Publishing House ASV

begell house, inc. publishers

Scientific coordination is carried out by the Russian Academy of Architecture and Construction Sciences (RAACS)

Volume 20 • Issue 2 • 2024

ISSN 2588-0195 (Online)
ISSN 2587-9618 (Print) Continues ISSN 1524-5845

International Journal for

Computational Civil and Structural Engineering

Международный журнал по расчету гражданских и строительных конструкций

https://ijccse.iasv.ru/

DOI: 10.22337/2587-9618
GICID: 71.0000.1500.2830

EXECUTIVE EDITOR

Vladimir I. Travush,
Full Member of RAACS, Professor, Dr.Sc.,
Vice-President of the Russian Academy
of Architecture and Construction Sciences;
Urban Planning Institute
of Residential and Public Buildings;
24, Ulitsa Bolshaya Dmitrovka, 107031, Moscow, Russia

EDITOR-IN-CHIEF

Vladimir N. Sidorov,
Corresponding Member of RAACS, Professor, Dr.Sc.,
National Research Moscow State University of Civil
Engineering; Russian University of Transport
(RUT – MIIT); Moscow Institute of Architecture
(State Academy); Perm National Research Polytechnic
University; 26, Yaroslavskoe Shosse, 129337,
Moscow, Russia

EDITORIAL DIRECTOR

Valery I. Telichenko,
Full Member of RAACS, Professor, Dr.Sc.,
The First Vice-President of the Russian Academy
of Architecture and Construction Sciences;
Honorary President of National Research
Moscow State University of Civil Engineering;
24, Ulitsa Bolshaya Dmitrovka, 107031, Moscow, Russia

MANAGING EDITOR

Nadezhda S. Nikitina,
Professor, Ph.D.,
Director of ASV Publishing House;
National Research Moscow State University
of Civil Engineering;
26, Yaroslavskoe Shosse, 129337, Moscow, Russia

ASSOCIATE EDITORS

Pavel A. Akimov,
Full Member of RAACS, Professor, Dr.Sc.,
Acting Rector of National Research
Moscow State University of Civil Engineering;
Vice-President of the Russian Academy
of Architecture and Construction Sciences;
Tomsk State University of Architecture and Building;
Russian University of Friendship of Peoples;
26, Yaroslavskoe Shosse, 129337, Moscow, Russia

Alexander M. Belostotsky,
Full Member of RAACS, Professor, Dr.Sc.,
Research & Development Center "STADYO";
National Research Moscow State University of Civil
Engineering; Russian University of Transport (RUT –
MIIT); Russian University of Friendship of Peoples;
Perm National Research Polytechnic University;
Tomsk State University of Architecture and Building;
Irkutsk National Research Technical University;
8th Floor, 18, ul. Tretya Yamskogo Polya,
125040, Moscow, Russia

Mikhail Belyi, Professor, Dr.Sc.,
Dassault Systèmes Simulia;
1301 Atwood Ave Suite 101W
02919 Johnston, RI, United States

Vitaly Bulgakov, Professor, Dr.Sc.,
Micro Focus;
Newbury, United Kingdom

Nikolai P. Osmolovskii, Professor, Dr.Sc.,
Systems Research Institute, Polish Academy of Sciences;
Kazimierz Pulaski University
of Technology and Humanities in Radom;
29, ul. Malczewskiego, 26-600, Radom, Poland

Gregory P. Panasenko, Professor, Dr.Sc.,
Equipe d'Analise Numerique; NMR CNRS 5585
University Gean Mehnet;
23 rue. P.Michelon 42023, St.Etienne, France

Scientific coordination is carried out by the Russian Academy of Architecture and Construction Sciences (RAACS)

PUBLISHER

ASV Publishing House
(ООО «Издательство АСВ»)
19/1,12, Yaroslavskoe Shosse, 120338, Moscow, Russia
Tel. +7(925)084-74-24; E-mail: iasv@iasv.ru; Интернет-сайт: http://iasv.ru/

ADVISORY EDITORIAL BOARD

Mojtaba Aslami, Ph.D,
Fasa University; Daneshjou blvd,
Fasa, Fars Province, Iran

Klaus-Jurgen Bathe, Professor
Massachusetts Institute
of Technology;
Cambridge, MA 02139, USA

Alexander T. Bekker,
Academician of RAACS,
Professor, Dr.Sc.,
Far Eastern Federal University;
Russian Academy of Architecture
and Construction Sciences;
8, Sukhanova Street, Vladivostok,
690950, Russia

Tomas Bock, Professor, Dr.-Ing.,
Technical University of Munich,
Arcisstrasse 21, D-80333
Munich, Germany

Jan Buynak, Professor, Ph.D.,
University of Žilina;
1, Univerzitná, Žilina, 010 26,
Slovakia

Vladimir T. Erofeev,
Full Member of RAACS,
Professor, Dr.Sc.,
Ogarev Mordovia State University;
68, Bolshevistskaya Str., Saransk
430005, Republic of Mordovia,
Russia

Victor S. Fedorov,
Full Member of RAACS,
Professor, Dr.Sc.,
Russian University of Transport
(RUT – MIIT);
9b9 Obrazcova Street, Moscow,
127994, Russia

Sergey V. Fedosov,
Full Member of RAACS,
Professor, Dr.Sc.,
Russian Academy of Architecture
and Construction Sciences;
24, Ul. Bolshaya Dmitrovka, 107031,
Moscow, Russia

Sergiy Yu. Fialko,
Professor, Dr.Sc.,
Cracow University of Technology;
24, Warszawska Street, Kraków,
31-155, Poland

Vladimir G. Gagarin,
Corresponding Member
of RAACS, Professor, Dr.Sc.,
Research Institute of Building
Physics of Russian Academy
of Architecture and Construction
Sciences;
21, Lokomotivny Proezd,
Moscow, 127238, Russia

Vyatcheslav A. Ilyichev,
Full Member of RAACS,
Professor, Dr.Sc.,
Russian Academy of Architecture
and Construction Sciences;
Podzemproekt Ltd.;
24, Ulitsa Bolshaya Dmitrovka,
Moscow, 107031, Russia

Marek Iwański,
Professor, Dr.Sc.,
Kielce University of Technology;
7, al. Tysiąclecia Państwa Polskiego
Kielce, 25 – 314, Poland

Sergey Yu. Kalashnikov,
Advisor of RAACS,
Professor, Dr.Sc.,
Volgograd State Technical
University; 28, Lenin avenue,
Volgograd, 400005, Russia

Semen S. Kaprielov,
Academician of RAACS,
Professor, Dr.Sc.,
Research Center of Construction;
6, 2nd Institutskaya St., Moscow,
109428, Russia

Nikolay I. Karpenko,
Full Member of RAACS,
Professor, Dr.Sc.,
Research Institute of Building
Physics of Russian Academy
of Architecture and Construction
Sciences; Russian Academy of
Architecture and Construction
Sciences; 21, Lokomotivny Proezd,
Moscow, 127238, Russia

Vladimir V. Karpov,
Professor, Dr.Sc., Saint Petersburg
State University of Architecture and
Civil Engineering;
4, 2-nd Krasnoarmeiskaya Steet,
Saint Petersburg, 190005, Russia

Galina G. Kashevarova,
Corresponding Member
of RAACS, Professor, Dr.Sc.,
Perm National Research
Polytechnic University;
29 Komsomolsky pros., Perm,
Perm Krai, 614990, Russia

John T. Katsikadelis,
Professor, Dr.Eng, PhD, Dr.h.c.,
National Technical University of
Athens; Zografou Campus
9, Iroon Polytechniou str
15780 Zografou, Greece

Vitaly I. Kolchunov,
Full Member of RAACS,
Professor, Dr.Sc., Southwest State
University; Russian Academy of
Architecture and Construction
Sciences; 94, 50 let Oktyabrya,
Kursk, 305040, Russia

Dmitry V. Kozlov, Dr. Sc.
Engineering, Professor, Head of
the Department of Hydraulics and
Hydrotechnical Construction, NRU
MGSU,
26, Yaroslavskoe Shosse., 129337,
Moscow, Russia

Markus König, Professor
Ruhr-Universität Bochum;
150, Universitätsstraße, Bochum,
44801, Germany

Sergey B. Kositsin,
Advisor of RAACS,
Professor, Dr.Sc.,
Russian University of Transport
(RUT – MIIT); 9b9 Obrazcova
Street, Moscow, 127994, Russia

Sergey B. Krylov,
Corresponding Member
of RAACS, Professor, Dr.Sc.,
Research Center of Construction;
6, 2nd Institutskaya St., Moscow,
109428, Russia

Sergey V. Kuznetsov,
Professor, Dr.Sc.,
Ishlinsky Institute for Problems
in Mechanics of the Russian
Academy of Sciences;
101-1, Prosp. Vernadskogo,
Moscow, 119526, Russia

Vladimir V. Lalin,
Professor, Dr.Sc.,
Peter the Great Saint-Petersburg Polytechnic University;
29, Ul. Politechnicheskaya, Saint-Petersburg, 195251, Russia

Leonid S. Lyakhovich,
Full Member of RAACS, Professor, Dr.Sc., Tomsk State University of Architecture and Building; 2, Solyanaya Sq., Tomsk, 634003, Russia

Rashid A. Mangushev,
Corresponding Member of RAACS, Professor, Dr.Sc., Saint Petersburg State University of Architecture and Civil Engineering;
4, 2-nd Krasnoarmeiskaya Steet, Saint Petersburg, 190005, Russia

Ilizar T. Mirsayapov,
Advisor of RAACS, Professor, Dr.Sc., Kazan State University of Architecture and Engineering; 1, Zelenaya Street, Kazan, 420043, Republic of Tatarstan, Russia

Vladimir L. Mondrus,
Corresponding Member of RAACS, Professor, Dr.Sc., National Research Moscow State University of Civil Engineering;
Yaroslavskoe Shosse 26, Moscow, 129337, Russia

Valery I. Morozov,
Corresponding Member of RAACS, Professor, Dr.Sc., Saint Petersburg State University of Architecture and Civil Engineering;
4, 2-nd Krasnoarmeiskaya Steet, Saint Petersburg, 190005, Russia

Anatoly V. Perelmuter,
Foreign Member of RAACS, Professor, Dr.Sc., SCAD Soft;
Office 1,2, 3a Osvity street, Kiev, 03037, Ukraine

Alexey N. Petrov,
Advisor of RAACS, Professor, Dr.Sc., Petrozavodsk State University; 33, Lenina Prospect, Petrozavodsk, 185910, Republic of Karelia, Russia

Vladilen V. Petrov,
Full Member of RAACS, Professor, Dr.Sc.,
Yuri Gagarin State Technical University of Saratov;
77 Politechnicheskaya Street, Saratov, 410054, Russia

Jerzy Z. Piotrowski,
Professor, Dr.Sc.,
Kielce University of Technology;
al. Tysiąclecia Państwa Polskiego 7, Kielce, 25 – 314, Poland

Chengzhi Qi, Professor, Dr.Sc.,
Beijing University of Civil Engineering and Architecture;
1, Zhanlanlu, Xicheng District, Beijing, China

Vladimir P. Selyaev,
Full Member of RAACS, Professor, Dr.Sc., Ogarev Mordovia State University;
68, Bolshevistskaya Str., Saransk 430005, Republic of Mordovia, Russia

Eun Chul Shin,
Professor, Ph.D.,
Incheon National University;
(Songdo-dong)119 Academy-ro, Yeonsu-gu, Incheon, Korea

D.V. Singh,
Professor, Ph.D,
University of Roorkee;
Roorkee, India, 247667

Wacław Szcześniak,
Foreign Member of RAACS, Professor, Dr.Sc.,
Lublin University of Technology;
Ul. Nadbystrzycka 40, 20-618 Lublin, Poland

Tadatsugu Tanaka,
Professor, Dr.Sc.,
Tokyo University; 7-3-1 Hongo, Bunkyo, Tokyo, 113-8654, Japan

Josef Vican,
Professor, Ph.D,
University of Žilina;
1, Univerzitná, Žilina, 010 26, Slovakia

Zbigniew Wojcicki,
Professor, Dr.Sc.,
Wroclaw University of Technology;
11 Grunwaldzki Sq., 50-377, Wrocław, Poland

Artur Zbiciak, Professor, Dr.Sc.,
Warsaw University of Technology;
Pl. Politechniki 1, 00-661 Warsaw, Poland

Segrey I. Zhavoronok, Ph.D.,
Institute of Applied Mechanics of Russian Academy of Sciences;
Moscow Aviation Institute (National Research University);
7, Leningradsky Prt., Moscow, 125040, Russia

Askar Zhussupbekov,
Professor, Dr.Sc.,
Eurasian National University;
5, Munaitpassov street, Astana, 010000, Kazakhstan

TECHNICAL EDITOR

Taymuraz B. Kaytukov,
Advisor of RAACS,
Associate Professor, Ph.D.,
Vice-Rector of National Research Moscow State University of Civil Engineering;
Yaroslavskoe Shosse 26,
Moscow, 129337, Russia

EDITORIAL TEAM

Vadim K. Akhmetov, Professor, Dr.Sc., National Research Moscow State University of Civil Engineering; 26, Yaroslavskoe Shosse, 129337 Moscow, Russia

Pavel A. Akimov, Full Member of RAACS, Professor, Dr.Sc., Acting Rector of National Research Moscow State University of Civil Engineering; Vice-President of the Russian Academy of Architecture and Construction Sciences; Tomsk State University of Architecture and Building; Russian University of Friendship of Peoples; 26, Yaroslavskoe Shosse, 129337, Moscow, Russia

Alexander M. Belostotsky, Full Member of RAACS, Professor, Dr.Sc., Research & Development Center "STADYO"; National Research Moscow State University of Civil Engineering; Russian University of Transport (RUT – MIIT); Russian University of Friendship of Peoples; Perm National Research Polytechnic University; Tomsk State University of Architecture and Building; Irkutsk National Research Technical University; 8th Floor, 18, ul. Tretya Yamskogo Polya, 125040, Moscow, Russia

Mikhail Belyi, Professor, Dr.Sc., Dassault Systèmes Simulia; 1301 Atwood Ave Suite 101W 02919 Johnston, RI, United States

Vitaly Bulgakov, Professor, Dr.Sc., Micro Focus; Newbury, United Kingdom

Charles El Nouty, Professor, Dr.Sc., LAGA Paris-13 Sorbonne Paris Cite; 99 avenue J.B. Clément, 93430 Villetaneuse, France

Natalya N. Fedorova, Professor, Dr.Sc., Novosibirsk State University of Architecture and Civil Engineering (SIBSTRIN); 113 Leningradskaya Street, Novosibirsk, 630008, Russia

Darya Filatova, Professor, Dr.Sc., Probability, Assessment, Reasoning and Inference Studies Research Group, EPHE Laboratoire CHART (PARIS) 4-14, rue Ferrus, 75014 Paris

Vladimir Ya. Gecha, Professor, Dr.Sc., Research and Production Enterprise All-Russia Scientific-Research Institute of Electromechanics with Plant Named after A.G. Iosiphyan; 30, Volnaya Street, Moscow, 105187, Russia

Taymuraz B. Kaytukov, Advisor of RAACS, Associate Professor, Ph.D, Vice-Rector of National Research Moscow State University of Civil Engineering; 26, Yaroslavskoe Shosse, 129337, Moscow, Russia

Marina L. Mozgaleva, Professor, Dr.Sc., National Research Moscow State University of Civil Engineering; 26, Yaroslavskoe Shosse, 129337 Moscow, Russia

Nadezhda S. Nikitina, Professor, Ph.D., Director of ASV Publishing House; National Research Moscow State University of Civil Engineering; 26, Yaroslavskoe Shosse, 129337 Moscow, Russia

Nikolai P. Osmolovskii, Professor, Dr.Sc., Systems Research Institute Polish Academy of Sciences; Kazimierz Pulaski University of Technology and Humanities in Radom; 29, ul. Malczewskiego, 26-600, Radom, Poland

Gregory P. Panasenko, Professor, Dr.Sc., Equipe d'Analise Numerique NMR CNRS 5585 University Gean Mehnet; 23 rue. P.Michelon 42023, St.Etienne, France

Andreas Rauh, Prof. Dr.-Ing. habil. Carl von Ossietzky Universität Oldenburg, Germany School II - Department of Computing Science Group Distributed Control in Interconnected Systems D-26111 Oldenburg, Germany

Zhan Shi, Professor LPSM, Université Paris VI 4 place Jussieu, F-75252 Paris Cedex 05, France

Marina V. Shitikova, National Research Moscow State University of Civil Engineering, Advisor of RAACS, Professor, Dr.Sc., Voronezh State Technical University; 14, Moscow Avenue, Voronezh, 394026, Russia

Igor L. Shubin, Corresponding Member of RAACS, Professor, Dr.Sc., Research Institute of Building Physics of Russian Academy of Architecture and Construction Sciences; 21, Lokomotivny Proezd, Moscow, 127238, Russia

Vladimir N. Sidorov, Corresponding Member of RAACS, Professor, Dr.Sc., National Research Moscow State University of Civil Engineering; Russian University of Transport (RUT – MIIT); Moscow Institute of Architecture (State Academy); Perm National Research Polytechnic University; 26, Yaroslavskoe Shosse, 129337, Moscow, Russia

Valery I. Telichenko, Full Member of RAACS, Professor, Dr.Sc., The First Vice-President of the Russian Academy of Architecture and Construction Sciences; National Research Moscow State University of Civil Engineering; 24, Ulitsa Bolshaya Dmitrovka, 107031, Moscow, Russia

Vladimir I. Travush, Full Member of RAACS, Professor, Dr.Sc., Vice-President of the Russian Academy of Architecture and Construction Sciences; Urban Planning Institute of Residential and Public Buildings; 24, Ulitsa Bolshaya Dmitrovka, 107031, Moscow, Russia

INVITED REVIEWERS

Akimbek A. Abdikalikov, Professor, Dr.Sc.,
Kyrgyz State University of Construction, Transport and Architecture n.a. N. Isanov;
34 Maldybayeva Str., Bishkek, 720020, Biskek, Kyrgyzstan

Vladimir N. Alekhin, Advisor of RAACS, Professor, Dr.Sc.,
Ural Federal University named after the first President of Russia B.N. Yeltsin;
19 Mira Street, Ekaterinburg, 620002, Russia

Irina N. Afanasyeva, Ph.D., University of Florida; Gainesville, FL 32611, USA

Ján Čelko, Professor, PhD, Ing., University of Žilina; Univerzitná 1, 010 26, Žilina, Slovakia

Tatyana L. Dmitrieva, Professor, Dr.Sc.,
Irkutsk National Research Technical University; 83, Lermontov street, Irkutsk, 664074, Russia

Petr P. Gaidzhurov, Advisor of RAACS, Professor, Dr.Sc.,
Don State Technical University; 1, Gagarina Square, Rostov-on-Don, 344000, Russia

Jacek Grosel, Associate Professor, Dr inz.
Wroclaw University of Technology; 11 Grunwaldzki Sq., 50-377, Wrocław, Poland

Stanislaw Jemioło, Professor, Dr.Sc.,
Warsaw University of Technology; 1, Pl. Politechniki, 00-661, Warsaw, Poland

Konstantin I. Khenokh, M.Ing., M.Sc.,
General Dynamics C4 Systems; 8201 E McDowell Rd, Scottsdale, AZ 85257, USA

Christian Koch, Dr.-Ing., Ruhr-Universität Bochum;
Lehrstuhl für Informatik im Bauwesen, Gebäude IA, 44780, Bochum, Germany

Gaik A. Manuylov, Professor, Ph.D.,
Moscow State University of Railway Engineering; 9, Obraztsova Street, Moscow, 127994, Russia

Alexander S. Noskov, Professor, Dr.Sc.,
Ural Federal University named after the first President of Russia B.N. Yeltsin;
19 Mira Street, Ekaterinburg, 620002, Russia

Grzegorz Świt, Professor, Dr.hab. Inż.,
Kielce University of Technology; 7, al. Tysiąclecia Państwa Polskiego, Kielce, 25 – 314, Poland

AIMS AND SCOPE

The aim of the Journal is to advance the research and practice in structural engineering through the application of computational methods. The Journal will publish original papers and educational articles of general value to the field that will bridge the gap between high-performance construction materials, large-scale engineering systems and advanced methods of analysis.

The scope of the Journal includes papers on computer methods in the areas of structural engineering, civil engineering materials and problems concerned with multiple physical processes interacting at multiple spatial and temporal scales. The Journal is intended to be of interest and use to researches and practitioners in academic, governmental and industrial communities.

ОБЩАЯ ИНФОРМАЦИЯ О ЖУРНАЛЕ

International Journal for Computational Civil and Structural Engineering

(Международный журнал по расчету гражданских и строительных конструкций)

Международный научный журнал "International Journal for Computational Civil and Structural Engineering (Международный журнал по расчету гражданских и строительных конструкций)" (IJCCSE) является ведущим научным периодическим изданием по направлению «Инженерные и технические науки», издаваемым, начиная с 1999 года (ISSN 2588-0195 (Online); ISSN 2587-9618 (Print) Continues ISSN 1524-5845). В журнале на высоком научно-техническом уровне рассматриваются проблемы численного и компьютерного моделирования в строительстве, актуальные вопросы разработки, исследования, развития, верификации, апробации и приложений численных, численно-аналитических методов, программно-алгоритмического обеспечения и выполнения автоматизированного проектирования, мониторинга и комплексного наукоемкого расчетно-теоретического и экспериментального обоснования напряженно-деформированного (и иного) состояния, прочности, устойчивости, надежности и безопасности ответственных объектов гражданского и промышленного строительства, энергетики, машиностроения, транспорта, биотехнологий и других высокотехнологичных отраслей.

В редакционный совет журнала входят известные российские и зарубежные деятели науки и техники (в том числе академики, члены-корреспонденты, иностранные члены, почетные члены и советники Российской академии архитектуры и строительных наук). Основной критерий отбора статей для публикации в журнале − их высокий научный уровень, соответствие которому определяется в ходе высококвалифицированного рецензирования и объективной экспертизы, поступающих в редакцию материалов.

Журнал входит в Перечень ВАК РФ ведущих рецензируемых научных изданий, в которых должны быть опубликованы основные научные результаты диссертаций на соискание ученой степени кандидата наук, на соискание ученой степени доктора наук по научным специальностям и соответствующим им отраслям науки:

- 1.1.8 – Механика деформируемого твердого тела (технические науки),
- 1.2.2 – Математическое моделирование численные методы и комплексы программ (технические науки),
- 2.1.1 – Строительные конструкции, здания и сооружения (технические науки),
- 2.1.2 – Основания и фундаменты, подземные сооружения (технические науки),
- 2.1.5 – Строительные материалы и изделия (технические науки),
- 05.23.07 – Гидротехническое строительство (технические науки),
- 2.1.9 – Строительная механика (технические науки)

В Российской Федерации журнал индексируется Российским индексом научного цитирования (РИНЦ).

Журнал входит в базу данных Russian Science Citation Index (RSCI), полностью интегрированную с платформой Web of Science. Журнал имеет международный статус и высылается в ведущие библиотеки и научные организации мира.

Издатели журнала – *Издательство Ассоциации строительных высших учебных заведений /АСВ/* (Россия, г. Москва) и до 2017 года *Издательский дом Begell House Inc*. (США, г. Нью-Йорк). Официальными партнерами издания является *Российская академия архитектуры и строительных наук* (РААСН), осуществляющая научное курирование издания, и *Научно-исследовательский центр СтаДиО* (ЗАО НИЦ СтаДиО).

Цели журнала – демонстрировать в публикациях российскому и международному профессиональному сообществу новейшие достижения науки в области вычислительных методов

решения фундаментальных и прикладных технических задач, прежде всего в области строительства.

Задачи журнала:

• предоставление российским и зарубежным ученым и специалистам возможности публиковать результаты своих исследований;

• привлечение внимания к наиболее актуальным, перспективным, прорывным и интересным направлениям развития и приложений численных и численно-аналитических методов решения фундаментальных и прикладных технических задач, совершенствования технологий математического, компьютерного моделирования, разработки и верификации реализующего программно-алгоритмического обеспечения;

• обеспечение обмена мнениями между исследователями из разных регионов и государств.

Тематика журнала. К рассмотрению и публикации в журнале принимаются аналитические материалы, научные статьи, обзоры, рецензии и отзывы на научные публикации по фундаментальным и прикладным вопросам технических наук, прежде всего в области строительства. В журнале также публикуются информационные материалы, освещающие научные мероприятия и передовые достижения Российской академии архитектуры и строительных наук, научно-образовательных и проектно-конструкторских организаций.

Тематика статей, принимаемых к публикации в журнале, соответствует его названию и охватывает направления научных исследований в области разработки, исследования и приложений численных и численно-аналитических методов, программного обеспечения, технологий компьютерного моделирования в решении прикладных задач в области строительства, а также соответствующие профильные специальности, представленные в диссертационных советах профильных образовательных организациях высшего образования.

Редакционная политика. Политика редакционной коллегии журнала базируется на современных юридических требованиях в отношении авторского права, законности, плагиата и клеветы, изложенных в законодательстве Российской Федерации, и этических принципах, поддерживаемых сообществом ведущих издателей научной периодики.

За публикацию статей плата с авторов не взымается. Публикация статей в журнале бесплатная. На платной основе в журнале могут быть опубликованы материалы рекламного характера, имеющие прямое отношение к тематике журнала.

Журнал предоставляет непосредственный открытый доступ к своему контенту, исходя из следующего принципа: свободный открытый доступ к результатам исследований способствует увеличению глобального обмена знаниями.

Индексирование. Публикации в журнале входят в системы расчетов индексов цитирования авторов и журналов. «Индекс цитирования» – числовой показатель, характеризующий значимость данной статьи и вычисляющийся на основе последующих публикаций, ссылающихся на данную работу.

Авторам. Прежде чем направить статью в редакцию журнала, авторам следует ознакомиться со всеми материалами, размещенными в разделах сайта журнала (интернет-сайт Российской академии архитектуры и строительных наук (http://raasn.ru); подраздел «Издания РААСН» или интернет-сайт Издательства АСВ (http://iasv.ru); подраздел «Журнал IJCCSE»): с основной информацией о журнале, его целями и задачами, составом редакционной коллегии и редакционного совета, редакционной политикой, порядком рецензирования направляемых в журнал статей, сведениями о соблюдении редакционной этики, о политике авторского права и лицензирования, о представлении журнала в информационных системах (индексировании), информацией о подписке на журнал, контактными данными и пр. Журнал работает по лицензии Creative Commons типа cc by-nc-sa (Attribution Non-Commercial Share Alike) – Лицензия «С указанием авторства – Некоммерческая – Копилефт».

Рецензирование. Все научные статьи, поступившие в редакцию журнала, проходят обязательное двойное слепое рецензирование (рецензент не знает авторов рукописи, авторы рукописи не знают рецензентов).

Заимствования и плагиат. Редакционная коллегия журнала при рассмотрении статьи проводит проверку материала с помощью системы «Антиплагиат». В случае обнаружения многочисленных заимствований редакция действует в соответствии с правилами COPE.

Подписка. Журнал зарегистрирован в Федеральном агентстве по средствам массовой информации и охраны культурного наследия Российской Федерации. Индекс в общероссийском каталоге РОСПЕЧАТЬ − 18076.

По вопросам подписки на международный научный журнал “International Journal for Computational Civil and Structural Engineering (Международный журнал по расчету гражданских и строительных конструкций)” обращайтесь в Агентство «Роспечать» (Официальный сайт в сети Интернет: http://www.rosp.ru/) или в издательство Ассоциации строительных вузов (АСВ) в соответствии со следующими контактными данными:

ООО «Издательство АСВ»

Юридический адрес: 129337, Россия, г. Москва, Ярославское ш., д. 26, офис 705;

Фактический адрес: 129337, Россия, г. Москва, Ярославское ш., д. 19, корп. 1, 5 этаж, офис 12 (ТЦ Соле Молл);

Телефоны: +7 (925) 084-74-24;

Интернет-сайт: www.iasv.ru. Адрес электронной почты: iasv@iasv.ru.

Контактная информация. По всем вопросам работы редакции, рецензирования, согласования правки текстов и публикации статей следует обращаться к главному редактору журнала члену-корреспонденту РААСН *Сидорову Владимиру Николаевичу* (адреса электронной почты: sidorov.vladimir@gmail.com, sidorov@iasv.ru, iasv@iasv.ru, sidorov@raasn.ru) или к техническому редактору журнала советнику РААСН *Кайтукову Таймуразу Батразовичу* (адреса электронной почты: tkaytukov@gmail.com; kaytukov@raasn.ru). Кроме того, по указанным вопросам, а также по вопросам размещения в журнале рекламных материалов можно обращаться к генеральному директору ООО «Издательство АСВ» *Никитиной Надежде Сергеевне* (адреса электронной почты: iasv@iasv.ru, nsnikitina@mail.ru, ijccse@iasv.ru).

Журнал становится технологичнее. Издательство АСВ с сентября 2016 года является членом Международной ассоциации издателей научной литературы (Publishers International Linking Association (PILA)), осуществляющей свою деятельность на платформе CrossRef. Оригинальным статьям, публикуемым в журнале, будут присваиваться уникальные номера (индексы DOI – Digital Object Identifier), что значительно облегчит поиск метаданных и местонахождение полнотекстового произведения. DOI – это система определения научного контента в сети Интернет.

С октября 2016 года стал возможен прием статей на рассмотрение и рецензирование через онлайн систему приема статей Open Journal Systems на сайте журнала (электронная редакция): https://ijccse.iasv.ru.

Автор имеет возможность следить за продвижением статьи в редакции журнала в личном кабинете Open Journal Systems и получать соответствующие уведомления по электронной почте.

В феврале 2018 года журнал был зарегистрирован в Directory of open access journals (DOAJ) (это один из самых известных поисковых сервисов в мире, который предоставляет открытый доступ к материалам и индексирует не только заголовки журналов, но и научные статьи), в сентябре 2018 года включен в продукты EBSCO Publishing.

В ноябре 2020 года журнал начал индексироваться в международной базе Scopus.

International Journal for
Computational Civil and Structural Engineering
(Международный журнал по расчету гражданских и строительных конструкций)
Volume 20, Issue 2 ***2024***

Scientific coordination is carried out by the Russian Academy of Architecture and Construction Sciences (RAACS)

CONTENTS

Filtration Regime and Stability of the Earth Dam During Reservoir Drawdown **14**
Nikolay A. Aniskin, Andrey V. Stupivtsev

Mathematical Modeling of Relaxation Process in Concrete **25**
Sergey B. Krylov, Petr D. Arleninov

Elastoplastic Deformation of Steel Concrete Beams with Local Commission Under Three-Point Bending **34**
Pavel A. Khazov, Vladimir I. Erofeev, Olga I. Vediaikina, Artyom P. Pomazov, Dmitrij A. Kozhanov

Hydraulic Analysis of Composite Hydraulic Structure Considering Existing of Pier **46**
Rafi M. Qasim, Ihsan A. Abdulhussein, Muna A. Hameed

Numerical Analysis of Stress-Strain State of the Steel Modular Block with Corrugated Webs **60**
Olga A. Tusnina, Anatoliy V. Alekseytsev

Numerical Simulation of the Operation of Aluminum Alloy Joints Made by Contact Capacitor Welding **76**
Andrey V. Korgin

Optimal Seismic Protection of Structures on Bearings with Bilinear Hysteretic Characteristic **88**
Elena V. Poznyak, Vladimir P. Radin, Olga V. Novikova, Alexey V. Kiselev, Yulia Y. Ivanova

Probabilistic Design of Flexural Cross-Laminated Timber Structural Elements **99**
Sergey A. Solovev, Valery M. Puchkov, Anastasia A. Soloveva

The Effect of Montmorillonite on the Rheological and Physico-Mechanical Properties of a Thermosetting Polymer Composite **109**
Pavel V. Monastyrev, Tatiana F. Elchishcheva, Maxim V. Makarchuk, Vladimir T. Erofeyev, Vladimir I. Rimshin, Irina V. Erofeeva

Concrete Delayed Failure Time **118**
Vu Ngoc Tuyen, Nataliya V. Fedorova

Calibration of the Nonlocal Dynamic Deformation Model of a Flexural Beam Based on Numerical Experiment Results **132**
Vladimir N. Sidorov, Elena. S. Badina, Roman O. Tsarev

Analytical Model for Buckling Length Coefficient Determination in Steel Trusses: A Lateral Torsional Buckling Approach **141**
D. Boukhalfa, T. Belaid, A. Slimani, F. Ammari

Implementation of BIM Technologies in the Management of Multi-Apartment Buildings During the Operation Phase **155**
Dmitriy A. Matveev

Overall Assessment of Deformation and Force of Diaphragm Wall Joints During the Stages of Deep Excavation Construction **163**
Phuong Tuan Nguyen, Truong Xuan Dang, Tuan Anh Nguyen, Hoa Van Vu Tran

The Coefficient of Longitudinal Bending for Composite Steel-Concrete Rods Under Short-Term Loads **177**
Denis V. Konin

Solution of the Problem of Two-Dimensional Theory of Elasticity with the Use of Discrete-Continual Finite Element Method in the Presence of a Crack **192**
Marina L. Mozgaleva, Pavel A. Akimov

International Journal for
Computational Civil and Structural Engineering
(Международный журнал по расчету гражданских и строительных конструкций)
Volume 20, Issue 2 ***2024***

Scientific coordination is carried out by the Russian Academy of Architecture and Construction Sciences (RAACS)

СОДЕРЖАНИЕ

Фильтрационный режим и устойчивость грунтовой плотины при сработке водохранилища **14**
Н.А. Анискин, А.В. Ступивцев

Математическое моделирование процесса релаксации в бетоне **25**
С.Б. Крылов, П.Д. Арленинов

Упругопластическое деформирование сталебетонных балок с локальным смятием при трехточечном изгибе **34**
П.А. Хазов, В.И. Ерофеев, О.И. Ведяйкина, А.П. Помазов, Д.А. Кожанов

Гидравлический анализ сложного гидротехнического сооружения, включающего пирс **46**
Рафи М. Касим, Эхсан А. Абдул-Хусейн, Муна А. Хамид

Численный анализ напряженно-деформированного состояния стального модульного блока со стенами из гофрированного листа **60**
О.А. Туснина, А.В. Алексейцев

Численное моделирование работы соединений из алюминиевых сплавов, выполненных методом контактной конденсаторной сварки **76**
А.В. Коргин

Оптимальная сейсмозащита конструкций на опорах с билинейной гистерезисной характеристикой **88**
Е.В. Позняк, В.П. Радин, О.В. Новикова, А.В. Киселев, Ю.Ю. Иванова

Вероятностное проектирование изгибаемых элементов из перекрестно-клееной древесины **99**
С.А. Соловьев, В.М. Пучков, А.А. Соловьева

Влияние монтмориллонита на реологические и физико-механические свойства термореактивного полимерного композита **109**
П.В. Монастырев, Т.Ф. Ельчищева, М.В. Макарчук, В.Т. Ерофеев, В.И. Римшин, И.В. Ерофеева

Время задержки разрушения бетона **118**
Ву Нгок Туен, Н.В. Федорова

Калибровка нелокальной модели динамического деформирования изгибаемой балки по результатам численного эксперимента **132**
В.Н. Сидоров, Е.С. Бадьина, Р.О. Царёв

Аналитическая модель для определения коэффициента длины смятия в стальных фермах: Подход к определению бокового крутильного смятия **141**
Д. Бухалф, Т. Белаид, А. Слимани, Ф. Аммари

Внедрение BIM-технологий в управление многоквартирными домами на этапе эксплуатации **155**
Д.А. Матвеев

Обобщенная оценка деформаций и усилий в соединениях мембранных стен на этапах возведения объектов глубокого заложения **163**
Фыонг Туан Нгуен, Чыонг Суан Данг, Туан Ань Нгуен, Хоа Ван Ву Чан

Коэффициент продольного изгиба сталежелезобетонных стоек при кратковременном действии нагрузок **177**
Д.В. Конин

Решение двумерной задачи теории упругости с использованием дискретно-континуального метода конечных элементов при наличии щели **192**
М.Л. Мозгалева, П.А. Акимов

DOI:10.22337/2587-9618-2024-20-2-14-24

FILTRATION REGIME AND STABILITY OF THE EARTH DAM DURING RESERVOIR DRAWDOWN

Nikolay A. Aniskin, Andrey V. Stupivtsev
National Research Moscow State University of Civil Engineering, Moscow, RUSSIA

Abstract. The results of numerical investigations of the filtration regime and stability of an earth dam under reservoir drawdown are considered. The problem of unsteady filtration in a homogeneous earth dam is solved. The parameters of the filtration flow are determined: the position of the depression surface, the values and direction of filtration gradients and flow velocities. The changes in the maximum filtration gradients and the probability of filtration deformations are analyzed. Calculations are made to assess the stability of the upstream slope during the stages of reservoir drawdown with different velocities. It is shown that a dam with a large stability margin when the reservoir is full may lose it and be destroyed in the process of drawdown. Conclusions are drawn about the necessary measures to ensure reliability and safety during operation of the structure.

Keywords: earth dam, reservoir drawdown, unsteady seepage, seepage gradient, slope stability

FUNDING. The research was funded by the National Research Moscow State University of Civil Engineering (grant for fundamental and applied scientific research, project No. 28-392/130).

ФИЛЬТРАЦИОННЫЙ РЕЖИМ И УСТОЙЧИВОСТЬ ГРУНТОВОЙ ПЛОТИНЫ ПРИ СРАБОТКЕ ВОДОХРАНИЛИЩА

Н.А. Анискин, А.В. Ступивцев
Национальный исследовательский Московский государственный строительный университет,
г. Москва, РОССИЯ

Аннотация. Рассматриваются результаты численных исследований фильтрационного режима и устойчивости грунтовой плотины при сработке водохранилища. Решается задача неустановившейся фильтрации в однородной земляной плотине. Определяются параметры фильтрационного потока: положение депрессионной поверхности, величины и направление фильтрационных градиентов и скоростей потока. Дается анализ изменения максимальных градиентов фильтрации и вероятность возникновения фильтрационных деформаций. Проведены расчеты по оценке устойчивости верхового откоса на этапах сработки водохранилища с разной скоростью. Показано, что плотина, имеющая большой запас устойчивости при наполненном водохранилище, может потерять его и быть разрушенной в процессе сработки. Сделаны выводы о необходимых мероприятиях по обеспечению надежности и безопасности при эксплуатации сооружения.

Ключевые слова: грунтовая плотина, сработка водохранилища, неустановившаяся фильтрация, градиент фильтрации, устойчивость откоса

Финансирование. Данная работа была поддержана грантом 2024 года на проведение фундаментальных и прикладных научных исследований (НИР/НИОКР) научными коллективами НИУ МГСУ, проект № 28-392/130.

INTRODUCTION

Problems of unsteady filtration are encountered in hydraulic engineering practice during construction and operation of dams, in cases of filling or drawdown of a reservoir, as well as during construction of reclamation dams.

The drawdown of a reservoir may be caused by the technological necessity of operation of a hydroelectric complex, which includes an earth dam, or by an emergency situation. The lowering of the water level upstream of the dam leads to a change in the filtration regime of the ground structure - the position of the depression surface, the values and directions of the gradients and velocities of the filtration flow change. The consequence of this process can be filtration deformations of soils and occurrence of concentrated filtration in the dam body [1-3]. Also in this case, in the upstream slope there is a

change in the direction of action of filtration hydrodynamic load towards the upstream, which reduces the stability of the slope of the structure [4-5]. In the practice of hydraulic engineering, there are quite a large number of cases of emergencies associated with the lowering of the reservoir water level [6-7]. The degree of change in the stability of the structure and the filtration regime depends on several factors: the permeability of the soils in the upstream prism of the dam, the magnitude and rate of drawdown, the top slope embedment, and a number of other factors [8-10].

At present, filtration calculations are mandatory in the design of earth dams, on the basis of which the filtration stability of the dam soils, foundation and banks, as well as the stability of the slopes of the structure are assessed (SP39.13330.2012 Dams made of earth materials. Updated version of SNiP2.06.05-84).

The assessment of the stability of the upstream slope in the design justification of the earth dam should be carried out for the case of the maximum possible drawdown of the reservoir water level with the highest possible velocity, where the filtration forces of unsteady filtration are as follows.

This paper investigates the effect of the drawdown rate on the maximum filter gradient and the stability of the upstream slope of a homogeneous earth dam. The changes in these parameters in the process of lowering the upstream water level are considered. Previous studies [10,11] have shown that the maximum filtration gradient can be recorded not at the end of drawdown, but at intermediate stages of water level lowering.

RESEARCH OBJECT

The object of research is a homogeneous earthen dam 24.0m high, located on an impermeable base (Figure 1). The dam slopes are -1:3 for upstream and downstream slopes. At the level mark of the dam foot level equal to 0.00, the upstream water level is 22.0m and the downstream water level is 3.0m. To ensure reliable operation of the dam, a 4m high drainage prism with a 1:3 slope is installed in the downstream prism.

The dam body is composed of clayed sand. The characteristics corresponding to this group of soils, included in filtration, stress-strain and

Table 1. Characteristics of the soil of the dam body under consideration

Type of soil	Particle size, mm	Percentage of soil particles, %	Filtration coefficient, m/day	Cohesion C, kN/m2	Density γ, kN/m3		Strain modulus E, kN/m2	Poisson's ratio ν	Angle of internal friction φ, °
					Saturated condition	Dry condition			
Clayed sand	< 0.002	22	0.10	4.0	19.0	18.0	20000	0.33	30.0
	0.002 - 0.05	25							
	0.05 - 2	53							

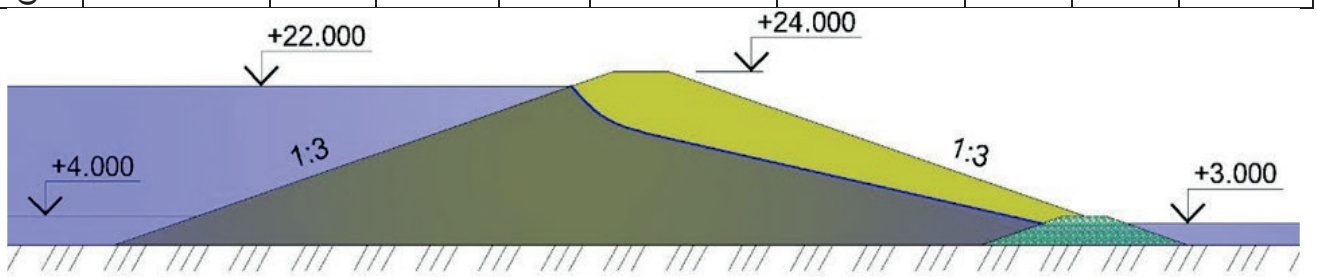


Figure 1. Schematic diagram of a homogeneous earth dam with drainage

stability calculations, are given in Table 1. Characteristics of the drainage prism soil: density in saturated and dry states 19 and 16 kN/m3; modulus of elasticity $E = 30000 kN/m^2$; Poisson's ratio $\nu = 0{,}3$; cohesion $c = 1\ kN/m^2$; angle of internal friction $\varphi = 30°$, filtration coefficient $k = 10 m/day$.

METHODS

Since the middle of the 20th century, due to the difficulty of solving the problem of unsteady filtration, hydraulic methods based on the solution of the Boussinesq equation with some assumptions [12] have become widespread. As the issue of improvement of calculation methods developed, new analytical [13] and hydraulic [14-15] calculation methods appeared.

In modern studies [16-19], the main task is to determine filtration parameters, such as the position of the depression curve, the height of the drawdown gap on the downstream slope of the dam, the filtration flow rate, gradients and filtration velocities. This is achieved using numerical methods of FEM, FVM and BEM.

Modern program complexes (PCs) designed to solve filtration problems are based on the solution of the basic differential equation of filtration theory with known boundary conditions [13]:

$$\frac{\partial}{\partial x}\left(K_x \frac{\partial H}{\partial x}\right) + \frac{\partial}{\partial y}\left(K_y \frac{\partial H}{\partial y}\right) + \frac{\partial}{\partial z}\left(K_z \frac{\partial H}{\partial z}\right) - \mu \frac{\partial H}{\partial t} = 0, \quad (1)$$

where $H = f\ (x, y, z, t)$ – head function in the considered area, varying along the coordinates x, y, z and in time t; K_x, K_y, K_z– filtration coefficients in axis directions x, y, z; μ – water loss coefficient in the ground.

In such calculations, water movement between particles is assumed when the pores are completely filled with water. Water moves from a higher-pressure region to a lower pressure region. Then, when excluding the finite elements from the computational domain, for which the obtained value of filtration head is less than their altitude position, the position of the depression curve will be determined [18]. Similar problems of soil hydrology were considered in the works of famous foreign [20-23] and Soviet-Russian scientists [24].

When solving filtration problems in soil hydrology, the L.A.Richards equation [25] based on the Darcy equation is used to solve problems of unsteady filtration. One of the modifications of this equation for moisture transport in vertical direction, with gravity pressure gradient equal to one, is presented in the form:

$$\mu\ (\partial \Psi\ /\ \partial t)\ =\ \partial\ (k\ (\partial \Psi / \partial z\ -1))\ /\partial z, \quad (2)$$

where Ψ – capillary pressure of ground (soil) moisture (cm of water column), k – ground (soil) hydraulic conductivity coefficient (cm/day, is a function of moisture pressure Ψ), μ- coefficient of differential soil water holding capacity (cm of waterstage -1), t - time (days), z – vertical axis coordinate (cm).

When solving such an equation, only numerical methods can be used. Coefficients $\mu = \mu(\Psi)\ and\ k = k\ (\Psi)$ are a function of capillary pressure of moisture, but these functions have empirical value [24, 26], which leads to inaccuracy of the obtained results. Value of soil volumetric moisture θ is determined under laboratory conditions and depends on the capillary pressure of moisture Ψ, called the basic hydrophysical characteristic (BHC) [25].

In 1980, Van Genuchten [22], using the Mualem method [21], proposed a model for describing the hydrophysical properties of soils (soils) using expressions of the Mualem-Van Genuchten model. Such a model is widely used in practice nowadays in the numerical modeling of filtration processes [6-7].

RESULTS

The effect of reservoir drawdown on the filtration regime and stability of the structure was studied for a homogeneous earth dam structure under consideration. The problem was solved in Plaxis PC using the finite element method. The computational domain was divided into 1984 elements and 16221 nodes, taking into account the elements and nodes of the impermeable foundation.

Three variants of drawdown were considered depending on its velocity in height with values of 0.25, 1.0, 2.0 s/day. Depletion rate in height was 18 meters: from elevation 22.0 to elevation 4.0 (Figure 1).

During the study, the design calculations were carried out in 3 phases:

Initial Phase - the first phase in which initial conditions of loading by own weight and hydraulic conditions under steady filtration level were set. At this phase depression curve was formed at filled reservoir.

The second phase, in which reservoir drawdown with different rates of water level drawdown was modeled. In this phase, deformations and pore pressure under unsteady filtration are calculated in time.

The third phase, in which the stability of the structure is calculated using the strength reduction method.

At each setback step with a height interval of 1.0 m, the 2nd and 3rd phases of the calculation were solved.

Safety calculation in Plaxis 2D PC is used to determine the calculated actual stability coefficients. During this calculation, the strength characteristics of soils (internal friction angle, cohesion and shear strength) are sequentially reduced until failure. The slope stability coefficient is defined as the ratio of the actual strength to the failure strength. The known criterion of slope stability is used:

$$\gamma_{lc} \; F \leq \gamma_c \, R / \gamma_n \qquad (3)$$

where F – design value of the generalized shear force, determined taking into account the load reliability factor; R – calculated value of the generalized bearing capacity of the system "structure - base", determined taking into account the reliability coefficient for soil, i.e. generalized calculated value of the ultimate shear resistance forces on the considered surface; γ_{lc} – load combination factor, taken as: γ_{lc} = 1,0 – for the main load combination; γ_{lc}= 0,9 – for special load combinations; γ_n – reliability coefficient by the degree of responsibility of structures. For the considered structure we can conditionally assume γ_n =1,20, which corresponds to reliability class II; γ_c – coefficient of working conditions, or taking into account the method of calculation: γ_c=1,0 – for calculation methods taking into account the stress-strain state.

The soil medium was modeled on the basis of the bilinear elastic-plastic Mohr-Coulomb model (Mohr-Coulomb) [20, 21].

Estimation of filtration regime. The solution of the unsteady filtration problem (2nd phase of calculations) allowed us to obtain a picture of changes in the filtration regime of a homogeneous dam at different drawdown rates. Figure 2 shows the position of the depression surface and the distribution of the filtration gradient at the moments of the end of the reservoir drawdown up to the 4.0 mark for the variants of drawdown rates of 0.25 and 2.0 m/day.

It can be noted that for the variant of 0.25 m/day drawdown rate, the depression curve decreased to a greater extent in the upper prism in comparison with the variant with 2.0 m/day drawdown rate (the

depression curve mark in the first variant is 12.0 m, in the second - 16.0 m). At elevations below the point of depression curve exit to the upper slope near the slope, zones with increased values of filtration gradients were obtained.

Based on the results obtained, the maximum filtration gradients were plotted (Figure 3) to provide a preliminary assessment of the ground filtration strength and to calculate, if necessary, the parameters of inverse filters. The maximum

output gradients occur on the upstream slope of the dam when the upstream slope is drawn down to the marks 14.0 -16.0. The maximum gradients for the 0.25, 1.0, and 2.0 m/day drawdown rates are 0.460, 0.518, and 0.532, respectively.

Estimation of the stability of the upper slope. Based on the results of the third phase calculation, a series of dam stability coefficients for different moments of failure were obtained, as summarized in Table 2. Graphical representation of some of the results is given in Figure 4.

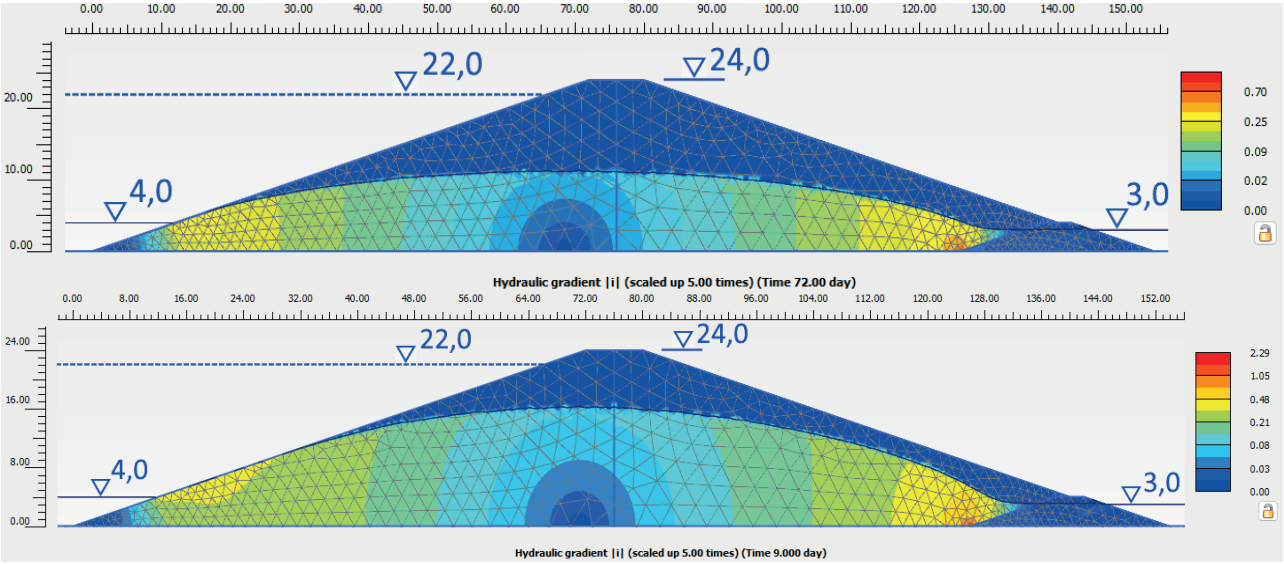


Figure 2. Position of the depression curve at drawdown with velocities of 0.25m/day and 2m/day for the period of the end of reservoir drawdown (isopoles show the distribution of hydraulic gradient)

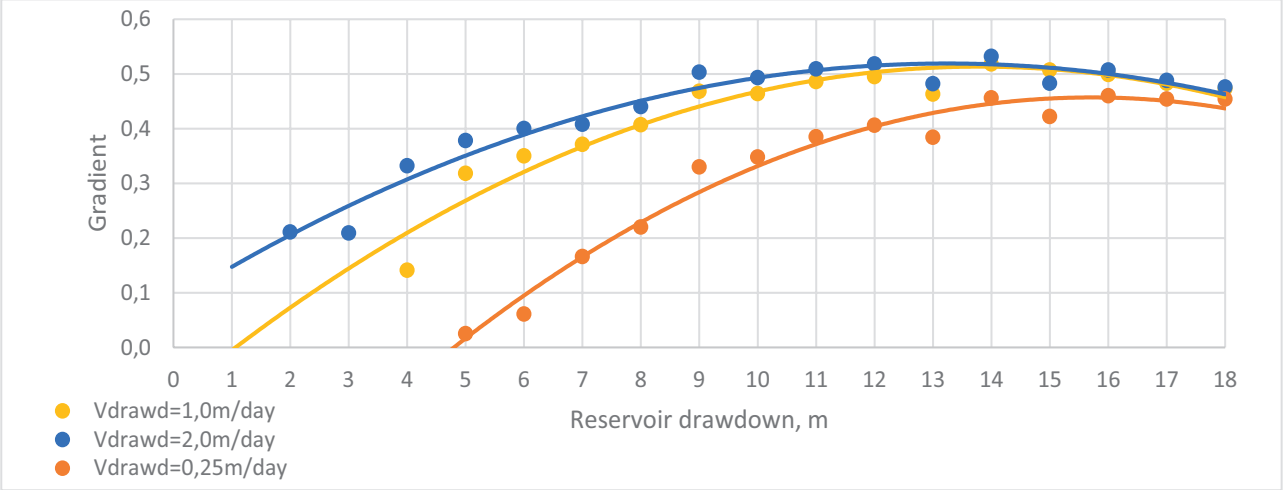


Figure 3. Variation of the maximum filtration gradient as a function of drawdown elevation for variants of drawdown rates

It is possible to note the influence of the displacement rate on the value of the minimum stability coefficients of the top slope (Table 2). As can be seen from the results, the stability coefficient is lower the higher the displacement rate. At the value of stability coefficient Ks =2.127 when the reservoir is filled, this value decreases at drawdown rates of 0.25. 1.0, 2.0 m/day respectively to values 1.360, 1.137 and 1.047.

It can be concluded that at displacement rates higher than 0.5 m/day the slope stability coefficient is less than the normative one (for conditionally assumed 2nd capitalization class K_n =1.2).

Next, the slope stability at different stages of reservoir drawdown was investigated. Step 1m of fixing the stability coefficient was set for cases with drawdown rates of 0.25m/day, 1m/day and 2m/day. At each step, the slope stability coefficient was determined taking into account the filtration hydrodynamic forces determined from the solution of the unsteady filtration problem. According to the results of the numerical experiment, the graphs of changes in the stability coefficient of the upper slope were plotted for the stages of depletion at the values of its velocity equal to 0.25, 1.0 and 2.0 m/day (Figure 5).

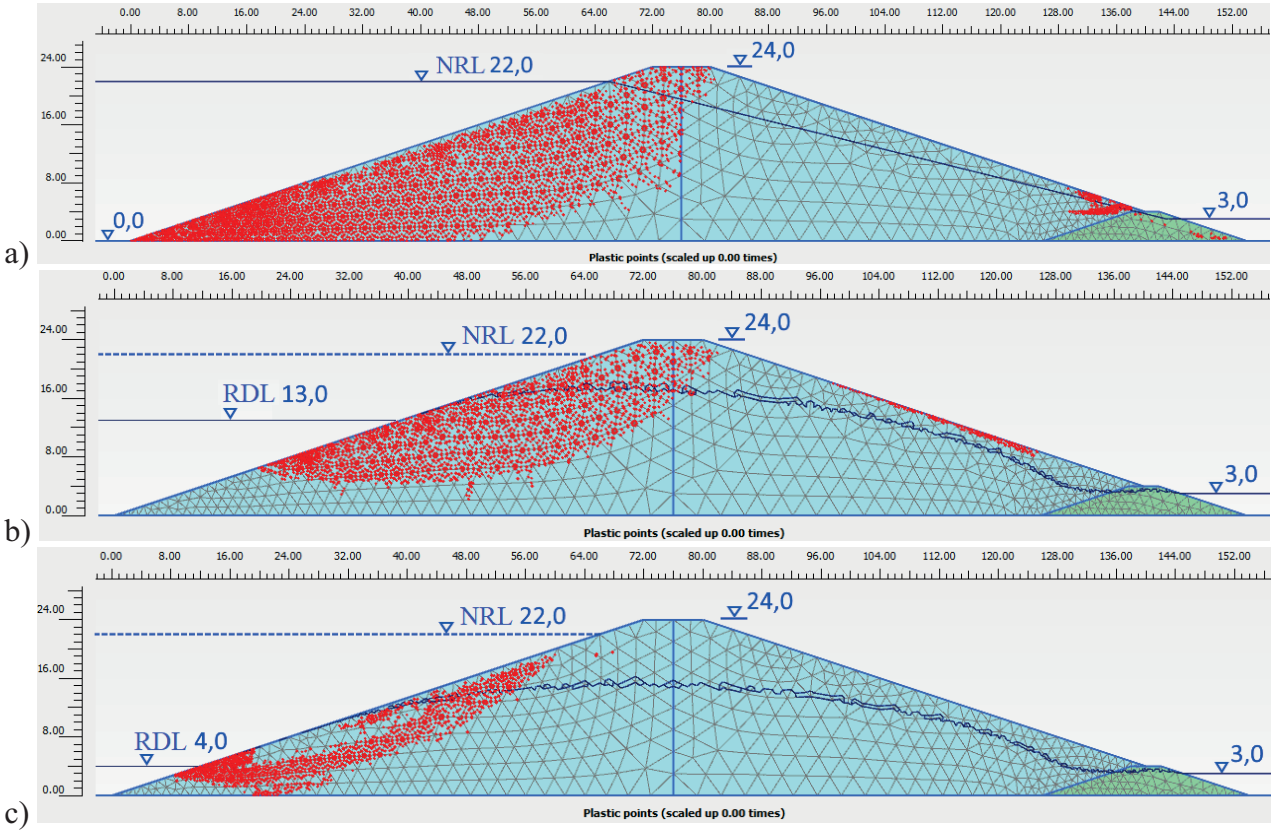


Figure 4. Collapse surfaces with minimum stability coefficients for cases of reservoir drawdown at a rate of 1 m/day: a) at fully filled reservoir; b) at 9.0 m drawdown; c) at 18.0 m drawdown

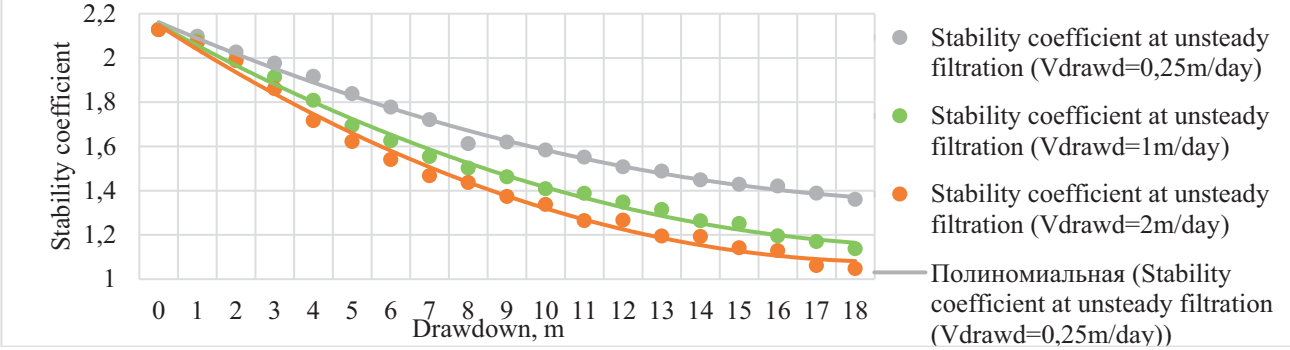


Figure 5. Plots of change in the stability coefficient of the upper slope depending on the degree of displacement and its velocity

Table 2. Calculation results of stability coefficient for different soil variants and displacement rates

Type of soil	Filtration coefficient, m/day	Slope stability coefficient					
		Reservoir drawdown rate, m/day					
		0.10	0,25	0,5	1,0	1,5	2,0
Clayed sand	0.10	1,506	1,360	1,233	1,137	1,072	1,047

As can be seen from the graphs in Figure 5, as the reservoir drawdown proceeds, the stability coefficient decreases significantly. The drawdown rate affects the slope stability: increasing the rate decreases the stability coefficient. At the same time, by the end of drawdown to the 4.0 mark, the minimum stability coefficients were recorded (Table 2, Figure 5).

For the considered variant of the earth dam, the drawdown rates of 1.0 and 2.0 m/day cause the stability coefficient to decrease to values lower than the normative one. Thus, for the rate of 1.0 m/day $K_s \leq K_n$ at reservoir drawdown exceeding 16.0 m from the NRL level, for the rate of 2.0 m/day - exceeding 12.0 m.

CONCLUSIONS

The design of earth dams must take into account the effect of unsteady filtration in the dam body in the event of reservoir drawdown. The degree to which drawdown affects the seepage regime and the stability of the upstream slope depends to a large extent on a number of factors, primarily the rate of water level drawdown.

1. The values of maximum filtration gradients necessary to evaluate the possibility of filtration deformations and to calculate the return filters in case of the top slope fixing device have been obtained for the considered design of the earth dam.
2. The value of the maximum filtration gradient during reservoir drawdown depends on its velocity. The highest gradients at the outlet of filtration flow to the upper reservoir with values 0.46 - 0.53 occur for the considered variant in the lower third of the drawdown interval at grades 13.0 - 16.0 depending on the drawdown rate. The higher is the discharge rate, the greater are the values of output gradients.
3. Reservoir drawdown reduces the stability of the upstream slope. The stability coefficient values are minimal at maximum upstream drawdown. For the considered variant of the dam and the conditions of drawdown at drawdown rates ≥ 1.0 m/day, the value of the slope stability coefficient is less than the normative value K_n=1.2, conventionally accepted for a structure of the 2nd capital class. This relationship occurs at drawdown to elevation 12.0 at 2.0 m/day and to elevation 16.0 at 1.0 m/day.

Further studies may consider the effect of anisotropy of the dam body soils caused by the placement technology and properties of the soils, as well as the effect of drawdown on the performance of earth dams with impervious elements.

REFERENCES

1. **Bellendir E.N., Ivashintsov D.A., Stefanishin D.V.** et al. Probabilistic methods of reliability assessment of ground hydraulic structures // St. Petersburg: VNIIG named after B.E. Vedeneev. B.E. Vedeneev. 2003- 2004. T. 1.
2. **Adamo, Nasrat & Al-Ansari, Nadhir & Sissakian, Varoujan & Laue, Jan & Knutsson, Sven**. Dam Safety Problems Related to Seepage. 2020; 10. 191-239
3. **López-Acosta N.P., Sánchez M.A. Soil Solution, G. Auvinet J.-M. Pereira.** Assessment of exit hydraulic gradients at the toe of levees in water drawdown conditions. Scour and Erosion – Cheng, Draper & An (Eds)©. 2015; Taylor &

Francis Group, London. Available from: https://www.researchgate.net/publication/283129540. DOI: 10.1201/b17703-21.
4. **Fattah M.Y., Hasan A. Omran, Mohammed A. Hassan.** Behavior of an Earth Dam during Rapid Drawdown of Water in Reservoir-Case Study. International Journal of Advanced Research. 2015; Vol. 3, Issue 10, 110 -122.
5. **Upomo T.C., Effendi M.K., Kusumawardani R.** Behaviour of levee on softsoil caused by rapid drawdown. AIP Conference Proceedings. American Institute of Physics Inc. 2018; 1941. DOI: 10.1063/1.5028103.
6. **Stark T.D., Jafari N.H., Zhindon J.S.L., & Baghdady A.** Unsaturated and Transient Seepage Analysis of San Luis Dam. Journal of Geotechnical and Geoenvironmental Engineering. 2017; 143(2), 04016093. DOI: 10.1061/(ASCE)GT.1943-5606.0001602.
7. **Vandenberge D.R.** Total Stress Rapid Drawdown Analysis of the Pilarcitos Dam Failure using the Finite Element Method. Frontiers of Structural and Civil Engineering. 2014; 8(2), 115–123. DOI: 10.1007/s11709-014-0249-7.
8. **Perzlmaier S.** Hydraulic criteria for internal erosion in cohesionless soil. In Internal erosion of dams and their Foundations. Editors R. Fell and J.J. Fry. Taylor & Francis. 2007; 179-190. DOI: 10.1201/9781482266146-20.
9. **Aniskin N.A., Sergeev S.A.** The effect of draw-off on filtration regime of earth-fill dam. International Journal for Computational Civil and Structural Engineering. 2022. 18(1) 40-50. DOI:10.22337/2587-9618-2022-18-1-40-50. Available from: https://ijccse.iasv.ru/index.php/ijccse/article/download/474/283/837.
10. **Aniskin, N.A.; Stupivtsev, A.V.** Influence of the factors on the filtration regime of the earth dam during the upper bank failure // Vestnik of MSCU. 2023. T. 18. Issue. 6. P. 917-926. DOI: 10.22227/1997-0935.2023.6.917-926.
11. **Aniskin N., Stupivtsev A.** Change in filtration gradients during head water drawdown //E3S Web of Conferences. – EDP Sciences, 2023. – T. 457. – P. 02046.
12. Development of research on filtration theory in the USSR // Institute of Hydrodynamics, SB AS USSR, VNIIG named after B.E.Vedeneev. B.E.Vedeneev. VNII of Natural Gases. M. "Nauka.".
13. **Anakhaev, K.N.** About filtration calculation of a cofferdam // Mathematical modeling. 2011. T. 23. № 2. P.148-158.
14. **Bukhartsev V.N., Petrichenko M.R.** Nonsteady filtration in a uniform soil mass. Power Technology and Engineering. 2012; Vol. 46, No. 3. 1-3
15. **Petrichenko M.R., Zaborova D.D., Kotov E.V., Musorina T.A.** Weak solutions of the limit problems of Crocco // Scientific and Technical Bulletins of St. Petersburg State Polytechnic University. Physico-mathematical sciences. 2018. T. 11(3). P.27-38. DOI: 10.18721/JPM.11303.
16. **Lee K.K., Darrell I.** Leap Simulation of a free- surface and seepage face using boundary-fitted coordinate system method. Journal of Hydrology. 1997; Vol.196 (1). pp.297–309. DOI: 10.1016/S0022-1694(96)03246-5.
17. **Billstein, M.** Development of a Numerical Model of Flow through Embankment Dams. Department of Environmental Engineering, Lulea University of Technology. 1998; Lulea, Sweden. P.59.
18. **Hsiao C.C., Chen J.T., Chen K.H.** Application of hypersingular equations to free-surface seepage problems. Computational Methods. 2006; Springer. pp. 73-77.
19. **Aniskin N.A., Antonov A.S**. Development geo-seepage models for solving seepage problems of large dam's foundations, on an example of ANSYS Mechanical APDL. Advanced Materials Research. 2015; Vols. 1079-1080. pp. 198-201. DOI:

10.4028/www.scientific.net/AMR.1079-1080.198.
20. **Burdine, N.T.** Relative permeability calculations from pore size distribution data. Petr. Trans. AIME. 1953; 198, Pp. 71–78. DOI: 10.2118/225-G.
21. **Mualem, Y.** A new model for predicting the hydraulic conductivity of unsaturated porous media. Water Resour. Res. 1976; 12(3), Pp. 513–522. DOI: 10.1029/WR012i003p00513.
22. **Van Genuchten, M.T.** A closed-form equation for predicting the hydraulic conductivity of unsaturated soils. Soil Sci. Soc. Am. J. 1980; 44(5), Pp. 892–898. DOI: 10.2136/sssaj1980.03615995004400050002x.
23. **Kosugi K.** General model for unsaturated hydraulic conductivity for soil with lognormal pore-size distribution. Soil Sci. Soc. Am. J. 1999; 63:Pp. 270-277. DOI: 10.2136/sssaj1999.03615995006300020003x.
24. **Terleev V.V., Mirschel W., Schindler U., Wenkel K.-O.** Estimation of soil water retention curve using some agrophysical characteristics and Voronin's empirical dependence. International Agrophysics. 2010; 24(4):381-387.
25. **Shein E.V.** Course of soil physics // M.: Izd-vo Moscow. unct. 2005. C. 432.
26. **Terleyev V.V.V., Narbut M.A., Topazh A.G., Mirschel V.** Modeling of hydrophysical properties of soil as a capillary-porous body and improvement of the Mualem - Van Genuchten method: theory. // Agrophysics. 2014. №2(14), c. 35 -44.

СПИСОК ЛИТЕРАТУРЫ

1. **Беллендир Е.Н., Ивашинцов Д.А., Стефанишин Д.В. и др**. Вероятностные методы оценки надежности грунтовых гидротехнических сооружений // СПб.: ОАО ВНИИГ им. Б.Е. Веденеева. 2003-2004. Т. 1.
2. **Adamo, Nasrat & Al-Ansari, Nadhir & Sissakian, Varoujan & Laue, Jan & Knutsson, Sven**. Dam Safety Problems Related to Seepage. 2020; 10. 191-239
3. **López-Acosta N.P., Sánchez M.A. Soil Solution, G. Auvinet J.-M. Pereira**. Assessment of exit hydraulic gradients at the toe of levees in water drawdown conditions. Scour and Erosion – Cheng, Draper & An (Eds)©. 2015; Taylor & Francis Group, London. Available from: https://www.researchgate.net/publication/283129540. DOI: 10.1201/b17703-21.
4. **Fattah M.Y., Hasan A. Omran, Mohammed A. Hassan.** Behavior of an Earth Dam during Rapid Drawdown of Water in Reservoir-Case Study. International Journal of Advanced Research. 2015; Vol. 3, Issue 10, 110 -122.
5. **Upomo T.C., Effendi M.K., Kusumawardani R.** Behaviour of levee on softsoil caused by rapid drawdown. AIP Conference Proceedings. American Institute of Physics Inc. 2018; 1941.DOI: 10.1063/1.5028103.
6. **Stark T.D., Jafari N.H., Zhindon J.S.L., & Baghdady A.** Unsaturated and Transient Seepage Analysis of San Luis Dam. Journal of Geotechnical and Geoenvironmental Engineering. 2017; 143(2), 04016093. DOI: 10.1061/(ASCE)GT.1943-5606.0001602.
7. **Vandenberge D.R.** Total Stress Rapid Drawdown Analysis of the Pilarcitos Dam Failure using the Finite Element Method. Frontiers of Structural and Civil Engineering. 2014; 8(2), 115–123. DOI: 10.1007/s11709-014-0249-7.
8. **Perzlmaier S.** Hydraulic criteria for internal erosion in cohesionless soil. In Internal erosion of dams and their Foundations. Editors R. Fell and J.J. Fry. Taylor & Francis. 2007; 179-190. DOI: 10.1201/9781482266146-20.
9. **Aniskin N.A., Sergeev S.A.** The effect of draw-off on filtration regime of earth-fill dam. International Journal for Computational Civil and Structural

Engineering. 2022. 18(1) 40-50. DOI:10.22337/2587-9618-2022-18-1-40-50. Available from: https://ijccse.iasv.ru/index.php/ijccse/article/download/474/283/837.

10. **Анискин Н.А., Ступивцев А.В.** Влияние факторов на фильтрационный режим земляной плотины при сработке верхнего бьефа // Вестник МГСУ. 2023. Т. 18. Вып. 6. С. 917–926. DOI: 10.22227/1997-0935.2023.6.917-926.
11. **Aniskin N., Stupivtsev A.** Change in filtration gradients during head water drawdown //E3S Web of Conferences. – EDP Sciences, 2023. – Т. 457. – С. 02046.
12. Развитие исследований по теории фильтрации в СССР // Институт гидродинамики СО АН СССР, ВНИИГ им. Б.Е.Веденеева. ВНИИ Природных газов. М. “Наука.”.
13. **Анахаев К.Н.** О фильтрационном расчете перемычки // Математическое моделирование. 2011. Т. 23. № 2. С.148–158.
14. **Bukhartsev V.N., Petrichenko M.R**. Nonsteady filtration in a uniform soil mass. Power Technology and Engineering. 2012; Vol. 46, No. 3. 1-3
15. **Петриченко М.Р., Заборова Д.Д., Котов Е.В., Мусорина Т.А.** Слабые решения предельных задач Крокко // Научно-технические ведомости Санкт-Петербургского государственного политехнического университета. Физико-математические науки. 2018. Т. 11(3). С.27-38. DOI: 10.18721/JPM.11303.
16. **Lee K.K., Darrell I.** Leap Simulation of a free- surface and seepage face using boundary-fitted coordinate system method. Journal of Hydrology. 1997; Vol.196 (1). pp.297–309. DOI: 10.1016/S0022-1694(96)03246-5.
17. **Billstein, M.** Development of a Numerical Model of Flow through Embankment Dams. Department of Environmental Engineering, Lulea University of Technology. 1998; Lulea, Sweden. P.59.
18. **Hsiao C.C., Chen J.T., Chen K.H.** Application of hypersingular equations to free-surface seepage problems. Computational Methods. 2006; Springer. pp. 73-77.
19. **Aniskin N.A., Antonov A.S.** Development geo-seepage models for solving seepage problems of large dam’s foundations, on an example of ANSYS Mechanical APDL. Advanced Materials Research. 2015; Vols. 1079-1080. pp. 198-201. DOI: 10.4028/www.scientific.net/AMR.1079-1080.198.
20. **Burdine, N.T.** Relative permeability calculations from pore size distribution data. Petr. Trans. AIME. 1953; 198, Pp. 71–78. DOI: 10.2118/225-G.
21. **Mualem, Y.** A new model for predicting the hydraulic conductivity of unsaturated porous media. Water Resour. Res. 1976; 12(3), Pp. 513–522. DOI: 10.1029/WR012i003p00513.
22. **Van Genuchten, M.T.** A closed-form equation for predicting the hydraulic conductivity of unsaturated soils. Soil Sci. Soc. Am. J. 1980; 44(5), Pp. 892–898. DOI: 10.2136/sssaj1980.03615995004400050002x.
23. **Kosugi K.** General model for unsaturated hydraulic conductivity for soil with lognormal pore-size distribution. Soil Sci. Soc. Am. J. 1999; 63:Pp. 270-277. DOI: 10.2136/sssaj1999.03615995006300020003x.
24. **Terleev V.V., Mirschel W., Schindler U., Wenkel K.-O.** Estimation of soil water retention curve using some agrophysical characteristics and Voronin’s empirical dependence. International Agrophysics. 2010; 24(4):381-387.
25. **Шеин Е.В**. Курс физики почв // М.: Изд-во Моск. ун-та. 2005. С. 432.
26. **Терлеев В.В., Нарбут М.А., Топаж А.Г., Миршель В**. Моделирование гидрофизических свойств почвы как каппилярно-пористого тела и усовершенствование метода Муалема - Ван Генухтена: теория. // Агрофизика. 2014. №2(14), с. 35 -44.

Aniskin Nikolay Alexeyevich, Professor, DSc, Acting Director of the Institute of Hydrotechnical and Power Engineering (IGES) of the National Research Moscow State University of Civil Engineering (NRU MGSU), 129337, Russia, Moscow, Yaroslavskoe shosse, 26, phone +7 (495) -287-49-14 ext. 14-19, e-mail: Aniskin@mgsu.ru

Stupivtsev Andrey Vladimirovich, postgraduate student of the Institute of Hydrotechnical and Power Engineering (IGES) of the National Research Moscow State University of Civil Engineering (NRU MGSU), 129337, Russia, Moscow, Yaroslavskoe shosse, 26, phone +7 (495) -287-49-14 ext. 14-19, e-mail: StupivtsevAV@gmail.com

Анискин Николай Алексеевич, профессор, доктор технических наук, исполняющий обязанности директора Института гидротехнического и энергетического строительства (ИГЭС) Национального исследовательского Московского государственного строительного университета (НИУ МГСУ), 129337, г. Москва, Ярославское ш., д. 26, тел. +7 (495)-287-49-14 доб.14-19. e-mail: Aniskin@mgsu.ru

Ступивцев Андрей Владимирович, аспирант кафедры «Гидравлики и гидротехнического строительства» Национального исследовательского Московского государственного строительного университета (НИУ МГСУ) 129337, г. Москва, Ярославское ш., д. 26, тел. +7 (495)-287-49-14 доб. 14-19. e-mail: StupivtsevAV@gmail.com

DOI:10.22337/2587-9618-2024-20-2-25-33

MATHEMATICAL MODELING OF RELAXATION PROCESS IN CONCRETE

Sergey B. Krylov [1], Petr D. Arleninov [1,2]

[1] JSC Research Center of Construction NIIZHB named after A.A. Gvozdev, Moscow, RUSSIA
[2] National Research Moscow State University of Civil Engineering, Moscow, RUSSIA

Abstract: The study provides experimental and theoretical investigations of stress relaxation in concrete under preset constant deformation of specimens and proposes an approach to the mathematical determination of stress relaxation in concrete. In addition to mathematical modeling, parallel long-term tests were performed on concrete specimens of the same class under four different regimes: determination of concrete creep in compression (concrete prism specimens in spring installations) according to GOST 24544; determination of concrete relaxation in compression (concrete prism specimens in special installations, determination of concrete creep in bending (concrete specimens-beams in rack-type installations working in bending and loaded with gravity load) according to GOST 24544; determination of concrete relaxation in bending (concrete specimen beams, with applied initial deformation in the middle of the span
Determination of stress drop was performed using electronic dynamometers built between the specimen and the point of load application. A new concept, "relaxation measure Rm", was proposed. This value is similar in meaning to the creep measure and characterizes the degree of stress reduction in time due to relaxation when loaded with a unit relative strain.
The introduction of relaxation measure allows to simplify the relaxation equation and significantly simplifies its solution. According to the results of calculation by the proposed computational algorithms for determining the relaxation measure in comparison with the experimental data, a satisfactory convergence of the results is obtained Qualitative conclusions about the applicability of the methodology of SP 63.13330 for reducing the modulus of elasticity of concrete in creep and relaxation.

Keywords: concrete, reinforced concrete, creep of concrete, relaxation of concrete

МАТЕМАТИЧЕСКОЕ МОДЕЛИРОВАНИЕ ПРОЦЕССА РЕЛАКСАЦИИ В БЕТОНЕ

С.Б. Крылов[1], П.Д. Арленинов[1,2]

[1] Научно-исследовательский, проектно-конструкторский и технологический институт бетона и железобетона (НИИЖБ) им. А.А. Гвоздева АО «НИЦ «Строительство», г. Москва, РОССИЯ
[2] ФГБОУ ВО «Национальный исследовательский Московский государственный строительный университет» Минобрнауки России (НИУ МГСУ), г. Москва, РОССИЯ

Аннотация: Рассматривается подход по математическому определению падения напряжения в бетонных образцах при заданной постоянной деформации образца – релаксации напряжений в бетоне. Работа, в рамках которой были проведены данные исследования, является экспериментально-теоретической. В дополнение к математическому моделированию были проведены параллельные длительные испытания на образцах из бетона одного класса в четырех различных режимах: определение ползучести бетона при сжатии (бетонные образцы-призмы в пружинных установках) по ГОСТ 24544; определение релаксации бетона при сжатии (бетонные образцы призмы в специальных установках), определение ползучести бетона при изгибе (бетонные образцы- балки в установках стеллажного типа, работающие на изгиб и загруженные гравитационной нагрузкой) по ГОСТ 24544; определение релаксации бетона при изгибе (бетонные образцы-балки, с приложенной начальной деформации в середине пролета
Определение падения напряжений выполнялось с помощью электронных динамометров, встроенных между образцом и точкой приложения нагрузки. Предложено новое понятие – «мера релаксации Rm». Эта величина по смыслу подобна мере ползучести и характеризует степень снижения напряжений во времени из-за релаксации при загружении единичной относительной деформацией. Введение меры релаксации позволяет упростить уравнение релаксации и существенно упрощает его решение. По результатам расчета по предложенным вычислительным алгоритмам, для определения меры релаксации

при сравнении с опытными данными, получена удовлетворительная сходимость результатов Сделаны качественные выводы о применимости методики СП 63.13330 по снижению модуля упругости бетона при ползучести и при релаксации.

Ключевые слова: бетон, железобетон, ползучесть бетона, релаксация напряжений в бетоне

INTRODUCTION

Usually, during the construction of unique buildings and structures using new high-strength concretes, experimental studies of creep and shrinkage characteristics of concrete are carried out. This direction is quite well studied [1-12]. At the same time, creep of concrete is just one of the deformation properties of a concrete specimen when working under the action of a long-term load. Another important property is stress relaxation.

The use of normative deformation characteristics of concretes even of the same strength class in compression in critical structures is not quite correct Modern concretes having the same strength class may differ greatly in composition, having different modifiers and additives. Therefore, creep, relaxation and elasticity characteristics for them may be slightly different. This can be easily seen by analyzing the tabulated values of the initial modulus of elasticity, tensile strength of concrete (standard and design) - these figures depend directly on the compressive strength class of concrete and are in fact their minimum values with the required security. Thus, for example, in works [13-14] shows a significant increase in modulus of elasticity, relative to that specified in SP 63.13330 due to the use of stronger coarse aggregate. Thus, for concrete B100, values of initial modulus of elasticity of more than 50GPa are achieved. In works [15-16] the true tensile behavior of concrete is investigated; the obtained values also differ from the tabulated values given in the norms.

The creep testing of concrete specimens itself, on the basis of which all subsequent processing is carried out, also has two serious disadvantages. The first is the need to constantly check that a constant compressive force is maintained in the test rig. And since this condition is violated, the compressive force must be adjusted at all times (this is especially true for spring systems, which are the most widely used for such tests). The second disadvantage is that the test setup is quite complex. As a result, only a few organizations in our country can perform such tests. Relaxation tests require simpler installations, in which specified deformations of specimens are maintained and forces in specimens are measured. Constant control and maintenance of such installations during testing is not required. This improves the accuracy of the results and makes the tests much simpler and more affordable.

In temperature and force redistribution problems, relaxation plays a more important role than creep. When performing such calculations, first the creep measure of concrete is determined, then the creep kernel is determined through the creep measure, and the relaxation kernel is determined through the creep kernel, then the predicted stresses in concrete at an arbitrary point in time are determined.

The introduction of the new test methodology will improve the accuracy of the results obtained, which in turn will make it possible to upgrade the accuracy of calculations, while at the same time with sufficient reliability will lead to a cheaper design. Simplification of the test method will allow the tests to be performed more widely. This in turn will enable objective data to be obtained on the properties of concrete over a wide range of compositions and strengths. In this regard, the topic under consideration is relevant and necessary for the development of modern construction industry.

Such studies have not been carried out either in our country or abroad. Therefore, the methodology of the proposed tests, their mathematical processing and results are new and essentially unique.

METHODS

The basic equations of modern creep theory have the form of three integral expressions (in addition to the equations of creep theory we can include expression (4) for the creep measure $C(t,\tau)$ through which the relaxation kernel function is already determined) and consist of the creep equation, the relaxation equation and the equation connecting the creep and relaxation kernels $L(t,\tau), R(t,\tau)$, they are based on a large number of experimental and theoretical works [17-22]. According to the first equation, the relative strains through elastic modulus, stresses and the function responsible for the creep strain buildup, the creep kernel, are determined. Using the second equation it is possible to determine the stresses, respectively through the relative strains, elastic modulus and the function responsible for the stress drop - the relaxation kernel. Using the third equation, it is possible to define separately, for example, the relaxation kernel through the creep kernel, the data for which are more readily available.

$$\varepsilon(t) = \frac{\sigma(t)}{E(t)} - \int_{t_0}^{t} \sigma(\tau)\, L(t,\tau)\partial\tau \qquad (1)$$

$$\sigma(t) = \varepsilon(t)E(t) + \int_{t_0}^{t} \varepsilon(\tau)\, R(t,\tau)\partial\tau \qquad (2)$$

$$L(t,\tau) - R(t,\tau) = \int_{t_0}^{t} R(,\tau)\, L(t,)\partial\tau \qquad (3)$$

$$C(t,\tau) = \mathrm{C}_{\infty}^{28} \cdot \Omega(t_0) \cdot F(t - t_0) \qquad (4)$$

In the above equations, the following notations are used:
t - test time, τ - loading time, C_{∞}^{28} is the limiting value of the creep measure $\Omega(\tau)$ is the ageing function, $F(t - t_0)$ is the function determining the shape of the creep curve.
Based on the above equations, let us introduce a new concept - relaxation measure (5) and give it the following definition "Relaxation measure is a function that determines the stress drop-in time when the specimen is loaded with a constant relative strain $\varepsilon = 1$. This equation is similar in structure to the creep measure. In this expression:
$\Omega(\tau)$ - the aging function is assumed to be the same as in the calculation of the creep measure, Rm_{∞}^{28} - defines the limiting value of the relaxation measure at the observation time $\Phi(t - t_0)$ - defines the shape of the relaxation function and is to be determined. The following notations are used in the equations:
t - test time, τ - loading time,
C_{∞}^{28} is the limiting value of the creep measure $\Omega(\tau)$ is the ageing function, $\Phi(t - t_0)$ is the function determining the shape of the creep curve.
Based on the above equations, let us introduce a new concept - relaxation measure (5) and give it the following definition "Relaxation measure is a function that determines the stress drop-in time when the specimen is loaded with a constant relative strain $\varepsilon = 1$. This equation is similar in structure to the creep measure. In this expression:
$\Omega(\tau)$ - the aging function is assumed to be the same as in the calculation of the creep measure, Rm_{∞}^{28} - defines the limiting value of the relaxation measure at observation time $\Phi(t - t_0)$ - defines the shape of the relaxation function and is to be determined.

$$Rm(t,\tau) = Rm_{\infty}^{28} \cdot 1\frac{1}{\Omega(t_0)} \cdot \Phi(t - t_0) \qquad (5)$$

In general, the functions $Rm_{\infty}^{28}$and $\Phi(t - t_0)$ should be determined from experimental data, just as the functionsC_{∞}^{28} and $F(t - t_0)$ were determined at one time. Since it is not possible to set up a large-scale experiment on concrete compositions with different strengths involving different laboratories, it is advisable to determine the above functions computationally from the creep equation (1) and the equation derived from it (8). This is due to the fact that detailed experimental data are available for the determination of all the quantities included in this equation. Therefore, it is reasonable to use

the same data to determine the relaxation parameters.

Next, let us derive an expression for the determination of the relaxation measure through the creep measure, for this purpose we write down the expressions for the total relative strain (6) at unit stresses and stresses at unit relative strain loading (7).

$$\lambda(t,\tau) = \frac{1}{E(t)} + Cm(t,\tau) \quad (6)$$

$$s(t,\tau) = E(t) - Rm(t,\tau) \quad (7)$$

Then the creep and relaxation equations will take the form (8), (9). According to the introduced definition, the relaxation measure is a function that determines the stress drop when the specimen is loaded with a constant relative strain $\varepsilon = 1$, then the creep equation will be written in the form 10.

$$\varepsilon(t,t_0) = \sigma(t_0)\cdot\lambda(t,t_0) + \int_{t_0}^{t}\frac{\partial}{\partial\tau}\sigma(\tau)\lambda(t,\tau)\partial\tau \quad (8)$$

$$\sigma(t,\tau) = \varepsilon(t_0)\cdot s(t,t_0) - \int_{t_0}^{t}\frac{\partial}{\partial\tau}\varepsilon(\tau)s(t,\tau)d\tau \quad (9)$$

$$s(t_0,t_0)\lambda(t,t_0) + \int_{t_0}^{t}\frac{\partial}{\partial\tau}s(t,\tau)\,\lambda(t,\tau)\partial\tau = 1 \quad (10)$$

Substituting (6) and (7) into (10), and considering that $\frac{\partial}{\partial\tau}E(t) = 0$ (partial derivative on a variable that is not included in the function), and the value of $Rm(t_0,t_0) = 0$ (relaxation does not have time to manifest itself at the initial time at loading), performing elementary transformations finally we obtain:

$$(E(t))\left(\frac{1}{E(t)} + Cm(t,t_0)\right) - \int_{t_0}^{t}\frac{\partial}{\partial\tau}Rm(t,\tau)\left(\frac{1}{E(t)} + Cm(t,\tau)\right)\partial\tau = 1 \quad (11)$$

In this expression, the calculation of $Rm(t,\tau)$ values are performed step by step at individual time points.

Within the framework of this study, a set of long-term tests was carried out. The research was carried out at the experimental site of JSC "VNIIG named after B.E. Vedeneev". The experimental part of the study is described in detail in [23].

Concrete specimens were made of two classes of compressive strength (B30 and B60), the tests were carried out from the age of 28 days. Compressive and flexural creep tests were carried out in accordance with GOST 24544. In parallel, tests were carried out to determine stress relaxation in concrete and creep in compression and bending for subsequent mathematical processing of the results.

Plants for determining the relaxation of concrete prisms in compression were prepared by dismantling spring creep test plants with the removal of springs in them to fix the required initial strains

Combined relaxation or flexural creep rigs were prepared by upgrading existing rack-type rigs for flexural creep testing. The upgraded plant allows flexural creep testing of beam specimens on the lower tier with constant gravity loading (using shot pails as loading devices) and concrete relaxation testing of beam specimens on the upper tier with constant strain loading.

Additionally, units were made to determine the relaxation in flexural mode by means of reverse loading. The essence of the method is that the specimen in the setup is in an inverted state to minimize creep strain, and the initial strain loading is from bottom to top.

Figure 1 below shows the compression and flexural relaxation test scheme, Figure 2 shows the test process.

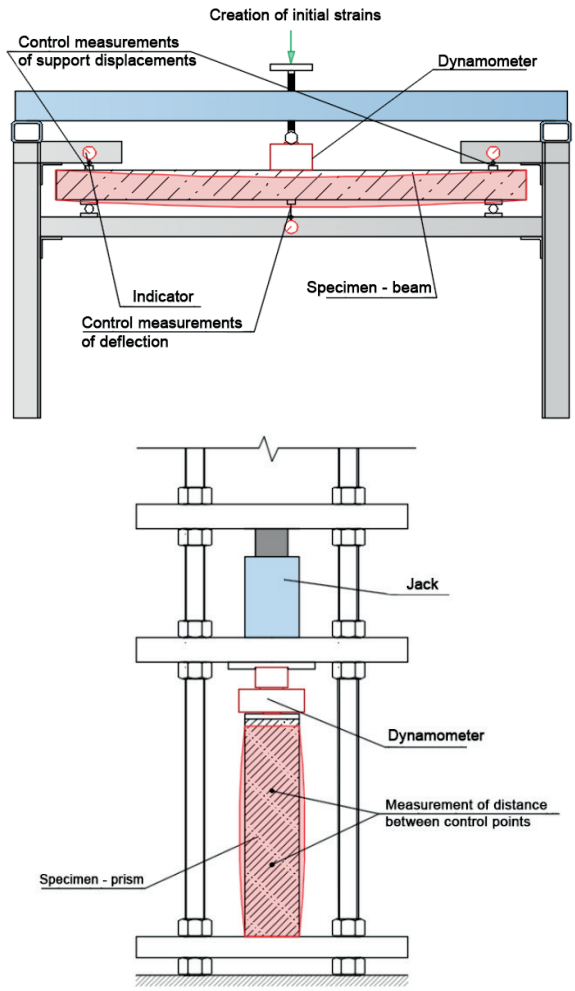


Figure 1. Schematic diagram of the relaxation test facilities

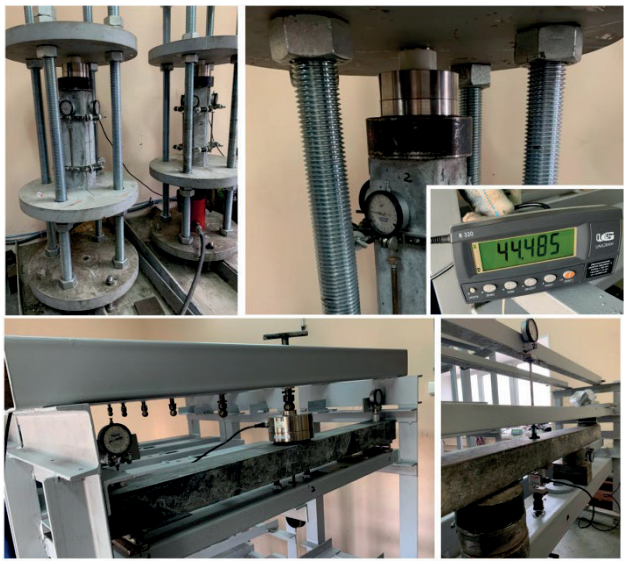


Figure 2. Compression (top) and bending (bottom) tests

RESULTS AND DISCUSSION

Using formula (11), the relaxation measure was determined by calculation. Figure 3 below shows graphically the exact and approximate plot (based on the proposed methodology) of stress drop over time when Rm is calculated based on the calculation for concrete of class B30. It can be seen that the limiting value of the relaxation measure can be expressed through the limiting value of the creep measure. The ratio of the limiting degree of increase in the initial relative strains (at infinitely long time compared to the moment of loading) to the degree of decrease in the limiting stresses (also at infinitely long time compared to the moment of loading) is 1.98, i.e. practically 2. Taking this into account leads to the relations:

$$Rm(\infty, 28) \cdot Cm(\infty, 28) = 2 \qquad (12)$$

$$Rm(\infty, 28) = \frac{2}{Cm(\infty, 28)} \qquad (13)$$

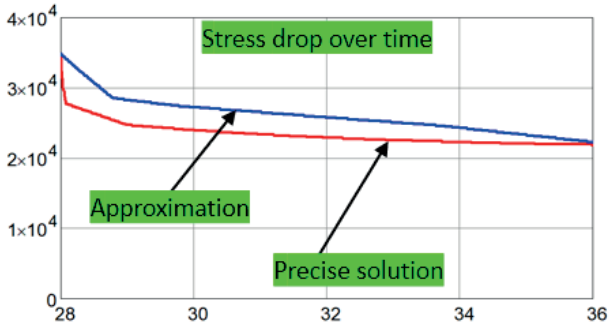


Figure 3. Calculated stresses (MPa) versus time (day) according to exact and approximate formula

Figure 4 shows a comparison of the calculation results using the proposed method with the simplified formula for the relaxation measure with the experimental curve. The graphs show that the error in the first day reaches 20%. After 7 days the error practically disappears. Taking into account that in technical and regulatory literature there are various expressions for the measure of creep, including those giving both very gentle and very steep graphs, calculations even at the initial stage after loading according to the above dependencies are acceptable.

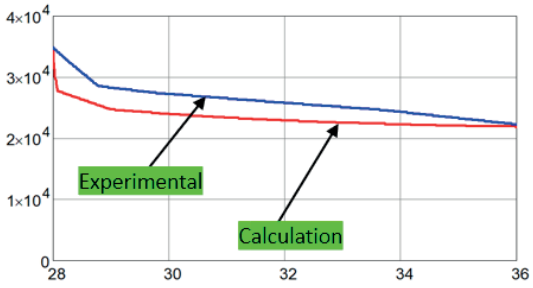


Figure 4. Comparison of stress relaxation curves (kN) over time (days)

CONCLUSION

1. According to calculations and experimental data, the rate of development of creep deformations is faster than the rate of stress drop during relaxation (approximately by a factor of 2). Therefore, strictly speaking, it is impossible to take both into account by reducing the modulus of elasticity of concrete according to the methodology of SP 63.13330 [21]. The reduction of modulus of elasticity at creep and at relaxation should be different.
2. To simplify the calculations of deflections of structures, it is proposed to introduce the concept of relaxation measure Rm(t,τ). This value is similar in meaning to the creep measure and characterises the degree of stress reduction in time due to relaxation when loaded with a unit relative strain.
3. Calculation of Rm(t,τ) values by the above equation (11) is performed step by step at separate time points. For calculations of stresses in real structures, it is necessary to convert the set of calculation results for the mentioned points into a function by selecting a suitable approximation.
4. Taking into account the relations between the limit values of the relaxation and creep measures, as well as the fact that the creep and relaxation phenomena are mutually related, it is proposed to use a function, also constructed on the basis of the creep measure, to approximate the relaxation measure at other points of time. This makes it possible to obtain an expression for the relaxation measure with acceptable accuracy without complicated calculations. Calculations show that good results can be obtained for the expression of the relaxation measure according to formula (5)

ACKNOWLEDGEMENT

The authors of the article thank their colleagues for their help in experimental work:

- Alexey Donov, Simas Bakanovichus, (Research Institute of Building Constructions (VNIIG) Named After B. E. Vedeneev – preparation of experimental models (installation of strain gauges)
- Polina Kalmakova Research Institute of Concrete and Reinforced Concrete (NIIZHB) named after A.A. Gvozdev JSC "Research center of Construction") – graphic design, text translation.

1. REFERENCES

1. **Yonghui Huang, Jiyang Fu, Ronghui Wang, Rui Rao, Niujing Ma** // Experimental study on creep behaviour of high-strength concrete filled steel tubular (HSCFST) columns. Case Studies in Construction Materials. Volume 20, July 2024, e02690.
2. **Cole Shurbert-Hetzel, Dana Daneshvar, Agathe Robisson, Behrouz Shafei** // Data-enabled comparison of six prediction models for concrete shrinkage and creep. Case Studies in Construction Materials. Volume 19, December 2023, e02406.
3. **Francisco Dias, Luis Fernando, Paullo Muñoz, Deane Roehl** // A numerical model for basic creep of concrete with aging and damage on beams. Applied Mathematical Modelling. Volume 121, September 2023, Pages 185-203.
4. **Bazant, Z.P.** // Stability of Elastic, Anelastic, and Disintegrating Structures, and Finite Strain Effects: an Overview. Comprehensive Structural Integrity, 2023, pp. V2-680-V2-710.
5. **Bazant Z. P., Yunping Xi** // Continuous retardation spectrum for solidification theory of concrete creep. Proceedings of

Engineering Mechanics - ASCE, 121(2), 1995, pp 281-288.
6. **Chiorino M.A., Carreira J.** Factors Affecting Creep and Shrinkage of Hardened Concrete and Guide for Modelling. The Indian Concrete Journal, 2012.
7. **Kolchunov, V.I., Kolchunov, V.I.** // Deformation Models of Reinforced Concrete under Special Effects. Industrial and Civil Engineering. - 2018. - № 8. - C. 54-60. - EDN UWOAEP.
8. **Travush V.I., Shakhramanyan Y.A., Kolotovichev A.M.** // "Lakhta Centre": automated monitoring of deformations of load-bearing structures and foundations. Academia. Architecture and Construction. - 2018. - № 4. - C. 94-108. DOI 10.22337/2077-9038-2018-4-94-108.
9. **Travush V.I., Arleninov P.D., Desyatkin M.A., Ivashchenko A.N., Kaprielov, S.S., Konin D.V., Krylov A.S., Krylov S.B., Chilin I.A. Sheinfeld A.V.** // Bearing capacity of steel-reinforced concrete walls with sheet reinforcement for static loads. International Journal for Computational Civil and Structural Engineering, (2023)19(4), 166-181.
10. **Chepurnenko A.S., Litvinov, S.V., Yazyev S.B.** // Determination of Rheological Parameters of Concrete by Nonlinear Optimisation Methods. International Journal for Computational Civil and Structural Engineering, (2023)19(4), 147-154.
11. **Rimshin V.I., Krishan A.L., Mukhametzyanov. A.I.** // Construction of deformation diagram of uniaxial compressed concrete. Vest. MSCU № 6 2015. - C. 23-31.
12. **Sanzharovsky R.S., Musabaev T.T.** Elastoplastic deformation of reinforced concrete shells and slabs with cracks // Izv. of Higher Education Institutions. Ser. Structural and Architectural Engineering. 1996.- №5. P.Z-11.
13. **Kaprielov S.S., Karpenko N.I., Sheinfeld A.V., Kuznetsov E.N.** // About regulation of elasticity and creep modulus of high-strength concrete with modifier MB-50S. Concrete and Reinforced Concrete. - 2003. - № 6. - C. 8-12.
14. **Kaprielov S.S., Karpenko N.I., Sheinfeld A.V., Kuznetsov E.N.** // Influence of organomineral modifier MB-50S on structure and deformability of cement stone and high-strength concrete. Concrete and Reinforced Concrete. - 2003. - № 3. - C. 2-7.
15. **Nesvetaev G.V., Kuzmenko T.G.** // About correlation of tensile strength limits of cement concrete in bending and compression. Engineering bulletin of Don. - 2023. - № 8(104). - C. 304-316.
16. **Bondarev B.A., Chernousov N.N., Chernousov R.N., Sturova V.A.** // Investigation of strength properties of steel-fibreslag concrete under axial tension and compression with account of its age. Construction Materials. - 2017. - № 5. - C. 20-25.
17. **Aleksandrovskiy S.V.** // Creep and Shrinkage of Concrete and Reinforced Concrete Structures - M.: Stroyizdat, 1976. - 349 c.
18. **Arutyunyan N.Kh.** // Creep of aging materials. Creep of concrete. Mechanics in the USSR for 50 Years, vol.Z. MTT. -M.: Nauka, 1972. C.155-202.
19. **Galustov K.Z.** // Nonlinear Theory of Concrete Creep and Calculation of Reinforced Concrete Structures - Moscow: Izd. fiz. mat. litt., 2006. - C. 94-110.
20. **Bondarenko V.M., Bondarenko S.V.** // Engineering methods of nonlinear theory of reinforced concrete. -M.: Stroyizdat, 1982. - C. 100-106.
21. Recommendations on taking into account creep and shrinkage of concrete in the

calculation of concrete and reinforced concrete structures. -M.: NIIZHB. 1988. - C. 5-15.
22. **Tamrazyan A.G., Yesayan. S.G.** // Mechanics of concrete creep - M.: MSCU, 2012. - 490 c.
23. **Arleninov, P.D.; Krylov, S.B.; Kalmakova, P.S.; Donov, A.V.** Experimental studies of concrete relaxation process in different modes. Vestnik SIC Stroitelstroy. 2023. № 1 (36). C. 86-98.

СПИСОК ЛИТЕРАТУРЫ

1. **Yonghui Huang, Jiyang Fu, Ronghui Wang, Rui Rao, Niujing Ma** // Experimental study on creep behavior of high-strength concrete filled steel tubular (HSCFST) columns. Case Studies in Construction Materials. Volume 20, July 2024, e02690.
2. **Cole Shurbert-Hetzel, Dana Daneshvar, Agathe Robisson, Behrouz Shafei** // Data-enabled comparison of six prediction models for concrete shrinkage and creep. Case Studies in Construction Materials. Volume 19, December 2023, e02406.
3. **Francisco Dias, Luis Fernando, Paullo Muñoz, Deane Roehl** // A numerical model for basic creep of concrete with aging and damage on beams. Applied Mathematical Modelling. Volume 121, September 2023, Pages 185-203
4. **Bazant, Z.P.** // Stability of Elastic, Anelastic, and Disintegrating Structures, and Finite Strain Effects: an Overview. Comprehensive Structural Integrity, 2023, pp. V2-680–V2-710.
5. **Bazant Z. P., Yunping Xi** // Continuous retardation spectrum for solidification theory of concrete creep. ournal of Engineering Mechanics — ASCE, 121(2), 1995, pp 281–288.
6. **Chiorino M.A., Carreira J.** Factors Affecting Creep and Shrinkage of Hardened Concrete and Guide for Modelling. The Indian Concrete Journal, 2012
7. **Колчунов, В.И., Колчунов, Вл.И.** // Деформационные модели железобетона при особых воздействиях. Промышленное и гражданское строительство. – 2018. – № 8. – С. 54-60. – EDN UWOAEP.
8. **Травуш В.И., Шахраманьян Ю.А., Колотовичев А.М.** // «Лахта центр»: автоматизированный мониторинг деформаций несущих конструкций и основания. Academia. Архитектура и строительство. – 2018. – № 4. – С. 94-108. DOI 10.22337/2077-9038-2018-4-94-108
9. **Травуш В.И., Арленинов П.Д., Десяткин М.А., Иващенко А.Н., Каприелов, С.С., Конин Д.В., Крылов А.С., Крылов С.Б., Чилин И.А. Шейнфельд А.В.** // Несущая способность сталежелезобетонных стен с листовым армированием на статические нагрузки. International Journal for Computational Civil and Structural Engineering, (2023)19(4), 166–181.
10. **Чепурненко А.С., Литвинов, С.В., Язьев С.Б.** // Определение реологических параметров бетона при помощи методов нелинейной оптимизации. International Journal for Computational Civil and Structural Engineering, (2023)19(4), 147–154.
11. **Римшин В.И., Кришан А.Л., Мухаметзянов. А.И**. // Построение диаграммы деформирования одноосного сжатого бетона. Вест. МГСУ №6 2015. - С. 23-31.
12. **Санжаровский Р.С., Мусабаев Т.Т.** Упругопластическое деформирование железобетонных оболочек и плит с трещинами // Изв. вузов. Сер. Стр-во и архит-ра. 1996.- №5. С.3-11.
13. **Каприелов С.С., Карпенко Н.И., Шейнфельд А.В., Кузнецов Е.Н.** // О

регулировании модуля упругости и ползучести высокопрочных бетонов с модификатором МБ-50С. Бетон и железобетон. – 2003. – № 6. – С. 8-12.
14. **Каприелов С.С., Карпенко Н.И., Шейнфельд А.В., Кузнецов Е.Н.** // Влияние органоминерального модификатора МБ-50С на структуру и деформативность цементного камня и высокопрочного бетона. Бетон и железобетон. – 2003. – № 3. – С. 2-7.
15. **Несветаев Г.В., Кузьменко Т.Г.** // О соотношении пределов прочности цементных бетонов на растяжение при изгибе и сжатие. Инженерный вестник Дона. – 2023. – № 8(104). – С. 304-316.
16. **Бондарев Б.А., Черноусов Н.Н., Черноусов Р.Н., Стурова В.А.** // Исследование прочностных свойств сталефиброшлакобетона при осевом растяжении и сжатии с учетом его возраста. Строительные материалы. – 2017. – № 5. – С. 20-25.
17. **Александровский С.В.** // Ползучесть и усадка бетона и железобетонных конструкций -М.: Стройиздат, 1976. - 349 с.
18. **Арутюнян Н.Х.** // Ползучесть стареющих материалов. Ползучесть бетона. Механика в СССР за 50 лет, т.3. МТТ. -М.: Наука, 1972. С.155-202.
19. **Галустов К.З**. // Нелинейная теория ползучести бетона и расчет железобетонных конструкций - М.: Изд. физ. мат. лит., 2006. - С. 94-110.
20. **Бондаренко В.М., Бондаренко С.В.** // Инженерные методы нелинейной теории железобетона. -М.: Стройиздат, 1982. - С. 100-106.
21. Рекомендации по учету ползучести и усадки бетона при расчете бетонных и железобетонных конструкции. -М.: НИИЖБ. 1988. - С. 5-15.
22. **Тамразян А.Г., Есаян. С.Г**. // Механика ползучести бетона – М.: МГСУ, 2012. - 490 с.
23. **Арленинов П.Д., Крылов С.Б., Калмакова П.С., Донов А.В.** Экспериментальные исследования процесса релаксации бетона в разных режимах. Вестник НИЦ Строительство. 2023. № 1 (36). С. 86-98.

Krylov S.B, Doctor of Engineering Sciences. JSC Research Center of Construction NIIZHB named after A.A. Gvozdev, Head of Laboratory of Reinforced Concrete Mechanics, 109428, 6, building 5., 2nd Institutskaya str., Moscow, Russia, e-mail: Krylov_s_b@mail.ru, telephone +7-499-174-74-07

Крылов Сергей Борисович, доктор технических наук, заведующий лабораторией Механики железобетона, Научно-исследовательский, проектно-конструкторский и технологический институт бетона и железобетона (НИИЖБ) им. А. А. Гвоздева АО «НИЦ «Строительство», 109428, Москва, 2-я Институтская ул., д.6, корп. 5, тел.: +7-499-174-74-07, e-mail: Krylov_s_b@mail.ru

Arleninov P.D., Department of Reinforced Concrete and Masonry Structures, National Research Moscow State University of Civil Engineering, 129337, Yaroslavskoye shosse, 26, Moscow, Russia; JSC Research Center of Construction NIIZHB named after A.A. Gvozdev, laboratory of reinforced concrete mechanics, 109428, 6, building 5., 2nd Institutskaya str., Moscow, Russia, e-mail: arleninoff@gmail.com, telephone +7-499-174-74-07

Арленинов Петр Дмитриевич, кандидат технических наук, ФГБ0У ВО «Национальный исследовательский Московский государственный строительный университет» Минобрнауки России (НИУ МГСУ), 129337, Москва, Ярославское шоссе, д. 26; заместитель заведующего лаборатории Механики железобетона, Научно-исследовательский, проектно-конструкторский и технологический институт бетона и железобетона (НИИЖБ) им. А.А. Гвоздева АО «НИЦ «Строительство», 109428, Москва, 2-я Институтская ул., д.6, корп. 5. тел.: +7-499-174-74-07, e-mail: arleninoff@gmail.com

International Journal for Computational Civil and Structural Engineering, 20(2) 34–45 (2024)

DOI:10.22337/2587-9618-2024-20-2-34-45

ELASTOPLASTIC DEFORMATION OF STEEL CONCRETE BEAMS WITH LOCAL BUCKLING UNDER THREE-POINT BENDING

Khazov Pavel Alekseevich [1], Erofeev Vladimir Ivanovich [2], Vediaikina Olga Ivanovna [1], Pomazov Artyom Pavlovich [1], Kozhanov Dmitrij Aleksandrvich [1]

[1] Nizhny Novgorod State University of Architecture and Civil Engineering, Nizhny Novgorod, RUSSIA
[2] Mechanical Engineering Research Institute of the RAS – Branch of Federal Research Center «A.V. Gaponov – Grekhov Institute of Applied Physics of the Russian Academy of Sciences», Nizhny Novgorod, RUSSIA

Abstract: In recent decades, there has been increased interest in studying the stress-strain state of concrete-filled steel tube constructions – composite elements consisting of a steel shell tube and a concrete core in a state of triaxial compression. In this combination, steel and concrete can achieve better strength and deformation characteristics than when they work separately, which makes it possible to design safe and economical structures. This article presents the results of an experimental study of the deformation process of bent concrete-filled steel tube elements of small circular sections. It is shown that with three-point transverse bending of a tubular concrete beam, in addition to deflection due to the curvature of the rod axis, deformations of local crumpling in places of application of concentrated loads have a significant effect on vertical displacement. The possibility of applying the classical theory of bending of a hollow steel beam according to the Bernoulli model is evaluated. The test results and deformation diagrams of hollow steel pipes (analytical and experimental data) and steel-reinforced concrete pipe beams filled with concrete are compared. A qualitative and quantitative assessment of the contribution of the presence of a concrete core to the bearing capacity and deformability (including local crumpling) of the element was carried out. The presence of a concrete core in a composite rod gives a significant weighting of the structure, however, in the case of off-center compression of the load-bearing vertical elements of multi-storey buildings, the effectiveness of using tubular concrete elements is very effective.

Keywords: pipe concrete, three-point bending, Bernoulli model, beam bending theory, elastoplastic deformation, triaxial compression of concrete, complex stress-strain state, efficiency of pipe concrete, load bearing capacity

УПРУГОПЛАСТИЧЕСКОЕ ДЕФОРМИРОВАНИЕ СТАЛЕБЕТОННЫХ БАЛОК С ЛОКАЛЬНЫМ СМЯТИЕМ ПРИ ТРЕХТОЧЕЧНОМ ИЗГИБЕ

Хазов Павел Алексеевич [1], Ерофеев Владимир Иванович [2], Ведяйкина Ольга Ивановна [1], Помазов Артём Павлович [1], Кожанов Дмитрий Александрович [1]

[1] Нижегородский государственный архитектурно-строительный университет, г. Нижний Новгород, РОССИЯ
[2] Институт проблем машиностроения РАН – филиал ФГБНУ «Федеральный исследовательский центр «Институт прикладной физики им. А.В. Гапонова – Грехова Российской академии наук», г. Нижний Новгород, РОССИЯ

Аннотация: В последние десятилетия наблюдается повышенный интерес к изучению напряженно-деформированного состояния трубобетонных конструкций – композитных элементов, состоящих из стальной трубы-оболочки и бетонного сердечника, находящегося в состоянии трехосного сжатия. В таком сочетании сталь и бетон позволяют достичь лучших прочностных и деформативных характеристик, чем при их раздельной работе, что позволяет проектировать безопасные и экономичные конструкции. В настоящей статье приводятся результаты экспериментального исследования процесса

деформирования изгибаемых трубобетонных элементов малогабаритных круглых сечений. Показано, что при трехточечном поперечном изгибе трубобетонной балки помимо прогиба за счет искривления оси стержня, существенное влияние на вертикальные перемещению оказывают деформации локального смятия в местах приложения сосредоточенных нагрузок. Проводится оценка возможности применения классической теории изгиба полой стальной балки по модели Бернулли. Сопоставляются результаты испытаний и диаграммы деформирования полых стальных труб (аналитические и экспериментальные данные) и сталежелезобетонных балок труб, заполненных бетоном. Произведена качественная и количественная оценка вклада наличия бетонного сердечника на несущую способность и деформативность (в т.ч. местное смятие) элемента. Наличие бетонного сердечника в композитном стержне дает существенное утяжеление конструкции, однако в случае внецентренного сжатия несущих вертикальных элементов многоэтажных зданий эффективность применения трубобетонных элементов весьма эффективно.

Ключевые слова: трубобетон, трехточечный изгиб, модель Бернулли, теория изгиба балок, упругопластическое деформирование, трехосное сжатие бетона, сложное напряженно-деформированное состояние, эффективность трубобетона, несущая способность

1. INTRODUCTION

In recent decades, steel-concrete rods have attracted increased interest from domestic [1-10] and foreign scientists [11-23], since they allow the most complete combination of the main advantages inherent in both metals and concrete, while leveling or completely eliminating their disadvantages [2, 3, 10]. Thus, steel structures are very strong, but, due to their good elastic properties, they practically don't damp mechanical energy. It makes their use in conditions of oscillations and vibrations difficult and requires the appliance of special vibration and seismic protection systems [11]. In turn, reinforced concrete elements with a commensurate load-bearing capacity are much more massive and have poor resistance to the accumulation of damage and the initiation and development of cracks. The use of steel-concrete elements formed by enclosing reinforced concrete or concrete in a steel cage also leads to a nonlinear increase in load-bearing capacity due to the transition of the core to a triaxial stress state [1, 4-10, 24-27].

At present, many experimental and numerical studies have been carried out to study the strength and stability of pipe concrete structures (PCS) under central and eccentric compression [1-3, 5-7, 9, 10]. However, the bending work of such rods remains poorly studied. The main reason for this is the irrationality of using PCS as a load-bearing bending element (pipe-concrete beam - hereinafter referred to as PCB) due to the small increase in load-bearing capacity with significant weight. At the same time, in real operating conditions [8], it is almost impossible to identify a purely compressed element, and to analyze compressed-bent elements, a detailed study of the work under pure and transverse bending of rods of various flexibility is necessary. Of particular interest is the bending of massive PCB, the characteristic cross-sectional size of which is about 10% of the length, since in such elements it is not always possible to apply the classical models of Bernoulli or Timoshenko beams. This is primarily due to the fact that the distribution of internal forces into elementary components (moment and shear force) becomes difficult, and the transition from forces to stresses is complicated by the "composite" nature and internal static indetermination of the steel-concrete section [1-3].

Under conditions of three-point bending, significant local stresses arise in the PCB, leading, in addition to general curvature, to local deformation at the force points (Fig. 1). Conducting experimental studies in this case is the most rational for assessing the general stress-strain state of a massive PCB during bending with local compression.

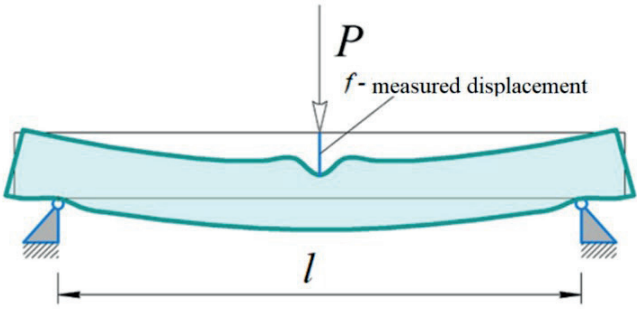


Figure 1. Deformation of the PCS under three-point bending

The research [31] considers the bending of PCB using Bernoulli beam theory, as a result of which the equivalent bending stiffness is determined. The main disadvantage of the study is the idealization and assumptions of work with a predominance of normal stresses (bending model of a Bernoulli beam), which is a very rough approximation due to the factors indicated above.

2. MATERIALS AND RESEARCH METHODS

To analyze the stress-strain state, experimental and numerical simulations were carried out under three-point bending. To conduct experiments, PCB samples with a length of 700 mm were made using steel pipes with a cross section of Ø76x3, Ø102x3.5 mm, steel grade 09G2S. To create the core, fine-grained concrete of class B12.5 was used. To confirm the grades and characteristics of the PCB components, compression tests were carried out on control samples [2, 3].

Fig. 2 shows the experimental setup. In the experiment, a span of 600 mm was assumed, i.e. the ratio of the span to the transverse size of the sample was l/D = 1/7.89; 1/5.88.

During testing, a smooth load was applied to sample 1 using a load crossbeam 2. Using indicator 4, the general approach of the traverses was recorded, that is, the curvature of the sample as a result of pure bending of the bend and local crushing.

To assess the contribution of the concrete core to the deformation of PCS, control samples of hollow pipes with a length of 700 mm and a cross section of Ø76x3, Ø102x3.5 mm (steel grade 09G2S) were additionally manufactured. The need for this part of the study is dictated by the fact that, based on the Bernoulli model, a hollow pipe has fairly good performance in transverse bending due to the high values of the moments of inertia of the undeformed section. However, studies on the performance of flexural thin-walled structures have shown that local deformation, cross-sectional bending and metal collapse are fundamental in structures of this type and significantly reduce the overall stiffness and load-bearing capacity [32]. Fig. 3 shows a basic view of the deformed state of a thin-walled beam and the difference between the Bernoulli model and the real structure.

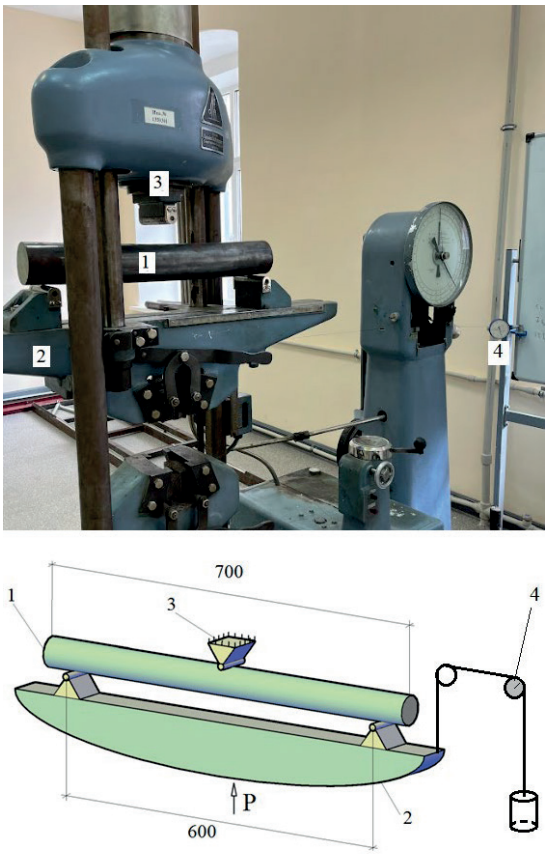


Figure 2. Experimental setup for testing PCS for three-point bending: 1 – sample under study, 2 – movable cargo cross-beam, 3 – static cross-beam, 4 – dial-type movement indicator

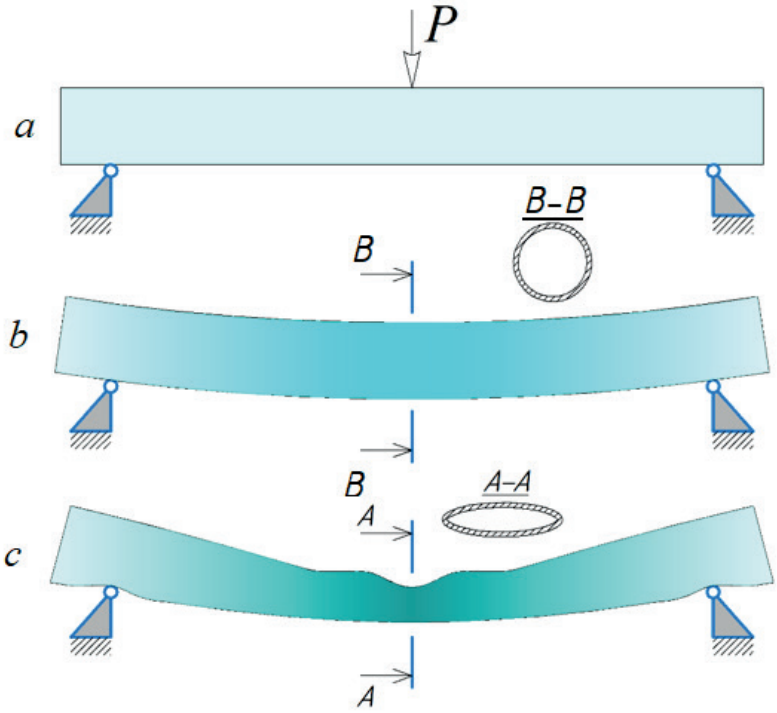


Figure 3. Calculation diagram of the bending element (a), diagram of deformations according to the Bernoulli model (b) and taking into account the curvature of sections and local crushing (c)

3. RESULTS OF THE EXPERIMENTAL RESEARCH

During the research, samples of PCB and hollow pipes were brought to destruction or complete loss of load-bearing capacity. In this case, the measured deformations were obviously not divided into "bending" and "bearing deformations", since in this study the interest is precisely the general stress-strain state of the sample with local collapse during three-point bending. Fig. 4 shows a typical type of PCB failure during three-point bending.

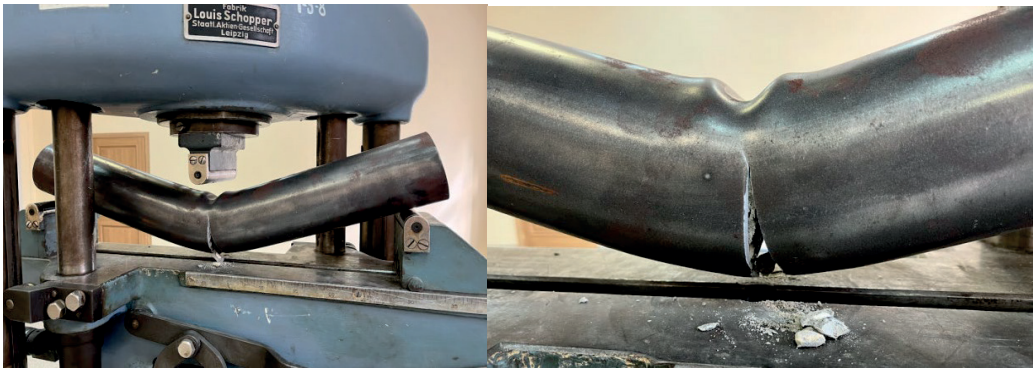


Figure 4. Destruction of PCB along the normal section

Fig. 5 shows diagrams of elastoplastic deformation of PCB samples, showing the dependence of the load on the sample and the approach of the traverses $P(f)$, (Fig. 1). The diagrams show that at the initial stage the work of the samples is close to elastic, and the transition to a nonlinear dependence occurs at the same displacements $f \approx 6$ mm.

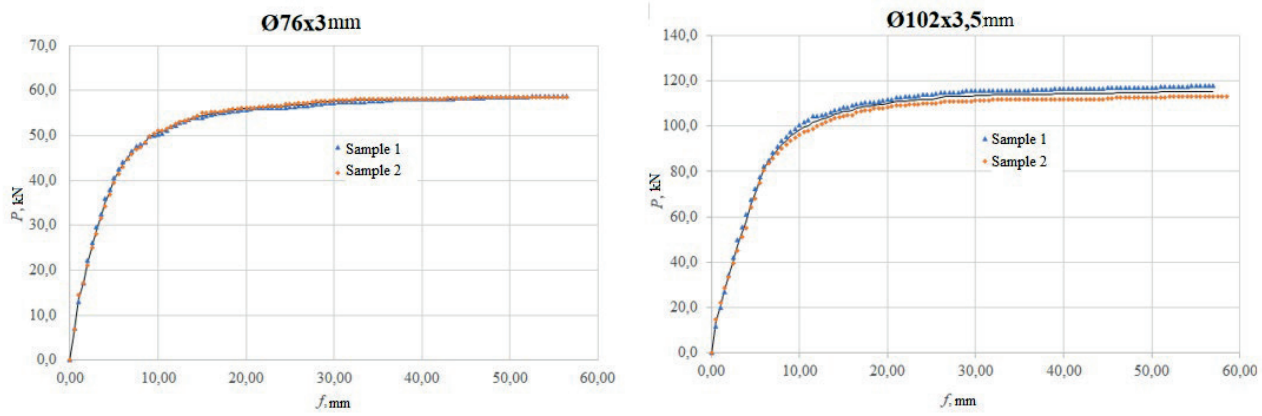


Figure 5. Deformation diagrams of PCB samples

As expected, despite the destruction along the normal section (Fig. 4), there are significant local deformations in the beam due to the collapse of the steel pipe. Nevertheless, the deformations did not lead to a global change in the shape and dimensions of the PCB cross sections. Moreover, in almost the entire linear section of the diagram (Fig. 5), bending deformations prevailed over crushing (Fig. 6).

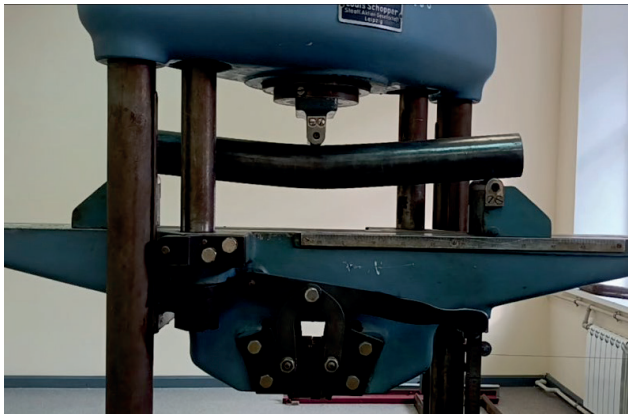


Figure 6. Appearance of the sample under linear deformation

In Fig. 7 compares the deformation of the PCB in a linear section with the deformation of an equivalent hollow pipe according to the Bernoulli beam model (Fig. 3b), according to which, in the absence of local deformations, the diagram is described by the dependence:

$$f = \frac{Pl^3}{48EJ}, \qquad (1)$$

where: f, P, l – measured displacement, load, beam span (Fig. 1); $E = 2{,}06 \cdot 10^5$ MPa – Young's modulus of pipe material; $J = \pi(D-d)^4/64$ – axial moment of inertia of the pipe section (D, d – outer and inner diameters), and the bearing capacity can be determined from the Navier condition:

$$\frac{M}{J} \cdot \frac{D}{2} \le R_c, \qquad (2)$$

where: $M = Pl/4$ – maximum bending moment in beam sections; R_c = 320 MPa – calculated resistance to the yield strength of steel grade 09G2S.

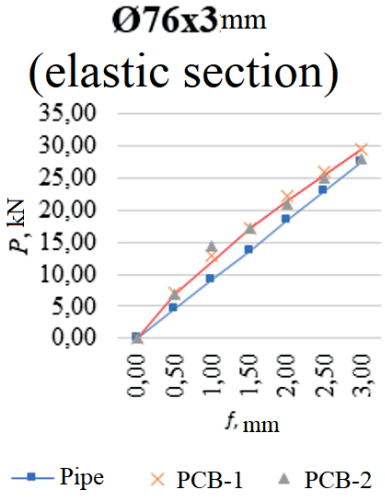


Figure 7. Diagrams of linear deformation of a hollow pipe (according to the Bernoulli model) and pipe-concrete samples

The diagrams show that, compared to the Bernoulli bending deformation model, the presence of a concrete core in the pipe leads to strengthening of the structure. It should be taken into account that the actual operation of a thin-walled pipe under three-point bending is noticeably different from the Bernoulli beam model. Fig. 8 shows experimental deformation diagrams and the appearance of hollow pipe samples after testing. Real data obtained experimentally (Fig. 8) indicate that the load-bearing capacity of a hollow pipe is significantly lower than the calculated values according to (2). Table 1 provides a comparative analysis of the load-bearing capacity of PCB and hollow pipes according to the Bernoulli model and according to experimental data (after the load-bearing capacity value, the percentage relative to the Bernoulli model is given). According to the data given in Table 1, it is clear that an increase in diameter critically affects the load-bearing capacity of a hollow sample, which is explained by an increase in the flexibility of its cross-section and a sharp increase in the influence of bearing deformations.

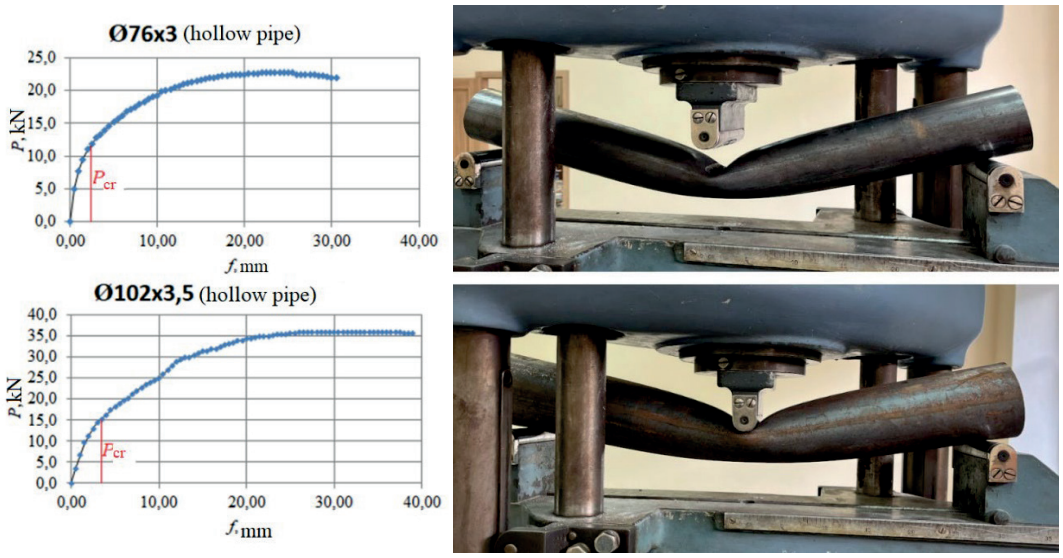


Figure 8. Deformation diagrams and view of hollow pipe samples after testing

Table 1. Comparison of the load-bearing capacity of hollow and pipe concrete beams

Sample size	Load-bearing capacity, kN		
	PCB (Fig.5)	Hollow pipe	
		Bernoulli model (formula 2)	Experiment (Fig. 8)
Ø76x3	44 (169%)	26 (100%)	12 (46%)
Ø102x3.5	87 (158%)	55 (100%)	15 (27 %)

Fig. 9 shows a comparison of the actual strain diagrams of a PCB and a hollow pipe under three-point bending. As can be seen from the diagrams, the presence of a core in a thin-walled bending pipe significantly improves its strength and deformation characteristics. It should also be noted that despite the plastic properties of concrete enclosed in a core, the deformation of PCB by its nature is more reminiscent of the behavior of metals (for example, with an obvious plastic zone in the graphs (Fig. 9). At the same time, a hollow pipe due to crushing and curvature cross sections immediately deform nonlinearly, which complicates the calculations when designing such structures.

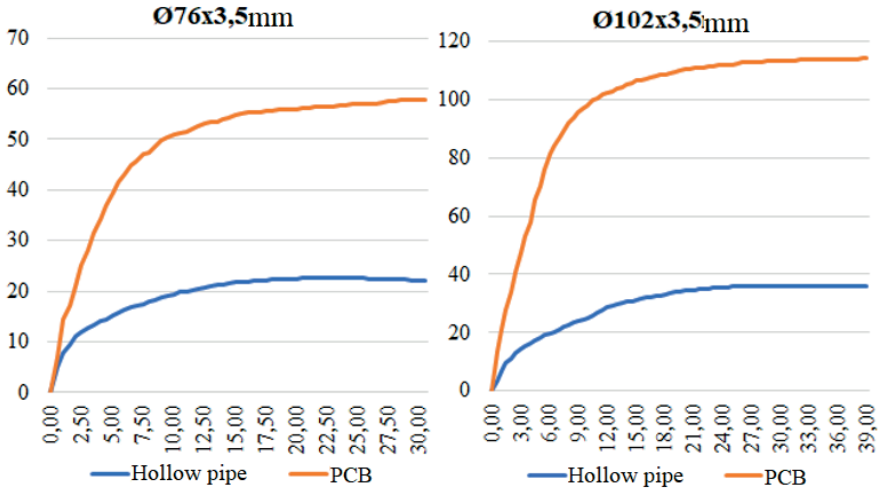


Figure 9. Experimental diagrams of deformation of PCB and hollow pip

4. CONCLUSIONS

Based on the results of the experimental research, it was established that the presence of a concrete core primarily ensures the resistance of the metal pipe to crushing and local deformation of the section. The contribution of the concrete core to the load-bearing capacity for the two diameters was about 60% compared to the Bernoulli model, and compared to the experimentally tested hollow pipe, the load-bearing capacity increased by about 3 times. Despite the significant weight, the use of bendable pipe-concrete structures may be advisable if, along with bending, compressive forces occur in the sections (for example, columns of multi-story buildings), since the concrete core significantly strengthens structures of this kind [1-3].

The use of classical models of beam bending in the case of thin-walled pipe structures is irrational and provides unnecessary margins, since it does not take into account local collapse and deformation of sections. The design of massive bendable PCB should be carried out taking into account local deformations.

REFERENCES

1. **Khazov, P.A**. Trekhosnoe napriazhennoe sostoianie betona pri prodol'nom deformirovanii trubobetonnykh obraztsov. [Triaxial stress state of concrete under longitudinal deformation of tube-concrete samples]. Problemy prochnosti i plastichnosti. 2023. T. 85. Vol. 2. S. 5-15.
2. **Khazov P.A., Erofeev V.I., Lobov D.M., Sitnikova A.K., Pomazov A.P.** Eksperimental'noe issledovanie prochnosti kompozitnykh trubobetonnykh obraztsov malogabaritnykh sechenii. [The experimental research of the strength of composite steel tube confined concrete samples of small-sized sections]. Privolzhskii nauchnyi zhurnal. 2022. Vol. 3 (63). S.36-43.
3. **Khazov P.A., Erofeev V.I., Lobov D.M., Pomazov A.P., Sitnikova A.K.** Eksperimental'noe issledovanie raschetnykh dlin i koeffitsientov prodol'nogo izgiba kompozitnykh trubobetonnykh obraztsov. [Experimental study of reduced lengths and longitudinal bending coefficients of composite concrete-filled steel tube samples]. Privolzhskii nauchnyi zhurnal. 2022. Vol. 4 (64). S. 16-24.
4. **Bragov A.M., Lomunov A.K., Konstantinov A.IU., Lamzin D.A., Balandin V.V.** Otsenka radial'noi deformatsii obraztsa na

osnove teoretiko-eksperimental'nogo analiza metodiki dinamicheskikh ispytanii materialov v zhestkoi oboime. [Estimation of radial strain of specimen on the basis of the theoretical and experimental analysis of a technique dynamic tests of materials in a rigid ferrule]. Problemy prochnosti i plastichnosti. 2016. T. 78. Vol. 4. S. 378-387.

5. **Krishan A.L., Rimshin V.I., Rakhmanov V.A. i dr.** Nesushchaia sposobnost' korotkikh trubobetonnykh kolonn kruglogo secheniia. [Bearing capacity of short concrete filled steel tube columns of circular cross-section]. Izvestiia vysshikh uchebnykh zavedenii. Tekhnologiia tekstil'noi promyshlennosti. 2017. Vol. 4 (370). S. 220-225.
6. **Krishan A.L., Gareev M.SH., Mukhametova F.I., Sitina IU.A**. Rezul'taty issledovaniia NDS szhatykh trubobetonnykh elementov s predvaritel'no obzhatym iadrom. [Results of a study of the stress-strain state of compressed pipe-concrete elements with a pre-compressed core]. Vestnik MGTU im. G.I. Nosova. 2005. Vol. 4. S. 74-77.
7. **Krishan A.L., Zaikin A.I., Kupfer M.S**. Opredelenie razrushaiushchei nagruzki szhatykh trubobetonnykh elementov. [determination of the breaking load of compressed tube-concrete elements]. Beton i zhelezobeton. 2008. Vol. 2. S. 22-25.
8. **Krishan A.L**. Trubobetonnye kolonny dlia mnogoetazhnykh zdanii. [The concrete-filled steel tube columns for high-rise buildings]. Stroitel'naia mekhanika inzhenernykh konstruktsii i sooruzhenii. 2009. Vol. 4. S. 75-80.
9. **Krishan A.L., Surovtsev M.M.** Eksperimental'nye issledovaniia prochnosti gibkikh trubobetonnykh kolonn. [Experimental reserches of strength of flexible concrete-filled tube (CFT) columns]. Vestnik Magnitogorskogo gosudarstvennogo tekhnicheskogo universiteta im. G.I. Nosova. 2013. Vol. 1(21). S. 90-92.
10. **Nesvetaev G.V., Rezvan I.V.** Otsenka prochnosti trubobetona. [Resistibility evaluation of the composite columns]. Fundamental'nye issledovaniia. 2011. no 12-3. S. 580-583.11.
11. **Lehman D.E., Kuder K.G., Gunnarrson A.K., Roeder C.W., Berman J.W.** Circular Concrete-Filled Tubes for Improved Sustainability and Seismic Resilience. Journal of Structural Engineering. 2015. No 141.
12. **Li P., Zhang T., Wang C.** Behavior of Concrete-Filled Steel Tube Columns Subjected to Axial Compression. Advances in Materials Science and Engineering. 2018. P. 1-15.
13. **Lu Y., Na Li, Li S., Liang H.** Behavior of steel fiber reinforced concrete-filled steel tube columns under axial compression. Construction and Building Materials. 2015. No 95. P. 74-85.
14. **Dai X.H., Lam D., Jamaluddin N.** Numerical analysis of slender elliptical concrete filled columns under axial compression. Thin-Walled Structures. 2014. No 77. Pp. 26–35.
15. **Lazovic Radovanovic M.M., Nikolic J.Z., Radovanovic J.R., Kostic S.M.** Structural Behaviour of Axially Loaded Concrete-Filled Steel Tube Columns during the Top-Down Construction Method. Applied Sciences. 2022. No 12(8).
16. **Manikandan K.B., Umarani C.** Understandings on the Performance of Concrete-Filled Steel Tube with Different Kinds of Concrete Infill. Advances in Civil Engineering. 2021. Vol. 2021. 12 p.

17. **Wang J., Sun Q., Li J.** Experimental study on seismic behavior of high-strength circular concrete-filled thin-walled steel tubular columns. Engineering Structures. 2019. Vol. 182. P. 403-415.
18. **Prasanta K., Arun C.B., Konjengbam D.S.** Experimental investigation of partially confined concrete-filled steel tubular square columns under lateral cyclic loading. Journal of Constructional Steel Research. 2023. Vol. 201.
19. **Zhang T., Gong Y.Z., Ding, F.X., Liu, X.M., Yu Z.W.** Experimental and numerical investigation on the behavior of concrete-filled rectangular steel tubes under bending. Structural Engineering and Mechanics, An Int'l Journal. 2021. Vol. 78. №. 3. P. 231-253.
20. **Terry P.J., Bradford M.A., Gilbert R.I.** Creep and shrinkage in concrete-filled steel tubes. Tubular structures VI. 2021. P. 293-298.
21. **Tran V.L., Thai D.K., Nguyen D.D.** Practical artificial neural network tool for predicting the axial compression capacity of circular concrete-filled steel tube columns with ultra-high-strength concrete. Thin-Walled Structures. 2020. Vol. 151.
22. **Lai M.H., Ho J.C.M.** A theoretical axial stress-strain model for circular concrete-filled-steel-tube columns. Engineering Structures. 2016. Vol. 125. P. 124-143.
23. **Wang Z.B., Tao Z., Han L.H., Uy B., Lam D., Kang, W.H**. Strength, stiffness and ductility of concrete-filled steel columns under axial compression. Engineering Structures. 2017. Vol. 135. P. 209-221.
24. **Karpenko N.I., Karpenko S.N.** Opredelenie prochnosti i orientatsii ploshchadok razrusheniia pri razlichnykh vidakh obemnogo napriazhennogo sostoianiia. [Determination of the strength and orientation of destruction concretes surfaces for different types of bulk stress state]. International Journal for Computational Civil and Structural Engineering. 2015. Vol. 11, Iss. 4. P. 52–61.
25. **Karpenko N.I., Korsun V.I., Karpenko S.N., Anushchenko A.M.** Kriterii prochnosti betona pri trekhosnom szhatii. [strength criterion of concrete under triaxial compression]. Privolzhskii nauchnyi zhurnal. 2022. Vol.4 (64). S. 8-16.
26. **Korsun, V., Kalmykov Yu., Niedoriezov A., Korsun A.** The Influence of the Initial Concrete Strength on its Deformation under Triaxial Compression. Procedia Engineering. 2015. № 117. P. 959–969.
27. **Markov I.P., Konstantinov A.IU.** Dinamicheskie ispytaniia obemnoszhimaemogo kompozitsionnogo materiala. [Dynamic testing of volumetric compressible composite material]. Problemy prochnosti i plastichnosti. 2018. T. 80. Vol. 3. S. 409-417.
28. **Geel van H.J.G.M.** Concrete behaviour in multiaxial compression: experimental research. Technische Universiteit Eindhoven. 1998. P. 178.
29. **He Z., Song Y.** Triaxial strength and failure criterion of plain high-strength and high-performance concrete before and after high temperatures. Cement and Concrete Research. 2010. № 40. P. 171–178.
30. **Sovjak R., Vogel F., Beckmann B.** Triaxial compressive strength of ultra high performance concrete. ActaPolytechnica. 2013. № 53 (6). P. 901–905.
31. **Khazov P.A., Vediaikina O.I., KHokhlova I.S., Artem'eva D.V.** Deformirovanie i razrushenie trubobetonnykh obraztsov pri poperechnom izgibe. [Deformation and destruction of concrete-filled steel tube sam-

ples during transverse bending]. Privolzhskii nauchnyi zhurnal. 2023. Vol. 2 (66). S.69-74.
32. Prochnost' tonkostennykh metallicheskikh konstruktsii [Strength of thin-walled metal structures]. / B.B. Lampsi. Moskva : Stroiizdat, 1987. 279 p.

СПИСОК ЛИТЕРАТУРЫ

1. **Хазов, П.А.** Трехосное напряженное состояние бетона при продольном деформировании трубобетонных образцов. Проблемы прочности и пластичности. – 2023. – Т. 85. – № 2. – С. 5-15.
2. **Хазов П.А., Ерофеев В.И., Лобов Д.М., Ситникова А.К., Помазов А.П.** Экспериментальное исследование прочности композитных трубобетонных образцов малогабаритных сечений. Приволжский научный журнал. – 2022. – № 3 (63). – С. 36-43.
3. **Хазов П.А., Ерофеев В.И., Лобов Д.М., Помазов А.П., Ситникова А.К.** Экспериментальное исследование расчетных длин и коэффициентов продольного изгиба композитных трубобетонных образцов. Приволжский научный журнал. – 2022. – №4 (64). – С. 16-24.
4. **Брагов А.М., Ломунов А.К., Константинов А.Ю., Ламзин Д.А., Баландин В.В.** Оценка радиальной деформации образца на основе теоретико-экспериментального анализа методики динамических испытаний материалов в жесткой обойме. Проблемы прочности и пластичности. – 2016. – Т. 78. – № 4. – С. 378-387.
5. **Кришан А.Л., Римшин В.И., Рахманов В.А. и др.** Несущая способность коротких трубобетонных колонн круглого сечения. Известия высших учебных заведений. Технология текстильной промышленности. – 2017. – № 4 (370). – С. 220-225.
6. **Кришан А.Л., Гареев М.Ш., Мухаметова Ф.И., Ситина Ю.А.** Результаты исследования НДС сжатых трубобетонных элементов с предварительно обжатым ядром. Вестник МГТУ им. Г.И. Носова. – 2005. – № 4. – С. 74-77.
7. **Кришан А.Л., Заикин А.И., Купфер М.С.** Определение разрушающей нагрузки сжатых трубобетонных элементов. Бетон и железобетон. – 2008. – №2. – С. 22-25.
8. **Кришан А.Л**. Трубобетонные колонны для многоэтажных зданий. Строительная механика инженерных конструкций и сооружений. – 2009. – №4. – С. 75-80.
9. **Кришан А.Л., Суровцев М.М.** Экспериментальные исследования прочности гибких трубобетонных колонн. Вестник Магнитогорского государственного технического университета им. Г.И. Носова. – 2013. – № 1(21). – С. 90-92.
10. **Несветаев Г.В., Резван И.В.** Оценка прочности трубобетона. Фундаментальные исследования. – 2011. – № 12-3. – С. 580-583.
11. **Lehman D.E., Kuder K.G., Gunnarrson A.K., Roeder C.W., Berman J.W.** Circular Concrete-Filled Tubes for Improved Sustainability and Seismic Resilience. Journal of Structural Engineering. 2015. No 141.
12. **Li P., Zhang T., Wang C.** Behavior of Concrete-Filled Steel Tube Columns Subjected to Axial Compression. Advances in Materials Science and Engineering. – 2018. – P. 1-15.
13. **Lu Y., Na Li, Li S., Liang H.** Behavior of steel fiber reinforced concrete-filled steel tube columns under axial compression.

Construction and Building Materials. – 2015. – No 95. – P. 74-85.

14. **Dai X.H., Lam D., Jamaluddin N.** Numerical analysis of slender elliptical concrete filled columns under axial compression. Thin-Walled Structures. – 2014. – No 77. – Pp. 26–35.
15. **Lazovic Radovanovic M.M., Nikolic J.Z., Radovanovic J.R., Kostic S.M.** Structural Behaviour of Axially Loaded Concrete-Filled Steel Tube Columns during the Top-Down Construction Method. Applied Sciences. – 2022. – No 12(8).
16. **Manikandan K.B., Umarani C.** Understandings on the Performance of Concrete-Filled Steel Tube with Different Kinds of Concrete Infill. Advances in Civil Engineering. – 2021. – Vol. 2021. – 12 p.
17. **Wang J., Sun Q., Li J.** Experimental study on seismic behavior of high-strength circular concrete-filled thin-walled steel tubular columns. Engineering Structures. – 2019. – Vol. 182. – P. 403-415.
18. **Prasanta K., Arun C.B., Konjengbam D.S.** Experimental investigation of partially confined concrete-filled steel tubular square columns under lateral cyclic loading. Journal of Constructional Steel Research. – 2023. – Vol. 201.
19. **Zhang T., Gong Y.Z., Ding, F.X., Liu, X.M., Yu Z.W.** Experimental and numerical investigation on the behavior of concrete-filled rectangular steel tubes under bending. Structural Engineering and Mechanics, An Int'l Journal. – 2021. – Vol. 78. – №. 3. – P. 231-253.
20. **Terry P.J., Bradford M.A., Gilbert R.I.** Creep and shrinkage in concrete-filled steel tubes. Tubular structures VI. – 2021. – P. 293-298.
21. **Tran V.L., Thai D.K., Nguyen D.D.** Practical artificial neural network tool for predicting the axial compression capacity of circular concrete-filled steel tube columns with ultra-high-strength concrete. Thin-Walled Structures. – 2020. – Vol. 151.
22. **Lai M.H., Ho J.C.M.** A theoretical axial stress-strain model for circular concrete-filled-steel-tube columns. Engineering Structures. – 2016. – Vol. 125. – P. 124-143.
23. **Wang Z.B., Tao Z., Han L.H., Uy B., Lam D., Kang, W.H**. Strength, stiffness and ductility of concrete-filled steel columns under axial compression. Engineering Structures. – 2017. – Vol. 135. – P. 209-221.
24. **Карпенко Н.И., Карпенко С.Н.** Определение прочности и ориентации площадок разрушения при различных видах объемного напряженного состояния. International Journal for Computational Civil and Structural Engineering. – 2015. – Vol. 11. – Iss. 4. – P. 52–61.
25. **Карпенко Н.И., Корсун В.И., Карпенко С.Н., Анущенко А.М**. Критерий прочности бетона при трехосном сжатии. Приволжский научный журнал. – 2022. – №4 (64). – С. 8-16.
26. **Korsun, V., Kalmykov Yu., Niedoriezov A., Korsun A.** The Influence of the Initial Concrete Strength on its Deformation under Triaxial Compression. Procedia Engineering. – 2015. – № 117. – P. 959–969.
27. **Марков И.П., Константинов А.Ю**. Динамические испытания объемно-сжимаемого композиционного материала. Проблемы прочности и пластичности. – 2018. – Т. 80. – № 3. – С. 409-417.
28. **Geel van H.J.G.M.** Concrete behaviour in multiaxial compression: experimental re-

search. Technische Universiteit Eindhoven. 1998. P. 178.
29. **He Z., Song Y.** Triaxial strength and failure criterion of plain high-strength and high-performance concrete before and after high temperatures. Cement and Concrete Research. – 2010. – № 40. – P. 171–178.
30. **Sovjak R., Vogel F., Beckmann B.** Triaxial compressive strength of ultra high performance concrete. ActaPolytechnica. – 2013. – № 53 (6). – P. 901–905.
31. **Хазов П.А., Ведяйкина О.И., Хохлова И.С., Артемьева Д.В**. Деформирование и разрушение трубобетонных образцов при поперечном изгибе. Приволжский научный журнал. – 2023. – № 2 (66). – С. 69-74.
32. Прочность тонкостенных металлических конструкций / Б.Б. Лампси . – М. : Стройиздат, 1987. – 279 с.

Khazov Pavel Alekseevich, Candidate of Technical Sciences, Associate Professor of the Department of Theory of Structures and Technical Mechanics, Head of the Laboratory for Continuous Monitoring of the Technical Condition of Buildings and Structures, Nizhny Novgorod State University of Architecture and Civil Engineering, 65, Ilyinskaya str., Nizhny Novgorod, 603950, Russia, e-mail: khazov.nngasu@mail.ru, tel: +7 (951) 919-0-919. ORCID: 0000-0003-1220-6930.

Vladimir Ivanovich Erofeev, Doctor of Physical and Mathematical Sciences, Professor, Director, Mechanical Engineering Research Institute of the RAS – Branch of Federal Research Center «A.V. Gaponov – Grekhov Institute of Applied Physics of the Russian Academy of Sciences», 85, Belinskogo str., Nizhny Novgorod, 603024, Russia, e-mail: erof.vi@yandex.ru, tel: +7(831) 432-05-76. ORCID: 0000-0002-6637-5564.

Olga Ivanovna Vediaikina, Candidate of Physical and Mathematical Sciences, Associate Professor of the Department of General Physics and Theoretical Mechanics, Nizhny Novgorod State University of Architecture and Civil Engineering, 65, Ilyinskaya str., Nizhny Novgorod, 603950, Russia, e-mail: razvnauki@rambler.ru, tel: +7 (831) 430-19-34. ORCID: 0009-0007-1686-2579.

Artyom Pavlovich Pomazov, post-graduate student of the Department of Theory of Structures and Technical Mechanics, assistant of the Department of Building Structures, Nizhny Novgorod State University of Architecture and Civil Engineering, 65, Ilyinskaya str., Nizhny Novgorod, 603950, Russia, e-mail: pomazov.a.p@yandex.ru, tel: +7 (915) 947-36-25. ORCID: 0009-0009-5465-3692.

Dmitrij Aleksandrvich Kozhanov, Candidate of Physical and Mathematical Sciences, Associate Professor of the Department of Theory of Structures and Technical Mechanics, Nizhny Novgorod State University of Architecture and Civil Engineering, 65, Ilyinskaya str., Nizhny Novgorod, 603950, Russia, e-mail: kozhanov@nngasu.ru, tel: +7 (831) 433-92-35. ORCID: 0000-0002-8443-1291.

Павел Алексеевич Хазов, кандидат технических наук, доцент кафедры Теории сооружений и технической механики, заведующий лабораторией непрерывного контроля технического состояния зданий и сооружений, Нижегородский государственный архитектурно-строительный университет (ННГАСУ), Адрес: д. 65, ул. Ильинская, г. Нижний Новгород, 603950, Россия, e-mail: khazov.nngasu@mail.ru, тел. +7 (951) 919-0-919. ORCID: 0000-0003-1220-6930.

Владимир Иванович Ерофеев, доктор физико-математических наук, профессор, директор, Институт проблем машиностроения РАН – филиал ФГБНУ «Федеральный исследовательский центр «Институт прикладной физики им. А.В. Гапонова – Грехова Российской академии наук» (ИПМ РАН), Адрес: д. 85, ул. Белинского, г. Нижний Новгород, 603024, Россия, e-mail: erof.vi@yandex.ru, тел. +7(831) 432-05-76. ORCID: 0000-0002-6637-5564.

Ольга Ивановна Ведяйкина, кандидат физико-математических наук, доцент кафедры Общей физики и теоретической механики, Нижегородский государственный архитектурно-строительный университет (ННГАСУ), Адрес: д. 65, ул. Ильинсская, г. Нижний Новгород, 603950, Россия, e-mail: razvnauki@rambler.ru, тел. +7 (831) 430-19-34. ORCID: 0009-0007-1686-2579.

Артём Павлович Помазов, аспирант кафедры Теории сооружений и технической механики, ассистент кафедры Строительных конструкций, Нижегородский государственный архитектурно-строительный университет (ННГАСУ), Адрес: д. 65, ул. Ильинская, г. Нижний Новгород, 603950, Россия, e-mail: pomazov.a.p@yandex.ru, тел. +7 (915) 947-36-25. ORCID: 0009-0009-5465-3692.

Дмитрий Александрович Кожанов, кандидат физико-математических наук, доцент кафедры Теории сооружений и технической механики, Нижегородский государственный архитектурно-строительный университет (ННГАСУ), Адрес: д. 65, ул. Ильинская, г. Нижний Новгород, 603950, Россия, e-mail: kozhanov@nngasu.ru, тел. +7 (831) 433-92-35. ORCID: 0000-0002-8443-1291.

International Journal for Computational Civil and Structural Engineering, 20(2) 46–59 (2024)

DOI:10.22337/2587-9618-2024-20-2-46-59

HYDRAULIC ANALYSIS OF COMPOSITE HYDRAULIC STRUCTURE CONSIDERING EXISTING OF PIER

Rafi M. Qasim [1], Ihsan A. Abdulhussein [1], Muna A. Hameed [2]

[1] Southern Technical University/ Basra Engineering Technical College, Basrah, IRAQ
[2] Southern Technical University/ Technical Institute of Basrah, Basrah, IRAQ

Abstract: A composite hydraulic structure is used to solve the problems of sediment and floating materials, respectively. A pier (obstacle) is used at the downstream of the composite hydraulic structure to increase water depth, decrease flow velocity, and dissipate the flow energy. The paper deals with the effect of single pier and double piers on the hydraulic characteristics of the composite structure. Circular and square shapes are adopted in the study with different spacing measured from the downstream of the composite structure. The experiments reveal how the level of the hydraulic characteristics is changed due to the existence of the pier/piers as compared to without the existence of the pier/piers. The statistical data which is collected from the experiments shows the alteration in the average downstream water depth, discharge coefficient, Reynolds number, upstream Froude number and downstream Froude number regardless of pier shape and spacing. The alteration happens owing to a change in the separation zone of water flow along the pier circumference. Nonlinear water surface profile is appeared when the pier is located at the downstream, while linear water surface profile is appeared clearly when the downstream without pier. Also the interference between overflow velocity and underflow velocity will be reflected in the hydraulic characteristics.

Keywords: open channel flow, weir, gate, pier

ГИДРАВЛИЧЕСКИЙ АНАЛИЗ СЛОЖНОГО ГИДРОТЕХНИЧЕСКОГО СООРУЖЕНИЯ, ВКЛЮЧАЮЩЕГО ПИРС

Рафи М. Касим [1], Эхсан А. Абдул-Хусейн [1], Муна А. Хамид [2]

[1] Южный технический университет/Басрский инженерно-технический колледж, г. Басра, ИРАК
[2] Южный технический университет/Технический институт Басры, г. Басра, ИРАК

Аннотация: Композиционное гидротехническое сооружение используется для решения проблем, связанных с отложениями и соответственно всплывающими веществами. Пирс (как препятствие) задействован в нижней части сложного гидротехнического сооружения для увеличения глубины воды, уменьшения скорости потока и рассеивания энергии потока. В статье рассмотрено влияние одиночных и двойных свай на гидравлические характеристики составной конструкции. В исследовании приняты круглые и квадратные формы с разным расстоянием, измеренным от нижней части композиционной конструкции. Эксперименты показывают, как изменяется уровень гидравлических характеристик при наличии препятствия/препятствий по сравнению с их отсутствием. Статистические данные, собранные в результате экспериментов, показывают изменение средней глубины воды ниже по течению, коэффициента расхода, числа Рейнольдса, числа Фруда выше по течению и числа Фруда ниже по течению независимо от формы и расстояния между опорами. Изменение происходит за счет изменения зоны отрыва потока воды по окружности пирса. Нелинейный профиль водной поверхности проявляется при расположении пирса в нижнем бьефе, а линейный профиль водной поверхности проявляется четко при нижнем бьефе без пирса. Также на гидравлических характеристиках будет отражаться взаимовлияние скорости перелива и скорости нижнего потока.

Ключевые слова: течение в открытом русле, плотина, затвор, препятствие

INTRODUCTION

The weir and gate composite hydraulic structure is the most common and significant discharge structure in irrigation engineering work. This structure is used for adjusting and controlling the water flow in the channel or canal. The function of using both a weir and a gate in the same structure is to remove the floating material by the weir structure and the sediment by the gate opening at the same time with high efficiency of the operation without any shortages in supply water flow rate. The free flow characteristics of the flow which passes over the weir and under the gate are investigated. The weir has a triangular shape, while the gate has a rectangular shape. Nine different weirs are used with three different angles over a gate with a rectangular section. Also, three different distances between the gate and the weir are considered in the study [1]. The discharge coefficient of a combined hydraulic structure is investigated. Nine different models are used, with the weir having a rectangular shape while the gate has a semi-circular shape. The discharge coefficient of the combined structure is estimated by using a multi-regression model with the percentage of the error equal to ±10% [2]. Also, the flow pattern over the weir and under the gate of the combined weir-gate structure is studied experimentally. In the experiments, four different opening gate heights were adopted. Four different angles for the weir were also adopted in the experiments. Statistical analysis principles are adopted to correlate the discharge coefficient with hydraulic and geometric variables [3]. The discharge coefficient and the free flow characteristics for composite weirs and sluice gates are examined by using experiments. The gate has a semicircular shape with fixed dimensions. Fifteen device models are employed and tested under the action of the different geometrical conditions, while the hydraulic conditions are considered constant. They obtained an expression to describe the device discharge coefficient [4]. As well, the discharge coefficient of the combined weir-gate structure is examined by using experiments under free flow conditions. The weir consists of two parts, and these parts are trapezoidal notch over rectangular notch, while the sluice gate has a semicircular shape. Fifteen device models are employed and tested. From the results of the experiments, they developed and predicted a formula for the discharge coefficient of the device [5]. Experimentally, the hydraulic characteristics of flow over a cipolletti weir and under an opening with a rectangular section are studied. Thirty-nine models are made with different geometrical dimensions. The experiments are done under the free flow condition and subcritical flow [6]. In addition, the characteristics of the combined flow under a rectangular opening and over a trapezoidal weir are studied experimentally. Also, the dimensional analysis with statistics program is employed to obtain an empirical formula to describe the discharge coefficient [7]. The mutual influence of the suspended material and the deposition on the combined hydraulic structure has been studied. Experimental work has been done to validate the composite models. The simulation analysis is based on the RNGK-ε turbulence model. From this study, the prediction of the discharge leads to the suggestion of two mathematical models with an acceptable discharge coefficient [8]. On the other hand, the composite hydraulic structure flow characteristics are studied experimentally under free flow conditions. The study dealt with the influence of the installation angle of the composite structure on the horizontal bed of the flume on hydraulic characteristics, considering different geometrical dimensions of the composite structure [9]. In addition, experimental work is performed to reveal the hydraulic characteristics of water flow that passes through the composite hydraulic structure and encounters obstacles with or without openings, which are located downstream of the composite structure. The experiments show the direct effect of the obstacles with openings on the hydraulic

characteristics and flow pattern [10]. The impact of using the barrier/barriers at the downstream region of the weir-gate structure has been studied experimentally. The experiments reveal the influence of the barrier/barriers on controlling the hydraulic characteristics of the composite hydraulic structure [11]. Also, an experimental study was carried out to show the effect of the downstream obstacle/obstacles on the hydraulic characteristics of the discharge structure (weir-gate structure). The experiments show that the obstacle/obstacles control the trend between the hydraulic variables [12]. The experiment study deals with assessment of the composite structure's hydraulic characteristics under the effect of the pier/piers' existence at the downstream of the composite structure. Here, the pier works as an obstacle and leads to an increased water level around the pier and reduced flow velocity. These factors will be reflected directly on the hydraulic characteristics of the hydraulic structure.

THEORETICAL ANALYSIS

The theoretical discharge, which crosses the rectangular weir, can be computed from the following equation [13].

$$Q_w = \frac{2}{3}\sqrt{2g}\; b\, h^{3/2} \tag{1}$$

The theoretical discharge, which crosses the gate, can be computed from:

$$Q_g = V\,.A = \sqrt{2g\,H}\;A \tag{2}$$

For free flow conditions,

$$H = d + y + h \tag{3}$$

For submerged flow conditions

$$H = d + y + h - h_d \tag{4}$$

For the composite hydraulic structure, which consists of weir and gate, the theoretical discharge and actual discharge can be computed according to:

$$Q_{theor} = Q_w + Q_g \tag{5}$$

$$Q_{act} = C_d \cdot Q_{theor} \tag{6}$$

$$Q_{act} = C_d\,[Q_w + Q_g] \tag{7}$$

Where, H: upstream water depth, h: water head over weir crest, h_d: downstream water depth, y: vertical distance between weir and gate, d: the gate depth, A: gate cross-section flow area, Vis the flow velocity, b: the width of the rectangular weir, g: acceleration due to gravity, Q_w:weir discharge ,Q_g: gate discharge,Q_{theor}: theoretical discharge ,Q_{act}: actual discharge ,C_d: discharge coefficient.

The Reynolds number [14] and Froude number [15] are computed by using the following equations:

$$R_e = \frac{V\,h_d}{\nu} \tag{8}$$

$$F_r = \frac{V}{\sqrt{g\,y}} \tag{9}$$

Where: ν is the kinematic viscosity of water, y: water depth.

EXPERIMENTAL SETUP

The experiments for the current study are done on the flume, which has the following dimensions: 2 m long, 7.5 cm wide, and 15 cm deep. The volume method is used to measure the actual discharge quantity, while the water depth at the upstream and downstream is measured by using a scale mounted on the side wall of the flume. Table 1 displays the dimensions of the test model that is made from wood sheet material; the thickness of wood sheet is equal to 5mm beveled

along all the edges at 45° with sharp edges of 1mm. The composite hydraulic structure is located at a certain distance equal to 80 cm from the beginning of the flume. For all experiments, the bed of the flume must be in a horizontal position. Two different shapes of the pier are used; the first one has a circular shape, while the second one has a square shape.

Table 1. The dimensions of the test models

Model No.	Hu(cm)	D(cm)	Y(cm)	H(cm)
1	3	4	2	9
2	2	4	2	8
3	1	4	2	7
4	3	3	3	9
5	2	3	3	8
6	1	3	3	7
7	2	4	3	9
8	1	4	3	8
9	3	2	4	9
10	2	2	4	8
11	1	2	4	7
12	1	4	4	9

Table 2 reviews the details of the pier. Piers are located at different distances measured from the downstream of the composite hydraulic structure. Also, table 2 illustrates the details of the distances. Here, the pier is made by using wood material. Figure 1-a shows the sketch of the composite structure, while Figure 1-b shows the sketch of the whole hydraulic system, which consists of the composite structure and the pier.

Table 2. Details of the pier with distance measured from the composite hydraulic structure

Circular Pier			
Case	Pier Shape	Diameter	Distance
Single pier	Circular	2cm	20cm
Single pier	Circular	2cm	30cm
Double pier	circular	2cm	20cm,30cm
Single pier	circular	3cm	20cm
Single pier	circular	3cm	30cm
Double pier	circular	3cm	20cm,30cm
Single pier	circular	4cm	20cm
Single pier	circular	4cm	30cm
Double pier	circular	4cm	20cm,30cm
Square Pier			
Case	Pier Shape	Diameter	Distance
Single pier	Square	2cm	20cm
Single pier	Square	2cm	30cm
Double pier	Square	2cm	20cm,30cm
Single pier	Square	3cm	20cm
Single pier	Square	3cm	30cm
Double pier	Square	3cm	20cm,30cm
Single pier	Square	4cm	20cm
Single pier	Square	4cm	30cm
Double pier	Square	4cm	20cm,30cm

RESULTS AND DISCUSSION

A series of experiments were carried out using various dimensions of the composite hydraulic structure with varying pier diameters, shapes, and spacing. Figure 2 shows the discharge coefficient of the composite model variation with the ratio (D/H), where D refers to the circular pier diameter and H refers to the upstream water depth. The figure shows a

comparative study based on two different flow conditions. The first condition refers to the free flow condition, which occurs without the existence of the pier, while the second condition refers to the submerged flow condition, which occurs due to the existence of the pier.

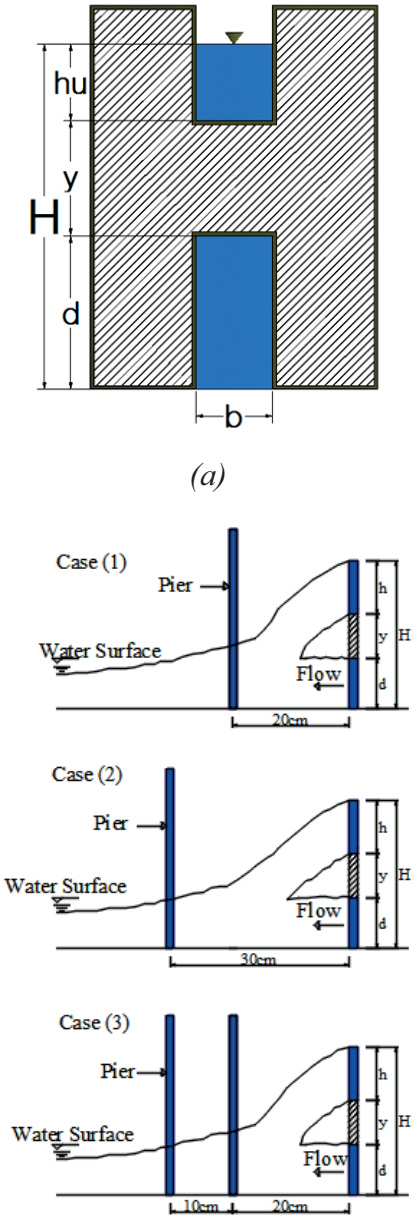


Figure 1. a) The composite structure. b) Composite structure and the Pier

The figure shows that the values of the discharge coefficient in the free flow condition are always greater than the discharge coefficient of the submerged flow condition. The trend in relation between the discharge coefficient and the ratio (D/H) for the submerged flow condition can be considered dramatic owing to the alteration in the pier cross section, spacing, and number of the piers. The variation in the composite discharge coefficient will be associated with the variation in the flow velocity. The variation in the flow velocity happens owing to the alteration in the separation points of the water stream along the circumference of the circular cylinder.

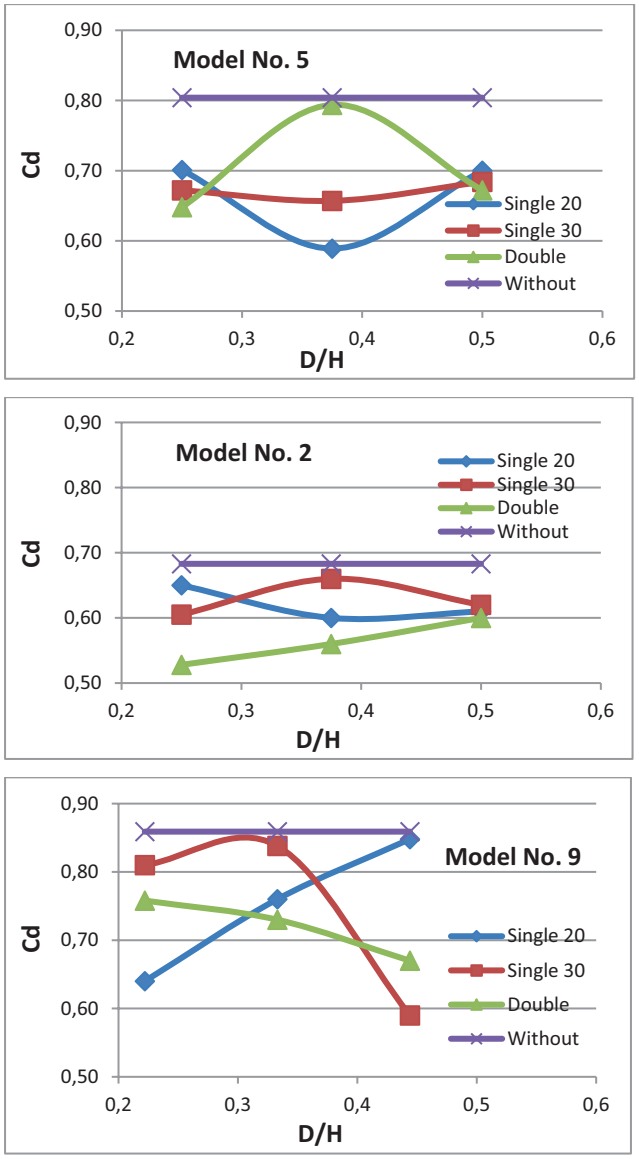


Figure 2. The variation of discharge coefficient with (D/H) ratio of circular pier and for different models

Figure 3 illustrates the variation of the ratio (h_d/H) against the ratio (D/H) for various cases and configurations, where h_d refers to the average downstream water depth. For submerged flow conditions, it is obvious that the ratio (h_d/H) decreases slightly and then increases slightly when the ratio (D/H) increases, while for free flow conditions, by increasing the ratio (D/H), the ratio (h_d/H) remains constant. The figure shows that the values of the submerged flow condition are always greater than the values of the free flow condition. Because of the existence of the pier (obstacle), which confines the water and leads to increasing the water depth, this condition will be satisfied for the submerged flow condition.

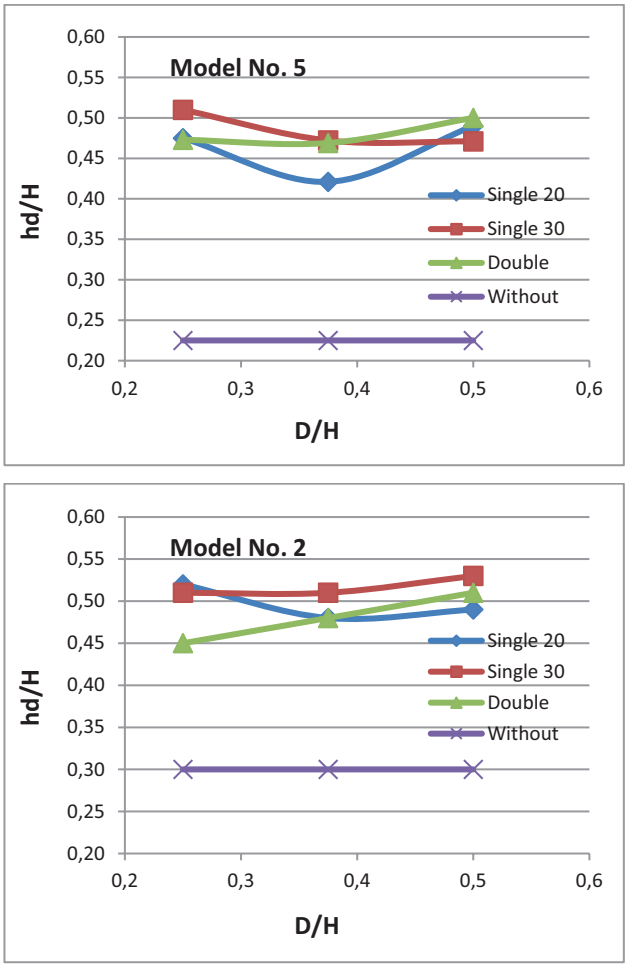


Figure 3. The variation of (h_d/H) ratio with (D/H) ratio of circular pier and for different models

Figure 4 illustrates the relationship between the composite hydraulic structure's actual discharge and the ratio (D/H). The relationship is identical to the trend of the relationship between discharge coefficient and the ratio (D/H), which is shown in figure 2. This happens owing to the direct proportion between actual discharge and discharge coefficient.

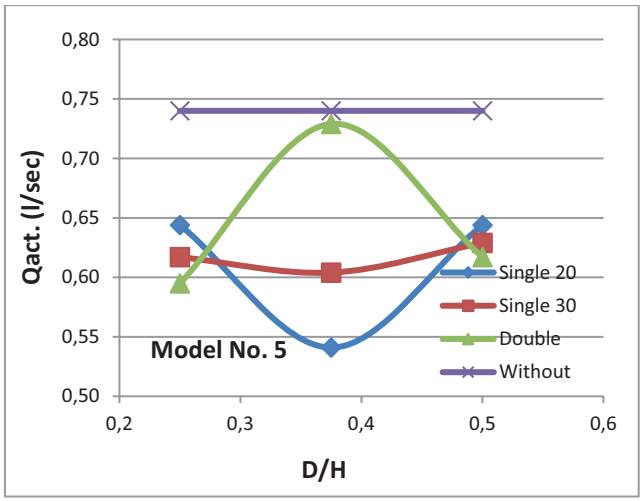


Figure 4. The variation of the actual discahrge with (D/H) ratio of circular pier and for model number 5

Figure 5 illustrates the comparison between free flow and submerged flow for the following relationships: relation between upstream Froude number and the ratio (D/H); downstream Froude number and the ratio (D/H); also the relation between Reynolds number and the ratio (D/H). In general, both the Froude number and the Reynolds number depend on flow velocity and flow depth. The figure shows that the values of the free flow condition are always greater than the values of the submerged flow condition. The justification of this situation is associated with the existence of the pier (obstacle), which leads to the rise in the water depth and decreases Froude number in the downstream region, and this occurs due to the inverse proportion between Froude number and the flow depth. Also, the same behaviour appears

for the Froude number in the upstream region. In the upstream, the flow depth is very high, and this leads to the low values for Froude number. The interaction between weir flow velocity and gate flow velocity has a greater influence on the Reynolds number value distribution than the interaction between flow depth and flow velocity. All three relationships are more influenced by the overlapping between weir velocity and gate velocity, pier diameter, and the spacing between pier and composite structure. Based on the Reynolds number, the flow is considered turbulent. Also, based on the Froude number at upstream, the flow type is considered subcritical and the flow type at downstream is changed from subcritical to supercritical.

Figures 6, 7 and 8 review the relationship between the ratio (h_d/H) and the ratio (X/H), where X refers to the distance along the downstream of the flume, and this distance is measured from the downstream of the composite hydraulic structure. Figures 6 and 7 take into account the existence of single piers and double piers, respectively, while Figure 8 is drawn for both single piers and double piers for a constant ratio of (D/H =0.429). Figures 6, 7 and 8 comprise two different cases. These cases are free flow and submerged flow. The figures show that the values of the average downstream water depth for the free flow are always less than the corresponding values in the case of the submerged flow. The nonlinear water surface profile happens due to the alteration in the water surface elevation around the pier (obstacle), which affects the stability of the water surface elevation along the downstream region. The fluctuation in the trend of the profile relies on pier diameter, spacing, and interference between weir velocity and gate velocity.

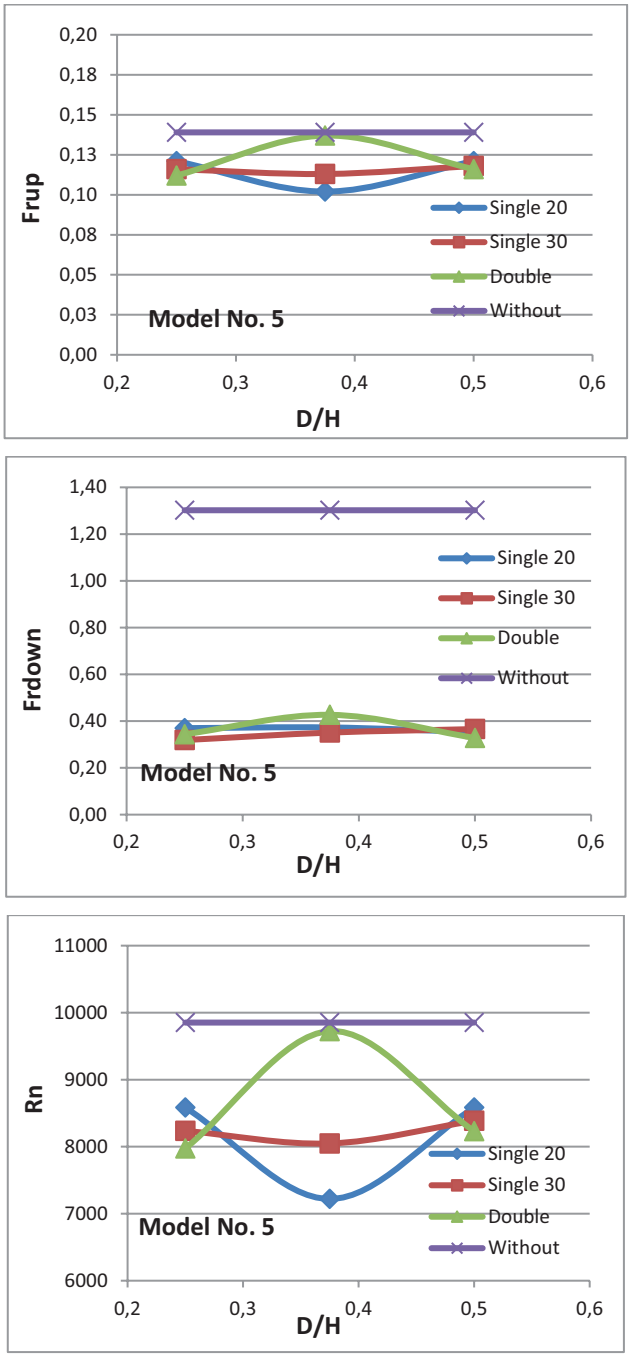


Figure 5. Variation of upstream Froude number, Downstream Froude number and Reynold's number with (D/H) ratio of circular pier and for model No. 5

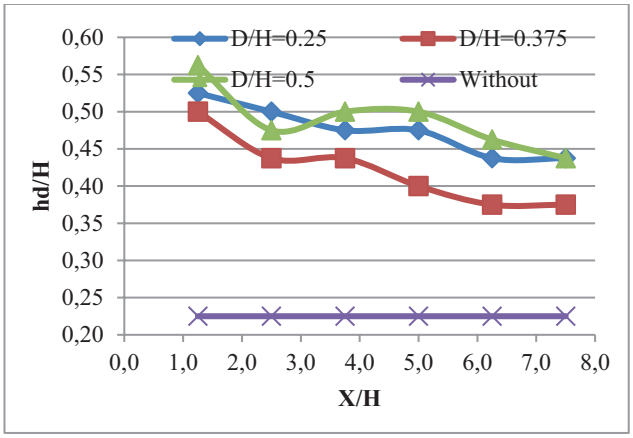


Figure 6. The relationship between (h_d/H) ratio and the ratio (X/H) for model No. 5, Single 20, circular pier

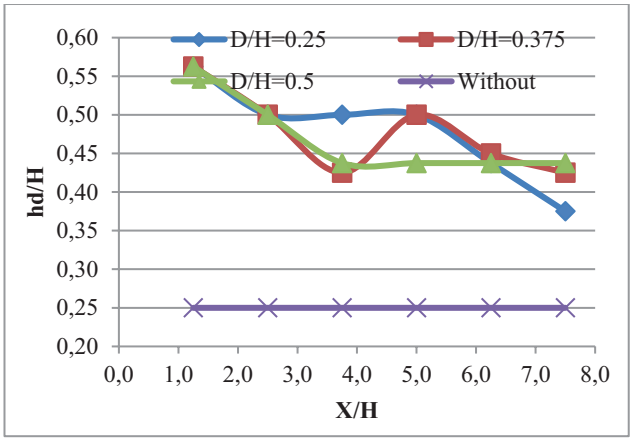


Figure 7. The relationship between (h_d/H) ratio and the ratio (X/H) for model No. 8, double, circular pier

Figure 9 shows the discharge coefficient of the composite model variation with the ratio (D/H), where D refers to the square pier diameter and H refers to the upstream water depth. The figure shows a comparative study based on two different flow conditions. The first condition refers to the free flow condition which occurs without the existence of the pier, while the second condition refers to the submerged flow condition which occurs due to the existence of the pier. The figure shows that the values of the discharge coefficient in the free flow condition are always greater than the discharge coefficient of the submerged flow condition. The trend in relation between the discharge coefficient and the ratio (D/H) for the submerged flow condition can be considered dramatic owing to the alteration in the pier cross section, spacing, and number of the piers. The variation in the composite discharge coefficient will be associated with the variation in the flow velocity. For a single pier, the trend in the relationship is considered identical owing to the separation point of the fluid being considered fixed along the circumference of the square pier. As for the trend, it is starting to increase gradually and drop dramatically. For the double piers, the variation depends on the change in the flow velocity between the front pier and the rear pier.

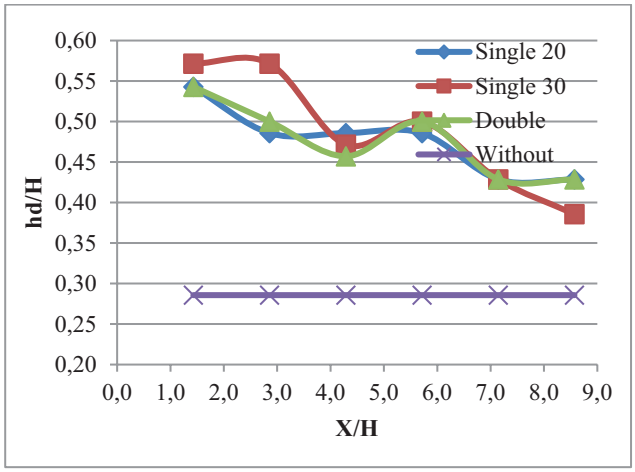


Figure 8. The relationship between (h_d/H) ratio and the ratio (X/H) for model No. 3, D/H=0.429, circular pier

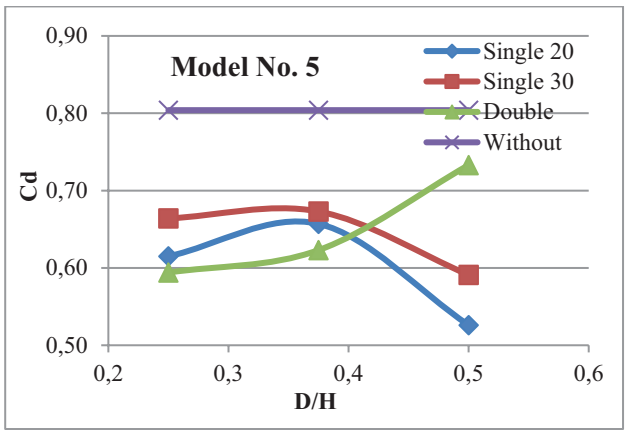


Figure 9. The variation of discharge coefficient with (D/H) ratio of square pier and for model No. 5

Figure 10 illustrates the variation of the ratio (h_d/H) against the ratio (D/H) for various configurations of the pier arrangement, where h_d refers to the average downstream water depth. For submerged flow conditions, it is obvious that the ratio (h_d/H) decreases slightly when the ratio (D/H) increases, while for free flow conditions, by increasing the ratio (D/H), the ratio (h_d/H) remains constant. The figure shows that the values of the submerged flow condition are always greater than the values of the free flow condition. Because of the existence of the pier (obstacle), which confines the water and leads to increasing the water depth, this condition will be satisfied for the submerged flow condition.

Figure 11 illustrates the comparison between free flow and submerged flow for the following relationships: relation between upstream Froude number and the ratio (D/H); downstream Froude number and the ratio (D/H); also the relation between Reynolds number and the ratio (D/H). In general, both the Froude number and the Reynolds number depend on flow velocity and flow depth.

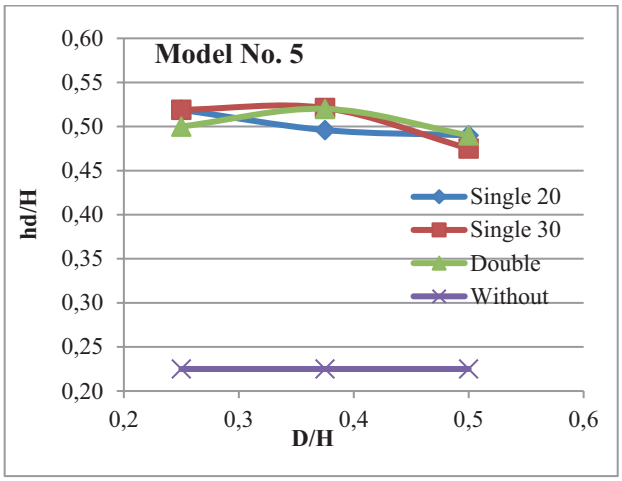
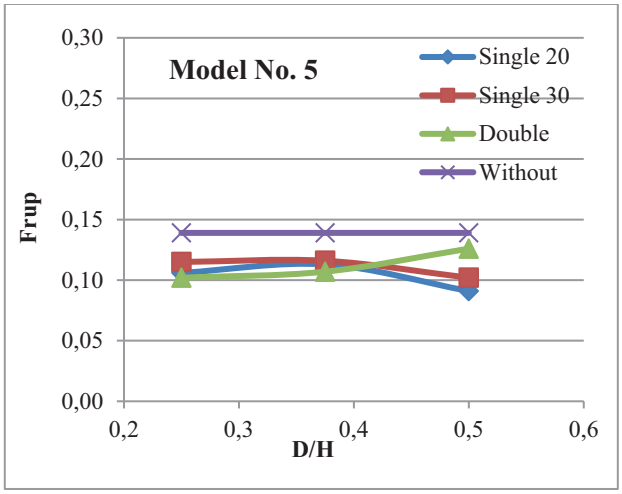
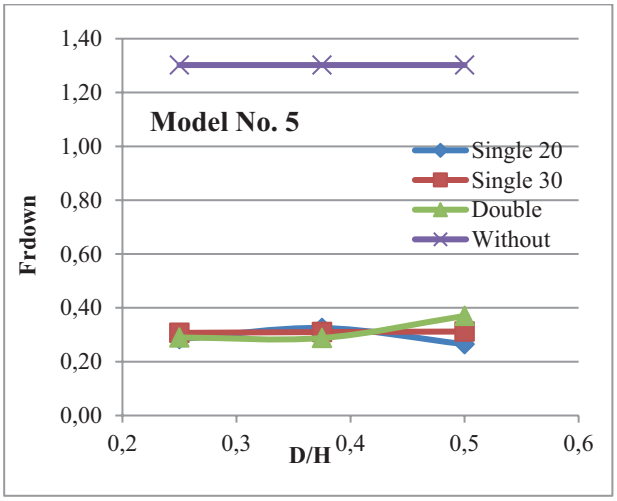


Figure 10. The variation of (h_d/H) ratio with (D/H) ratio of square pier and for model No. 5

The figure shows that the values of the free flow condition are always greater than the values of the submerged flow condition. The justification of this situation is associated with the existence of the pier (obstacle), which leads to the rise in the water depth and decreases Froude number in the downstream region, and this occurs due to the inverse proportion between Froude number and the flow depth. Also, the same behaviour appears for the Froude number in the upstream region. In the upstream, the flow depth is very high, and this leads to the low values for Froude number. The interaction between weir flow velocity and gate flow velocity has a greater influence on the Reynolds number value distribution than the interaction between flow depth and flow velocity. All three relationships are more influenced by the overlapping between weir velocity and gate velocity, pier diameter, and the spacing between pier and composite structure. Based on the Reynolds number, the flow is considered turbulent. Also, based on the Froude number at upstream, the flow type is considered subcritical and the flow type at downstream is changed from subcritical to supercritical.

Figures 12, 13 and 14 review the relationship between the ratio (h_d/H) and the ratio (X/H), where X refers to the distance along the downstream of the flume, and this distance is measured from the downstream of the composite hydraulic structure. Figures 12 and 13 take into account the existence of single piers and double piers, respectively, while Figure 14 is drawn for both single piers and double piers for a constant ratio of (D/H = 0.571). Figures 12, 13 and 14 comprise two different cases. These cases are free flow and submerged flow. The figures show that the values of the average downstream water depth for the free flow are always less than the corresponding values in the case of the submerged flow. The nonlinear water surface profile happens due to the alteration in the water surface elevation around the pier (obstacle), which affects the stability of the water surface elevation along the downstream region. The fluctuation in the trend of the profile relies on pier diameter, spacing, and interference between weir velocity and gate velocity.





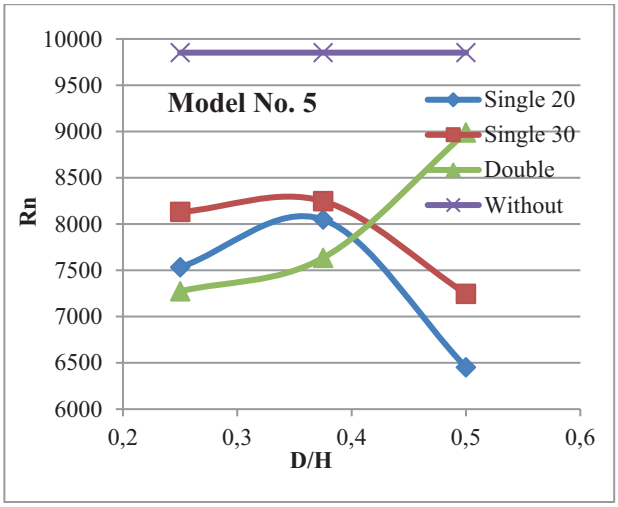


Figure 11. Variation of upstream Froude number, Downstream Froude number and Reynold's number with (D/H) ratio of square pier and for model No. 5

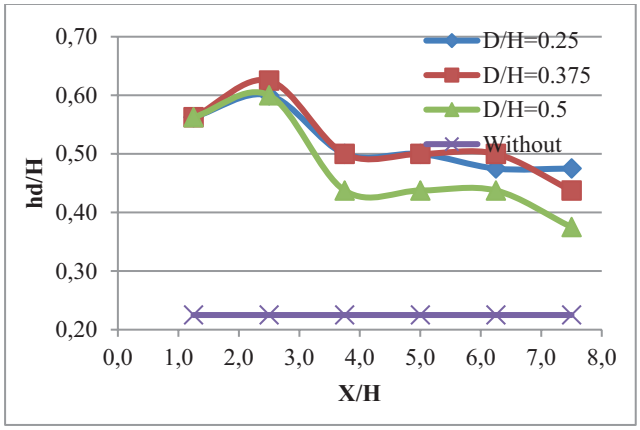


Figure 12. The relationship between (h_d/H) ratio and the ratio (X/H) for model No. 5, Single 30, square pier

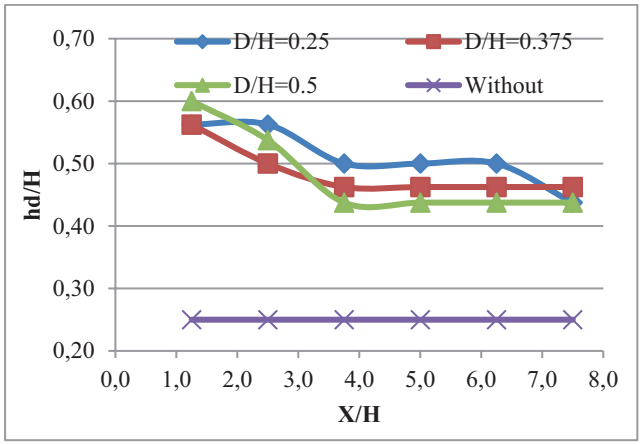


Figure 13. The relationship between (h_d/H) ratio and the ratio (X/H) for model No. 5, double, square pier

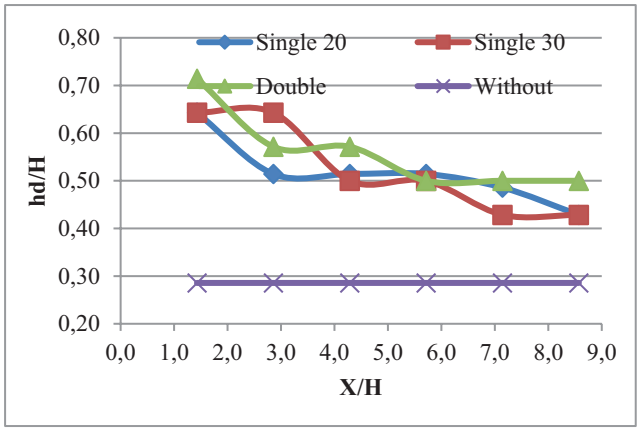


Figure 14. The relationship between (h_d/H) ratio and the ratio (X/H) for model No. 3, D/H=0.571, square pier

Table 3 shows the maximum, minimum, and average values of discharge coefficient; average downstream water depth; upstream Froude number; downstream Froude number; and Reynolds number. Table 3 includes two different shapes of pier. These shapes are the circular pier and the square pier. Also, table 3 reviews the values for single pier and double piers. From table 3, the following is obvious: The existence of a single square pier with a diameter of 20 cm leads to a higher discharge coefficient, with little fluctuation in the average value. But in the case of double piers, the existence of the double circular piers leads to a higher discharge coefficient as compared with the existence of the double square piers. Also, for a single circular pier with a 30 cm diameter and a single square pier with a 30 cm diameter, the variation in discharge coefficient values appears clearly. For the average downstream water depth, the existence of the square pier leads to higher water depth as compared with the existence of the circular pier regardless of the pier numbers (single or double). A small difference appeared in values of the Froude number upstream regardless of the pier shapes and numbers (single or double). The Froude number downstream has a higher value with a single circular pier with a diameter of 20 cm. Also, Froude number has higher values with double circular piers, but for a single square pier with a diameter of 30 cm, Froude number has higher values as compared with a single square pier with a 20 cm diameter and double square piers. In terms of Reynolds number, the variation in values is obvious regardless of pier shape and configuration (single or double). Variation in all values will be produced by the change in fluid separation zone; flow velocity change from section to section; water depth alteration from section to section; and the change in momentum transfer due to the existence of the pier (obstacle). Also, the table indicates a comparative between two cases; the first case deals with pier existence while the second is without pier existence.

Table 3. Comparison between ferr and submerged output models parameters

Parameter		Circular			Square			Case without
		Single 20cm	Single 30cm	Double	Single 20cm	Single 30cm	Double	
Cd	Maximum	0.892	0.892	0.926	0.897	0.838	0.781	0.859
	Minimum	0.444	0.020	0.502	0.496	0.426	0.434	0.586
	Average	0.630	0.630	0.641	0.602	0.593	0.601	0.750
h_{davg} (cm)	Maximum	4.500	4.683	4.400	4.617	4.617	4.633	3.500
	Minimum	2.783	2.967	3.067	3.167	3.283	3.333	0.850
	Average	3.758	3.925	3.823	4.037	4.082	4.087	1.854
Fr_{up}	Maximum	0.143	0.146	0.147	0.143	0.130	0.153	0.178
	Minimum	0.066	0.003	0.073	0.064	0.068	0.082	0.094
	Average	0.110	0.111	0.111	0.105	0.103	0.106	0.132
Fr_{down}	Maximum	0.470	0.413	0.427	0.397	0.358	0.370	3.919
	Minimum	0.250	0.009	0.262	0.193	0.166	0.222	0.522
	Average	0.352	0.332	0.351	0.303	0.290	0.300	1.483
Rn	Maximum	10695	11257	11407	10959	9852	10870	10999
	Minimum	3810	182	5289	3711	3953	4779	5467
	Average	8125	8194	8313	7795	7571	7830	9597

CONCLUSION

In the current study, flow over weir and under gates with and without single pier or double piers has been studied experimentally. Depending on the experimental results of the current investigation, the following conclusions can be found:

1- The water flow separation zone along the circumference of the pier has a major effect on the hydraulic characteristics, especially the flow velocity.
2- The interaction between gate flow velocity and weir flow velocity produces a variation in the hydraulic characteristics of the composite structure.
3- The pier shape and spacing have a direct effect on the control of the hydraulic behavior of the composite hydraulic structure.
4- The change in water depth, flow velocity, and momentum transfer will have an effect directly on the hydraulic characteristics of the composite structure.
5- Actual discharge and discharge coefficient have the same trend regardless of the presence of the pier/piers.
6- The Reynolds number and Froude number are more sensitive to the existence of the pier/piers.
7- The hydraulic characteristics of the composite structure under the action of the pier/piers are not similar to the hydraulic characteristics without the pier/piers.

REFERENCES

1. **Hayawi, H.A.M., Yahia, A.A.G., Hayawi, G.A.M.** Free combined flow over a triangular weir and under rectangular gate. Damascus Univ. Journal. 2008. 24 (1).
2. **Hayawi, H.A.M., Hayawi, G.A.M., Alniami, A.A.G.** Coefficient of discharge for a combined hydraulic measuring device. Al-Rafidain Engineering. 2009. 17(6). http://dx.doi.org/10.33899/rengj.2009.43616.
3. **Jalil, A.S., Sarhan, A.S.** Experimental study of combined oblique weir and gate structure. ARPN Journal of Engineering and Applied Sciences. 2013. 8(4).
4. **Khassaf, S.I., Yost, S.A., Abbas, H.A.** Coefficient of discharge for a compound weir with semicircular gate. International Journal of Advance Research. IJOAR.org. 2013. 1(Issue 9).
5. **Khassaf, S.I., Abbas, H.A.** Study the free flow over compound weir and below semi circular gate. International Journal of Scientific & Engineering Research. 2013. 4(Issue 10).
6. **Al-Suhili, R.H., Shwana, A.J.** Prediction of the discharge coefficient for a cipolletti weir with rectangular bottom opening. Int. Journal of Engineering Research and Applications. 2014. 4(Issue 1). (Version 4), 80-89.
7. **Khassaf, S.I., Habeeb, M.** Experimental investigation for flow through combined trapezoidal weir and rectangular gate. International Journal of Scientific & Engineering Research. 2014. 5(Issue 4).
8. **Sarhan, S.A., Jalil, S.A.** Analysis of simulation outputs for the mutual effect of flow in weir and gate system. Journal of Babylon University/Engineering Sciences. 2018. 26(6).
9. **Qasim, R.M., Abdulhussein, I.A., AL-Asadi, K.** Experimental study of composite inclined weir – gate hydraulic structure. WSEAS TRANSACTIONS on FLUID MECHANICS, 2020. 15. DOI: 10.37394/232013.2020.15.5
10. **Qasim, R.M., Abdulhussein, I.A., Mohammed, A.A., Maatooq, Q.A.** The effect of the obstacle on the hydraulic response of the composite hydraulic structure. INCAS BULLETIN. 2020. 12(Issue 3). 159 – 172. DOI: 10.13111/2066-8201.2020.12.3.13
11. **Qasim, R.M. Abdulhussein, I.A., AL-Asadi, K.** The effect of barrier on the hydraulic response of composite weir-gate structure. Archives of Civil Engineering.

2020. 66 (Issue 4). DOI: 10.24425/ace.2020.135211
12. **Qasim, R.M., Mohammed, A.A., Abdulhussein, I.A., Maatooq, Q.A.** Experimental invistigation of multi obsticales impact on weir-gate discharge structure. International Journal of Mechatronics and Applied Mechanics. 2021. Issue 9. dx.doi.org/10.17683/ijomam/issue9.11
13. **Streeter, V.L., Wylie, E.B.** Fluid mechanics, First SI Metric Edition, Copy right©. 1983.
14. **Negm, A.M., AL- Brahim, M., ALHamid, A.A.** Combined-free flow over weirs and below gates. J. Hydraul. Res. 2002. 40. 1–7.
15. **Fox, R.W., McDonald, A.T.** Introduction to fluid mechanics. Fourth Edition. SI version Copyright © John Wiley and Sons, Inc. 1994.

СПИСОК ЛИТЕРАТУРЫ

1. **Hayawi, H.A.M., Yahia, A.A.G., Hayawi, G.A.M.** Free combined flow over a triangular weir and under rectangular gate. Damascus Univ. Journal. 2008. 24 (1).
2. **Hayawi, H.A.M., Hayawi, G.A.M., Alniami, A.A.G.** Coefficient of discharge for a combined hydraulic measuring device. Al-Rafidain Engineering. 2009. 17(6). http://dx.doi.org/10.33899/rengj.2009.43616.
3. **Jalil, A.S., Sarhan, A.S.** Experimental study of combined oblique weir and gate structure. ARPN Journal of Engineering and Applied Sciences. 2013. 8(4).
4. **Khassaf, S.I., Yost, S.A., Abbas, H.A.** Coefficient of discharge for a compound weir with semicircular gate. International Journal of Advance Research. IJOAR.org. 2013. 1 (Issue 9).
5. **Khassaf, S.I., Abbas, H.A.** Study the free flow over compound weir and below semi circular gate. International Journal of Scientific & Engineering Research. 2013. 4 (Issue 10).
6. **Al-Suhili, R.H., Shwana, A.J.** Prediction of the discharge coefficient for a cipolletti weir with rectangular bottom opening. Int. Journal of Engineering Research and Applications. 2014. 4 (Issue 1). (Version 4), 80-89.
7. **Khassaf, S.I., Habeeb, M.** Experimental investigation for flow through combined trapezoidal weir and rectangular gate. International Journal of Scientific & Engineering Research. 2014. 5(Issue 4).
8. **Sarhan, S.A., Jalil, S.A.** Analysis of simulation outputs for the mutual effect of flow in weir and gate system. Journal of Babylon University/Engineering Sciences. 2018. 26(6).
9. **Qasim, R.M. Abdulhussein, I.A., AL-Asadi, K.** Experimental study of composite inclined weir – gate hydraulic structure. WSEAS TRANSACTIONS on FLUID MECHANICS, 2020. 15.DOI: 10.37394/232013.2020.15.5
10. **Qasim, R.M. Abdulhussein, I.A., Mohammed, A.A., Maatooq, Q.A.** The effect of the obstacle on the hydraulic response of the composite hydraulic structure. INCAS BULLETIN. 2020. 12 (Issue 3). 159 – 172. DOI: 10.13111/2066-8201.2020.12.3.13
11. **Qasim, R.M. Abdulhussein, I.A., AL-Asadi, K.** The effect of barrier on the hydraulic response of composite weir-gate structure. Archives of Civil Engineering. 2020. 66 (Issue 4). DOI: 10.24425/ace.2020.135211
12. **Qasim, R.M., Mohammed, A.A., Abdulhussein, I.A., Maatooq, Q.A.** Experimental invistigation of multi obsticales impact on weir-gate discharge structure. International Journal of Mechatronics and Applied Mechanics. 2021. Issue 9. dx.doi.org/10.17683/ijomam/issue9.11
13. **Streeter, V.L., Wylie, E.B.** Fluid mechanics, First SI Metric Edition, Copy right©. 1983.

14. **Negm, A.M., AL- Brahim, M., ALHamid, A.A.** Combined-free flow over weirs and below gates. J. Hydraul. Res. 2002. 40. 1–7.

15. **Fox, R.W., McDonald, A.T.** Introduction to fluid mechanics. Fourth Edition. SI version Copyright © John Wiley and Sons, Inc. 1994.

Rafi Mohammed Qasim, Assistant Professor at Energy and Fuel Engineering Department, Southern Technical University (Basrah, Iraq). His research interests are in the application of hydraulic structure, flow on an open channel, flow around obstacles, soil and foundation engineering. Phone: +9647814154013, e-mail: *rafi.mohammed@stu.edu.iq*, ORCID: *https://orcid.org/0000-0002-1882-0766*.

Ihsan Abdulkareem Abdulhussein,* Professor of Civil Engineering - Hydraulic Structures at Environment and Pollution Engineering Department, Southern Technical University (Basrah, Iraq). He is also a member of particular promotion committee at Basrah Engineering Technical College (Basrah, Iraq) and teaches environmental statistics and wastewater pollution control. His research interests are in the area of seepage under hydraulic structures, composite structures, scour around pile and abutment, seepage through earth dams, optimization, uncertainty, and statistical analysis. Phone:+9647801151917, e-mail: drengihssan@stu.edu.iq, ORCID: *https://orcid.org/0000-0002-0281-0870*
*Corresponding Author drengihssan@stu.edu.iq

Muna A. Hameed, Assistant Lecturer at Survey Department, Technical Institute of Basrah, Southern Technical University. She teaches Engineering Surveying and Mathematics Applications. Her research interests are in composite structures and flow on an open channel. Phone: +9647801234202, e-mail: *mona.hameed@stu.edu.iq*, ORCID: *https://orcid.org/0000-0001-9904-406X*.

Рафи Мохаммед Касим, доцент кафедры энергетики и топливной инженерии Южного технического университета (Басра, Ирак). Его исследовательские интересы связаны с применением гидротехнических сооружений, течением в открытом русле, обтеканием препятствий, проектированием грунтов и фундаментов. Телефон: +9647814154013, электронная почта: rafi.mohammed@stu.edu.iq, ORCID: https://orcid.org/0000-0002-1882-0766.

*Ихсан Абдулкарим Абдул-Хуссейн**, доцент кафедры гражданского строительства – гидротехнические сооружения на факультете экологии и загрязнения окружающей среды Южного технического университета (Басра, Ирак). Он также является членом специального комитета по продвижению в Инженерно-техническом колледже Басры (Басра, Ирак) и преподает статистику окружающей среды и контроль загрязнения сточных вод. Его научные интересы лежат в области фильтрации под гидротехническими сооружениями, составными конструкциями, размывом свай и устоя, просачиванием через земляные дамбы, оптимизацией, неопределенностью и статистическим анализом. Телефон: +9647801151917, электронная почта: drengihssan@stu.edu.iq, ORCID: https://orcid.org/0000-0002-0281-0870
* Автор, ответственный за переписку drengihssan@stu.edu.iq

Муна А. Хамид, ассистент кафедры геодезии, Технический институт Басры, Южный технический университет. Она преподает инженерные изыскания и математические приложения. Ее исследовательские интересы связаны с составными структурами и течением в открытом канале. Телефон: +9647801234202, электронная почта: mona.hameed@stu.edu.iq, ORCID: https://orcid.org/0000-0001-9904-406X.

DOI:10.22337/2587-9618-2024-20-2-60-75

NUMERICAL ANALYSIS OF STRESS-STRAIN STATE OF THE STEEL MODULAR BLOCK WITH CORRUGATED WEBS

Olga A. Tusnina, Anatoliy V. Alekseytsev

National Research Moscow State University of Civil Engineering, Moscow, RUSSIA

Abstract. Modular blocks are widely used in industrial and civil engineering both as stand-alone structures and combined into block-modular buildings. Modular block consists of the load bearing frame, wall fencing, roof and floor decking. The modular block, with wall fencing made of corrugated sheet continuously welded to the beams, is a spatial system, with beams and corrugated webs working together. The steel modular block for the gas pumping unit on a gas turbine power plant is considered in the paper. Assessment of the corrugated web thickness effect on the load bearing capacity of the block is performed. Numerical investigation of stress-strain state of the blocks with different thickness of corrugated web is carried out by the finite element method. The values of the ultimate destructive load on the blocks with different thickness of the corrugated web are determined. The values of the allowable load on the block and the criteria for its limitation have been established depending on the stress-strain state of the block and the causes of destruction.
For comparison, a calculation was made of a block with walls made of sandwich panels that are not included in the work of the frame. It is determined that ultimate load on the block with corrugated webs is 1,5-6 times greater than on the block with wall sandwich panels.

Key words: modular building, steel modular block, corrugated web, critical load, buckling, finite-element analysis

ЧИСЛЕННЫЙ АНАЛИЗ НАПРЯЖЕННО-ДЕФОРМИРОВАННОГО СОСТОЯНИЯ СТАЛЬНОГО МОДУЛЬНОГО БЛОКА СО СТЕНАМИ ИЗ ГОФРИРОВАННОГО ЛИСТА

О.А. Туснина, А.В. Алексейцев

Национальный исследовательский Московский государственный строительный университет, г. Москва, РОССИЯ

Аннотация. Строительство промышленных и гражданских зданий из модульных блоков получает широкое распространение благодаря эффективности и экономичности таких конструкций. Модульные блоки используют как отдельно стоящие сооружения, так и объединяют между собой в блочно-модульные здания. В статье рассмотрен стальной модульный блок газоперекачивающего аппарата на газотурбинной электростанции. Модульный блок, в котором гофрированная стенка, непрерывно приваривается к балкам, представляет собой пространственную систему с совместно работающими балками и стенкой. Выполнен численный анализ влияния толщины гофрированной стенки на несущую способность блока. Определена разрушающая нагрузка на блок и параметры напряженно-деформированного состояния конструктивных элементов блоков при различной толщине гофрированных стенок (1 мм, 2 мм, 2,5 мм и 3 мм). Установлены величины допускаемой нагрузки на блок и критерии ее ограничения, в зависимости от напряженно-деформированного состояния блока и причин разрушения. Для сравнения выполнен расчет блока с навесными стенами из сэндвич-панелей, не включающимися в работу каркаса. Получено, что разрушающая нагрузка для рассмотренных блоков с гофрированными стенками в 1,5-6 раз выше, чем для блока со стеновыми сэндвич-панелями.

Ключевые слова: модульное здание, стальной модульный блок, гофрированная стенка, критическая нагрузка, потеря устойчивости, конечно-элементный расчет

1. INTRODUCTION

Structures made of modular blocks are widely used in civil and industrial construction. Modular blocks are used as standalone structures as well as part of buildings consisting of several blocks.

A typical example of modular structure is shipping container. A standard ISO container represents a spatial block, with its frame composed of main beams and racks welded together. The cold formed hollow rectangular sections are used for beams and racks. The wall fencing of a standard container is made of corrugated sheet with a thickness of 2.5 mm, attached by continuous welds to the upper and lower main beams. Corner fittings are located at the corners of the container at the top and bottom of the columns, transmitting loads to supports and receiving loads from containers placed on top. The block works on a beam scheme with a span equal to its length.

Standard ISO containers can withstand heavy loads, primarily due to the combined action of load-bearing beams and columns with the corrugated sheet. Furthermore, due to the nature of load application on the container: about 80% of the allowable load is transmitted through the corner fittings to the container's columns, and only 20% of the load representing the payload on the container floor from the cargo weight. The permissible maximum weight of a loaded 12-meter container is limited to 30.4 tons [1], while the container can withstand a load of up to 192 tons. Therefore, it is permissible to stack up to 6 containers on top of each other.

When such a container is used as building structures, the load distribution will be different. The roof beams will bear snow load, technical loads from equipment placed on the roof and the payload. Therefore, for the use of standard containers in construction of buildings and structures [2], it is necessary to conduct special studies taking into account the actual structural design of the block, the loads acting on it, and other factors [3]. Several studies are dedicated to the analysis and design of modular blocks. Typical structural solutions for modular blocks are developed for use in building construction [4-7], questions regarding the selection of optimal cross-sections for load-bearing structures of the blocks are studied [7], standard connections between modular blocks are developed [8-10], etc.

When loads are applied to the roof of the container, the main beams experience bending and transfer the loads to the corrugated web. As a result, each plane of the longitudinal walls of the block can be represented as a beam with a corrugated web [11-15], where the flanges are the top and bottom longitudinal beams of the block frame. The load-bearing capacity of beams with corrugated webs is influenced by the shape of the corrugations, the presence, shape, and location of openings in the web [16-20].

Studying the influence of the profile and thickness of the corrugated web, the presence of door and window openings, as well as the localization and magnitude of the applied loads on the stress-strain state of the modular block is a relevant and practically significant task.

This article presents a numerical study of the stress-strain state of a steel modular block for a gas pumping unit on a gas turbine power plant. Blocks with different thicknesses of corrugated webs loaded with local and full roof loads were analyzed.

2. METHODS

Modular block for gas pumping unit (GP-block) is a space structure with sizes 12x3,2x3,2 m (length (L) x width (b) x height (H)). There are 4 support points in the corners of the block. Generally, block can be represented as a beam with the span 12 m. Distinctive feature of the considered block is its big height H in comparison to the span L: span to height ratio (L/H) of the block is 3,75. Beams with values of L/H ratio below 5 ($L/H < 5$) are deep beams. For deep beams the fundamental principle that a plane section before bending remains plane after bending is violated. For beams with small span-

to-height ratio section warping should be taken into account. Stress distribution across the section of the deep beam is nonlinear due to the shear warping of the cross-section.

The considered block contains openings in the walls and roof, unlike standard ISO containers. Furthermore, the height and width of the GP-block are larger than the dimensions of standard containers.

The main beams and racks of the frame are constructed from cold-formed welded rectangular hollow sections. Walls of the block consists of corrugated sheets continuously welded to the top and bottom main beams. The floor and roof decking are made of flat steel sheets with a thickness of t=4 mm with L-stiffeners. The steel sheet is supported by secondary beams with hollow rectangular sections welded to the main longitudinal frame beams. In the roof there is a rectangular opening with sizes 3,2x4,9 m for tube of gas pumping equipment.

Structures of the considered block are made of steel S255 (GOST 27772-2015). Normative yielding stress is R_{yn}=245 MPa.

Numerical analyses of the stress-strain state of the blocks with various corrugated web thicknesses have been conducted.

A finite element model of the GP-block has been developed using the computational program Simcenter Femap and depicted in Figure 1. The models with corrugated web thicknesses of 1 mm, 2 mm, 2,5 mm and 3 mm are considered.

Corrugated webs, roof and floor sheets, sections of the main beams are modeled by PLATE finite elements. The racks, secondary beams and stiffeners of the flat sheets are modeled by BEAM finite elements. Boundary conditions include constraints to prevent displacements in all linear directions at the four bottom corners of the block.

In addition to the cases with different corrugated sheets on the walls, an analysis was conducted on the model without corrugated webs to estimate the effect of the corrugated web presence on the stress-strain state of the block. In this case, the block has walls made of sandwich panels, which are hung on the frame structures and practically do not participate in load distribution. So, their effect on the behavior of the block can be neglected.

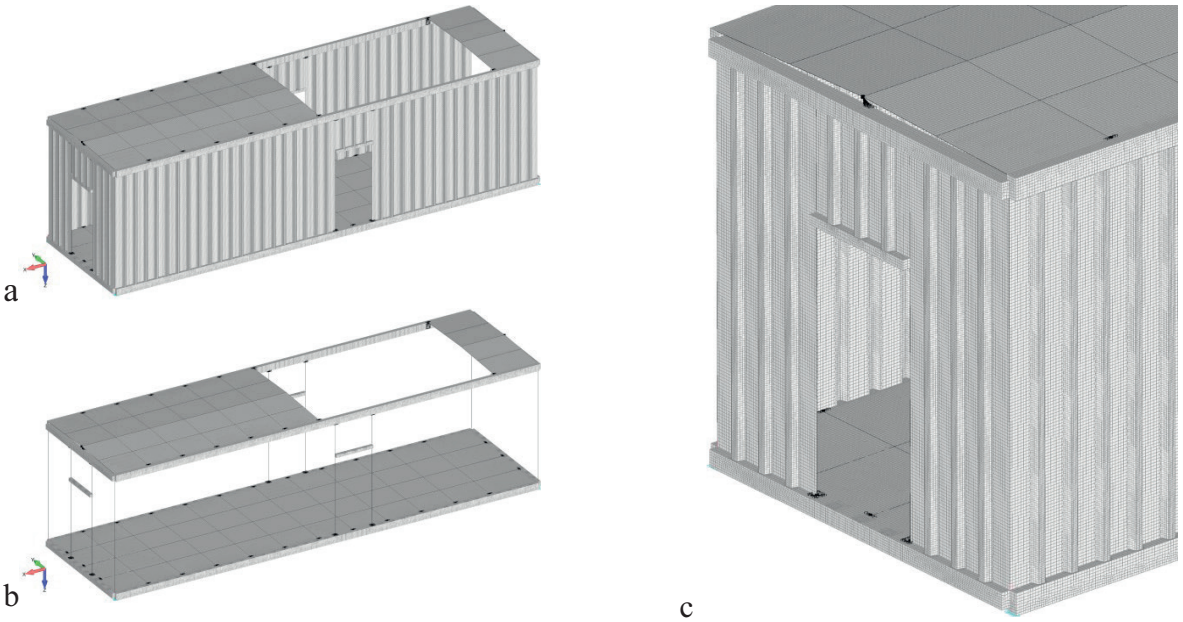


Figure 1. Finite-element model of block for gas pumping unit: a – with corrugated webs; b – without corrugated web (block with wall sandwich panels); c - fragment

Two loading schemes of the blocks are considered: “full load” – payload over the entire area of the roof and “local load” – payload over the local area of the roof. The uniform load was applied to the top longitudinal beam. (fig. 2).

Geometrical and physical nonlinear analyses have been made. Stress-strain curve for steel S255 according SP 16.13330.2017 is taken into analysis and shown on fig. 3. The values of stress and strain in the key points of the diagram are represented in table 1.

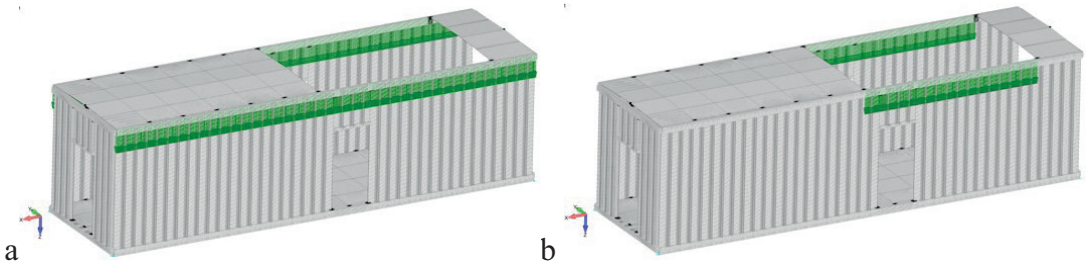


Figure 2. Schemes of loading: a – “full load”; b – “local load”

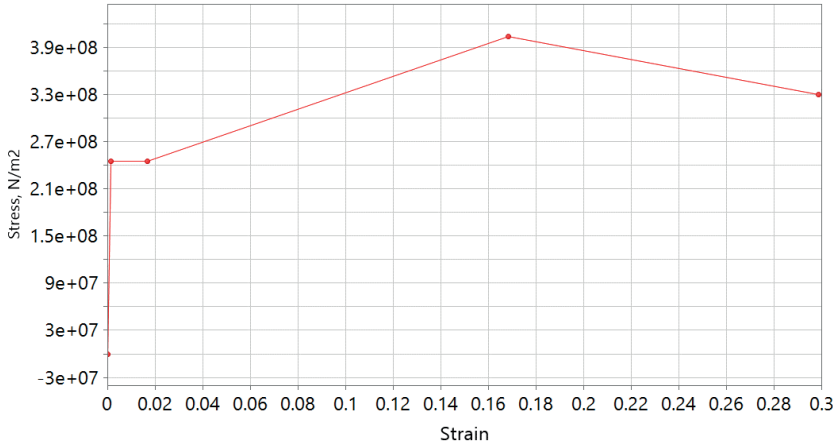


Figure 3. Stress–strain curve for steel S255 taken into analysis

Table 1. Characteristics of steel S255

Point of curve	$\bar{\varepsilon} = \varepsilon E / R_{yn}$	$\bar{\sigma} = \sigma / R_{yn}$	ε	σ, MPa
Yield strength (Beginning of yield plateau)	1	1	0,00119	245
End of yield plateau	14	1	0,01665	245
Ultimate strength	141,6	1,653	0,16840	404,99
Fracture	251	1,35	0,29850	330,75

The geometrically nonlinear analysis was performed using the step-by-step iterative method (ITER), with the following parameters: number of increments – 40, iterations before update – 25, convergence tolerances by load - 0.001.

The buckling and yielding criteria are established to determine the ultimate load on the particular structural elements of the block and on the block as whole.

Theoretically, the buckling criterion can be defined as a sudden increase in displacement

increment $\Delta\delta$ at a constant load increment ΔP. Buckling can be identified on the graph as the inflection point of the displacement-load curve. The load corresponds to a sudden change in the slope of the tangent line to the displacement-load curve is considered the ultimate load according to the buckling criterion for the particular structural element.

The following equation is proposed to define the **buckling criterion**:

$$\frac{tg\alpha_{i+1}}{tg\alpha_i} \geq 3, \qquad (1)$$

where $tg\alpha_{i+1} = \frac{\Delta\delta_{i+1}}{\Delta P_{i+1}}$, $tg\alpha_i = \frac{\Delta\delta_i}{\Delta P_i}$ - tangents of the displacement-load curve on the (i+1)-step and i-step of load increment, respectively.

Assuming a constant load increment $\Delta P_i = \Delta P_{i+1} = const$ equation (1) for the buckling criterion can be written as follows:

$$\frac{\Delta\delta_{i+1}}{\Delta\delta_i} \geq 3, \qquad (2)$$

where $\Delta\delta_{i+1}$ and $\Delta\delta_i$ - displacement increments at the (i+1)-step and i-step of the load increment ΔP_i. respectively.

The graphical interpretation of the buckling criterion is depicted on fig. 4.

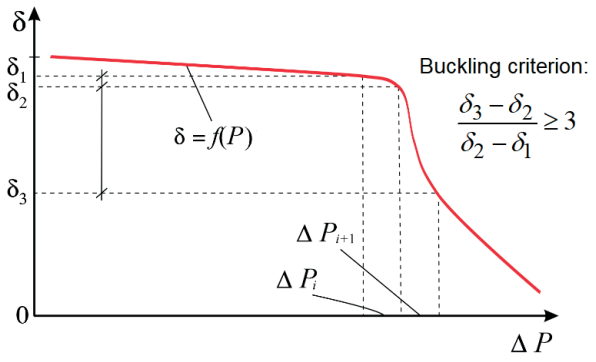


Figure 4. Graphical interpretation of the buckling criterion

To define the **yielding criterion**, we adopt the following condition: the criterion of yielding is met when the values of Von Mises strain ε falling within the specified range:

$$R_y / E \leq \varepsilon < \varepsilon_u \qquad (3)$$

where R_y – design resistance of steel determined based on the nominal value of yield strength; E=210000 N/mm^2 – modulus of elasticity of the steel; ε_u – ultimate strain corresponding to the ultimate tensile strength.

3. RESULTS AND DISCUSSION

In the results of carried out analyses the stress-strain state of the block with different corrugated web thickness is defined depending on load value and scheme of loading ("full load" or "local load"). The stress-strain parameters of the block structures in the key positions are determined (fig. 5):

- Von Mises stress and horizontal transverse (Y-direction) displacement of the corrugated web in the corner support zone (pos. A);
- Von Mises stress and horizontal transverse (Y-direction) displacement of the top longitudinal beam in the span (pos. B);
- Von Mises stress and vertical (Z) displacement of the roof sheet between stiffeners (pos. C).

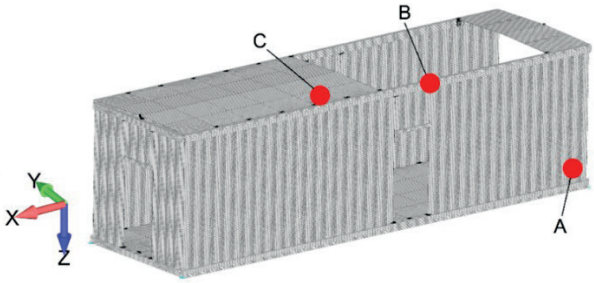


Figure 5. Key positions for determine stress-strain state of the block

Diagrams of displacement and Von Mises stress dependence from load in the key positions of the top longitudinal beam and corrugated web are represented on fig. 6 and 7. Curves depicted results for loading scheme "full load" are drawn by continuous line and for loading scheme "local load" - by dashed line.

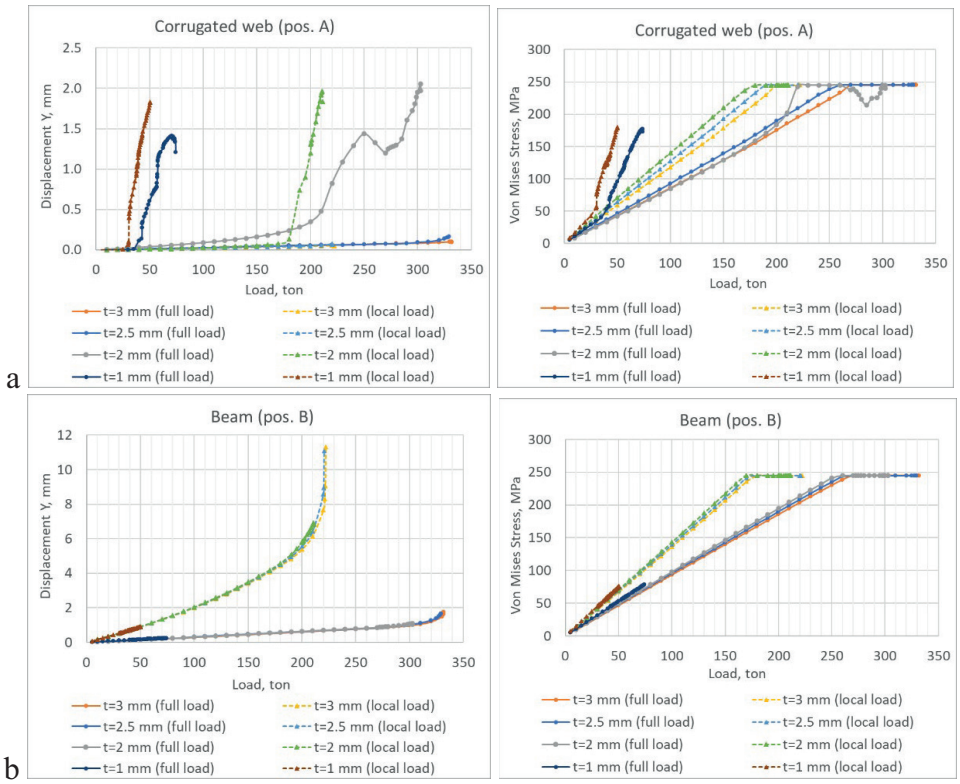


Figure 6. Displacement – Load curves and Von Mises stress – Load curves in the key positions of the blocks: a – corrugated web; b – top longitudinal beam

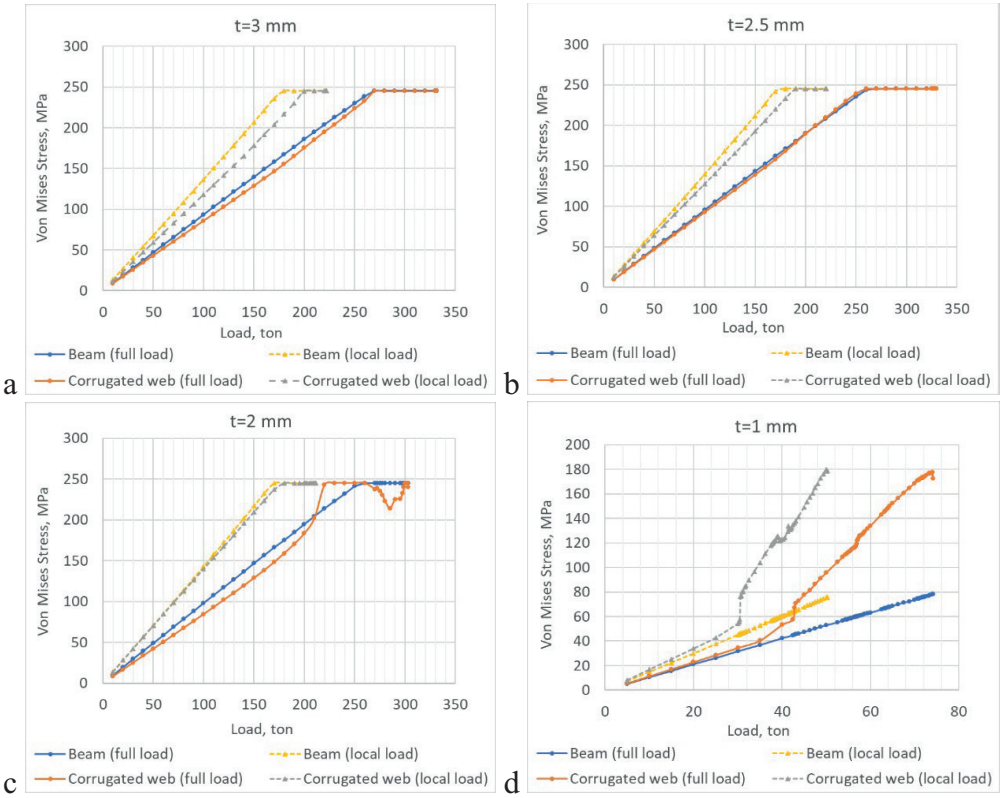


Figure 7. Von Mises stress – Load curves for blocks with corrugated web thickness (t): a – t=3 mm; b – t=2.5 mm; c – t=2 mm; d – t=1 mm

Von Mises stress in the key positions of the structural elements of the considered blocks are represented in table 3.

The values of ultimate load P_{ult} for the considered modular blocks are obtained in the results of numerical analyses and represented in table 4. Ultimate load for each structural element and block entire is the load when buckling or yielding criterion for the appropriate structure is reached – see equation (1-3) and fig. 4.

Table 3. Von Mises stress in the structural elements of considered modular blocks

Corrugated web thickness	Load, ton	Von Mises stress, MPa					
		Roof sheet (pos. C)		Top longitudinal beam (pos. B)		Corrugated web (pos. A)	
		Full load	Local load	Full load	Local load	Full load	Local load
t=1 mm	30	7,41	6,40	31,62	45,06	34,42	54,42
	40	9,94	8,54	42,14	60,26	53,12	122,70
	50	12,48	10,67	52,65	75,40	95,59	179,72
	50,3	-	10,74	-	75,87	-	178,88
	70	17,75	-	73,72	-	168,50	-
	74,2	18,89	-	78,16	-	172,45	-
t=2 mm	50	12,14	10,72	49,21	70,86	42,10	70,71
	130	37,83	28,21	127,34	187,37	110,67	181,35
	160	62,90	38,43	156,43	232,49	138,22	223,83
	170	71,73	54,83	166,07	245,00	148,22	237,17
	180	79,48	67,47	175,69	245,00	159,11	245,00
	210	98,10	91,00	204,30	245,00	202,08	245,00
	211,2	-	90,66	-	245,00	-	245,00
	220	103,38	-	213,75	-	245,00	-
	260	122,85	-	245,00	-	245,00	-
	300	142,53	-	245,00	-	245,00	-
	302,8	143,16	-	245,00	-	239,88	-
t=2,5 mm	50	12,06	10,71	47,97	69,07	46,47	64,21
	130	37,32	27,99	124,10	182,54	120,33	165,82
	160	62,00	36,28	152,43	226,41	148,31	206,23
	180	78,71	67,39	171,17	245,00	167,98	233,40
	190	85,59	76,74	180,50	245,00	178,59	245,00
	220	102,70	97,12	208,26	245,00	209,44	245,00
	220,6	-	97,64	-	245,00	-	245,00
	260	122,05	-	245,00	-	245,00	-
	325	154,03	-	245,00	-	245,00	-
	329,7	156,83	-	245,00	-	245,00	-
t=3 mm	50	11,99	10,69	46,93	67,54	42,98	59,25
	130	36,93	27,82	121,39	178,41	111,43	153,50
	160	61,30	34,41	149,08	221,23	137,60	191,72
	180	78,11	67,14	167,40	245,00	155,48	216,82
	200	91,24	84,32	185,60	245,00	175,26	245,00
	220	102,20	97,05	203,66	245,00	195,11	245,00
	222,1	-	98,50	-	245,00	-	245,00
	270	126,18	-	245,00	-	245,00	-
	330	155,65	-	245,00	-	245,00	-
	331,8	156,66	-	245,00	-	245,00	-
Without corrugated web	10	26,80	20,54	50,56	102,49	-	-
	20	85,16	83,11	130,94	245,00	-	-
	30	207,17	101,28	245,00	245,00	-	-
	40	245,00	88,39	245,00	245,00	-	-
	50	245,00	-	245,00	-	-	-

For example, buckling of the top longitudinal beam and corrugated web is characterized by an abrupt increase of its Y-displacements. This can be observed on the displacement-load curves (fig. 6).

The yielding criterion for structural element is determined by the load applied to the block that causes the yield stress in structural element (see fig. 7).

In the table 4, cells containing the ultimate load, corresponding to the earliest attainment of the buckling or yielding criterion for one of the structural elements are highlighted in color. This load can be used as allowable load - the upper limit to the load that can be applied to the block without causing failure of its structural elements.

Table 4. Ultimate load P_{ult} for the considered modular blocks

Corrugated web thickness	Structural element	Ultimate load P_{ult}, ton		Criterion
		Full load	Local load	
t=1 mm	Roof sheet	-	-	-
	Corrugated web	**40**	**30**	**Buckling**
		-	-	Yielding
	Top longitudinal beam	-	-	-
	Block entire	74,2	50,3	Buckling of the corrugated web
t =2 mm	Roof sheet	130	160	Buckling
	Corrugated web	**210**	**170**	**Buckling**
		220	180	Yielding
	Top longitudinal beam	-	210	Buckling
		260	170	Yielding
	Block entire	302,8	211,2	Buckling of the corrugated web
t =2,5 mm	Roof sheet	130	160	Buckling
	Corrugated web	-	-	Buckling
		260	190	Yielding
	Top longitudinal beam	325	220	Buckling
		260	**180**	**Yielding**
	Block entire	329,6	220,6	Buckling of the top longitudinal beam
t=3 mm	Roof sheet	130	160	Buckling
	Corrugated web	-	-	Buckling
		270	200	Yielding
	Top longitudinal beam	330	220	Buckling
		270	**180**	**Yielding**
	Block entire	331,8	222,1	Buckling of the top longitudinal beam
Without corrugated web	Roof sheet	40	-	Yielding
	Top longitudinal beam	50	40	Buckling
		27,5	**20**	**Yielding**
	Block entire	50	40	Buckling of the top longitudinal beam

Depending on the corrugated web thickness the following types of failure modes of the block are defined (fig. 8):

- 1st type: destruction of the corrugated web (buckling);
- 2nd type: destruction of the top longitudinal beams (yielding and subsequent buckling).

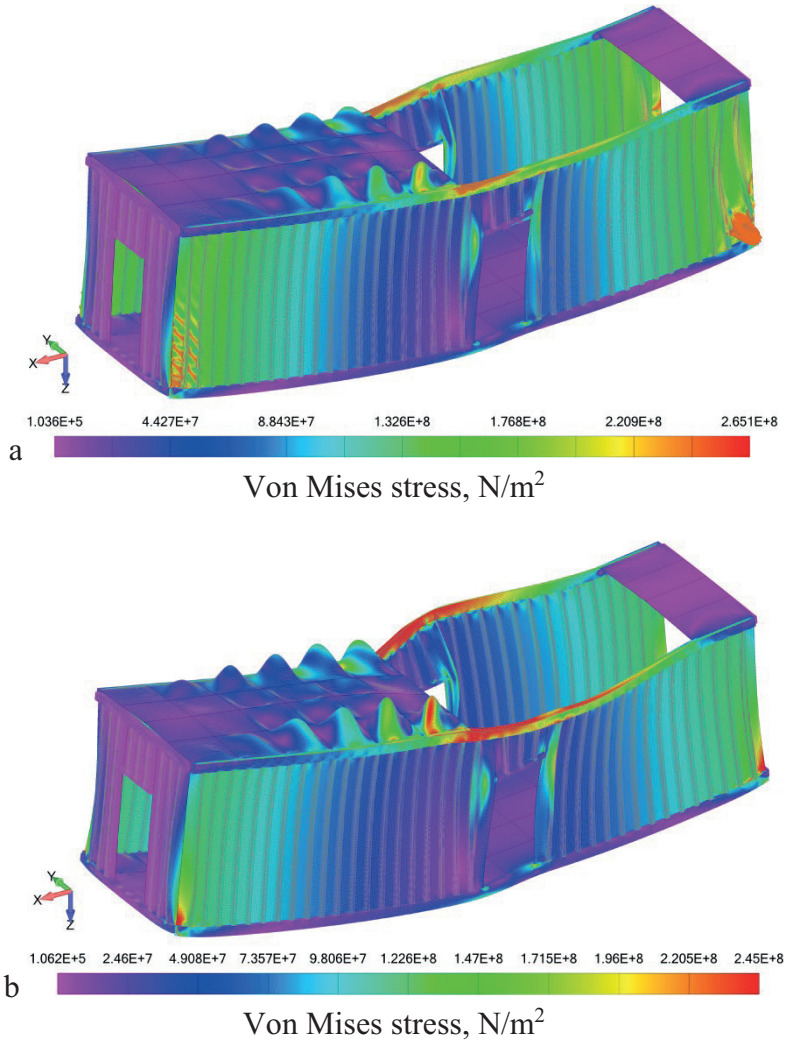


Figure 8. Failure modes of the block: a – buckling of the corrugated web (corrugated web thickness 2 mm); b – destruction of the top longitudinal beam (corrugated web thickness 3 mm)

The failure of the blocks with 2,5 mm and 3 mm thick corrugated web is caused by destruction of the top longitudinal beams and correspond to 1st type of failure mode. The ultimate load for loading scheme "full load" is about 330 tons and for scheme "local load" – 220 tons. This is the critical buckling load for top longitudinal beams. Yielding of the top longitudinal beams and corrugated web is observed before failure of the block. Buckling of the corrugated web 2,5 mm and 3 mm thick is not reached during the loading.

The failure of the blocks with corrugated web 1 mm and 2 mm thick is occurred by 1st type because of the corrugated web buckling. When the load reaches some critical value, the corrugated web begin bulges out from the plane of the block wall in the corner zones near the supports. Mainly the shear stresses cause local buckling of the corrugated web. At the same

time, the block overall retains its load-bearing capacity. With increasing load, the area of the corrugated web experienced buckling increases. The finite element analysis continues until the ultimate load is reached, at which complete failure of the block occurs.

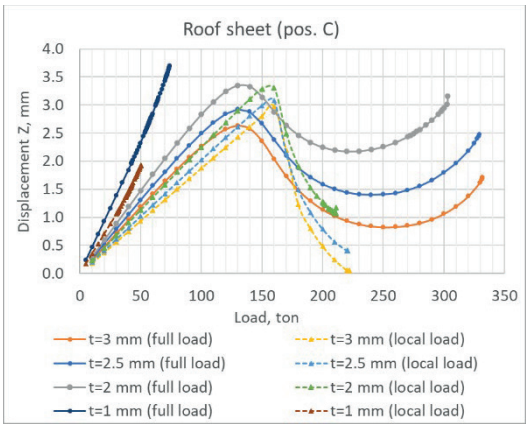
With a corrugated web thickness of 2 mm, yielding is observed at a load of 220 tons, while at a load of 260 tons, yield stress is noted in the top longitudinal beams. With a corrugated web thickness of 1 mm, the load causing yielding is not reached for all structural elements until failure of the block.

The values of ultimate load on the block loaded by “local load” scheme are on average 25% lower in comparison with “full load” loading scheme.

It should be noted that during the loading process, there is a local loss of stability in certain sections of the roof sheet (fig. 9).

In all loading scenarios of the block under the "full load" scheme, the critical load for the roof sheet was 130 tons, while under the "local load" scheme, it was 160 tons. Areas of the decking that have buckle are taken out of operation, but overall, the block retains its load-bearing capacity and can withstand further increases in load. Therefore, the buckling of the roof sheet was not considered as a criterion for limiting the allowable load on the block.

a



b

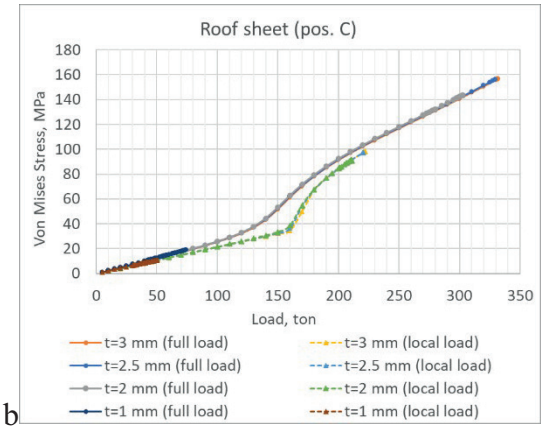


Figure 9. Diagrams for roof sheet: a – displacement-load curves; b – Von Mises stress – load curves

The failure of the block without the corrugated web occurs due to the buckling of the top longitudinal beam. The ultimate load for calculating a block without the corrugated web is 1.5-6 times lower than for a block with a corrugated web (see Table 4).

The corrugated web significantly reduces the stresses in the beams. For example, under a load of 50 tons according to the "full load" scheme, the stresses in the beams of a block without the corrugated web are 245 MPa, which corresponds to the yield stress. With the presence of the corrugated web, the Von Mises stress determined in the beam under the same load is on average 5 times lower (see fig. 10). At the same time, the thickness of the corrugated web has a negligible effect on the stress value in the beam (see Table 5).

Table 5. Comparison of the Von Mises stress in the structural elements of block with and without corrugated web

Structural element	Loading scheme	Corrugated web thickness				
		Without corrugated web	t=1 mm	t=2 mm	t=2,5 mm	t=3 mm
Top longitudinal beam	Full load	245,00	52,65	49,21	47,97	46,93
	Local load	-	75,40	70,86	69,07	67,54
Roof sheet	Full load	245,00	12,48	12,14	12,06	11,99
	Local load	-	10,67	10,72	10,71	10,69

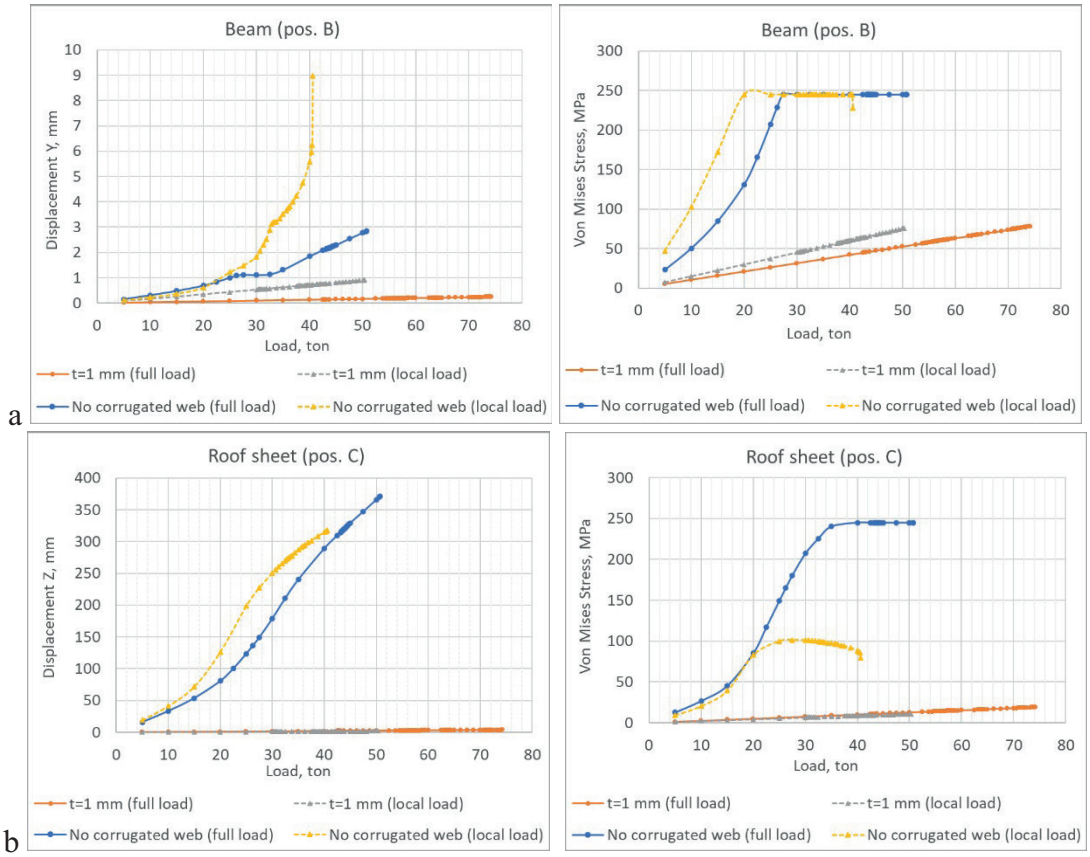


Figure 10. Comparative diagrams for blocks with and without corrugated webs: a – top longitudinal beam; c – roof sheet

Table 6 shows the values of the maximum allowable load on the block P_{max} and the ultimate load P_{ult} that caused block failure, as obtained in the results of the carried-out finite-element analyses. To ensure the necessary reliability of the structures, the allowable load on the block P_{max} is taken as 95% of the ultimate load, corresponding to the earliest attainment of the buckling or yielding criterion (see highlighted cells in table 4). For web thicknesses of 1 mm and 2 mm, the allowable load was limited by buckling criterion corresponding to the onset of local buckling of the corrugated web. For larger web thicknesses (2.5 mm and 3 mm), the limitation of allowed load is adopted by the yielding criterion, which is the onset of yielding strain in the top longitudinal beams.

Table 6. Allowable and ultimate load on the block

Corrugated web thickness	Allowable load P_{max}, ton		Ultimate load P_{ult}, ton		Criterion
	Full load	Local load	Full load	Local load	
Without corrugated web	25	19	50,8	40,6	Yielding of the top longitudinal beam
t=1 mm	38	28	74,2	50,3	Buckling of the corrugated web
t =2 mm	199	161	302,8	211,2	Buckling of the corrugated web
t =2,5 mm	247	161	329,6	220,6	Yielding of the top longitudinal beam
t=3 mm	256	171	331,8	222,1	Yielding of the top longitudinal beam

The adopted limitation of the allowable load on the block that provided in table 6, ensures a reserve of block load-bearing capacity, amounting to 49%, 34%, 25%, and 22% for blocks with corrugated web thicknesses of 1 mm, 2 mm, 2.5 mm, and 3 mm, respectively. The calculation results showed that local buckling of the corrugated web does not lead to complete failure if the block, and the block is able to withstand increased loads. Experimental tests on full-scale specimens of beams with corrugated webs [21, 22] also indicate that a beam with a partially buckled web retains its load-bearing capacity.

The presence of reserves allows ensuring the reliability of the block and increases its resistance to various emergency situations associated with the disruption of normal equipment operation, sudden changes in loads, explosions, and impacts [23].

The prospects for further research include the development of methods and tools for practical calculation of modular block structures.

Finite-element computational models of various levels of detail (LOD-cm) are used in design [24]. The use of highly detailed finite-element models for practical design is not always justified due to their complexity. In such cases, simplified equivalent models that describe the actual stress-strain state of the structure with sufficient engineering accuracy are used. For example, the corrugated web of beams can be replaced with an equivalent flat sheet [25, 26] or beam elements. A similar approach can be applied for the analysis of the stress-strain state of the modular blocks. For this purpose, based on numerical studies using high-detailed computational models, it is necessary to determine the characteristics of simplified equivalent models.

Another way to solve the practical problem of a modular block design is to use artificial intelligence, which can predict the stress-strain state and load-bearing capacity of the block based on given input parameters such as block dimensions, corrugated web thickness, applied load, etc.

4. CONCLUSIONS

As a result of the carried out numerical studies of the stress-strain state of the modular block for gas pumping unit, the following findings are obtained:

1. The load-bearing capacity of the considered modular blocks with corrugated webs is 1.5-6 times higher than that of a block with hanging wall cladding, such as sandwich panels.
2. The corrugated web, continuously welded to the beams, significantly relieves the beams, reducing stresses in them by 5 times compared to the case of its absence.
3. The following failure modes of the blocks with corrugated webs are defined:
- 1st type: destruction of the corrugated web (buckling) - observed for the blocks with corrugated web thicknesses of 1 mm and 2 mm);
- 2nd type: destruction of the top longitudinal beams (yielding and subsequent buckling) - observed for the blocks with corrugated web thicknesses of 2.5 mm and 3 mm).
4. Criteria for limiting the allowable load on the modular block are defined depending on the type of failure mode. The allowable load is taken as 95% of the ultimate load causes either yielding stress in the top longitudinal beams or buckling of the corrugated web.
5. The values of the maximum allowable load on the block with different thicknesses of the corrugated web and without it are determined based on the adopted criteria. Limiting the load on the block by allowable value provides a reserve of load-bearing capacity of the block ranging from 49% to 22% for corrugated web thicknesses from 1 to 3 mm, respectively.
6. The type and localization of the payload on the block affect its load-bearing capacity. The ultimate load on the block loaded by the "local load" scheme is on average 25% lower compared to the "full load" loading scheme.

REFERENCES

1. **Turkay Y.** (2019) Design and analysis of a lightweight composite shipping container made of carbon fiber laminates. *Logistics*, vol. 3, no. 3, 18.
2. **Kotnik J.** (2008) *Container architecture*, Barcelona: Links Books.
3. **Giriunas K., Sezen H., Dupaix R.B.** (2012) Evaluation, modeling, and analysis of shipping container building structures. *Engineering Structures*, vol. 43, pp. 48-57.
4. **Tusnin A.R.** (2017) Stal'noy karkas maloetazhnogo zdaniya [Steel framework of a low-rise building]. *Industrial and Civil Engineering*, no. 11, pp. 18-22. (In Russ.).
5. **Tusnin A.R., Varaksin P.A.** (2018) Tipovoy stal'noy karkas pyatietazhnogo zdaniya [Standard Steel Frame of a 5-Story]. *Industrial and Civil Engineering*, no. 10, pp. 45-49. (In Russ.).
6. **Su M., Yang B., Wang X.** (2022) Research on integrated design of modular steel structure container buildings based on BIM. *Advances in Civil Engineering*, vol. 2022, 4574676.
7. **Ha T.-H., Cho B.-H., Kim H., Kim D.-J.** (2016) Development of an efficient steel beam section for modular construction based on six-sigma. *Advances in Materials Science and Engineering*, vol. 2016, 9687078.
8. **Nadeem G., Safiee N.A., Abu Bakar N., Abd Karim I., Mohd Nasir N. A.** (2021) Connection design in modular steel construction: A review. *Structures*, vol. 33, pp. 3239-3256.
9. **Ma H., Huang Z., Song X., Ling Y.** (2023) A Study on Mechanical Performance of an Innovative Modular Steel Building Connection with Cross-Shaped Plug-In Connector. *Buildings*, vol. 13, no. 9, 2382.
10. **Tusnina O.A.** (2017) Konstruktivnye resheniya uzlov stal'nogo karkasa dlya maloetazhnykh zhilykh zdaniy [Structural Solutions of Joints of a Steel Frame for Low-Rise Residential Buildings]. *Industrial and Civil Engineering*, 2017, no. 11, pp. 23-27. (In Russ.).
11. **Gataullina K.R.** (2023) Effektivnost' primeneniya balok s gofrirovannoy stenkoy v balochnoy kletke [Efficiency of using beams with corrugated webs in a beam platform]. *Young Scientist*, no. 20 (467), pp. 85-90. (In Russ.).
12. **Bryantsev A.A., Absimetov V.E., Lalin V.V.** (2017) Effektivnost' primeneniya dvutavrov s gofrirovannymi stenkami v proizvodstvennykh zdaniyakh [Effective application of I-beams with corrugated webs in the industrial building]. *Construction of Unique Buildings and Structures*, no. 3(54). pp. 93-104. (In Russ).
13. **Bal'zannikov M.I., Kholopov I.S., Solov'ev A.V., Lukin A.O.** (2013) Primenenie stal'nykh balok s gofrirovannoy stenkoy v gidrotekhnicheskikh sooruzheniyakh [Using Steel Beams with Corrugated Web in Hydraulic Structures]. *Vestnik MGSU*, no. 11, pp. 34-41. (In Russ.).
14. **Tian Z.** (2023) Review of Research on Corrugated Web Steel Beams. *Journal of Engineering Mechanics and Machinery*, vol. 8(4), pp. 11-14.
15. **Al-Kannoon M.A., Suhiel I.A.** (2020) Experimentally flexural behaviour study of steel beams with corrugated webs. *IOP Conf. Series: Materials Science and Engineering*, vol. 888, 012084.
16. **Solov'ev A.V., Lukin A.O., Alpatov V.Yu., Savost'yanov V.N.** (2012) Uchet osobennostey raboty balok s gofrirovannoy stenkoy v raschetakh na stesnennoe kruchenie [Account for performance of corrugated web beams in the analysis of constrained torsion]. *Vestnik MGSU*, no. 11, pp. 105-112. (In Russ.).
17. **Al-Mawashee H.S. and Al-Kannoon M.A.-A.** (2021) Flexural Strength of Castellated Beams with Corrugated Webs. *Journal of Physics: Conference Series*, vol. 1973, 012213.

18. **Elamary A.S., Saddek A.B., Alwetaishi M.** (2017) Effect of corrugated web on flexural capacity of steel beams. *International Journal of Applied Engineering Research*, vol. 12(4), pp. 470-481.
19. **Kumar U.M., Reddy D.P., Patel R.R., Pandian M.S., Karthikeyan K.** (2018) A study on flexural capacity of steel beams with corrugated web. *International Journal of Civil Engineering and Technology*, vol. 9(4), pp. 679-689.
20. **Kudryavtsev S.** (2018) Influence of web openings on bearing capacity of triangularly corrugated web beam. *IOP Conf. Series: Materials Science and Engineering*, vol. 365, 042034.
21. **Zubkov V., Lukin A., Alpatov V.** (2018) Experimental research of beams with corrugated web. *MATEC Web of Conferences*, vol. 196, 01005.
22. **Zubkov V.A., Lukin A.O.** (2013) Eksperimental'nye issledovaniya vliyaniya tekhnologicheskikh i konstruktsionnykh parametrov na nesushchuyu sposobnost' metallicheskikh balok s gofrirovannoy stenkoy [Experimental research into the influence produced by processrelated and structural parameters on the bearing capacity of metal beams with corrugated webs]. *Vestnik MGSU*, no. 2, pp. 37-46. (In Russ.).
23. **Alekseytsev A.V.** (2023) Ensuring the safety of steel moment frames subjected to uncertain impacts. *Buildings,* vol. 13, no. 8, 2038.
24. **Tusnina O., Alekseytsev A.** (2023) LOD of a computational numerical model for evaluating the mechanical safety of steel structures. *Buildings*, vol. 13, no. 8, 1941.
25. **Sherman D., Fisher J.** (1971) Beams with corrugated webs. Proceedings of the *1st International Specialty Conference on Cold-Formed Steel Structures (Rolla, Missouri, August 19-20, 1971)*, pp. 198-204.
26. **Ye Z., Berdichevsky V.L., Yu W.** (2014) An equivalent classical plate model of corrugated structures. *International Journal of Solids and Structures*, vol. 51(11-12), pp. 2073-2083.

СПИСОК ЛИТЕРАТУРЫ

1. **Turkay Y.** (2019) Design and analysis of a lightweight composite shipping container made of carbon fiber laminates // Logistics, 2019, Vol. 3, no. 3, 18.
2. **Kotnik J.** Container architecture. Links Books, Barcelona, 2008, 253 pages.
3. **Giriunas K., Sezen H., Dupaix R.B.** Evaluation, modeling, and analysis of shipping container building structures // Engineering Structures, 2012, Vol. 43, pp. 48-57.
4. **Туснин А.Р.** Стальной каркас малоэтажного здания // Промышленное и гражданское строительство, 2017, № 11. С. 18-22.
5. **Туснин А.Р., Вараксин П.А.** Типовой стальной каркас пятиэтажного здания // Промышленное и гражданское строительство, 2018, № 10. С. 45-49.
6. **Su M., Yang B., Wang X.** Research on integrated design of modular steel structure container buildings based on BIM // Advances in Civil Engineering, 2022, Vol. 2022, 4574676.
7. **Ha T.-H., Cho B.-H., Kim H., Kim D.-J.** Development of an efficient steel beam section for modular construction based on six-sigma // Advances in Materials Science and Engineering, 2016, Vol. 2016, 9687078.
8. **Nadeem G., Safiee N.A., Abu Bakar N., Abd Karim I., Mohd Nasir N. A.** Connection design in modular steel construction: A review // Structures, 2021, Vol. 33, pp. 3239-3256.
9. **Ma H., Huang Z., Song X., Ling Y.** A Study on Mechanical Performance of an Innovative Modular Steel Building

Connection with Cross-Shaped Plug-In Connector // Buildings, 2023, Vol. 13, no. 9, 2382.
10. **Туснина О.А.** Конструктивные решения узлов стального каркаса для малоэтажных жилых зданий // Промышленное и гражданское строительство. 2017. № 11. С. 23-27.
11. **Гатауллина К.Р.** Эффективность применения балок с гофрированной стенкой в балочной клетке // Молодой ученый, 2023, № 20(467). С. 85-90.
12. **Брянцев А.А., Абсиметов В.Э., Лалин В.В.** Эффективность применения двутавров с гофрированными стенками в производственных // Строительство уникальных зданий и сооружений, 2017, №3 (54). С. 93-104.
13. **Бальзанников М.И., Холопов И.С., Соловьев А.В., Лукин А.О.** Применение стальных балок с гофрированной стенкой в гидротехнических сооружениях // Вестник МГСУ, 2013, № 11. С. 34-41.
14. **Tian Z.** Review of Research on Corrugated Web Steel Beams // Journal of Engineering Mechanics and Machinery, 2023, Vol. 8(4), pp. 11-14.
15. **Al-Kannoon M.A., Suhiel I.A.** Experimentally flexural behaviour study of steel beams with corrugated webs // IOP Conf. Series: Materials Science and Engineering, 2020, Vol. 888, 012084.
16. **Соловьев А.В., Лукин А.О., Алпатов В.Ю., Савостьянов В.Н.** Учет особенностей работы балок с гофрированной стенкой в расчетах на стесненное кручение // Вестник МГСУ, 2012, № 11. С. 105-112.
17. **Al-Mawashee H.S. and Al-Kannoon M.A.-A.** Flexural Strength of Castellated Beams with Corrugated Webs // Journal of Physics: Conference Series, 2021, Vol. 1973, 012213.
18. **Elamary A.S., Saddek A.B., Alwetaishi M.** Effect of corrugated web on flexural capacity of steel beams // International Journal of Applied Engineering Research, 2017, Vol. 12(4), pp. 470-481.
19. **Kumar U.M., Reddy D.P., Patel R.R., Pandian M.S., Karthikeyan K.** A study on flexural capacity of steel beams with corrugated web // International Journal of Civil Engineering and Technology, 2018, Vol. 9(4), pp. 679-689.
20. **Kudryavtsev S.** Influence of web openings on bearing capacity of triangularly corrugated web beam // IOP Conf. Series: Materials Science and Engineering, 2018, Vol. 365, 042034.
21. **Zubkov V., Lukin A., Alpatov V.** Experimental research of beams with corrugated web // MATEC Web of Conferences, 2018, Vol. 196, 01005.
22. **Зубков В.А., Лукин А.О.** Экспериментальные исследования влияния технологических и конструкционных параметров на несущую способность металлических балок с гофрированной стенкой // Вестник МГСУ, 2013, №. 2. С. 37-46.
23. **Alekseytsev A.V.** Ensuring the safety of steel moment frames subjected to uncertain impacts // Buildings, 2023, Vol. 13, no. 8, 2038.
24. **Tusnina O., Alekseytsev A.** LOD of a computational numerical model for evaluating the mechanical safety of steel structures. Buildings, 2023, Vol. 13, no. 8, 1941.
25 **Sherman D., Fisher J.** Beams with corrugated webs // Proceedings of the 1st International Specialty Conference on Cold-Formed Steel Structures. Rolla, Missouri, August 19-20, 1971, pp. 198-204.
26. **Ye Z., Berdichevsky V.L., Yu W.** An equivalent classical plate model of corrugated structures // International Journal of Solids and Structures, 2014, Vol. 51(11-12), pp. 2073-2083.

Olga A. Tusnina, docent, PhD, Associated Professor of the Department "Metal and timber structures"; National Research Moscow State University of Civil Engineering (NRU MGSU); Russia, 129337 Moscow, Yaroslavskoe sh., 26. Tel. +7 (495) 287-49-14 ext. 3005; e-mail: TusninaOA@mgsu.ru. Scopus ID: 55975424400; Researcher ID: U-7848-2018; ORCID: 0000-0002-5595-2784.

Anatoliy V. Alekseytsev, docent, DSc, Professor of the Department «Industrial and civil engineering», Associated Professor of the Department "Reinforced concrete and stone structures"; National Research Moscow State University of Civil Engineering (NRU MGSU); Russia, 129337 Moscow, Yaroslavskoe sh., 26. Tel. +7 (495) 287-49-14 ext. 3036; e-mail: AlekseytsevAV@ mgsu.ru. Scopus ID: 57191530761; Researcher ID: I-3663-2017; ORCID: 0000-0002-4765-5819.

Туснина Ольга Александровна, доцент, кандидат технических наук, доцент кафедры «Металлические и деревянные конструкции»; Национальный исследовательский московский государственный строительный университет (НИУ МГСУ); Россия, 129337 Москва, Ярославское шоссе, 26. Тел. +7 (495) 287-49-14 доб. 3005; e-mail: TusninaOA@mgsu.ru
Scopus ID: 55975424400; Researcher ID: U-7848-2018; ORCID: 0000-0002-5595-2784.

Алексейцев Анатолий Викторович, доцент, доктор технических наук, профессор кафедры «Промышленное и гражданское строительство», доцент кафедры «Железобетонные и каменные конструкции»; Национальный исследовательский московский государственный строительный университет (НИУ МГСУ); Россия, 129337 Москва, Ярославское шоссе, 26. Тел. +7 (495) 287-49-14 доб. 3036; e-mail: AlekseytsevAV@ mgsu.ru
Scopus ID: 57191530761; Researcher ID: I-3663-2017; ORCID: 0000-0002-4765-5819.

International Journal for Computational Civil and Structural Engineering, 20(2) 76–87 (2024)

DOI:10.22337/2587-9618-2024-20-2-76-87

NUMERICAL SIMULATION OF THE OPERATION OF ALUMINUM ALLOY JOINTS MADE BY CONTACT CAPACITOR WELDING

Andrey V. Korgin

National Research Moscow State University of Civil Engineering (NRU MGSU), Moscow, RUSSIA

Abstract. Currently, structures made of modern aluminum alloys are increasingly used and widespread in almost all areas of industrial and construction production, which is a consequence of the unique properties of physico-mechanical aluminum alloys, which make it possible to create structures of various purposes that are effective in weight, strength and aesthetic parameters, while having increased corrosion resistance compared to steel structures. However, the manufacture of structures made of aluminum alloys is a more complex technological process due to the need to use special aluminum welding methods compared to traditional methods of welding steel structures. he most common argon arc method and friction welding method with mixing of aluminum alloy structures are more difficult to implement in the field during installation and assembly of structural elements on a construction site, and require qualified personnel. For this reason, it is relevant to use other methods of welding elements of aluminum structures that do not require complex equipment and qualified personnel, similar to classical electric welding of steel structures, compared with the above more complex methods of welding aluminum structures. These technologies include modern methods of laser welding and contact capacitor spot welding, the equipment for which is very compact and mobile and does not require highly qualified personnel as for other aluminum welding technologies. The current regulatory documentation of the Russian Federation on contact capacitor spot welding is descriptive and does not allow reliable design and calculation of the strength of joints of this type, which requires additional experimental and theoretical studies of such joints. Earlier laboratory tests of samples of aluminum alloy compounds by condenser welding showed in some cases a significant difference between experimental data and strength calculations according to the normative methodology of compounds of this type. For this reason, the purpose of this work was to clarify regulatory solutions using numerical FEM modeling of the operation of experimentally tested 18 connections – nodes of the ceiling suspension of aluminum alloy sheets AMG2M to threaded rods made of aluminum alloy AMG3. The obtained data were compared with experimental results and previously performed data of normative calculations.

Keywords: aluminum alloy, spot capacitor welding, tension, shear, stress, strength, fracture, finite element method

ЧИСЛЕННОЕ МОДЕЛИРОВАНИЕ РАБОТЫ СОЕДИНЕНИЙ ИЗ АЛЮМИНИЕВЫХ СПЛАВОВ, ВЫПОЛНЕННЫХ МЕТОДОМ КОНТАКТНОЙ КОНДЕНСАТОРНОЙ СВАРКИ

А.В. Коргин

Национальный исследовательский Московский государственный строительный университет, г. Москва, РОССИЯ

Аннотация. в настоящее время конструкции из современных алюминиевых сплавов находят все большее применение практически во всех сферах промышленного и строительного производства, что является следствием уникальных физико-механических свойств алюминиевых сплавов, позволяющих создавать эффективные по весовым, прочностным и эстетическим параметрам конструкции самого разнообразного назначения, обладающие при этом повышенной коррозионной стойкостью по сравнению со стальными конструкциями. Однако изготовление конструкций из алюминиевых сплавов является более сложным технологическим процессом из-за необходимости применять специальные методы сварки алюминия по сравнению с традиционными методами сварки стальных конструкций. Наиболее распространенные в настоящее время аргонодуговой метод и метод сварки трением с перемешиванием конструкций из алюминиевых сплавов более сложно реализуются в полевых условиях при монтаже и сборке элементов конструкций на строительной площадке, и требуют квалифицированного персонала. По этой причине является актуальным использование иных методов сварки элементов алюминиевых конструкций, не требующих сложного оборудования и квалифицированного персонала аналогично классической электросварке

стальных конструкций, по сравнению с вышеперечисленными более сложными методами сварки алюминиевых конструкций. К данным технологиям следует отнести современные методы лазерной сварки и контактной конденсаторной точечной сварки, оборудование для которой весьма компактно и мобильно и не требует персонала высокой квалификации как для других технологий сварки алюминия. Действующая нормативная документация РФ по контактной конденсаторной точечной сварке носит описательный характер, и не позволяет надежно осуществлять проектирование и расчет прочности соединений данного типа, что требует дополнительных экспериментально-теоретических исследований таких соединений. Проведенные ранее лабораторные испытания образцов соединений алюминиевых сплавов конденсаторной сваркой показали в ряде случаев существенное различие экспериментальных данных с расчетами прочности по нормативной методике соединений данного типа. По этой причине целью настоящей работы явилось уточнение нормативных решений с помощью численного МКЭ моделирования работы экспериментально испытанных 18 соединений – узлов потолочной подвески листов алюминиевого сплава АМГ2М к стержневым резьбовым тягам из алюминиевого сплава АМГ3. Полученные данные сравнивались с экспериментальными результатами и проведенных ранее данными нормативных расчетов.

Ключевые слова: алюминиевый сплав, точечная конденсаторная сварка, растяжение, срез, напряжение, прочность, разрушение, метод конечных элементов

INTRODUCTION

Currently, structures made of modern aluminum alloys are increasingly used and widespread in almost all areas of industrial and construction production. This is a consequence of the unique properties of physical and mechanical aluminum alloys, which allow to create effective in weight, strength and aesthetic parameters of structures for a variety of purposes with increased corrosion resistance compared to steel ones. However, the manufacture of aluminum alloy structures is a more complex technological process due to the need to apply special methods of welding aluminum compared to traditional welding methods of steel structures. The most common at present argon-arc method and friction stir welding methods for aluminum alloy structures are more difficult to implement in the field during installation and assembly of structural elements at the construction site, and require qualified personnel [1,2,3,4,5,6,7,8]. Because of this, it is relevant to use other methods of welding elements of aluminum structures, which do not require complex equipment and qualified personnel similar to the classical electric welding of steel structures, compared to the above mentioned more complex methods of welding aluminum structures. These technologies should include modern methods of laser welding and contact capacitor spot welding, the equipment for which is very compact, mobile and does not require highly qualified personnel [9,10,11,12,13,14].

The current standards of the Russian Federation on contact capacitor spot welding (GOST 15878-79) are descriptive in nature and do not allow reliable design and calculation of the strength of this type of joints, which requires additional experimental and theoretical studies of such joints.

Previous laboratory tests of samples of aluminum alloy joints performed using condenser welding have shown in a number of cases a significant difference between experimental data and strength calculations according to the normative methodology for joints of this type. For this reason, the purpose of this study was to clarify the normative solutions by means of numerical FEM simulation of the experimentally tested 18 assemblies which are the joints of ceiling suspension of aluminum alloy sheets AMG2M to threaded tie rods made of aluminum alloy AMG3. The obtained data were compared with experimental results and earlier data of computations. Examples of similar studies in Russia and abroad are also given in [15,16,22,23].

The main stages of the study are as follows:

- development of FEM-models of the tested assemblies based on the data of experimental studies conducted earlier;

- numerical modeling of stress-strain state changes during tensile and shear tests of two types of assembly specimens;
- comparing the results of numerical modeling with experimental data and results of verification calculations performed by normative methods in order to be able to correct normative calculation methods for the design of similar assemblies and for the determination of the values of fracture loads;
- drawing conclusions and recommendations on the general calculation of assemblies of this type.

RESEARCH METHODS

Laboratory testing of joints

Previously, there were tested two types of specimens in NIU MGSU which involves joints of plates with dimensions 100×100 mm made of 3 mm thick sheet metal and parts of rolled Taurus with dimensions 100×70×70 mm made of aluminum alloy AMG2M. Studs with internal thread M4 made of aluminum alloy AMG3 were welded to these joints by the method of spot condenser welding [17].

The number of specimens of each type is 9 pieces, total 18 pieces (Fig. 1).

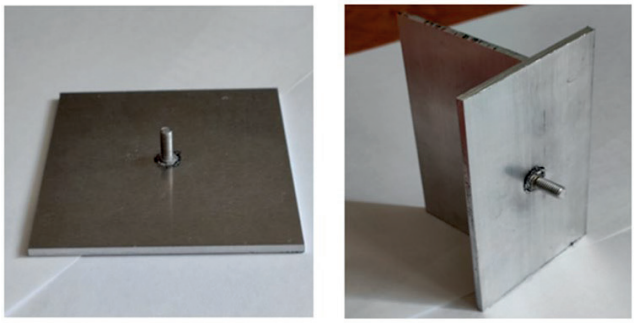


Figure 1. General view of tensile and shear test samples

The joints were subjected to tensile tests with a concentrated force perpendicular to the plane of the plates (type 1), and shear tests by concentrated force parallel to the plane of the plate flange (type 2). The tests were carried out in a universal testing machine Instron 3382 under static loading (Fig. 2) [18].

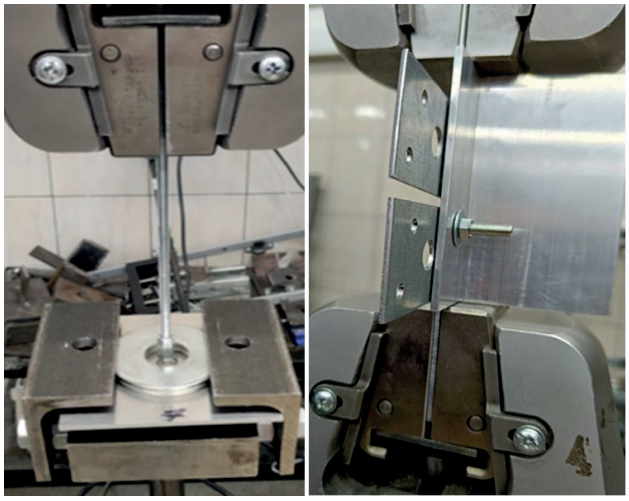


Figure 2. General view of the tensile and shear test samples in the testing machine

Joint strength calculations

In the course of earlier studies, the tested assemblies were subjected to verification calculations according to the standard methodology [17].

Within the framework of the present study, numerical FEM modeling of the tested joints was performed to improve the accuracy of calculations in comparison with the standard methodology and to compare the results of numerical analysis with the results of previously conducted laboratory tests.

RESULTS AND DISCUSSION

Tensile tests

The tensile tests with concentrated tensile force result in failure of the specimens solely by welding (Fig.3).

t

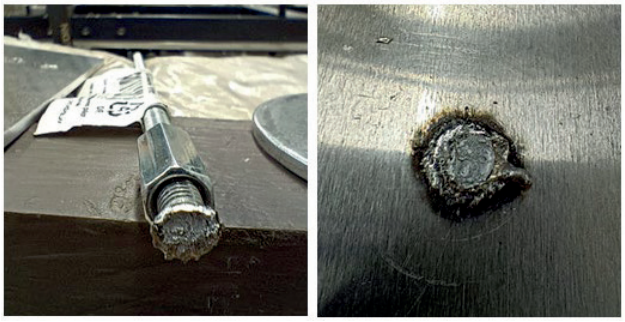


Figure 3. Type of destruction in the welded zone during tensile tests

The results of tensile tests are presented in Table 1. Evaluation of the mean values of failure load obtained was made both without rejection and with rejection of the value for specimen No. 9 due to the deviation from the mean value by more than 50%.

Table 1. Destructive forces during tensile tests.

Sample№	Maximal force, kN	Deviation from average value %	
		Before rejection	After rejection
1	1.68	-19	-17
2	2.32	13	14
3	1.75	-15	-14
4	1.63	-21	-20
*5	2.90	41	42
6	2.41	17	18
7	1.74	-16	-15
8	1.86	-10	-9
***9**	**0.74**	**-64**	**-**
Average value before rejection			**2.06**
Standard deviation			0.608
Coefficient of variation			32%
Average value after rejection			**2.04**
Standard deviation			0.457
Coefficient of variation			22%

* – samples subjected to rejection.

Shear tests

Similarly, shear tests of specimens show that the failure of this type of joints also occurred only by welding (Fig.4).



Figure 4. View of Type 2 samples after the shear tests

The results of the shear tests of the specimens are presented in Table 2.

Table 2. Destructive forces during shear tests.

Sample №	Maximal force, kN	Deviation from average value %	
		Before rejection	After rejection
1	14	26	14
2	-6	4	-6
3	-21	-12	-21
4	0.5	11	0.5
*5	5	15	5
6	-	-72	-
7	0.9	18	0.9
***8**	-	-	-
9	7	18	7
Average value before rejection			**2.08**
Standard deviation			0,608
Coefficient of variation			32%
Average value after rejection			**2.29**
Standard deviation			0.25
Coefficient of variation			11%

* – samples subjected to rejection.

Verification calculations

Tensile and shear test calculations of the two types of joints were performed based on the provisions of SP 128.13330.2016 “Aluminum structures”.

Dimensions of threaded rod M4 PT according to DIN EN ISO 13918 (Fig.5) are as follows:

Diameter of the welding zone (D1+0.5 mm) D_{sv}=6 mm.

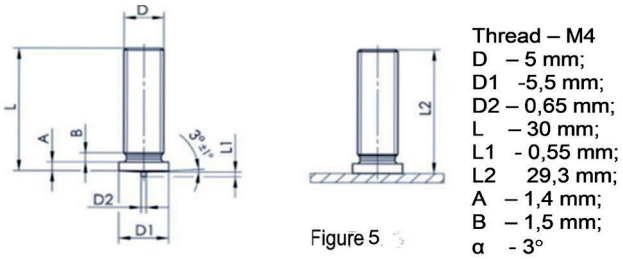


Figure 5. Geometric dimensions of the welded studs. Diameter of welding zone (D_1+0,5 mm) D_w=6 mm. The area of the welding zone A=28.3 mm^2.

Strength properties of the aluminum alloys used in the tested assemblies are given in accordance with the current standards (GOST 21631-2019 “Sheets of aluminum and aluminum alloys”, SP

128 and materials [19] with rounding to 5 MPa (Table 3)).

Table 3. Strength parameters of aluminum alloys

Node element	Tension[MPa]		Shear (срез) [MPa]	
	Yield strength $\sigma_{0,2}$	Maximum resistance $\sigma_в$	Yield strength $\tau_{0,2}$	Maximum resistance $\tau_в$
Plate АМГ2М	70	125	55	90
Threaded stud АМГ3	100	165	70	115

CALCULATION OF TENSILE STRENGTH

Experimental values of normal tensile stresses are presented in Table 4.

Table 4. Normal tensile stresses during tension

Sample №	P (kN)	δP (%)	σ (Pa)	δσ (%)	$\delta\sigma_B$ (%)
1	1,68	-17	5,94E+07	-17	-26
2	2,32	14	8,20E+07	14	2
3	1,75	-14	6,18E+07	-14	-23
4	1,63	-20	5,76E+07	-20	-28
5	2,90	42	1,02E+08	42	28
6	2,41	18	8,52E+07	18	6
7	1,74	-15	6,15E+07	-15	-23
8	1,86	-9	6,57E+07	-9	-18
Average	**2,04**	**0**	**7,20E+07**	**0**	**-10**

Stress in the weld zone for the mean value of fracture force P=2.04 kN:

$$\sigma = \frac{P}{A} = \frac{2{,}04 \cdot 10^3}{28{,}3 \cdot 10^{-6}} = 72 \cdot 10^6 = 72\ MPa < \sigma_B = 80\ MPa\ (\delta = -10\%)$$

Fracture stress range.
σ=68,5÷122 MPa (deviation from σ_B -±28%)

CALCULATION FOR SHEAR

Experimental values of shear tangent stresses are given in Table 5.

Table 5. Shear stresses during cutting

Sample №	P (kN)	δP (%)	τ (Pa)	δτ (%)	$\delta\tau_B$ (%)
1	2,61	14	9,22E+07	28	54
2	2,16	-6	7,63E+07	6	27
3	1,82	-21	6,43E+07	-11	7
4	2,3	0	8,13E+07	13	35
5	2,39	4	8,45E+07	17	41
6	2,31	1	8,16E+07	13	36
7	2,44	7	8,62E+07	20	44
Average	**2,29**	**0**	**8,09E+07**	**12**	**35**

Tangential stress in the weld zone for the mean value of fracture force P=2.29 kN:

$$\sigma = \frac{P}{A} = \frac{2{,}29 \cdot 10^3}{28{,}3 \cdot 10^{-6}} = 80{,}9 \cdot 10^6 = 80{,}9\ MPa > \sigma_B = 55\ MPa\ (\delta = 35\%)$$

Fracture stress range:.
τ=64,3÷92,2 MPa (deviation from τ_B 7÷54%)/

COMPUTER SIMULATION

Strength and deformation properties accepted in the modeling

Strength properties of aluminum alloys are presented in Table 3.
Deformation properties of materials are given in accordance with SP 128 and SP 16.13330.2020 “Steel structures”:
for aluminum alloys:
modulus of elasticity – E=0,7·10^6 MPa;
Poisson's ratio – γ=0,3;
for steel:
modulus of elasticity – E=2,1·10^6 MPa;
Poisson's ratio – γ=0,27.
FEM modeling was conducted in the ANSYS software [20] within the nonlinear elastic-plastic formulation using conventional bilinear elastic-plastic deformation diagrams of the aluminum alloys with regard to [21] (Fig. 6).

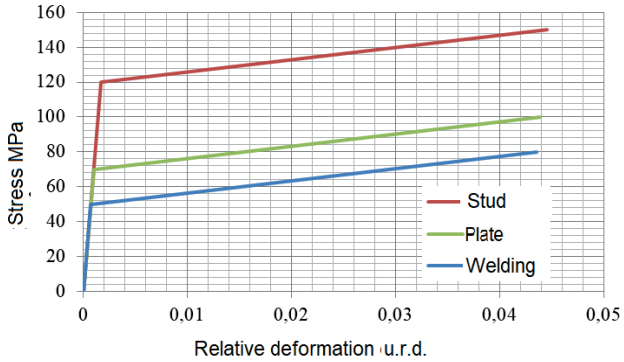


Figure 6. Conditional bilinear diagrams deformations

During modeling, the loading was carried out in stages up to the maximum value of the loading force of 3000 N, which exceeds the values of the failure force achieved during the experiment with a reserve.

Finite elements used

During modeling the SOLID 185 finite elements were used, which represents a three-dimensional three-dimensional cone element with 8 nodes, three degrees of freedom in each (Fig.7).

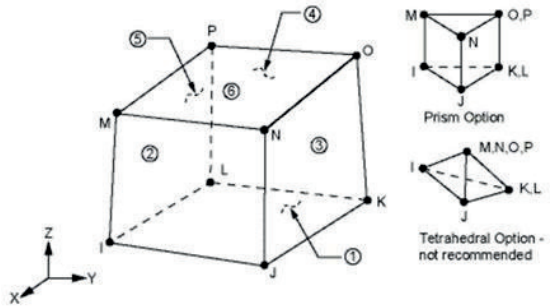


Figure 7. Solid 185 element

The numerical model of the tensile specimen is presented in Fig. 8.

The numerical model of the specimen tested in tension is a spatial model consisting of 4 zones: a stud, a plate, a welded zone made of the aluminum alloys used, and a steel base plate with a circular outline. In accordance with the test design, support was applied along the inner contour of the steel backing plate. The load was applied at the level of the top section of the stud.

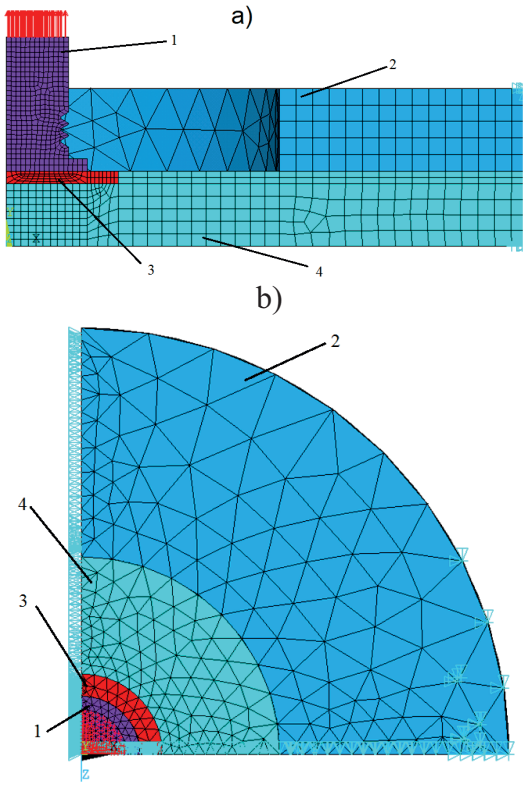


Figure 8. Numerical model of the sample a) front view; b) top view

Based on the symmetry of the model geometry and the applied load, the calculation was performed for ¼ of the model with the corresponding conditions of fixation of the sides of ¼ of the model along the symmetry axes (Fig. 8).

Results of tensile modeling of type 1 specimen.

Isopoles of vertical displacements [mm] are presented in Fig. 9.

The graph of displacements of the center point of the stud surface is shown in Fig.10.

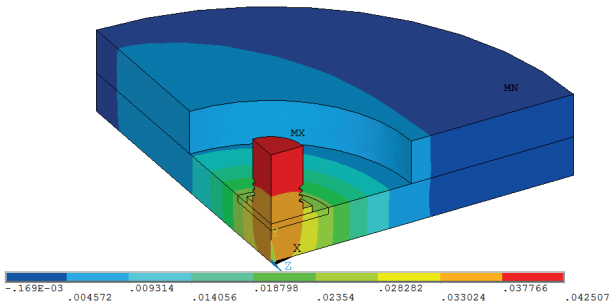


Figure 9. Isofields of vertical movements of the model at a load of 1800 N

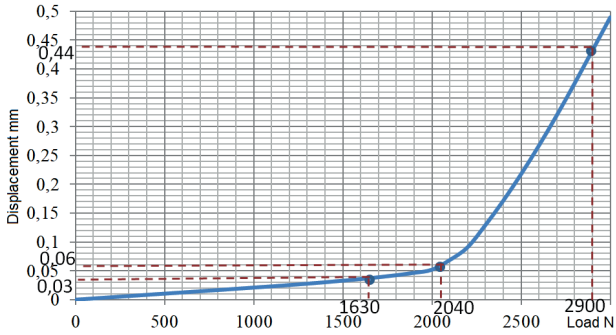


Figure 10. Movements of the upper point of the stud at minimum (1630 N), average (2040 N), and maximum (2900 N) load [mm]

Strains [u.r.d.] and normal stresses [MPa]

The isopoles of strain [u.r.d.] and normal stress[MPa] are shown in Fig. 11:

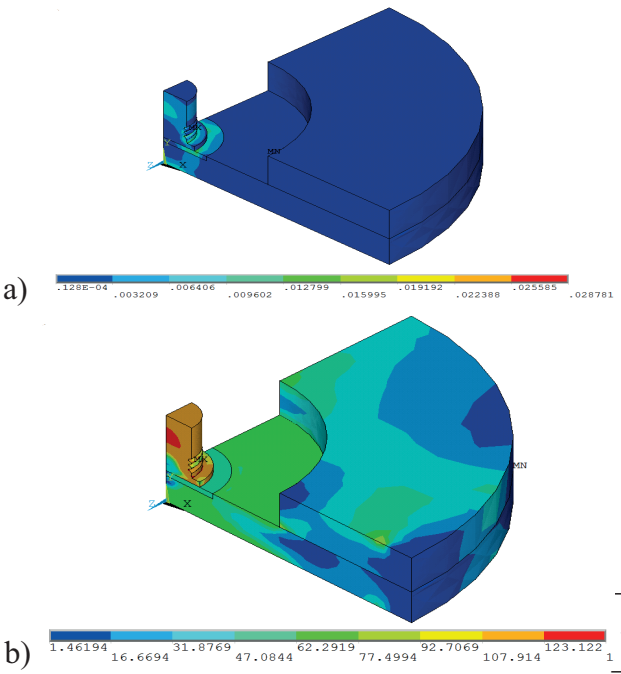


Figure 11. Isofields of a) – deformations, b) – stresses at a load of 1800 N

Fig. 12 shows the graphs of strain in the joint elements and their maximum values at characteristic levels of axial load.

Strain levels in joint elements at recorded values of failure load:

– 0.005 – at minimum load value – 1.63 kN,
– 0.01 – at an average load – 2.04 kN,
– 0.042 – at maximum load value – 2.9 kN.

Relation of maximum values of normal stresses σ in the elements of the node of type 1 to the load is presented in Fig. 13.

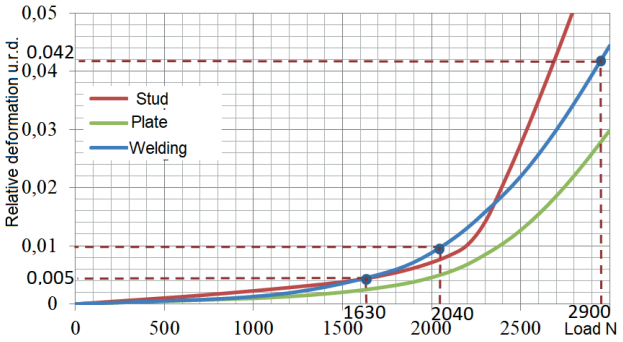


Figure 12. Dependence of the maximum values of relative deformation in the elements of the type 1 node on the load

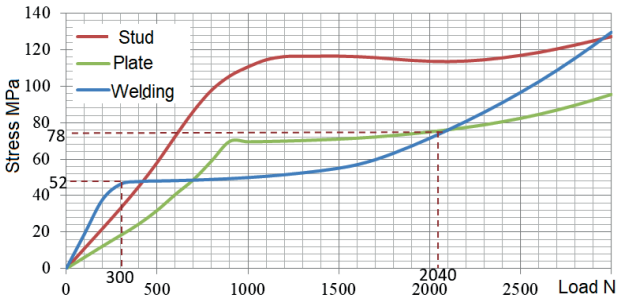


Figure 13. Dependence of the maximum values of normal stresses in the elements of the type 1 node on the load

There is a good correlation between the calculated values of normal stresses in the welding zone and the strength parameters of this zone:

– at the reaching of the yielding point σ=52 MPa ($\sigma_{0.2}$=55 MPa);
– at the value of failure load 2.04 kN – σ=78 MPa (σ_B=80 MPa).

Numerical model of type 2 shear specimen (Fig. 14)

The numerical model of the specimen being tested for shear is a spatial model fixed along the contour and loaded with a concentrated load at a node on the side surface of the stud by means of rigid inserts (MPC).

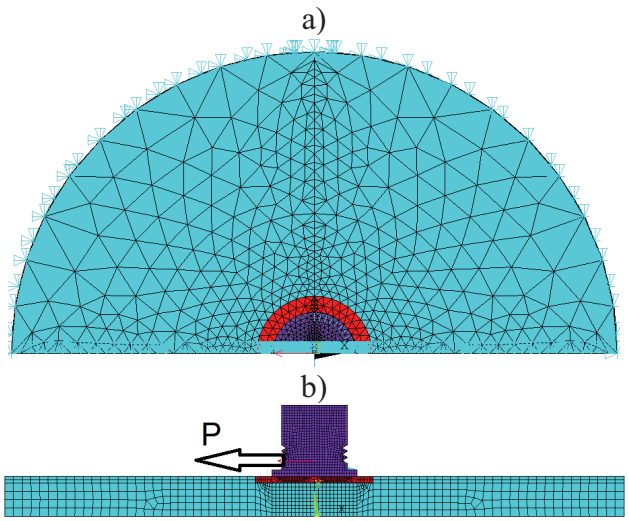


Figure 14. Numerical model of the type 2 sample on a slice: a) top view; b) side view

Based on the symmetry of the specimen geometry and the applied load in one plane, the calculation was performed for ½ of the model with symmetrical fixation along the symmetry axis. The force is applied in the horizontal direction along the symmetry axis.

Results of shear modeling of type 2 specimen

Horizontal displacements [mm] are shown in Fig. 15:

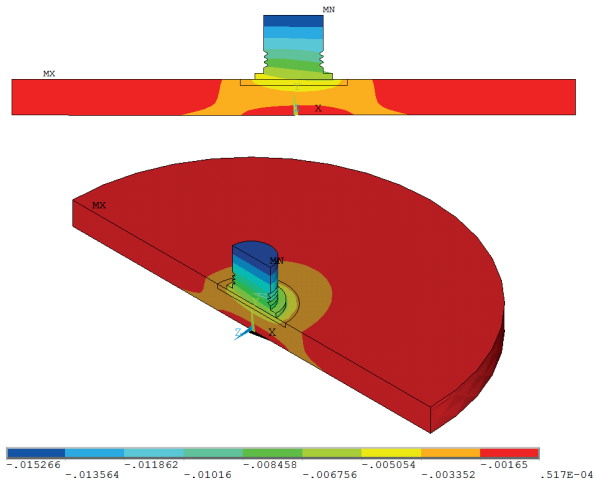


Figure 15. Isofields of horizontal model displacements at a load of 1000 N

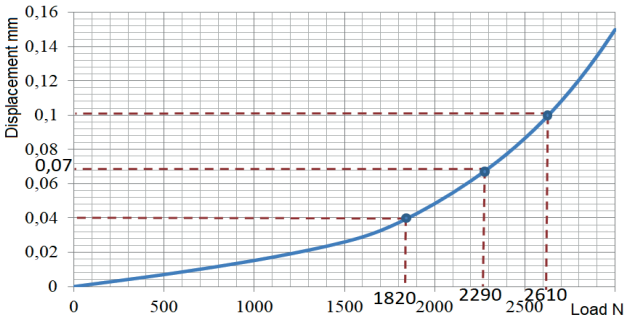


Figure 16. Horizontal movement of the upper point of the stud from the load

Strains γ [u.r.d] and tangential stresses τ [MPa]

The distribution of shear strains and stresses is shown in Figure 17.

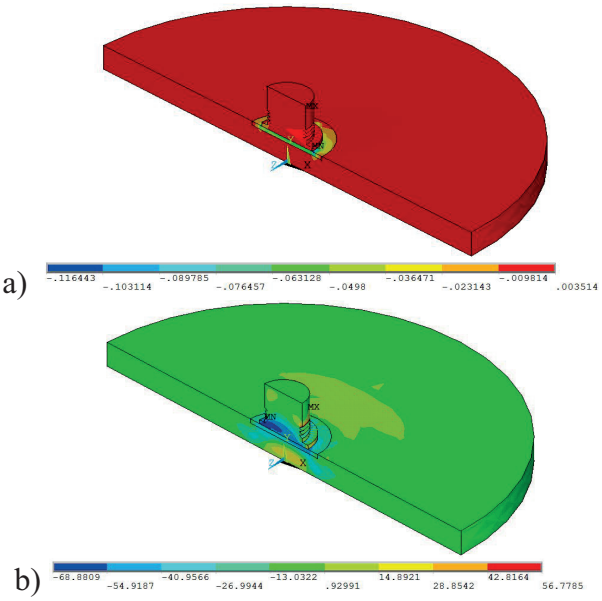


Figure 17. Isofields of a) deformations and b) stresses at a load of 2000 N

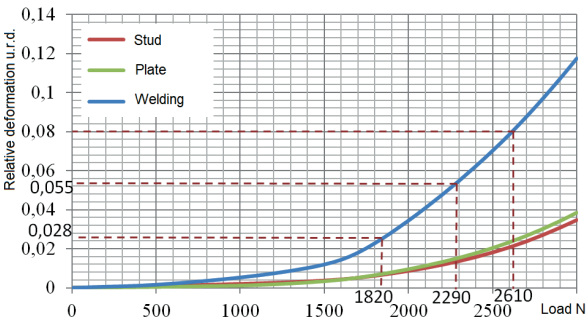


Figure 18. The dependence of the relative deformation in the elements of the type 2 node on the load

The relationship between the maximum values of tangential stresses τ in the elements of the node of type 2 and the load is shown in Fig. 19.

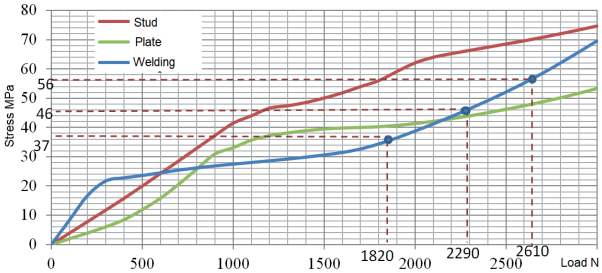


Figure 19. Dependence of the maximum tangential stresses in the elements of the type 2 node on the load

There is a satisfactory correlation of calculated values of tangential stresses τ in the welding zone with strength parameters of this zone in the range of experimental failure loads:
τ=37 MPa for P_{min}=1,82 kN;
τ=46 MPa for P_{cp} =2,29 kN; (δ=16%);
τ=56 MPa for P_{max}=2,61 kN; (τ_B=55 MPa),

CONCLUSIONS AND RECOMMENDATIONS BASED ON COMPARISON OF EXPERIMENTAL RESULTS, VERIFICATION CALCULATIONS AND FEM MODELING

1. Test results

1.1. According to the test results, all specimens of types 1 and 2 were failed along the welded zone.
1.2. The tensile failure force of the joint of type 1 lies within the range of 1.68÷2.9 kN, the mean value is 2.04 kN, the deviation from the mean value is within the range of -20÷+42%.
1.3. The failure force of the joint of type 2 at shear lies within the limits of 1.68÷2.9 kN, the mean value is 2.29 kN, the deviation from the mean value is within the limits of -11÷+20%.

2. Results of verification calculations

2.1. The discrepancy between the results of the calculation of tensile strength and the experiment is satisfactory. It lies within ±28%, from 59.4 MPa to 102 MPa, the mean value is 72 MPa. The average deviation from the tensile strength value of 80 MPa is δ = -10%.
2.2. The discrepancy between the results of the calculation for shear and the experiment is more significant than for tensile. It lies within the range of 7÷54%, from 64.3 MPa to 92.2 MPa. The mean value is 80.9 MPa. The average deviation from the value of shear time resistance 55 MPa is δ=35%.
2.3. The significantly greater difference between the results of calculations for shear and experiment than for tension is a consequence of the more complex actual stress state when the joint is loaded by the shear force caused by the design of the joint than for pure shear. For this reason, the shear performance of the type 2 joint, as well as the tensile performance of the type 1 joint, was analyzed using FEM modeling.

3. Results of FEM modeling

3.1. In tensile testing of type 1 assemblies, there is a good correlation between the calculated values of normal stresses in the weld zone at fracture and the strength parameters of the zone, with the mean value of the failure load kN - σ=78 MPa at σ_B =80 MPa, δ=4%, (with manual calculation δ=10%).
3.2. In shear tests of type 2 assemblies, there is a satisfactory correlation between the calculated values of tangential stresses in the weld zone at fracture and the strength parameters of the zone at an mean value of the failure load of 2.29 kN - τ=46 MPa at τ_B =55 MPa, δ=16% (with manual calculation δ=35%).
3.3. FEM-modeling provides a significantly better match between the results of calculations and experimental results than manual calculations due to more efficient analysis of the actual stress-strain state of the assemblies.
3.4. The design of such nodal joints of aluminum alloys, planned to be performed by means of contact welding, should be carried out on the basis of the results of computer simulation of the joint performance of the constituent elements of the joints under the action of load.

REFERENCES

1. **Shavnev A.A., Kurbatkina E.I., Kosolapov D.V.** Methods of joining aluminum composite materials (review) // Materials and technologies, 2017, No. 3 (48), pp. 35-42.
2. **Krylov D.S., Nazarov S.V.** Some features of argon arc welding of aluminum-magnesium alloys // In the collection: Actual problems of aviation and cosmonautics, Collection of materials of the VI International Scientific and Practical Conference dedicated to the Day of Cosmonautics, in 3 volumes under the general editorship of Yu.Yu. Loginov, 2020, pp. 466-467.
3. **Drits A.M., Ovchinnikov V.V.** Weldability and properties of welds of high-strength aluminum alloys of the Al - Cu - Li system // Metal Science and Heat Treatment, 2012, V. 53, No. 9-10, p.p. 445-449.
4. **Ovchinnikov V.V., Drits A.M.** Welding friction with mixing of aluminum alloys with additional cooling of the joint // Electrometallurgy, 2021. No. 10, pp. 2-14.
5. **Ovchinnikov V.V., Berezina V.A., Skakova T.Y.** Mechanical properties of aluminum alloy joints made by friction welding with static and dynamic loading // High-tech technologies in mechanical engineering, 2021, No. 11 (125), pp. 20-29.
6. **Laptev E.A., Mikhailitsyn S.V., Belyaev A.I.** Friction welding with mixing of aluminum alloys // Actual problems of modern science, technology and education, 2013, Vol. 1, No. 71. pp. 377-379.
7. **Drits A.M., Ovchinnikov V.V.** Properties of the joints of sheets of 1565ch alloy in combination with other aluminum alloys that were performed by friction welding with mixing // Russian Metallurgy (Metally), 2016, V. 2016, № 6, p.p. 537-546.
8. **Amirov A.I., Beloborodov V.A., Ivanov A.N., Zhukov L.L.** Lap welded joint of aluminum and titanium alloy by friction stir welding // Collection of AIP Conference Proceedings, Proceedings of the Advanced Materials with Hierarchical Structure for New Technologies and Reliable Structures, 2018, 020013.
9. **Milyutin V.S., Bliznik M.G. Kataev R.F.** Theory and technology of contact welding // Yekaterinburg, Ural University Publishing House, 2015, 255 p.
10. **Malikov A.G., Orishich A.M., Vitoshkin I.E., Karpov E.V., Ancharov A.I.** Laser welding of heterogeneous materials based on thermally hardened aluminum alloys // Applied Mechanics and Technical Physics, 2021, Vol. 62, No. 5 (369), pp. 161-171.
11. **Wang Z., Shao X., Bu X., Oliveira J.P., Zeng Z., Peng B.** Laser beam oscillating welding of 5a06 aluminum alloys: microstructure, porosity and mechanical properties // Optics & Laser Technology, 2019, V. 11, p.p. 58-65.
12. **Kuchuk A.V.,-Yatsenko S.I., Chvertko P.N., Semenov L.A., Gushchin K.V., Sabotryasov S.M.** Contact butt welding of products made of high-strength alloys based on aluminum // Automatic welding, 2013, No. 7 (723), pp. 3-7.
13. **Chvertko P.N., Semenov L.A., Gushchin K.V.** Contact butt welding by melting thin-walled profiles from thermally hardened aluminum alloys // Automatic welding, 2014, No. 12 (738), pp. 37-40.
14. **Dimitrescu A., Alecusan A.M., Babiş C., Chivu O., Ungureanu L.** Alternative non-demountable assembly technologies for aluminum alloy // In collection of 18th International Multidisciplinary Scientific GeoConference SGEM 2018., Conference proceedings, 2018, pp. 17-24.
15. **Gureeva M.A., Grushko O.E., Klochkov G.G.** Investigation of the properties of welded joints of aluminum alloy B1341 made by contact spot welding // Procurement production in mechanical engineering. 2016, No. 7, pp. 8-12.
16. **Hasan I.Kh ., Pan'kin N.A., Kyashkin V.M.** Xrd study of the surface of aluminum alloy AK5M7 after electric-spark alloying //

Letters about materials, 2021, V. 11. No. 1 (41), pp. 84-89.
17. **Korgin A.V.** Strength of aluminum alloy joints made by contact capacitor welding Vol. 19 No. 2 (2023): International Journal for Computational Civil and Structural Engineering, pp. 42-50.
18. Universal electromechanical machine Instron 3382, User Manual, Instron, USA, 2015, 235 p.
19. **NIL IIMSK NIU MGSU** Technical report for JSC Rusal TD "Development of a set of rules "Bridges with structures made of aluminum alloys. Design rules // NRU MGSU, Moscow, 2020, 230 p.
20. **WWW.Ans.Com.ru** Руководство по основным методам проведения анализа в программе ANSYS, https://vestnik.bsau.ru/netcat_files/File/CIT/manuals/ANSYS.pd, pp. 15-111.
21. **Anisimov A.G., Ahmed S.M.** Experimental investigation and numerical modeling of aluminum sample throwing for magnetic pulse welding // Nauka i innovatsii, 2022, No. 3 (123), pp. 58-62.
22. **Maksimov N.N., Sergeev V.Y**. Improving the technological process of contact welding of aluminum alloy parts // Alley of Science, 2017, Vol. 4, No. 10, pp. 150-157.
23. **Andreeva L.P., Ovchinnikov V.V., Sidorov A.A.** Optimization of point joint sizes during electric contact welding of aluminum alloys // Modern Materials, Technique and Technology, 2015, No. 3 (3), pp. 23-32.

СПИСОК ЛИТЕРАТУРЫ

1. **Шавнев А.А., Курбаткина Е.И., Косолапов Д.В.** Методы соединения алюминиевых композиционных материалов (обзор) // Материалы и технологии, 2017, № 3 (48), стр. 35-42.
2. **Крылов Д.С., Назаров С.В.** Некоторые особенности аргонодуговой сварки алюминиево-магниевых сплавов // В сборнике: Актуальные проблемы авиации и космонавтики, Сборник материалов VI Международной научно-практической конференции, посвященной Дню космонавтики, в 3-х томах под общей редакцией Ю.Ю. Логинова, 2020, стр. 466-467.
3. **Drits A.M., Ovchinnikov V.V.** Weldability and properties of welds of high-strength aluminum alloys of the Al - Cu - Li system // Metal Science and Heat Treatment, 2012, V. 53, № 9-10, pp. 445-449.
4. **Овчинников В.В., Дриц А.М.** Сварка трением с перемешиванием алюминиевых сплавов с дополнительным охлаждением соединения // Электрометаллургия, 2021. № 10, стр. 2-14.
5. **Овчинников В.В., Березина В.А., Скакова Т.Ю.** Механические свойства соединений алюминиевых сплавов, выполненных сваркой трением с, при статическом и динамическом нагружении // Наукоемкие технологии в машиностроении, 2021, № 11 (125), стр. 20-29.
6. **Лаптев Е.А., Михайлицын С.В., Беляев А.И.** Сварка трением с перемешиванием алюминиевых сплавов // Актуальные проблемы современной науки, техники и образования, 2013, Т. 1, № 71.стр. 377-379.
7. **Drits A.M., Ovchinnikov V.V.** Properties of the joints of sheets of 1565ch alloy in combination with other aluminum alloys that were performed by friction welding with mixing // Russian Metallurgy (Metally), 2016, V. 2016, № 6, pp. 537-546.
8. **Amirov A.I., Beloborodov V.A., Ivanov A.N., Zhukov L.L.** Lap welded joint of aluminum and titanium alloy by friction stir welding // Collection of AIP Conference Proceedings, Proceedings of the Advanced Materials with Hierarchical Structure for New Technologies and Reliable Structures, 2018, 020013.
9. **Милютин В.С., Близник М.Г. Катаев Р.Ф.** Теория и технология контактной сварки // Екатеринбург, изд-во Уральского университета, 2015, 255 стр.

10. **Маликов А.Г., Оришич А.М., Витошкин И.Е., Карпов Е.В., Анчаров А.И.** Лазерная сварка разнородных материалов на основе термически упрочняемых алюминиевых сплавов // Прикладная механика и техническая физика, 2021, Т. 62, № 5 (369), стр. 161-171.
11. **Wang Z., Shao X., Bu X., Oliveira J.P., Zeng Z., Peng B.** Laser beam oscillating welding of 5a06 aluminum alloys: microstructure, porosity and mechanical properties // Optics & Laser Technology, 2019, V. 11, pp. 58-65.
12. **Кучук А.В.,-Яценко С.И., Чвертко П.Н., Семёнов Л.А., Гущин К.В. Самотрясов С.М.,** Контактная стыковая сварка изделий из высокопрочных сплавов на основе алюминия // Автоматическая сварка, 2013, № 7 (723), стр. 3-7.
13. **Чвертко П.Н., Семенов Л.А., Гущин К.В.** Контактная стыковая сварка оплавлением тонкостенных профилей из термически упрочняемых алюминиевых сплавов // Автоматическая сварка, 2014, № 12 (738), стр. 37-40.
14. **Dimitrescu A., Alecusan A.M., Babiş C., Chivu O., Ungureanu L.** Alternative non-demountable assembly technologies for aluminium alloy // In collection of 18th International Multidisciplinary Scientific GeoConference SGEM 2018., Conference proceedings, 2018, pp. 17-24.
15. **Гуреева М.А., Грушко О.Е., Клочков Г.Г.** Исследование свойств сварных соединений алюминиевого сплава В1341, выполненных контактной точечной сваркой // Заготовительные производства в машиностроении. 2016, № 7, стр. 8-12.
16. **Hasan I.Kh., Pan'kin N.A., Kyashkin V.M.** Xrd study of the surface of aluminum alloy AK5M7 after electric-spark alloying // Letters about materials, 2021, V. 11. № 1 (41), pp. 84-89.
17. **Korgin A.V.** Strength of aluminum alloy joints made by contact capacitor welding Vol. 19 No. 2 (2023): International Journal for Computational Civil and Structural Engineering, pp. 42-50.
18. Универсальная электромеханическая машина Instron 3382, Руководство пользователя, Instron, USA, 2015, 235 стр.
19. **НИЛ ИИМСК НИУ МГСУ** Технический отчет для АО «Русал ТД» «Разработка свода правил «Мосты с конструкциями из алюминиевых сплавов. Правила проектирования // НИУ МГСУ, Москва, 2020, 230 стр.
20. **WWW.Ans.Com.ru** Руководство по основным методам проведения анализа в программе ANSYS, https://vestnik.bsau.ru/netcat_files/File/CIT/manuals/ANSYS.pd, pp. 15-111.
21. **Анисимов А.Г., Ахмед С.М.** Экспериментальное исследование и численное моделирование метания алюминиевого образца для магнитно-импульсной сварки // Наука и инновации, 2022, № 3 (123), стр. 58-62.
22. **Максимов Н.Н., Сергеев В.Ю.** Совершенствование технологического процесса контактной сварки деталей из алюминиевых сплавов // Аллея науки, 2017, Т. 4, № 10, стр. 150-157.
23. **Андреева Л.П., Овчинников В.В., Сидоров А.А.** Оптимизация размеров точечных соединений при электроконтактной сварке алюминиевых сплавов // Современные материалы, техника и технологии, 2015, № 3 (3), стр. 23-32.

Korgin Andrey Valentinovich, Doctor of Technical Sciences, Professor, Professor of the Department of Testing Structures of the National Research Moscow State University of Civil Engineering (NRU MGSU), Moscow, 129337, Yaroslavskoye sh., 26. e-mail: korguine@mgsu.ru , anvakorg@gmail.com. tel. +7 495 183-54-29 (office) +7 985 765-46-38 (mobile)

Коргин Андрей Валентинович, Доктор технических наук, профессор, профессор кафедры испытаний сооружений Национального Исследовательского Московского Государственного Строительного Университета (НИУ МГСУ), Москва, 129337, Ярославское ш., д.26. e-mail: korguine@mgsu.ru, anvakorg@gmail.com. тел. +7 495 183-54-29 (раб.) +7 985 765-46-38 (моб.)

DOI:10.22337/2587-9618-2024-20-2-88-98

OPTIMAL SEISMIC PROTECTION OF STRUCTURES ON BEARINGS WITH BILINEAR HYSTERETIC CHARACTERISTIC

Elena V. Poznyak, Vladimir P. Radin, Olga V. Novikova, Alexey V. Kiselev, Yulia Y. Ivanova

National Research University «Moscow Power Engineering Institute» (NRU MPEI), Moscow, RUSSIA

Abstract: The design of optimal seismic protection systems on bearings with hysteresis behavior leads to a conditional multidimensional global optimization problem with a nonlinear and non-differentiable objective function. In this paper, bearings with bilinear characteristic with hysteresis are considered, i.e. for each nonlinear bearing there are four parameters to optimize: ultimate elastic displacement and stiffness for the elastic mode and ultimate displacement and stiff-ness for the inelastic mode.

We study the seismic response of an elastic beam on four nonlinear bearings under vertical seismic ground motion. The perturbation functional as an integral of the quadratic form of the state vector with a weight matrix formed from the stiffness and inertia matrices of the system on equivalent elastic supports is considered as the objective function. Minimization of the functional means the minimum of the total energy of the system on equivalent elastic bearings. Genetic algorithm is used to solve the optimization problem.

Keywords: seismic protection, bilinear characteristic, global multidimensional optimization, optimality criterion, seismic action, genetic algorithm

ОПТИМАЛЬНАЯ СЕЙСМОЗАЩИТА КОНСТРУКЦИЙ НА ОПОРАХ С БИЛИНЕЙНОЙ ГИСТЕРЕЗИСНОЙ ХАРАКТЕРИСТИКОЙ

Е.В. Позняк, В.П. Радин, О.В. Новикова, А.В. Киселев, Ю.Ю. Иванова

ФГБОУ ВО «Национальный исследовательский университет «МЭИ» (НИУ «МЭИ»), г. Москва, РОССИЯ

Аннотация: Проектирование оптимальных систем сейсмозащиты на опорах с гистерезисным поведением приводит к условной многомерной глобальной задаче оптимизации с нелинейной и недифференцируемой целевой функцией. В этой статье рассматриваются опоры с билинейной характеристикой с гистерезисом, т.е. для каждой опоры необходимо оптимизировать четыре параметра: предельное упругое перемещение и жесткость для упругого режима и предельное смещение и жесткость для неупругого режима.

Исследуется сейсмический отклик упругой балки на четырех нелинейных опорах при вертикальном сейсмическом движении грунта. В качестве целевой функции рассматривается функционал возмущения как интеграл квадратичной формы вектора состояния с весовой матрицей, сформированной из матриц жесткости и инерции системы на эквивалентных упругих опорах. Минимизация функционала означает минимум общей энергии системы на эквивалентных упругих опорах. Для решения задачи оптимизации используется генетический алгоритм.

Ключевые слова: сейсмозащита, билинейная характеристика, глобальная многомерная оптимизация, критерий оптимальности, сейсмическое воздействие, генетический алгоритм

1. INTRODUCTION

In this work, the objective function corresponds to the total energy of some elastic structure (called an equivalent system below in the text) whose natural frequencies are very close to the resonant frequencies of the original structure on nonlinear bearings. Scientific publications describe extensive experience in optimal design of structures based on elements with bilinear hys-

teretic characteristic, such as lead rubber bearings, elastomeric isolators and other devices [1-16]; many researchers apply stochastic optimization methods [11-16], solving the problem of compromise between displacements and stresses in structures. In many works take the sum of dimensionless relative dynamic response parameters (relative displacements, velocities, accelerations, forces, etc.) with weight coefficients as the objective function [4-7]. By adjusting the weighting coefficients, researchers emphasize the most significant parameters. For example, in [4], the ratio of peak roof acceleration to peak ground acceleration is minimized. The optimality criterion given in [7] minimizes both top floor acceleration and bearing displacement.

For optimal seismic protection, we take an objective function as quadratic perturbation functional of the state vector with a weight matrix, which is formed from the stiffness and/or inertia matrices of the equivalent system. Then the minimum of the objective function will be close to the minimum of the potential and/or kinetic energy of the structure on the nonlinear bearings. The complication of the problem is multidimensionality with possible multi-extremality, nonlinearity and non-differentiability of the objective function, parametrical limitations of the structure and vibration protection. Not all optimization methods are suitable for solving this problem. The most effective methods are based on the direct calculation of the objective function, for example, random search methods including population methods (genetic and other evolutionary algorithms). Intelligence algorithms of optimization of nonlinear vibration isolators are applied in many works, for example, in [13-16].

Bilinear force-displacement hysteretic curve of the bearing is shown in Fig. 1. Such system has special properties, for example, as shown for a one-dimensional oscillator in [3], resonant frequencies depend on the amplitude of cyclic load. At small cyclic load amplitudes, the oscillator works in elastic regime $A'OA$ with stiffness c_1 (Fig.1). At large amplitudes, the support goes to the AB line with stiffness c_2 and works in inelastic regime with hysteresis on the loop $ABCDE$. Frequencies $\omega_1 = \sqrt{c_1/M}$ and $\omega_2 = \sqrt{c_2/M}$ correspond to these two regimes accordingly, here M is the mass of the oscillator. Depending on the regime, the resonant frequency of the oscillator will be close to one of the frequencies.

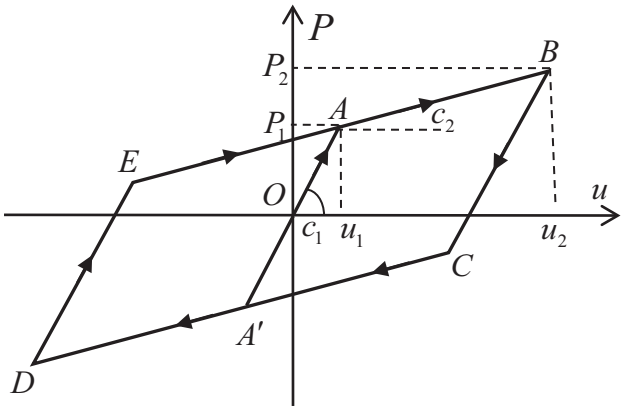


Figure 1. Bilinear curve of cyclic deformation

To design of elastomeric isolators it is common to consider elements with bilinear characteristic as linear–elastic bearings with effective stiffness $c_{eff} = P_2/u_2$, where P_2 is the ultimate force (Fig. 1) and $c_1 > c_{eff} > c_2$ [12]. However, it is very problematic to accurately calculate the resonant frequencies of multidimensional systems because they depend on the amplitude of cyclic loads.

Note that the work of the bearing in plastic regime with large deformations is undesirable because it leads to off-center compression of bearings, residual displacements and the need to restore it after an earthquake. In addition, as follows from [12], the damping of the nonlinear bearing is significantly reduced at large plastic strains. Consequently, the ultimate displacements should ensure that nonlinear elements operate predominantly in the elastic regime with greater damping and more predictable resonant frequencies.

In the study, we assume that each bearing works mainly in elastic regime, therefore the resonant frequencies are close to the natural frequencies

of the system on elastic bearings with stiffness c_1. This system is almost equivalent to the system on nonlinear histeretic bearings in terms of resonant frequencies. Despite on the nonlinear "damping - shear deformations" function and new damping models [8], we take a simple model of damping from [12] as $\xi_e = \frac{2}{\pi}\left(\frac{F_1}{F_2} - \frac{d_1}{d_2}\right)$.

Before designing of earthquake–resistant structures, it is necessary to find out whether the nonlinear bearings can reduce the seismic response of the structure? Bearings with bilinear characteristics reduce resonant frequencies, therefore it is necessary to determine natural frequencies of the original structure (on absolutely rigid bearings) and the prevailing frequencies of seismic action. If natural frequencies of the original structure are already far from the prevailing frequencies of seismic action, the bearings are not only unnecessary, but can also seriously harm, enhancing structural dynamic response. The nonlinear bearings are effective when the lowest resonant frequencies of a system with them are lower than the prevailing frequencies of seismic action.

2. OPTIMIZATION PROBLEM

We consider a structure with n degrees of freedom on N bearings. Each bilinear hysteretic bearing has four parameters, which should be optimized: $\mathbf{h}_i = \left[u_1^{(i)} \quad u_2^{(i)} \quad c_1^{(i)} \quad c_2^{(i)}\right]$, where c_1 and u_1 – stiffness of elastic mode and maximal elastic displacement, c_2 and u_2 – stiffness of inelastic mode and maximal displacement of the bearings, $i = 1, ..., N$. A simple example of the structure shown in Fig. 2. Vertical seismic ground motion is given by accelerogram $a(t)$ with duration T. At each the moment of time the state of the structure is described by a $2n$ – dimensional vector $\mathbf{X}(t) = \left[\mathbf{q} \quad \dot{\mathbf{q}}\right]^{\mathrm{T}}$, $\mathbf{q}$ and $\dot{\mathbf{q}}$ are nodal displacements and velocities.

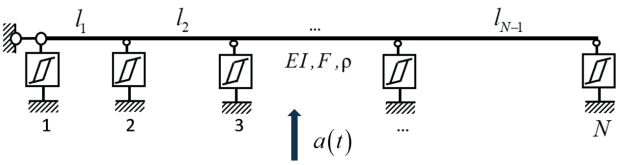


Figure 2. Beam on bilinear hysteretic bearings

We take the objective function as a quadratic functional:

$$f(\mathbf{H}) = \frac{1}{2T}\int_0^T \mathbf{X}^{\mathrm{T}}\mathbf{Q}\mathbf{X}dt,$$

where $\mathbf{H} = \left[\mathbf{h}_1 \quad \mathbf{h}_2 \quad ... \quad \mathbf{h}_N\right]$ – vector of optimized parameters, $\mathbf{Q}^{[2n\times 2n]}$ – weight matrix, $\mathbf{X}^{\mathrm{T}}\mathbf{Q}\mathbf{X} \geq 0$. We choose the matrix $\mathbf{Q}$ to give to the objective function an energy meaning. Let the matrix $\mathbf{Q}$ consists four zero blocks of the same size (two rows of two blocks). If we put stiffness matrix of the equivalent system in the first (upper left) block, the objective function will be equal to the average value of the potential energy of elastic deformation U on the interval $[0,T]$. This weight matrix is denoted by $\mathbf{Q}_U$. Minimization of the objective function $f(\mathbf{H})$ using the weight matrix $\mathbf{Q}_U$ leads to a decrease of internal forces and stresses. Similarly, if weight matrix $\mathbf{Q}_{\mathrm{T}}$ has only inertia matrix in the fourth (lower right) block, then objective function $f(\mathbf{H})$ is equal to average value of the kinetic energy T on the interval $[0,T]$. In this case, the kinematic parameters of the structure will be reduced.

The objective functions corresponding to potential, kinetic and total energy are denoted as follows:

$$J_U = f\left(\mathbf{H}\middle|\mathbf{Q}_U\right), \quad J_{\mathrm{T}} = f\left(\mathbf{H}\middle|\mathbf{Q}_{\mathrm{T}}\right),$$
$$J_E = f\left(\mathbf{H}\middle|\mathbf{Q}_E\right), \quad \mathbf{Q}_E = \mathbf{Q}_U + \mathbf{Q}_{\mathrm{T}}.$$

Consider the optimization problem:

$$\min_{\mathbf{H}\in D} f\left(\mathbf{H}\right) = f\left(\mathbf{H}_*\right) = f_*, \qquad (1)$$

where $\mathbf{H}_*$ – optimal solution, f_* – value of the optimized objective function, D – acceptable values of the vector $\mathbf{H}$:

$$D = \left\{\mathbf{H}\middle|\ \mathbf{H}_{low} \le \mathbf{H} \le \mathbf{H}_{up},\ \mathbf{A}_{cond}\mathbf{H} \le \mathbf{b}_{cond}\right\}. \quad (2)$$

Depending on the weight matrix $\mathbf{Q}_U$, $\mathbf{Q}_\mathrm{T}$ or $\mathbf{Q}_E$, problem (1) is the optimality criterion in terms of potential, kinetic or total energy.

Conditions $\mathbf{H}_{low} \le \mathbf{H} \le \mathbf{H}_{up}$ are acceptable parameters of a bilinear diagram (stiffnesses and ultimate displacements):

$$\mathbf{H}_{low} = \left[\mathbf{h}_{1_low} \quad \mathbf{h}_{2_low} \quad \ldots \quad \mathbf{h}_{N_low}\right],$$
$$\mathbf{h}_{i_low} = \left[u_{1_low}^{(i)} \quad u_{2_low}^{(i)} \quad c_{1_low}^{(i)} \quad c_{2_low}^{(i)}\right],$$
$$\mathbf{H}_{up} = \left[\mathbf{h}_{1_up} \quad \mathbf{h}_{2_up} \quad \ldots \quad \mathbf{h}_{N_up}\right],$$
$$\mathbf{h}_{i_up} = \left[u_{1_up}^{(i)} \quad u_{2_up}^{(i)} \quad c_{1_up}^{(i)} \quad c_{2_up}^{(i)}\right],$$

where

$$c_{1_low}^{(i)} < c_1^{(i)} < c_{1_up}^{(i)},\ \ c_{2_low}^{(i)} < c_2^{(i)} < c_{2_up}^{(i)},$$
$$u_{1_low}^{(i)} < u_1^{(i)} < u_{1_up}^{(i)},\ \ u_{2_low}^{(i)} < u_2^{(i)} < u_{2_up}^{(i)},\quad i = 1,\ldots,N.$$

The conditions $\mathbf{A}_{cond}\mathbf{H} \le \mathbf{b}_{cond}$ correspond to the bilinear hysteresis algorithm and are a matrix form of the following inequalities:

$$u_2^{(i)} - u_1^{(i)} \ge 0, \quad c_1^{(i)} - c_2^{(i)} \ge 0.$$

Both conditions (2) are set before the optimization process. Displacement of $i-$th bearing must not exceed predetermined value $u_*^{(i)}$:

$$\left|u^{(i)}\right| \le u_*^{(i)}. \qquad (3)$$

Constraint (3) cannot be satisfied before the optimization procedure starts. Consequently, the optimization algorithm must include a penalty: if at some time the condition (3) is not satisfied, the calculation stops and some large value (penalty) is assigned to the objective function.

We will not introduce additional constraints related to reliability of the structure, such as strength and stiffness conditions, assuming that the minimization of dynamic response of the structure is provided by the criterion of smallness of perturbations (1). Additional constraints will complicate the optimization procedure. If it found out that the global minimum of the objective function does not satisfy the strength or stiffness conditions, this means that hysteretic bearings is ineffective for this design.

Problem (1) with conditions (2-3) is a multidimensional global conditional optimization problem with a nonlinear non-differentiable objective function. Optimization methods based on the computation of the objective function without computing derivatives, such as random search algorithms, e.g., annealing simulation, hypersphere algorithm, "greedy" adaptive algorithms, genetic and other evolutionary algorithms, are suitable for finding the optimal solution [11]. The following example illustrates the results of solving the optimization problem (1) with conditions (2-3) obtained using the genetic algorithm (GA).

3. EXAMPLE OF OPTIMAL SOLUTION

We consider a steel hinged beam on four bearings, the cross-section profile is I–beam No. 20 (height 200 mm), the lengths of the three spans are 6, 8 and 12 m. The beam is under seismic action determined by the accelerogram of the vertical ground motion of the foundation; we use accelerogram synthesized at the Institute of Physics of the Earth, Moscow, Russia. The dynamic model of the beam was developed by using the finite element method; structural damping was neglected. The seismic response was

determined by direct integration of equations of motion in Simulink.

Figure 3 shows the estimates of the seismic ground motion power spectral density: the raw periodogram and its smoothed estimate found using the Welch window transformation with 50% overlap. The first three natural frequencies of the hinged supported beam are marked by red vertical lines (5.76, 14.33 and 22.85 Hz). It can be seen that the first frequency is dangerously close to one of the prevailing frequencies of the seismic action.

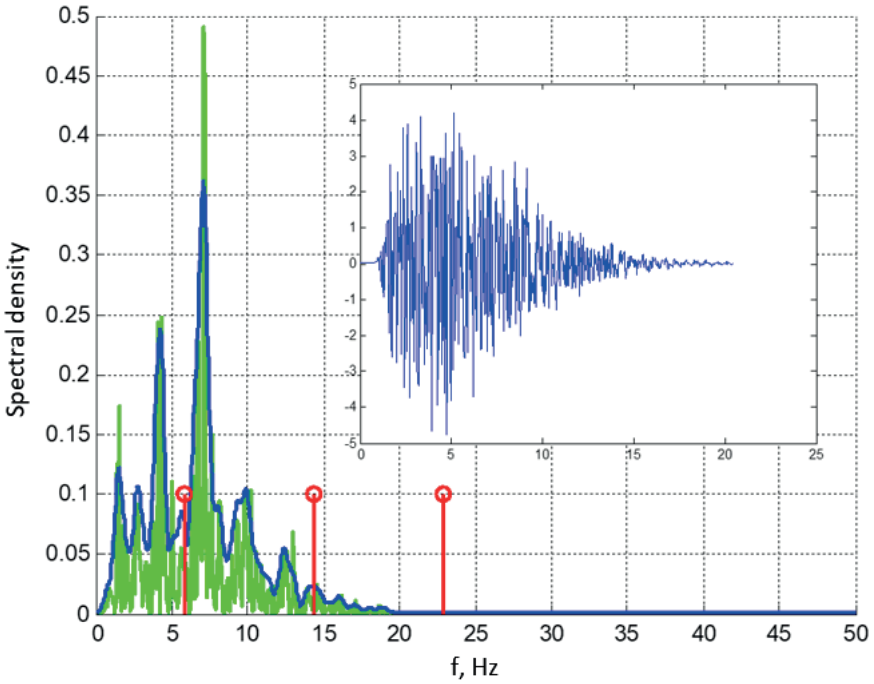


Figure 3. Anapa earthquake Z3G2–A. Spectral density: raw periodogram (green), smoothed periodogram (blue); natural frequencies of the hinged supported beam (red); in the box – accelerogram Z3G2–A (acceleration - m/s^2, time - s)

By analyzing Fig. 3, we conclude that the best way to reduce the dynamic response of the beam is to make the structure more rigid (e.g., add another supports) to shift its natural frequencies to the right. But for the purpose of this study, we place the beam on four bilinear hysteretic bearings (Fig. 2, $N = 4$) and try to find an optimal solution of problem (1-3) by applying a genetic algorithm. To solve this problem, the beam model on the bilinear hysteretic bearings was developed in Simulink. The model is a system with incomplete dissipation, since damping is present only in the bearings.

GA implemented in MATLAB Optimtool was used to find the optimal solution. The optimality criterion is the minimum of the total mechanical energy: $J_E = f\left(\mathbf{H}\middle|\mathbf{Q}_E\right) \to \min$. The dimensionality of the optimization problem is 16 (4 bearings, each with 4 optimized parameters). For conditions (2-3) we assign:

$$\mathbf{h}_{i_low} = \left(0.02\ \text{m} \quad 0.03\ \text{m} \quad 10^3\ \text{N/m} \quad 10^2\ \text{N/m}\right),$$
$$\mathbf{h}_{i_up} = \left(0.05\ \text{m} \quad 0.05\ \text{m} \quad 10^7\ \text{N/m} \quad 10^5\ \text{N/m}\right),$$
$$u_*^{(i)} = 0.10\ \text{m},\ i = 1,\ 2,\ 3,\ 4.$$

GA parameters: initial population contains 20 agents found manually, selection and mutation operators have uniform distribution, elite is 5 agents, two-point crossover, maximum number of iterations is 100. As a result, the following solution was obtained:

$$\mathbf{H}_* = \left[\mathbf{h}_1 \quad \mathbf{h}_2 \quad \mathbf{h}_3 \quad \mathbf{h}_4\right],$$

$$\mathbf{h}_1 = \left[0.03\ \text{m} \quad 0.05\ \text{m} \quad 10^5\ \text{N/m} \quad 10^3\ \text{N/m}\right],$$

$$\mathbf{h}_2 = \left[0.03\ \text{m} \quad 0.05\ \text{m} \quad 1.5\cdot 10^4\ \text{N/m} \quad 2.5\cdot 10^2\ \text{N/m}\right],$$

$$\mathbf{h}_3 = \left[0.03\ \text{m} \quad 0.05\ \text{m} \quad 2\cdot 10^4\ \text{N/m} \quad 10^2\ \text{N/m}\right],$$

$$\mathbf{h}_4 = \left[0.03\ \text{m} \quad 0.05\ \text{m} \quad 10^5\ \text{N/m} \quad 5\cdot 10^2\ \text{N/m}\right].$$

Seismic responses of the initial and optimized system are shown in Fig. 3, 4. Optimization resulted in a reduction of the maximum bending moment by more than a factor of two with a small allowable increase in kinematic parameters. The bearings work mainly in the elastic regime; there are no plastic displacements in bearings 1, 2, 4, and they are minimal in the third bearing. Table 1 summarizes the natural frequencies of the beam on bilinear hysteretic bearings and beams on equivalent elastic bearings.

Table 1

N	Natural frequencies, Hz	
	Hinged supported beam	Beam on equivalent elastic bearings
1	5.76	1.80
2	14.33	3.50
3	22.85	6.20
4	26.64	9.17
5	52.04	13.80
6	70.13	21.30

Table 2 shows the values of the objective function J_E before and after optimization, and values of the objective function with weight matrices $\mathbf{Q}_U$ and $\mathbf{Q}_\text{T}$.

Table 2. Objective function values before and after optimization

	Hinged supported beam	Beam on equivalent elastic bearings
J_E	3.133e05	1.287e05
J_U	1.570e05	3.029e04
J_T	1.563e05	9.845e04

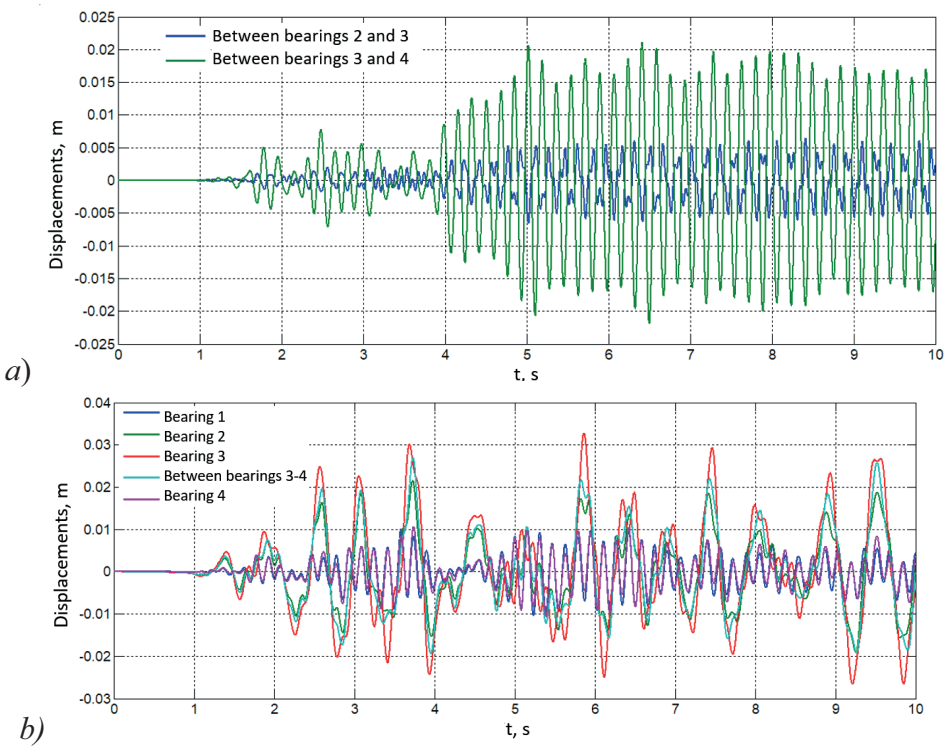


Figure 4. Displacements of cross-sections of: a) the hinged supported beam: $u_{\max} = 0.022$ m, $\sigma_{\max} = 0.010$ m; b) the optimized beam: $u_{\max} = 0.028$ m, $\sigma_{\max} = 0.009$ m.

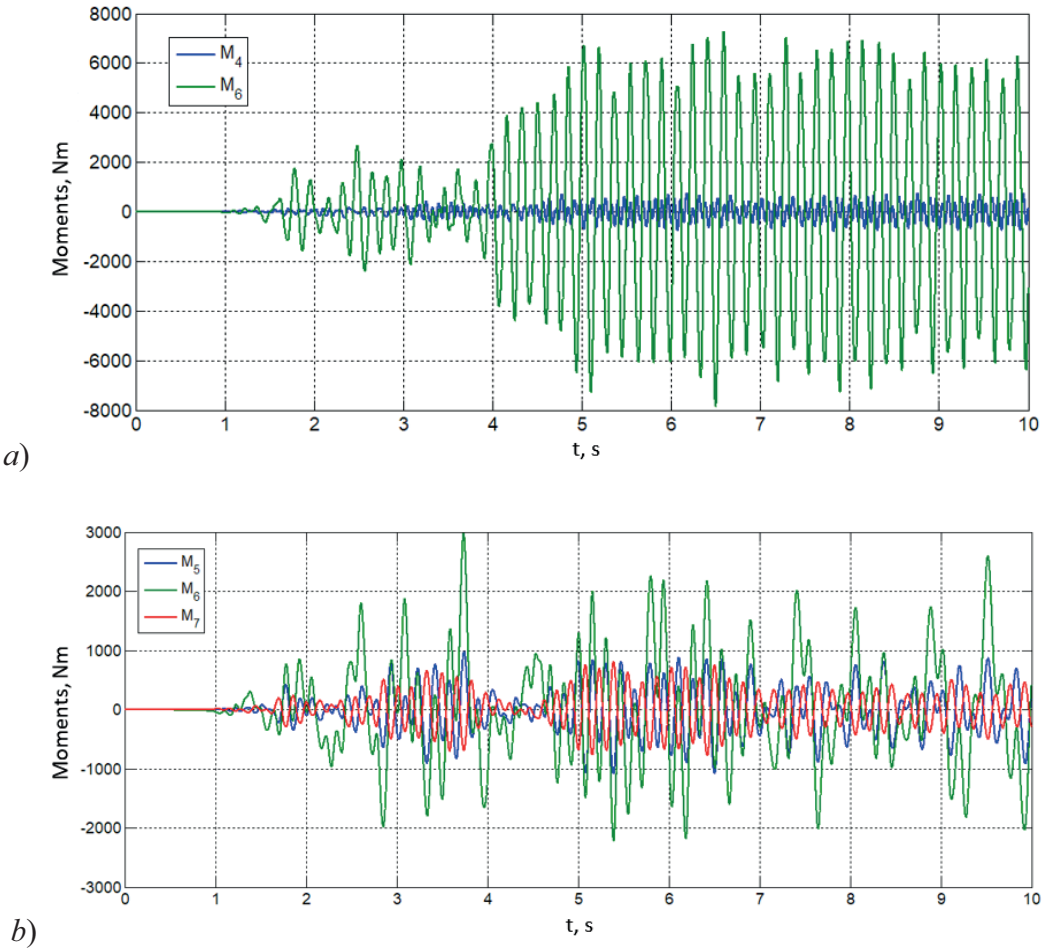


Figure 5. Bending moments: a) the hinged supported beam: M_4 – moment at the center of the second span, M_6 – moment at the center of the third span, $M_{max} = M_6 = 7.84$ kNm, $\sigma_{max} = 3.30$ kNm; b) the optimized beam: M_5 – moment at the center of the second span, M_6 – moment over the third bearing, M_7 – moment at the center of the third span, $M_{max} = M_6 = 2.98$ kNm, $\sigma_{max} = 0.860$ kNm.

4. EXPERIENCE OF USING A GENETIC ALGORITHM

Using GA to optimize a multidimensional dynamic system, you should not expect a fast and unambiguous solution. For multidimensional optimization, GA requires multiple calculations of the objective function, for example, for default parameters of the GA in the MATLAB Optimtool, if the number of parameters to be optimized is greater than 5, the initial population is $n = 200$ agents-solutions, maximal number of iterations is equal to $10n$ generations. For the above problem, we need to compute the objective function for 200 variants of the vector $\mathbf{H}$ at one iteration, and there can be 1600 such iterations. To speed up the process, it is necessary take more suitable solutions as the initial population and using elitism. Since the genetic algorithm is a stochastic method, by solving the same problem several times, you can get different solutions. The vector of optimal parameters $\mathbf{H}_*$ isn't a single best solution. Some solutions were rejected for various reasons, because they led, for example, to large plastic deformations. It was necessary to correct the initial population several times and adjust the parameters of genetic operators.

Fig. 6 shows the natural frequencies of the beam on equivalent elastic bearings and the estimates of the spectral density of the Anapa earthquake Z3G2 – A. Comparing the results in Fig. 3 and 6, we can draw a simple conclusion: the optimization resulted in a shift of the natural frequencies of the equivalent system to the minima of the seismic periodogram. To avoid such "adaptability" of the system on the bilinear hysteretic bearings to a single accelerogram, it is necessary to solve the optimization problem on a series of accelerograms. The random nature of earthquakes and the uncertainty with the resonant frequencies of the systems on nonlinear bearings make accurate tuning of resonant frequencies very unreliable. Hence, the nonlinear bearings should be used for the design of earthquake-resistant structures only if the lowest natural frequencies of the system on equivalent elastic bearings are lower than the prevailing seismic frequencies. In this case, a reasonable solution will be obtained without high computational costs.

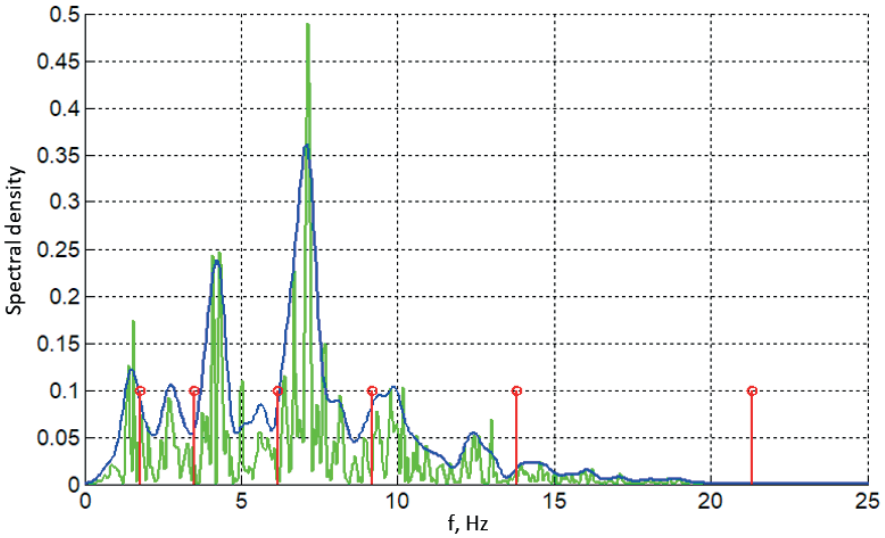


Figure 6. Anapa earthquake Z3G2–A. Spectral density: raw periodogram (green), smoothed periodogram (blue); resonant frequencies of the optimized beam (red)

5. CONCLUSIONS

In the study, an energy approach was formulated to solve the optimization problem of the structure on the bilinear hysteretic bearings. The approach is illustrated on the example of optimization of an earthquake-resistant structure. Multidimensional conditional nonlinear optimization has a complicated mathematical formulation and computationally "hard" solution. However, the optimal solution, as well as the answer to the question about the feasibility of installing a vibration protection system based on the bilinear hysteretic bearings, can be obtained by preliminary frequency analysis of the structure and seismic effects.

ACKNOWLEDGEMENTS

The work is executed within the Framework of the Project “Design of software modules for modeling the dynamic behavior of structural elements with hysteresis” with the support of a subvention from the National Research University “MPEI” for Implementation of the internal Research Program “Priority 2030: Future Technologies” in 2022-2024.

REFERENCES

1. **Radin V.P., Poznyak E.V., Chirkov V.P., Novikova O.V.** Dinamicheskie harakteris-

tiki i nastrojka vibroizolyatorov s bilinejnym gisterezisom [Dynamic characteristics and adjustment of vibration isolators with bilinear hysteresis]. *Izvestiya vysshih uchebnyh zavedenij. Mashinostroenie*, 2022, No. 12, pp. 14–23. (in Russian). doi: 10.18698/0536–1044–2022–12–14–23

2. **Radin V.P., Poznyak E.V., Novikova O.V., Chirkov V.P.** Razrabotka i issledovanie modeli zdaniya na rezinometallicheskih sejsmooporah [Development and Study of a Building Model on Lead Rubber Bearings]. *Vestnik MEI*, 2022, No. 2, pp. 105–112. (in Russian). doi: 10.24160/1993–6982–2022–2–105–112
3. **K. Ye, Y. Xiao, L. Hu** A direct displacement-based design procedure for base-isolated building structures with lead rubber bearings (LRBs), Engineering Structures, Volume 197, 2019, https://doi.org/10.1016/j.engstruct.2019.109402
4. **A.E. Çerçevik, Ö. Avşar, O. Hasançebi** Optimum design of seismic isolation systems using metaheuristic search methods, Soil Dynamics and Earthquake Engineering, Volume 131, 2020, https://doi.org/10.1016/j.soildyn.2019.106012
5. **P. Shoaei, M. Mahsuli** Reliability-based design of steel moment frame structures isolated by lead-rubber bearing systems, Structures, Volume 20, 2019, pp. 765-778, https://doi.org/10.1016/j.istruc.2019.06.020
6. **P. Shoaei, H. T. Orimi, S. M. Zahrai** Seismic reliability-based design of inelastic base-isolated structures with lead-rubber bearing systems, Soil Dynamics and Earthquake Engineering, Volume 115, 2018, pp. 589-605, https://doi.org/10.1016/j.soildyn.2018.09.033
7. **R.S. Jangid** Optimum lead–rubber isolation bearings for near-fault motions, Engineering Structures, Volume 29, Issue 10, 2007, pp. 2503-2513, ISSN 0141-0296, https://doi.org/10.1016/j.engstruct.2006.12.010
8. **T. Zordan, T. Liu, B. Briseghella, Q. Zhang** Improved equivalent viscous damping model for base-isolated structures with lead rubber bearings, Engineering Structures, Volume 75, 2014, pp. 340-352, https://doi.org/10.1016/j.engstruct.2014.05.044
9. **Bakaeva L., Egarmin K., Galikhanova E.** Effect of using rubber-metal seismic bearings on the dynamic and static characteristics of a multi–storey building. *AlfaBuil,* 2019, No. 5(12), pp. 15-26, doi: 10.34910/ALF.12.2. – EDN SERRFG.
10. **S. Eem, D. Hahm** Large strain nonlinear model of lead rubber bearings for beyond design basis earthquakes, Nuclear Engineering and Technology, Volume 51, Issue 2, 2019, pp. 600-606, https://doi.org/10.1016/j.net.2018.11.001
11. **Karpenko A.P.** Sovremennye algoritmy poiskovoj optimizacii. Algoritmy, vdohnovlennye prirodoj [Modern search engine optimization algorithms. Algorithms inspired by nature]: ucheb. posobie. – M.: Izd-vo MGTU im. N.E. Baumana, 2014. (in Russian).
12. Lead Rubber Bearings, S03. FIP Indusriale. https://www.pretensa.com.pt/upload/pdf/content_our_work/FZhd5uLx/S03_LRB-eng.pdf
13. **Y. Tu, G. Yang, Q. Cai, L. Wang, X. Zhou** Optimal design of SINS's Stewart platform bumper for restoration accuracy based on genetic algorithm, Mechanism and Machine Theory, Volume 124, 2018, pp. 42-54, https://doi.org/10.1016/j.mechmachtheory.2018.01.016
14. **A. Tsipianitis, Y. Tsompanakis** Optimizing the seismic response of base-isolated liquid storage tanks using swarm intelligence algorithms, Computers & Structures, Volume 243, 2021, 106407, https://doi.org/10.1016/j.compstruc.2020.106407
15. **J. Pérez-Aracil, C. Camacho-Gómez, P. Reynolds, E. Pereira, S. Salcedo-Sanz** Optimal vibration isolation and alignment over non-rigid bases with the CRO-SL ensemble, Engineering Applications of Artificial Intelli-

gence, Volume 113, 2022, 104984, https://doi.org/10.1016/j.engappai.2022.104984
16. **S. Etedali, K. Hasankhoie, M. R. Sohrabi** Optimal design of pure-friction isolators with and without restoring device: A multi-objective cuckoo search-based approach for seismic-excited structures, Structures, Volume 25, 2020, pp. 708-719, https://doi.org/10.1016/j.istruc.2020.03.041

СПИСОК ЛИТЕРАТУРЫ

1. **Радин В. П., Позняк Е. В., Чирков В. П., Новикова О. В.** Динамические характеристики и настройка виброизоляторов с билинейным гистерезисом. Известия высших учебных заведений. Машиностроение, 2022, № 12, С. 14–23, doi: 10.18698/0536–1044–2022–12–14–23
2. **Радин В.П., Позняк Е.В., Новикова О.В., Чирков В.П.** Разработка и исследование модели здания на резинометаллических сейсмоопорах. Вестник МЭИ, 2022, № 2, С. 105–112, doi: 10.24160/1993–6982–2022–2–105–112
3. **K. Ye, Y. Xiao, L. Hu.** A direct displacement-based design procedure for base-isolated building structures with lead rubber bearings (LRBs), Engineering Structures, Volume 197, 2019, https://doi.org/10.1016/j.engstruct.2019.109402
4. **A.E. Çerçevik, Ö. Avşar, O. Hasançebi** Optimum design of seismic isolation systems using metaheuristic search methods, Soil Dynamics and Earthquake Engineering, Volume 131, 2020, https://doi.org/10.1016/j.soildyn.2019.106012
5. **P.Shoaei, M. Mahsuli** Reliability-based design of steel moment frame structures isolated by lead-rubber bearing systems, Structures, Volume 20, 2019, pp. 765-778, https://doi.org/10.1016/j.istruc.2019.06.020
6. **P. Shoaei, H. T. Orimi, S. M. Zahrai** Seismic reliability-based design of inelastic base-isolated structures with lead-rubber bearing systems, Soil Dynamics and Earthquake Engineering, Volume 115, 2018, pp. 589-605, https://doi.org/10.1016/j.soildyn.2018.09.033
7. **R.S. Jangid** Optimum lead–rubber isolation bearings for near-fault motions, Engineering Structures, Volume 29, Issue 10, 2007, pp. 2503-2513, ISSN 0141-0296, https://doi.org/10.1016/j.engstruct.2006.12.010
8. **T. Zordan, T. Liu, B. Briseghella, Q. Zhang** Improved equivalent viscous damping model for base-isolated structures with lead rubber bearings, Engineering Structures, Volume 75, 2014, pp. 340-352, https://doi.org/10.1016/j.engstruct.2014.05.044
9. **Bakaeva L., Egarmin K., Galikhanova E.** Effect of using rubber-metal seismic bearings on the dynamic and static characteristics of a multi–storey building. *AlfaBuil,* 2019, No. 5(12), pp. 15-26, doi: 10.34910/ALF.12.2. – EDN SERRFG.
10. **S. Eem, D. Hahm** Large strain nonlinear model of lead rubber bearings for beyond design basis earthquakes, Nuclear Engineering and Technology, Volume 51, Issue 2, 2019, pp. 600-606, https://doi.org/10.1016/j.net.2018.11.001
11. **Карпенко А.П.** Современные алгоритмы поисковой оптимизации. Алгоритмы, вдохновленные природой. М.: Издательство МГТУ им. Н. Э. Баумана, 2014.
12. Lead Rubber Bearings, S03. FIP Indusriale. https://www.pretensa.com.pt/upload/pdf/content_our_work/FZhd5uLx/S03_LRB-eng.pdf
13. **Y. Tu, G. Yang, Q. Cai, L. Wang, X. Zhou** Optimal design of SINS's Stewart platform bumper for restoration accuracy based on genetic algorithm, Mechanism and Machine Theory, Volume 124, 2018, pp. 42-54, https://doi.org/10.1016/j.mechmachtheory.2018.01.016
14. **A. Tsipianitis, Y. Tsompanakis** Optimizing the seismic response of base-isolated liquid storage tanks using swarm intelligence algorithms, Computers & Structures, Volume 243, 2021, 106407,

International Journal for Computational Civil and Structural Engineering, 20(2) 60–75 (2024)

DOI:10.22337/2587-9618-2024-20-2-60-75

NUMERICAL ANALYSIS OF STRESS-STRAIN STATE OF THE STEEL MODULAR BLOCK WITH CORRUGATED WEBS

Olga A. Tusnina, Anatoliy V. Alekseytsev

National Research Moscow State University of Civil Engineering, Moscow, RUSSIA

Abstract. Modular blocks are widely used in industrial and civil engineering both as stand-alone structures and combined into block-modular buildings. Modular block consists of the load bearing frame, wall fencing, roof and floor decking. The modular block, with wall fencing made of corrugated sheet continuously welded to the beams, is a spatial system, with beams and corrugated webs working together. The steel modular block for the gas pumping unit on a gas turbine power plant is considered in the paper. Assessment of the corrugated web thickness effect on the load bearing capacity of the block is performed. Numerical investigation of stress-strain state of the blocks with different thickness of corrugated web is carried out by the finite element method. The values of the ultimate destructive load on the blocks with different thickness of the corrugated web are determined. The values of the allowable load on the block and the criteria for its limitation have been established depending on the stress-strain state of the block and the causes of destruction.
For comparison, a calculation was made of a block with walls made of sandwich panels that are not included in the work of the frame. It is determined that ultimate load on the block with corrugated webs is 1,5-6 times greater than on the block with wall sandwich panels.

Key words: modular building, steel modular block, corrugated web, critical load, buckling, finite-element analysis

ЧИСЛЕННЫЙ АНАЛИЗ НАПРЯЖЕННО-ДЕФОРМИРОВАННОГО СОСТОЯНИЯ СТАЛЬНОГО МО-ДУЛЬНОГО БЛОКА СО СТЕНАМИ ИЗ ГОФРИРОВАННОГО ЛИСТА

О.А. Туснина, А.В. Алексейцев

Национальный исследовательский Московский государственный строительный университет, г. Москва, РОССИЯ

Аннотация. Строительство промышленных и гражданских зданий из модульных блоков получает широкое распространение благодаря эффективности и экономичности таких конструкций. Модульные блоки используют как отдельно стоящие сооружения, так и объединяют между собой в блочно-модульные здания. В статье рассмотрен стальной модульный блок газоперекачивающего аппарата на газотурбинной электростанции. Модульный блок, в котором гофрированная стенка, непрерывно приваривается к балкам, представляет собой пространственную систему с совместно работающими балками и стенкой. Выполнен численный анализ влияния толщины гофрированной стенки на несущую способность блока. Определена разрушающая нагрузка на блок и параметры напряженно-деформированного состояния конструктивных элементов блоков при различной толщине гофрированных стенок (1 мм, 2 мм, 2,5 мм и 3 мм). Установлены величины допускаемой нагрузки на блок и критерии ее ограничения, в зависимости от напряженно-деформированного состояния блока и причин разрушения. Для сравнения выполнен расчет блока с навесными стенами из сэндвич-панелей, не включающимися в работу каркаса. Получено, что разрушающая нагрузка для рассмотренных блоков с гофрированными стенками в 1,5-6 раз выше, чем для блока со стеновыми сэндвич-панелями.

Ключевые слова: модульное здание, стальной модульный блок, гофрированная стенка, критическая нагрузка, потеря устойчивости, конечно-элементный расчет

DOI:10.22337/2587-9618-2024-20-2-99-108

PROBABILISTIC DESIGN OF FLEXURAL CROSS-LAMINATED TIMBER STRUCTURAL ELEMENTS

Sergey A. Solovev, Valery M. Puchkov, Anastasia A. Soloveva
Vologda State University, Vologda, RUSSIA

Abstract: The article presents a probabilistic approach to the design of flexural elements made of cross-laminated timber (CLT) as one of the promising materials for sustainable construction. The variability of the elasticity modulus and the ultimate strength of the timber layers effects on the structural safety. Such uncertainty can be modeled by using probabilistic and statistical methods. Information is presented on tests of a three-layer CLT panel during bending, and statistical parameters are given for wooden control samples of the CLT panel layers. The implementation of the presented approach makes it possible to obtain an estimate of the reliability index or the failure probability for the CLT structural element according to the criterion of normal cross-sections strength. With a given target level of reliability or risk value, the reliability level of the design solution of a cross-laminated structure can be quantified.

Keywords: cross-laminated timber, CLT, reliability index, probabilistic design, failure probability, flexural element, risk analysis

ВЕРОЯТНОСТНОЕ ПРОЕКТИРОВАНИЕ ИЗГИБАЕМЫХ ЭЛЕМЕНТОВ ИЗ ПЕРЕКРЕСТНО-КЛЕЕНОЙ ДРЕВЕСИНЫ

С.А. Соловьев, В.М. Пучков, А.А. Соловьева
ФГБОУ ВО «Вологодский государственный университет», Вологда, РОССИЯ

Аннотация: В статье представлен вероятностный подход к проектированию изгибаемых элементов из перекрестно-клееной древесины как одного из перспективных материалов для устойчивого строительства. Изменчивость модуля упругости и предела прочности слоев древесины влияет на безопасность эксплуатации конструкции, что может быть достоверно смоделировано путем использования вероятностно-статистических методов. Приведены данные об испытаниях трехслойной CLT панели при изгибе, а также статистическая информация об испытаниях контрольных образцов древесины слоев панели. Реализация представленного подхода позволяет получить оценку индекса надежности или вероятности безотказной работы для CLT элемента по критерию прочности нормальных сечений. При заданном целевом уровне надежности или значении риска можно количественно выразить уровень надежности проектного решения конструкции из перекрестно-клееной древесины.

Ключевые слова: перекрестно-клееная древесина, CLT, индекс надежности, вероятностное проектирование, вероятность отказа, изгибаемый элемент, анализ риска

INTRODUCTION

Cross-laminated timber (CLT), an engineered wood product that was originally developed in Europe in the 1990s, has been gaining worldwide popularity in helping to define a new class of timber products known as massive or “mass” timber. By GOST 56706-2022, cross-laminated timer is a massive wooden slab, manufactured in a factory manner and consisting of at least three orthogonally glued layers of solid or fused boards along a toothed joint and intended for use as a load-bearing and enclosing structural element. Besides gluing, nails, screws, or wooden dowels can be used to attach the layers. Innovative CLT products such as Interlocking Cross-Laminated Timber (ICLT) are in the process of development. As noted in Canadian CLT Handbook [1], “CLT is one of several mass timber products considered to be the “game changer” in this endeavor and the catalyst to enable other wood products to be used in those applications”. Regarding the

ongoing global activities, CLT production volume is expected to significantly increase over the next decade [2].

Since CLT is a relatively new structural material, at the moment there is not a large amount of statistical data on failures of CLT structural elements during construction or maintenance. The design of CLT elements is based on the semi-probabilistic methods (limit state design or partial safety factor method).

Eurocode 0 "Basis of structural design" divides the structural design methods into three levels: Semi-probabilistic methods (Level I), First-Order Reliability Methods (FORM) (Level II) and Full probabilistic methods (Level III). It is noted, that full probabilistic methods (Level III) give in principle correct answers to the reliability problem. Thus, the research and development of probabilistic methods for designing CLT elements is an urgent task aimed at developing the design theory of such structures.

There are some researches of probabilistic problems in cross laminated timer elements behavior. The article [3] presents the stochastic-mechanical multivariate model approach was established describing the load–displacement behavior of self-tapping screws. In the research [4] noted that "the present work should have shown the capability of the employed probabilistic methods to efficiently predict the variability of glued laminated timber. In future, probabilistic simulations will help in accomplishing more efficient timber structures, starting at the grading of wooden boards and development of timber products to engineering design of complex timber structures". A probabilistic approach is used in [5] for analyze the mechanical properties of three types of CLT connections.

The article [6] presents use of probabilistic methods for determination of stiffness and strength parameters of the CLT panels based on test data. Authors of the fundamental research of glued laminated timber beams stochastic behavior [7] notes "Due to the natural growth process of trees, wooden boards show a high amount of random fluctuation in their mechanical properties. Currently, in engineering practice, a homogeneous material behavior is assumed within wooden boards and uncertainties in loading and load-bearing capacity are considered through design procedures based on partial safety factors. These partial safety factors are not directly linked to the individual mechanical behavior of the considered structural system/element. Thus, a stochastic framework opening up the possibility to establish such links, by combining structural analysis tools with probabilistic descriptions of wooden boards, could be an important step in timber design, also to improve the competitiveness of wood against other building materials".

This paper considers the problem of probabilistic design of flexural CLT structural elements by the normal cross-section strength criterion on a target reliability level.

MATERIALS AND METHODS

According to Canadian CLT Handbook (2019) [1], the limit state condition for normal sections of flexural CLT structural elements can be written as:

$$\sigma = \frac{0{,}5 \cdot M \cdot h \cdot E_{mean}}{(E \cdot I)_{eff}} \le \sigma_{ult}, \qquad (1)$$

where M is a bending moment in the cross-section; h is a thickness of the CLT panel; E_{mean} is an average elasticity modulus of the cross-section; $(E \cdot I)_{eff}$ is effective bending stiffness of the panel for the major strength axis; σ_{ult} is bending strength or ultimate stress in the cross-section.

The effective bending stiffness can be determined as:

$$(E \cdot I)_{eff} = \sum_{i=1}^{n} E_i \cdot b_y \cdot \frac{t_i^3}{12} + \sum_{i=1}^{n} E_i \cdot b_y \cdot t_i \cdot z_i^2, \qquad (2)$$

where b_y is a width of the panel for the major strength axis; E_i is a modulus of elasticity of laminations in the *i*-th layer; t_i is a thickness of laminations in the *i*-th layer; z_i is a distance between the center point of the *i*-th layer and the neutral axis (Fig. 1).

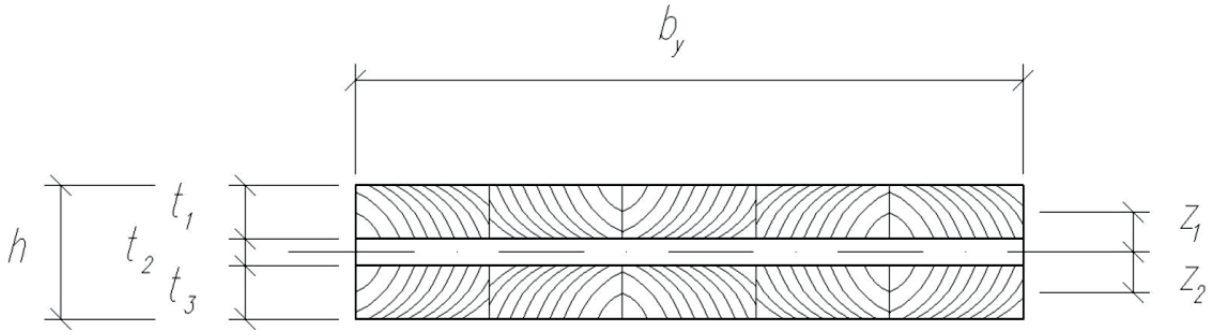


Figure 1. Cross-section parameters for a CLT structural element

The resistance factor of CLT in bending $\phi = 0{,}9$ and the strength modification factor $K_{rb,y} = 0{,}85$ as the partial safety factors are neglected in (2) because probabilistic approach will be used further. Some other safety factors by National Building Codes are also neglected in probabilistic models because it should be taken into account in probability distribution functions and parameters directly.

The dimensions of the geometric parameters are assumed to be deterministic, because the production technology of CLT panels allows controlling woodworking process with high precision.

The limit state function can be written as:

$$g = \frac{0{,}5 \cdot \widetilde{M} \cdot h \cdot E_{mean}}{\widetilde{\sigma}_{ult} \cdot b_y \cdot \left[\sum_{i=1}^{n} \widetilde{E}_i \cdot \frac{t_i^3}{12} + \sum_{i=1}^{n} \widetilde{E}_i \cdot t_i \cdot z_i^2 \right]} \le 1, \quad (3)$$

where are random variables denoted by the wavy lines.

The Mechanically Jointed Beams Theory can also be used of estimation of normal cross-section's bearing capacity. This method, also named Gamma Method (γ-method), was developed in 1955 by Professor Karl Möhler. According to this method, the stiffness properties of the mechanically jointed beams are defined using the Effective Bending Stiffness $(E \cdot I)_{eff}$, which is dependent on the section properties of the beams and the connection efficiency factor γ. The γ factor depends on the slip characteristics of the fasteners (also called *s*/*K* ratio), being zero for no mechanical connection between the beams and equaling unity for rigidly connected beams.

$$g = \frac{\widetilde{M} \cdot E_1}{\widetilde{\sigma}_{ult} \cdot (\widetilde{E} \cdot I)_{eff}} \left[\gamma_1 a_1 + \frac{h_1}{2} \right] \le 1,$$

where a_1 is the distance between the centroid of the first lamina and the centroid of the panel cross-section, and h_1 is the thickness of the first (outermost) lamina. As noted in [1], the γ factor may typically vary from 0.85 to 0.9.

The reliability index for CLT structural element by the normal cross-section strength can be expressed as:

$$\beta = \frac{1 - m_g}{S_g},$$

where m_g is an expected value and S_g is a standard deviation for limit state function *g*.

The failure probability of normal cross-sections is presented as $P_f = \Pr(g > 1)$, or $P_f = \Phi(\beta)$ if all random variables is described by the normal distribution, where Φ(.) is the value from the standard normal table (z-value table).

Two groups of methods for probabilistic reliability analysis can be distinguished:

- Analytical methods: FOSM (First Order Second Moment); FORM (First Order Reliability Method); SORM (Second Order Reliability Method); TANA (Two-point Adaptive Nonlinear Approximation), etc.
- Numerical methods: Monte Carlo methods, data sampling, discretization into Dempster-Shafer structures, etc.

Analytical methods obtain an accurate solution for the probability of non-failure of structural elements, but have a number of limitations: approximation of highly nonlinear limit state functions leads to computational errors; complexity of constructing models for mechanical systems taking into account the dependence of random variables; influence of the type and form of the mathematical model of the limit state (invariance problem); the complexity of the combination of different models of random variables – within the framework of one practical task, fuzzy variables, interval parameters, random sets, etc. may be present simultaneously.

Numerical methods make it possible to effectively model highly nonlinear mathematical models of limit states and analyze the reliability of complex systems, but the accuracy of such approaches may be low in cases of low probabilities of failure [8]. Computational time costs should also be taken into account when probabilistic reliability analysis using numerical methods, which can be quite high in the case of complex systems.

The Monte Carlo method in [9] refers to the methods of the level III (see above). It is also noted that for tasks with a low probability of failure, which is often found in engineering and construction practice, a large number of random variable generations are needed to achieve the required accuracy of the results.

The failure probability P_f based on the Monte Carlo simulations is defined as:

$$P_f \approx \frac{1}{N}\sum_{j=1}^{N} I\left[g\left(\mathrm{X}_j\right) > 1\right], \qquad (4)$$

where $I[.]$ is an indicator function, which takes value 1 if *I*[.] equal "true" and 0 if *I*[.] equal "fall"; *N* is number of simulations.

The simulation of random variables according to the basic probability distributions (normal, uniform, etc.) can be performed, for example, in the MathCAD software. However, often the probability distribution function may differ from well-known distributions or represent a model of a partially nonparametric p-box [10]. In this case, N.V. Smirnov's inverse transformation method can be used: N values of a uniformly distributed random variable u_i are simulated ranging from [0; 1]. The values of a random variable in the form are obtained by the inverse transformation method $x_i = F^{-1}(u_i)$. For more information, see the research [10].

RESULTS AND DISCUSSION

The CLT panel was tested in the laboratory of structural researches in Vologda State University. The design scheme and the general view of tested element are presented at the Fig. 2.

The strain gauges were installed in the middle of the span of the CLT-panel. The deflection gauge (the clock-type indicator) was also installed in the span middle. A test load was created by reinforced concrete beams. The test load was maintained until the strains and deformations were stabilized.

The load-strain curve and the load-deflection are presented at the Fig. 3 and Fig. 4.

a)



b)

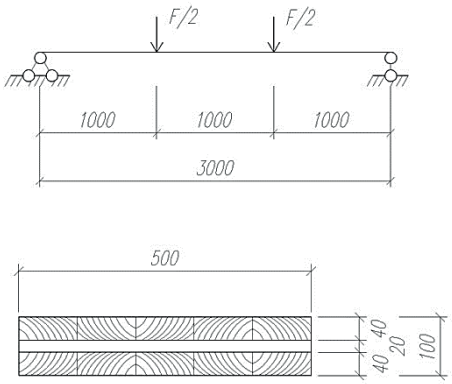


Figure 2. a) general view b) design parameters of the CLT panel

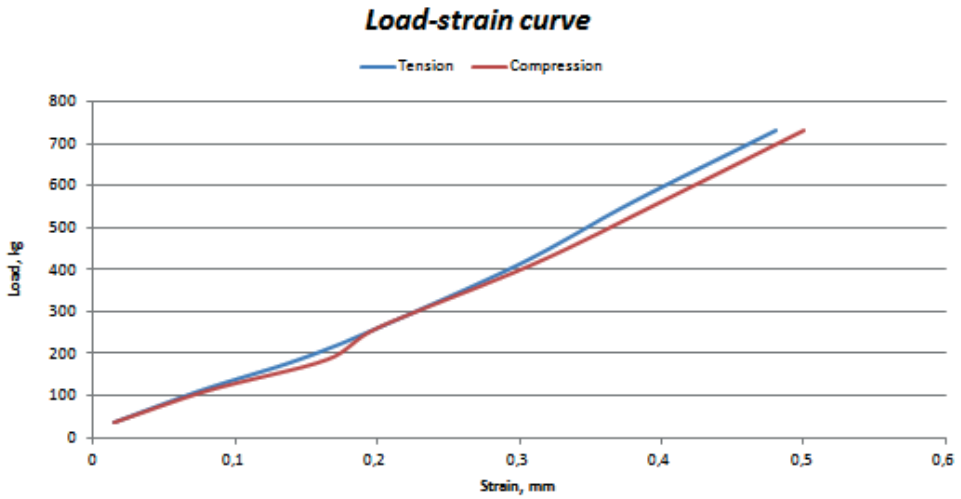


Figure 3. Load-strain curves for the CLT panel

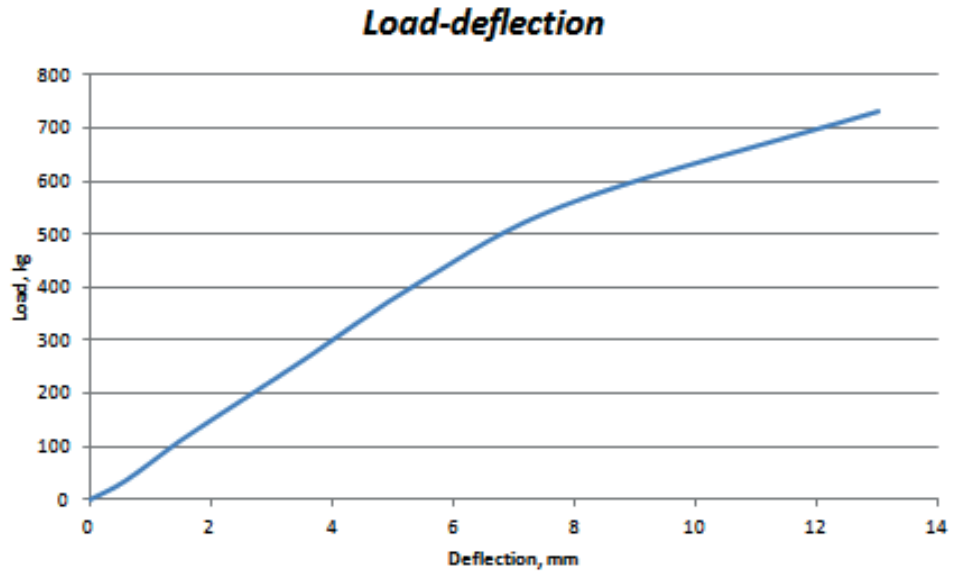


Figure 4. Load-deflection diagram

The design parameters of cross-section are $t_1 = 0.04$ m, $t_2 = 0.02$ m, $t_3 = 0.04$ m, $b_y = 0.50$ m, $h = 0.10$ m, $l = 3.00$ m. If we consider the codified design, the following values can be taken $E_1 = E_2 = E_{mean} = 10$ GPa, $\sigma_{ult} = 21$ MPa. Based on this values, the ultimate bending moment by eq. (3) is $M_{ult} = 34.7$ kN·m.

As can be seen from above, the linear function can be adopted for the load-deflection and load-strain relationships at the elastic stage of CLT-panels behavior.

The variation coefficient of elasticity modulus for coniferous wood is about to 15-20 percent [11].

Ten control samples of wood were taken from every layer of CLT panel for standard tests.

The empirical distribution functions $F_E^{emp}(E)$ and the estimated cumulative distribution functions $F_E(E)$ are presented on the Fig. 5 for upper and lower layers of the CLT panel.

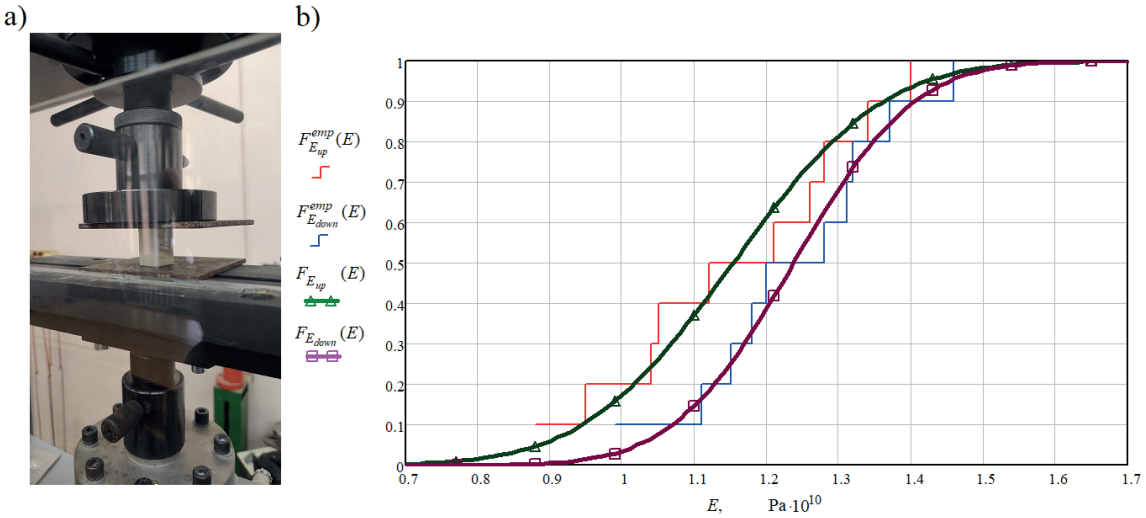


Figure 5. Statistical tests for elasticity modulus of the CLT panel's upper and lower layers: a) Test of a control sample; b) Cumulative density functions for elasticity modulus

As can be seen from Fig. 5(b), the random variable models for the elasticity modulus of upper and lower layers of the CLT panel are quite different. The coefficient of variation is higher and the expected value is lower for upper layer. The graphs in Fig. 5 also reflect the fact that the lower and upper layers of the CLT panel can be made of different timber, which can lead to a shift of the neutral axis and a redistribution of stresses. As a rule, the variability of this value is small and can be ignored at the first analytical stage of calculation. Probabilistic design can take into account such aspects. It will be taken into account in numerical calculations.

Normal distribution is adopted for the elasticity modulus of upper and lower layers. Following parameters are taken: $m_{E,up} = 11.53$ GPa, $S_{E,up} = 1.63$ GPa, $m_{E,down} = 12.37$ GPa, $S_{E,down} = 1.31$ GPa.

Ten control samples were also tested on bending. By the same way, following sample parameters were obtained: $m_{\sigma,ult} = 38.93$ MPa, $S_{\sigma,ult} = 4.85$ MPa.

It should be noted that for more accurate modeling of random variables by a small sample, it is necessary to use alternative models, for example, such as p-boxes [10]. However, to demonstrate the method, the hypothesis is used that the sample parameters estimates correspond to the parameters of the population.

Next, 100'000 values of random variables are generated in PTC MathCAD by the above statistical data. The number of failures is

calculated on given value of the bending moment for tested CLT panel. Substituting the bending moment values according to Table 1 into the g function (3) for each of the 100,000 cases, it is possible to obtain the number of failed CLT panels for the total number of generations and to estimate the failure probability P_f and the corresponding reliability index β.

The relationship between reliability (probability of non-failure $P_s = 1 - P_f$) and bending moment is presented on Fig. 6.

Table 1. Reliability of the tested CLT panel

Bending moment M, kN·m	Reliability index β	Failure probability P_f
30.00	5.00	0.00004
35.00	3.40	0.00033
40.00	2.74	0.00312
45.00	2.12	0.01709
50.00	1.53	0.06253

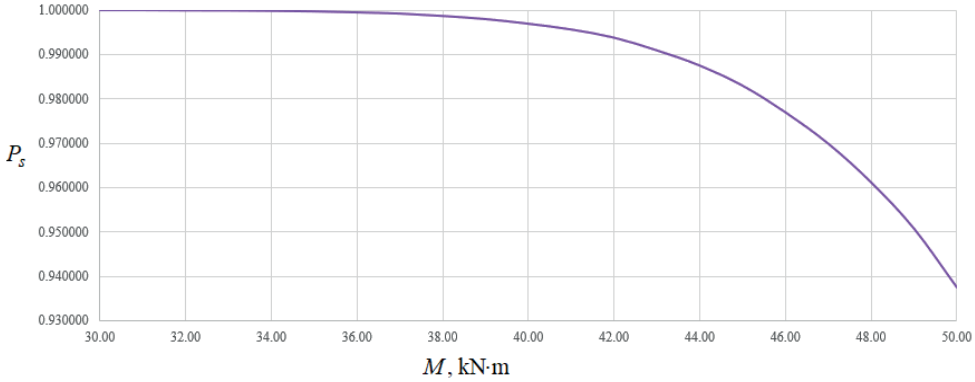


Figure 6. Relationship between reliability and test load on the CLT panel

To obtain a more accurate solution, it becomes necessary to take into account the inhomogeneities of each individual board in each layer of the CLT element. The solution of such problems is the domain of numerical solutions, for example, the finite element method [12-15]. The task is to build a model in a FEM program, and then simulate inhomogeneities by generating initial data (elasticity modulus, timber strength, etc.) using the Monte Carlo method. Reliability will also be determined by the ratio of the number of non-failure FEM models to the total number of initial data generations. However, as a rule, the use of such algorithms is associated with high costs of time and computing power.

CONCLUSIONS

Cross-laminated timber (CLT) is an innovative timber product that was introduced in the early 1990s in Austria and Germany and has been gaining popularity in many civil applications. The article presents a probabilistic approach to estimate the reliability level (reliability index or failure probability) of a CLT element in bending according to the strength criterion of normal cross-sections. The elasticity modulus and bending strength of wood have a high coefficient of variation (up to 20-25%), which is important to model in CLT elements, since they consist of many sub-elements (glued boards). The Monte Carlo method based on wood test data can be used in both analytical and numerical methods for structural design of CLT elements to further assess their reliability in probabilistic terms. P-boxes as random variables models can be used in case of limited statistical data.

ACKNOWLEDGMENTS

The research was funded by Russian Science Foundation (RSF) No. 23-79-01035. https://rscf.ru/en/project/23-79-01035/.

REFERENCES

1. **Karacabeyli E., Gagnon S.** Pointe-Claire Canadian CLT Handbook, 2019, 812 p.
2. **Schickhofer G., Brandner R., Bauer H.** (2016) Introduction to CLT, Product Properties, Strength Classes, in: Cross Laminated Timber - a Competitive Wood Product for Visionary and Fire Safe Buildings: Joint Conference of COST Actions FP1402 and FP1404, KTH, Stockholm, Sweden.
3. **Brandner R., Ringhofer A., Grabner M.** (2018) Probabilistic models for the withdrawal behavior of single self-tapping screws in the narrow face of cross laminated timber (CLT). European Journal of Wood and Wood Products, vol. 76, pp. 13-30.
4. **Kandler G., Füssl J.A.** (2017) Probabilistic approach for the linear behaviour of glued laminated timber. Engineering structures, vol. 148, pp. 673-685.
5. **Cao, J., Xiong, H., Chen, J., & Huynh, A.** (2019) Bayesian parameter identification for empirical model of CLT connections. Construction and Building Materials, vol.218, pp. 254-269.
6. **Dobeš P., Lokaj A.** (2020) Use of probabilistic methods for design of CLT panels. ARPN Journal of Engineering and Applied Sciences, vol. 15, no. 8, pp. 977-982.
7. **Kandler, G., Lukacevic, M., Zechmeister, C., Wolff, S., & Füssl, J.** (2018) Stochastic engineering framework for timber structural elements and its application to glued laminated timber beams. Construction and Building Materials, vol. 190, pp. 573-592.
8. **Grooteman F.** Adaptive radial-based importance sampling method for structural reliability // Structural Safety. – 2008. – Vol. 30. – No. 6. – Pp. 533-542.
9. **Cardoso J.B., de Almeida J.R., Dias J.M., Coelho P.G.** (2008) Structural reliability analysis using Monte Carlo simulation and neural networks. Advances in Engineering Software, vol. 39(6), pp. 505-513.
10. **Soloveva, A.A.** (2021) Reliability Analysis of RHS Steel Trusses Joints Based on the P-Boxes Approach. International Journal for Computational Civil and Structural Engineering, vol. 17, no. 1, pp. 87-97. DOI 10.22337/2587-9618-2021-17-1-87-97.
11. **Volynskij V.N.** Vzaimosvyaz I izmenchivost pokazatelej fiziko-mehanicheskih svojstv drevisiny [Interrelation and variability of indicators of physical and mechanical properties of wood]. Moscow, 2006, 215 p.
12. **Marjanović, M., Marković, N., Damnjanović, E., & Cvetković, R.** (2020) Three-dimensional stress analysis and design of cross-laminated timber panels using full-layerwise-theory-based finite element method. Thin-Walled Structures, vol. 157, pp. 107-156.
13. **Berg, S., Turesson, J., Ekevad, M., Huber, J.A.** (2019) Finite element analysis of bending stiffness for cross-laminated timber with varying board width. Wood Material Science & Engineering, vol. 14, pp. 392-403.
14. **Furtmüller T., Adam C.A**. (2023) Finite element for static and dynamic analyses of cross-laminated timber floors. Engineering Structures, vol. 293, pp. 116-669.
15. **Autengruber, M., Lukacevic, M., Gröstlinger, C., & Füssl, J.** (2021) Finite-element-based prediction of moisture-induced crack patterns for cross sections of solid wood and glued laminated timber exposed to a realistic climate condition. Construction and Building Materials, vol. 271, pp.121-775.
16. **Brandner R., Flatscher G., Ringhofer A., Schickhofer G**. (2016) Theil, Cross laminated timber (CLT): overview and development. European Journal of Wood and Wood Products, vol. 74, pp. 331–351. https://doi.org/10.1007/s00107-015-0999-5.
17. **Gaugris J.Y., van Rooyen M.W**. (2019) Evaluating Patterns of Wood Use for

Building Construction Evaluating patterns of wood use for building construction in Maputaland, South Africa. South African Journal of Wildlife Research, vol. 39, pp. 85–96.
18. **Lewis K., Shrestha R., Crews K.** (2014) Introduction to cross laminated timber and development of design procedures for Australia and New Zealand. 23rd Australasian Conference on the Mechanics of Structures and Materials, pp. 601–606.
19. **Amini M.O., van de Lindt J.W., Pei S., Rammer D., Line P., Popovski, M**. (2014) Overview of a project to quantify seismic performance factors for cross laminated timber structures in the United States. In Materials and Joints in Timber structures, pp. 531-541.
20. **Pei S., Popovski M., van de Lindt J.W**. (2013) Analytical study on seismic force modification factors. Canadian Journal of Civil Engineering, vol. 40, no.9, pp. 887-896.

СПИСОК ЛИТЕРАТУРЫ

1. **Karacabeyli E., Gagnon S.** Pointe-Claire Canadian CLT Handbook, 2019, 812 pages.
2. **Schickhofer G., Brandner R., Bauer H.** Introduction to CLT, Product Properties, Strength Classes, in: Cross Laminated Timber - a Competitive Wood Product for Visionary and Fire Safe Buildings // Joint Conference of COST Actions FP1402 and FP1404, KTH, Stockholm, Sweden, 2016.
3. **Brandner R., Ringhofer A., Grabner M.** Probabilistic models for the withdrawal behavior of single self-tapping screws in the narrow face of cross laminated timber (CLT) // European Journal of Wood and Wood Products, 2018, vol. 76, pp. 13-30.
4. **Kandler G., Füssl J.** A probabilistic approach for the linear behaviour of glued laminated timber // Engineering structures, 2017, vol. 148, pp. 673-685.
5. **Cao, J., Xiong, H., Chen, J., & Huynh, A.** Bayesian parameter identification for empirical model of CLT connections // Construction and Building Materials, 2019, vol. 218, pp. 254-269.
6. **Dobeš P., Lokaj A.** Use of probabilistic methods for design of clt panels // ARPN Journal of Engineering and Applied Sciences, 2020, vol. 15, no. 8, pp. 977-982.
7. **Kandler, G., Lukacevic, M., Zechmeister, C., Wolff, S., & Füssl, J.** Stochastic engineering framework for timber structural elements and its application to glued laminated timber beams // Construction and Building Materials, 2018, vol. 190, pp. 573-592.
8. **Grooteman F.** Adaptive radial-based importance sampling method for structural reliability // Structural Safety, 2008, vol. 30, no. 6, pp. 533-542.
9. **Cardoso J.B., de Almeida J.R., Dias J.M., Coelho P.G.** Structural reliability analysis using Monte Carlo simulation and neural networks // Advances in Engineering Software, 2008, vol. 39(6), pp. 505-513.
10. **Soloveva, A.A.** Reliability Analysis of RHS Steel Trusses Joints Based on the P-Boxes Approach // International Journal for Computational Civil and Structural Engineering, 2021, vol. 17, no. 1, pp. 87-97. – DOI 10.22337/2587-9618-2021-17-1-87-97.
11. **Волынский, В.Н.** Взаимосвязь и изменчивость показателей физико-механических свойств древесины. – Архангельск, 2006. – 215 с.
12. **Marjanović, M., Marković, N., Damnjanović, E., & Cvetković, R.** Three-dimensional stress analysis and design of cross-laminated timber panels using full-layerwise-theory-based finite element method // Thin-Walled Structures, 202, vol. 157, pp. 107-156.
13. **Berg, S., Turesson, J., Ekevad, M., & Huber, J.A.** Finite element analysis of bending stiffness for cross-laminated timber with varying board width // Wood Material

Science & Engineering, 2019, vol. 14, pp. 392-403.
14. **Furtmüller T., Adam C.** A finite element for static and dynamic analyses of cross-laminated timber floors // Engineering Structures, 2023, vol. 293, pp. 116-669.
15. **Autengruber, M., Lukacevic, M., Gröstlinger, C., & Füssl, J.** Finite-element-based prediction of moisture-induced crack patterns for cross sections of solid wood and glued laminated timber exposed to a realistic climate condition // Construction and Building Materials, 2021, vol. 271, pp. 121-775.
16. **Brandner R., Flatscher G., Ringhofer A., Schickhofer G.** Theil, Cross laminated timber (CLT): overview and development // European Journal of Wood and Wood Products, 2016 vol. 74, pp. 331–351. https://doi.org/10.1007/s00107-015-0999-5.
17. **Gaugris J.Y., van Rooyen M.W.** Evaluating Patterns of Wood Use for Building Construction Evaluating patterns of wood use for building construction in Maputaland, South Africa // South African Journal of Wildlife Research, 2019, vol. 39, pp. 85–96.
18. **Lewis K., Shrestha R., Crews K.** Introduction to cross laminated timber and development of design procedures for Australia and New Zealand // 23rd Australasian Conference on the Mechanics of Structures and Materials, 2014, pp. 601–606.
19. **Amini M. O., van de Lindt J. W., Pei S., Rammer D., Line P., Popovski, M.** Overview of a project to quantify seismic performance factors for cross laminated timber structures in the United States // In Materials and Joints in Timber structures, 2014, pp. 531-541.
20. **Pei S., Popovski M., van de Lindt J.W**. Analytical study on seismic force modification factors // Canadian Journal of Civil Engineering, 2013, vol. 40, no.9, pp. 887-896.

Solovev Sergey, Candidate of Technical Sciences, Associate Professor of the Industrial and Civil Engineering Department, Vologda State University (VSU), 160000, Russia, Vologda, ul. Lenina, 15, tel. +7 (8172) 51-83-96, e-mail: solovevsa@vogu35.ru

Puchkov Valery, Post-Graduate Student of the Industrial and Civil Engineering Department, Vologda State University (VSU), 160000, Russia, Vologda, ul. Lenina, 15, tel. +7 (8172) 51-83-96, e-mail: puchkovvm@vogu35.ru

Soloveva Anastasia, Post-Graduate Student, Lecturer of the Industrial and Civil Engineering Department, Vologda State University (VSU), 160000, Russia, Vologda, ul. Lenina, 15, tel. +7 (8172) 51-83-96, e-mail: solovevaaa@vogu35.ru

Соловьев Сергей Александрович, кандидат технических наук, доцент кафедры промышленного и гражданского строительства, Вологодский государственный университет (ВоГУ), 160000, Россия, г. Вологда, ул. Ленина, д. 15, тел. +7 (8172) 51-83-96, e-mail: solovevsa@vogu35.ru

Пучков Валерий Михайлович, аспирант кафедры промышленного и гражданского строительства, Вологодский государственный университет (ВоГУ), 160000, Россия, г. Вологда, ул. Ленина, д. 15, тел. +7 (8172) 51-83-96, e-mail: puchkovvm@vogu35.ru

Соловьева Анастасия Андреевна, аспирант, старший преподаватель кафедры промышленного и гражданского строительства, Вологодский государственный университет (ВоГУ), 160000, Россия, г. Вологда, ул. Ленина, д. 15, тел. +7 (8172) 51-83-96, e-mail: solovevaaa@vogu35.ru

DOI:10.22337/2587-9618-2024-20-2-109-117

THE EFFECT OF MONTMORILLONITE ON THE RHEOLOGICAL AND PHYSICO-MECHANICAL PROPERTIES OF A THERMOSETTING POLYMER COMPOSITE

Pavel V. Monastyrev [1], Tatiana F. Elchishcheva [1], Maxim V. Makarchuk [1], Vladimir T. Erofeyev [2], Vladimir I. Rimshin [2], Irina V. Erofeeva [2]

[1] Tambov state technical University, Tambov, RUSSIA
[2] NRU Moscow State University of Civil Engineering (National Research University), Moscow, RUSSIA

Abstract: The study investigates a thermosetting polymer filled with montmorillonite. Montmorillonite is a naturally occurring layered mineral with particle sizes ranging from 8 to 12 μm. The thermosetting polymer was DER-330 epoxy resin and FCH-S hardener. Rheological and physical-mechanical studies of the properties of epoxy resin modified with montmorillonite were carried out. Viscosity versus shear rate is shown for uncured pure epoxy resin and resin modified with montmorillonite particles at room temperature. At low shear rates, a significant effect of montmorillonite on the properties of the composite is observed. The low shear rate further allowed epoxy molecules to leak between the layers of montmorillonite platelets, causing swelling and increasing the distance between them. As the shear rate increased from 8 to 20 s-1, the percolation time of montmorillonite decreased, which affected the decrease in viscosity. When the shear rate increases above 20 s-1, no significant changes in viscosity occur; for both samples a monotonic line is observed on the graph. The addition of montmorillonite to epoxy resin changes the chemical composition of the composite, which leads to changes in rheological and physical-mechanical properties. The addition of montmorillonite retards gelation, which can affect processability, cure time, and final properties of the composite. Morphological studies were carried out to determine the degree of dispersion of montmorillonite particles in the polymer composite using a transmission electron microscope. The uneven distribution of montmorillonite particles predominated in all samples. Apparently this is due to the curing conditions of the polymer composite and insufficient dispersion time. Physical and mechanical studies were carried out on samples made of a composite with montmorillonite in comparison with samples from pure epoxy resin. The flexural strength of samples made from the resulting composite is comparable to the strength of samples made from pure epoxy resin. In turn, the viscosity increased by 170%.

Keywords: polymer materials, epoxy composite, montmorillonite, polymer fillers, thermosetting resins

ВЛИЯНИЕ МОНТМОРИЛЛОНИТА НА РЕОЛОГИЧЕСКИЕ И ФИЗИКО-МЕХАНИЧЕСКИЕ СВОЙСТВА ТЕРМОРЕАКТИВНОГО ПОЛИМЕРНОГО КОМПОЗИТА

П.В. Монастырев [1], Т.Ф. Ельчищева [1], М.В. Макарчук [1], В.Т. Ерофеев [2], В.И. Римшин [2], И.В. Ерофеева [2]

[1] Тамбовский государственный технический университет, г. Тамбов, РОССИЯ
[2] НИУ Московский государственный инженерно-строительный университет (Национальный исследовательский университет), г. Москва, РОССИЯ

Аннотация: В данной работе были проведены исследования терморактивного полимера, наполненного монтмориллонитом. Монтмориллонит представляет собой встречающийся в природе слоистый минерал, размер частиц которого составляет от 8 до 12 мкм. В качестве термореактивного полимера использовалась эпоксидная смола DER-330 и отвердитель FCH-S. Проведены реологические и физико-механические исследования свойств эпоксидной смолы, модифицированной монтмориллонитом. Показана зависимость вязкости от скорости сдвига для неотвержденной чистой эпоксидной смолы и

смолы, модифицированной частицами монтмориллонита при комнатной температуре. При низкой скорости сдвига наблюдается значительное влияние монтмориллонита на свойства композита. Низкая скорость сдвига дополнительно позволила молекулам эпоксидной смолы просачиваться между слоями пластинок монтмориллонита, вызывая набухание и увеличение расстояния между ними. По мере увеличения скорости сдвига с 8 до 20 c^{-1} время перколяции монтмориллонита уменьшалось, что повлияло на уменьшение вязкости. При увеличение скорости сдвига выше значения 20 c^{-1} каких-либо значимых изменений вязкости не происходит, для обоих образцах наблюдается на графике монотонная линия. Добавление монтмориллонита в эпоксидную смолу изменяет химический состав композита, что приводит к изменениям реологических и физико-механических свойств. Добавление монтмориллонита замедляет гелеобразование, что может влиять на технологичность, время отверждения и конечные свойства композита. Были проведены морфологические исследования для определения степени дисперсности частиц монтмориллонита в полимерном композите с использованием просвечивающего электронного микроскопа. Неравномерное распределение частиц монтмориллонита преобладало во всех образцах. По-видимому это связано с условиями отверждения полимерного композита и недостаточности времени диспергирования. Проводились физико-механические исследования образцов из композита с монтмориллонитом в сравнении с образцами из чистой эпоксидной смолы. Прочность на изгиб образцов из полученного композита сопоставима с прочностью образцов из чистой эпоксидной смолы. В свою очередь вязкость увеличилась на 170%.

Ключевые слова: полимерные материалы, эпоксидный композит, монтмориллонит, наполнители для полимеров, термореактивные смолы

1. INTRODUCTION

Thermosetting polymers are widely used in the construction industry as repair compounds for cracks (defects), anti-corrosion protection of building structures, and in decorative and finishing works. Depending on the conditions of use of thermosetting polymers, it is necessary to use various structural and functional fillers to obtain the necessary physical, mechanical and rheological properties. To improve the mechanical and thermal properties of the composite, small amounts of montmorillonite are introduced into its composition [1-3]. Montmorillonite has a unique morphology in the form of flakes with a thickness of about 1 nm with linear surface dimensions of 50–150 nm, which provides good barrier properties to moisture and volatile substances [4]. Studies [5] have shown that montmorillonite accelerates the rate of chemical reaction of the polymer composite. The interaction of montmorillonite particles with epoxy resin molecules affects the viscosity and mobility of the reacting particles during the curing process, which changes the curing rate, reaction time, enthalpy, glass transition, activation energy, viscoelastic properties and cross-linking density of the final composite [5, 6]. In addition, it was shown in [7, 8] that the type and amount of fillers and organic modifiers, as well as their interaction with the polymer base and their hardeners, affect the properties of the resulting composites.

The fillers introduced into its composition have a significant impact on the curing parameters of a polymer composite. Therefore, the manufacturer's recommended instructions for the use of thermosetting polymers and hardeners are not suitable for correct use. It is necessary to take into account the influence of fillers on the kinetic parameters of curing (activation energy) of polymer composites.

Gelation is of decisive importance in a thermosetting reaction. The use of a liquid polymer composite beyond the gelation point becomes virtually impossible due to the onset of crosslinking coupled with the rapid increase in viscosity. Therefore, understanding the influence of montmorillonite morphology on the rheological properties of thermoset polymer composites is critical, since it is directly related to the consistency of fluidity during use and the effect on the physical and mechanical properties of the thermoset polymer composite product.

2. MATERIALS AND METHODS

The following materials were used for the study: epoxy resin DER-330 (diglycidyl ether of bisphenol A, DGEBA); slow hardener FCH-S, manufactured by The Dow Chemical Company (Germany); montmorillonite Garamite 7305 (BYK, Germany). The montmorillonite used is a naturally occurring layered mineral with a chemical composition of $A_{0.3}(Al_{1.3}Mg_{0.7})[Si_4]O_{10}(OH)_2H_2O$, where "A" is the exchange cation, K^+, Na^+ or $0.5Ca^{2+}$. The chemical structure is shown in Figure 1. The particle size distribution of montmorillonite clusters ranged from 8 to 12 microns. This section specifies and describes in detail the chosen research method. The description should be in such a way that a qualified reader can reproduce it as a whole.

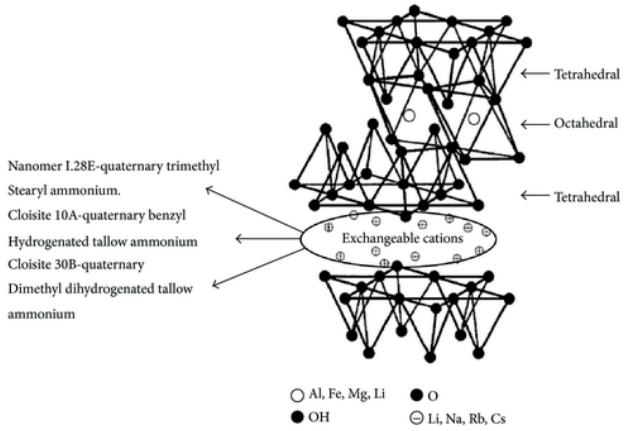


Figure 1. Chemical structure of montmorillonite [9]

The components were mixed using a magnetic stirrer MSH-300 (Biosan, Latvia). All formulations contained 10.0 g of resin and 3.3 g of hardener. A hardener and montmorillonite were alternately added to the working epoxy mixer. The mixing time of each component was 2 minutes, which made it possible to obtain a homogeneous mixture.

Morphological studies were carried out using an EMV-100A electron microscope (JSC SELMI, Ukraine).

The rheological properties of the formulations were measured under normal environmental conditions using a REOTEST RV2.1 rotary viscometer (VEB MLW, Germany) with a cylinder–cylinder working unit in the concentration range of 0.5 – 20.0%. The shear rate range was 0.3–1312 s^{-1}.

Samples for physico-mechanical studies were carried out with dimensions of 61×12×3.2 mm. The obtained samples were hardened in two stages at two temperature conditions – first at 100 °C for 24 hours, and then at 220 °C for 2 hours in a drying cabinet SHSU-M1 (manufactured by NPO Laborkomplekt, Russia).

Before taking measurements, the samples were purified with acetone. Three samples were tested for each composition. Bending tests were performed at room temperature on a universal testing machine TC 101-5-1-U (TEST SYSTEM production, Russia). In accordance with GOST R 56810-2015 "Polymer composites. Bending test method for flat samples" the dimensions of the sample span are regulated depending on its thickness. With a thickness greater than 1,6 mm, the span between the supports should be 16 times the thickness of the sample (tolerance ± 1 time). Therefore, during the bending test, the span between the supports was 51 mm, and the slider speed was 1.3 mm/min.

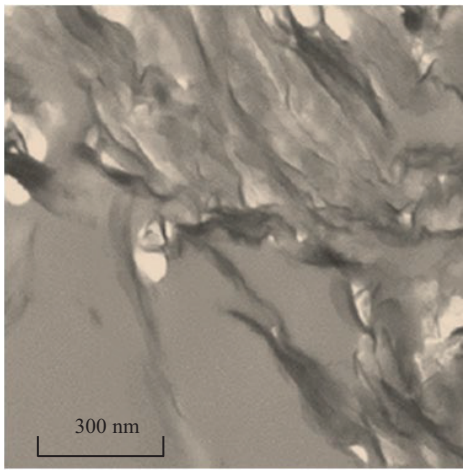
3. RESULTS AND DISCUSSION

The change in the rheological and physicomechanical properties of a thermosetting polymer composite using montmorillonite directly depends on the degree of dispersion, the uniform distribution of montmorillonite in the volume of the composite. Improving the properties of the composite also depends on the chemical reaction of the epoxy resin molecules occurring on the large surface area of the montmorillonite particles.

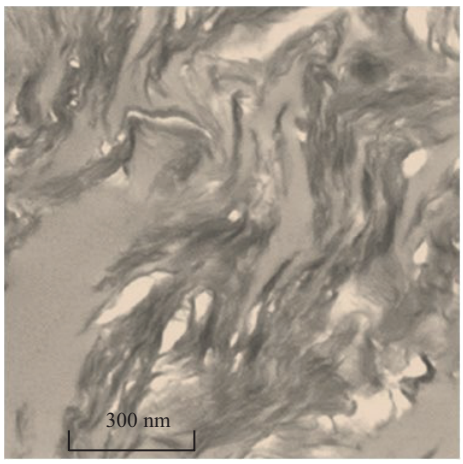
The greatest change in the rheological and physicomechanical properties of a thermosetting polymer composite and the effectiveness of

using montmorillonite particles will be achieved with a uniform distribution of the latter in the volume of the polymer composite with the largest surface area of montmorillonite particles participating in a chemical reaction with epoxy resin molecules.

Morphological studies were carried out to determine the degree of dispersion of montmorillonite particles in the polymer composite using a transmission electron microscope. The distribution of montmorillonite particles in the polymer composite is shown in Figure 2.



a)



b)

Figure 2. Polymer composite with montmorillonite particles

The uneven distribution of montmorillonite particles predominated in all samples. Apparently, this is due to the curing conditions of the polymer composite and insufficient dispersion time.

Experimental viscosity versus shear rate curves for uncured pure epoxy resin and resin modified with montmorillonite particles at room temperature are shown in Figure 3.

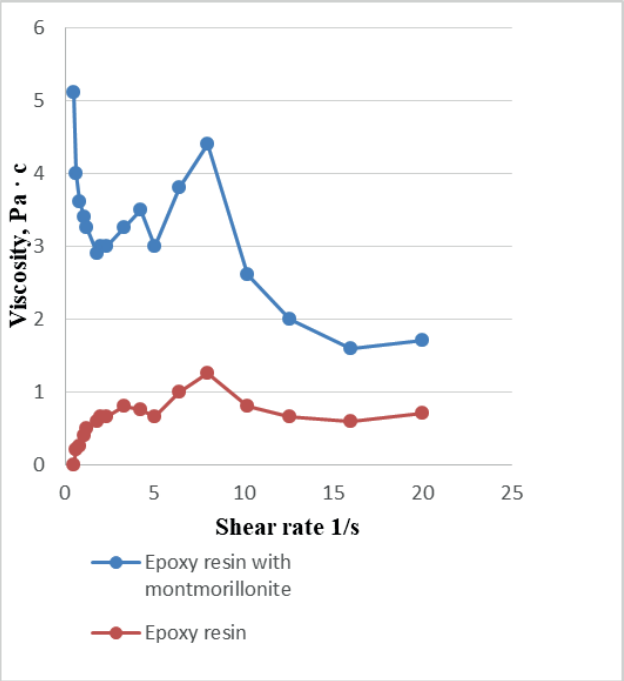


Figure 3. Dependence of viscosity on shear rate

At low shear rates, the effect of montmorillonite on the properties of the composite is very noticeable. The interaction of the montmorillonite particles with the epoxy resin significantly influenced the initial viscosity response to the applied shear stress. These interactions, combined with interactions between montmorillonite particles within the epoxy resin in response to applied stress, resulted in higher viscosity values at low shear rates (0–5 s^{-1}). The low shear rate further allowed epoxy molecules to leak between the layers of montmorillonite platelets, causing swelling and increasing the distance between them. As the shear rate increased from 8 to 20 s^{-1}, the percolation time of montmorillonite decreased, which affected the decrease in viscosity. When the shear rate increases above 20 s^{-1}, no significant changes in viscosity occur;

a monotonic line is observed in both samples. This behavior may have been due to insufficient time for the epoxy molecules to move further into the montmorillonite layers to form a mesoscopic mixture in response to increasing shear rates. Identical rheological properties at different viscosities demonstrate the dependence of viscosity on "particle–particle" and "particle–host interactions", as studies have shown [5, 10–14]. In general, the viscosity of the montmorillonite sample showed higher values throughout the study compared to pure epoxy resin. This indicates an anisotropic microstructural behavior in which epoxy molecules move into the interlayer space of the montmorillonite flakes and cause them to swell. It can be assumed that with an increase in the dispersion time of the composite, the epoxy resin molecules will penetrate more deeply between the montmorillonite flakes, with its subsequent swelling, affecting the viscosity and final properties of the composite. By the end of the study, the viscosity of the composite, compared to pure epoxy resin, increased by 170%. Montmorillonite significantly affects the viscosity of the base polymer, which can affect processability and cure, leading to changes in rheological and physical-mechanical properties [15–18].

The flexural test results for epoxy resin and epoxy-montmorillonite composite specimens are shown in Table 1. The cast pure epoxy resin has a flexural modulus of 2.8 GPa and a flexural strength of 83.0 MPa.

The composite containing 2 wt% montmorillonite showed a flexural modulus of 4.7 GPa and a flexural strength of 82.0 MPa. The elastic modulus of the composite increased by 25% compared to pure epoxy resin. The flexural strength of a composite with montmorillonite compared to pure epoxy resin is not significantly different. Thus, montmorillonite significantly affects the elastic modulus of the composite, which can have a significant impact on its technological and operational properties [19, 20].

Table 1. The modulus of elasticity and bending strength of cast and layered samples

Name of material	Elastic modulus, GPa	Flexural strength, MPa
Epoxy resin	2.8	83.0
Epoxy resin with montmorillonite	3.5	81.0

4. CONCLUSION

The work investigated the influence of montmorillonite on the rheological and physical-mechanical properties of composites of two compositions - two-component (from epoxy resin and hardener) and three-component (from epoxy resin, hardener and montmorillonite).

The scaly, branched surface of montmorillonite has a significant influence on the gelation and curing time of the composite. More research is needed on composites with different percentages of montmorillonite to obtain predictable properties of the final composites.

The results of the study showed that montmorillonite increases the viscosity of the composite by 170%, which affects its technological, rheological and physical-mechanical properties. The elastic modulus of the composite increased by 25% compared to pure epoxy resin. Montmorillonite significantly affects the elastic modulus of the composite, which can change its technological and operational properties. The flexural strength of a composite with montmorillonite compared to pure epoxy resin does not differ significantly.

REFERENCES

1. **Duty C.E., Kunc V., Compton B., Post B., Erdman D., Smith R., Lind R., Lloyd P., Love L.** (2017) Structure and mechanical behavior of big area additive manufacturing (BAAM) materials. *Rapid Prototyp Journal*, no. 23 (1), pp. 181–189.

doi: 10.1108/RPJ-12-2015-0183 ISSN 13552546.

2. **Kishore V., Ajinjeru C., Nycz A., Post B., Lindahl J., Kunc V., Duty C.** (2017) Infrared Preheating to Improve Interlayer Strength of Big Area Additive Manufacturing (BAAM) Components. *Additive Manufacturing*, no. 14, pp. 7–12. doi: 10.1016/j.addma.2016.11.008.
3. **Xidas P.I., Triantafyllidis K.S**. (2010) Effect of the type of alkylammonium ion clay modifier on the structure and thermal/mechanical properties of glassy and rubbery epoxy-clay nanocomposites, *European Polymer Journal*, vol. 46, no. 3, pp. 404–417. doi: 10.1016/j.eurpolymj.2009.11.004.
4. **Kiliaris P., Papaspyrides C.D.** (2010) Polymer/layered silicate (clay) nanocomposites: an overview of flame retardancy. *Progress in Polymer Science*, vol. 35, no. 7, pp. 902–958. doi: 10.1016/j.progpolymsci.2010.03.001.
5. **Litchfield D.W., Baird D.G.** (2006) The rheology of high aspect ratio nanoparticle filled liquids. *The British Society of Rheology* (electronic journal), pp. 1–60. Available at: https://www.researchgate.net/publication/265071718_The_rheology_of_high_aspect_ratio_nanoparticle_filled_liquids/citation/download.
6. **Cai H., Li P., Sui G. et al.** (2008) Curing kinetics study of epoxy resin/flexible amine toughness systems by dynamic and isothermal DSC. *Thermochimica Acta*, vol. 473, no. 1–2, pp. 101–105. doi: 10.1016/j.tca.2008.04.012.
7. **Ray S.S., Okamoto M.** (2003) Polymer/layered silicate nanocomposites: a review from preparation to processing. *Progress in Polymer Science*, vol. 28, no. 11, pp. 1539–1641. doi:10.1016/j.progpolymsci.2003.08.002.
8. **Cai H., Li P., Sui G. et al.** (2008) Curing kinetics study of epoxy resin/flexible amine toughness systems by dynamic and isothermal DSC. *Thermochimica Acta*, vol. 473, no. 1–2, pp. 101–105. doi: 10.1016/j.tca.2008.04.012.
9. **Giannelis E.P., Krishnamoorti R., Manias E.** (1999) Polymer-Silicate Nanocomposites: Model Systems for Confined Polymers and Polymer BrushesPolymers in Confined Environments. *Advances in Polymer Science*, vol 138, pp. 107–147. doi: 10.1007/3-540-69711-X_3.
10. **Mohan T.P., Velmurugan R., Kumar M.R.** (2005) Rheology and curing characteristics of epoxy-clay nanocomposites. *Polymer International*, vol. 54, no. 12, pp. 1653–1659. doi: 10.1002/pi.1897.
11. **Erofeev V.T., T.F. Elchishcheva, Preobrazhenskaya E.M., Makarchuk M.V.** (2020) Research of new materials and approaches in additive technologies in the manufacture of prototypes in industrial design. *SPCECI 2019. IOP Conference Series: Materials Science and Engineering*, vol. 972, P. 012057. doi: 10.1088/1757-899X/ 972/1/012057.
12. **Erofeev V.T., Elchishcheva T.F., Preobrazhenskaya E.M., Makarchuk M.V., Afonin V.V.** (2020) Optimization of the Strength Characteristics of the Cellular Structure in Samples of Thermoplastic Polyester. SPCECI 2019. IOP Conference Series: Materials Science and Engineering, vol. 972, P. 012056. doi: 10.1088/1757-899X/972/1/012056.
13. **Erofeev V.T., Elchishcheva T.F., Makarchuk M.V., Preobrazhenskaya E.M., Tingaev A.V.** (2022) Properties of Samples from Polymer Materials Manufactured by the Additive Method. Solid State Phenomena (SSP) (29 July 2022), vol. 335, pp. 79–84 doi: 10.4028/p-6n2zb7.
14. **Erofeev V.T., Ivlev V.I., Myshkin A.V., Yudin V.A., Elchishcheva T.F. etc.** (2021) Mekhanicheskiye svoystva otverzhdennoy poliefirakrilatnoy smoly MGF-9 [Mechanical properties of cured polyester acrylate resin MGF-9] Izvestiya Vysshikh

Uchebnykh Zavedenii, Seriya Teknologiya Tekstil'noi Promyshlennosti, no 6 (396), pp. 311–319. doi: 10.47367/0021-3497_2021_6_311.

15. **Erofeev V.T., Elchishcheva T.F., Makarchuk M.V.** (2022) Epoksidnyy kompozit s uglerodnymi strukturami v additivnoy tekhnologii izgotovleniya izdeliy dlya tekstil'noy promyshlennosti [Epoxy composite with carbon structures in additive technology for manufacturing products for the textile industry] Izvestiya Vysshikh Uchebnykh Zavedenii, Seriya Teknologiya Tekstil'noi Promyshlennosti, no 2 (398), pp. 346–354. doi: 10.47367/0021-3497_2022_2_346.
16. **Pahomova E.G., Monastyrev P.V., Mishchenko E.S., Yezerskiy V.A., Ivanov I.A., Balthazar A.D.** (2019) House-building analysis when usi ng additive technologies: Classification, advantages and disadvanta ges, Journal of Applied Engineering Science, vol. 17, no 4, pp. 449–456. doi: 10.5937/jaes17-23635.
17. **Ezersky V.A., Monastyrev P.V., Ivanov I.A.** (2019) The Analysis of The rmal Properties of a Wall Fragment Made with 3D Construction Te chnology, International Journal for Computational Civil and Structur al Engineering, vol. 15, no 4, pp. 34–47. doi: 10.22337/2 587-9618-2019-15-4-34-47.
18. **Pakhomova E.G., Andrianov K., Zubkov A., Monastyrev, P.** (2020) In fluence of thickness and granulometric composition of granular asp halt on its strength characteristics when placing into the road pave ment, Journal of Applied Engineering Science, vol. 18(2), pp.192–197, doi: 10.5937/jaes18-26311.
19. **Pakhomova E., Emelyanov S., Yartsev V., Danilov V., Monastyrev P.** (2023) The Influence of Climatic Aging on the Performance of Woo d-Based Panels, Civil Engineering Journal (Iran), no. 9(6), pp. 1491 –1508, doi: 10.28991/CEJ-2023-09-06-015.
20. **Sakoshev Z.G., Blaznov A.N.** (2022) Issledovaniye reologicheskikh i fiziko-mekhanicheskikh svoystv epoksidnykh sistem s otverditelyami raznoy prirody [Study of rheological and physical-mechanical properties of epoxy systems with hardeners of different nature] Plasticheskiye massy, no. 9-10, pp. 7–9. doi: 10.35164/0554-2901-2022-9-10-7-9.

СПИСОК ЛИТЕРАТУРЫ

1. **Duty C.E., Kunc V., Compton B., Post B., Erdman D., Smith R., Lind R., Lloyd P., Love L.** Structure and mechanical behavior of big area additive manufacturing (BAAM) materials // Rapid Prototyp Journal, 2017, No. 23 (1), pp. 181–189. doi: 10.1108/RPJ-12-2015-0183.
2. **Kishore V., Ajinjeru C., Nycz A., Post B., Lindahl J., Kunc V., Duty C.** Infrared Preheating to Improve Interlayer Strength of Big Area Additive Manufacturing (BAAM) Components // Additive Manufacturing, 2017, No. 14, pp. 7–12. doi: 10.1016/j.addma.2016.11.008.
3. **Xidas P.I., Triantafyllidis K.S.** Effect of the type of alkylammonium ion clay modifier on the structure and thermal/mechanical properties of glassy and rubbery epoxy-clay nanocomposites // European Polymer Journal, 2010, vol. 46, No. 3, pp. 404–417. doi: 10.1016/j.eurpolymj.2009.11.004.
4. **Kiliaris P., Papaspyrides C.D.** Polymer/layered silicate (clay) nanocomposites: an overview of flame retardancy // Progress in Polymer Science, 2010, vol. 35, No. 7, pp. 902–958. doi: 10.1016/j.progpolymsci.2010.03.001.
5. **Litchfield D.W., Baird D.G.** The rheology of high aspect ratio nanoparticle filled liquids // The British Society of Rheology (electronic journal), 2006, pp. 1–60. Available at: https://www.researchgate.net/publication/265071718_The_rheology_of_high_aspect_ratio_nanoparticle_filled_liquids/citation/download.

6. **Cai H., Li P., Sui G.** et al. Curing kinetics study of epoxy resin/flexible amine toughness systems by dynamic and isothermal DSC // Thermochimica Acta, 2008, vol. 473, No. 1–2, pp. 101–105. doi: 10.1016/j.tca.2008.04.012.
7. **Ray S.S., Okamoto M.** Polymer/layered silicate nanocomposites: a review from preparation to processing // *Progress in Polymer Science*, 2003, vol. 28, No. 11, pp. 1539–1641. doi:10.1016/j.progpolymsci.2003.08.002.
8. **Cai H., Li P., Sui G.** et al. Curing kinetics study of epoxy resin/flexible amine toughness systems by dynamic and isothermal DSC // Thermochimica Acta, 2008, vol. 473, No. 1–2, pp. 101–105. doi: 10.1016/j.tca.2008.04.012.
9. **Giannelis E.P., Krishnamoorti R., Manias E.** Polymer-Silicate Nanocomposites: Model Systems for Confined Polymers and Polymer BrushesPolymers in Confined Environments // Advances in Polymer Science, 1999, vol. 138, pp. 107–147. doi: 10.1007/3-540-69711-X_3.
10. **Mohan T.P., Velmurugan R., Kumar M.R.** Rheology and curing characteristics of epoxy-clay nanocomposites // Polymer International, 2005, vol. 54, No. 12, pp. 1653–1659. doi: 10.1002/pi.1897.
11. **Erofeev V.T., T.F. Elchishcheva, Preobrazhenskaya E.M., Makarchuk M.V.** Research of new materials and approaches in additive technologies in the manufacture of prototypes in industrial design // SPCECI 2019. IOP Conference Series: Materials Science and Engineering, 2020, vol. 972, P. 012057. doi: 10.1088/1757-899X/ 972/1/012057.
12. **Erofeev V.T., Elchishcheva T.F., Preobrazhenskaya E.M., Makarchuk M.V., Afonin V.V.** Optimization of the Strength Characteristics of the Cellular Structure in Samples of Thermoplastic Polyester // SPCECI 2019. IOP Conference Series: Materials Science and Engineering, 2020, Vol. 972, P. 012056. doi: 10.1088/1757-899X/972/1/012056.
13. **Erofeev V.T., Elchishcheva T.F., Makarchuk M.V., Preobrazhenskaya E.M., Tingaev A.V.** Properties of Samples from Polymer Materials Manufactured by the Additive Method // Solid State Phenomena (SSP) (29 July 2022), 2022. Vol. 335, pp. 79–84. doi: 10.4028/p-6n2zb7.
14. **Ерофеев В.Т., Ивлев В.И., Мышкин А.В., Юдин В.А., Ельчищева Т.Ф.** и др. Механические свойства отвержденной полиэфиракрилатной смолы МГФ-9 // Известия высших учебных заведений. Технология текстильной промышленности, 2021, № 6(396). С. 311-319. doi: 10.47367/0021-3497_2021_6_311.
15. **Ерофеев В.Т., Ельчищева Т.Ф., Макарчук М.В.** Эпоксидный композит с углеродными структурами в аддитивной технологии изготовления изделий для текстильной промышленности // Известия высших учебных заведений. Технология текстильной промышленности, 2022, № 2(398). С. 346-354. doi: 10.47367/0021-3497_2022_2_346.
16. **Pahomova E.G., Monastyrev P.V., Mishchenko E.S., Yezerskiy V.A., Ivanov I.A., Balthazar A.D.** House-building analysis when usi ng additive technologies: Classification, advantages and disadvanta ges, Journal of Applied Engineering Science, 2019, vol. 17, No. 4, pp. 449-456. doi: 10.5937/jaes17-23635.
17. **Ezersky V.A., Monastyrev P.V., Ivanov I.A.** The Analysis of The rmal Properties of a Wall Fragment Made with 3D Construction Te chnology // International Journal for Computational Civil and Structur al Engineering, 2019, vol. 15, No. 4, pp. 34-47. doi: 10.22337/2 587-9618-2019-15-4-34-47.
18. **Pakhomova E., Andrianov K., Zubkov A., Monastyrev P.** In fluence of thickness and granulometric composition of granular asp halt on its strength characteristics when placing

into the road pave ment // Journal of Applied Engineering Science, 2020, vol. 18(2), pp.192-197, doi: 10.5937/jaes18-26311.

19. **Pakhomova E., Emelyanov S., Yartsev V., Danilov V., Monastyrev P**The Influence of Climatic Aging on the Performance of Woo d-Based Panels // Civil Engineering Journal (Iran), 2023, No. 9(6), pp. 1491-1508. doi: 10.28991/CEJ-2023-09-06-015.
20. **Сакошев З.Г., Блазнов А.Н.** Исследование реологических и физико-механических свойств эпоксидных систем с отвердителями разной природы // Пластические массы, 2022, №9-10, С. 7-9. DOI: 10.35164/0554-2901-2022-9-10-7-9.

Pavel Vladislavovich Monastyrev, Doctor of Technical Sciences, Director of the Institute of Architecture, Construction and Transport of the Federal State Budgetary Educational Institution of Higher Education "Tambov State Technical University", Associate Professor, Corresponding Member of the RAASN, room 2, 106/5, st. Sovetskaya, Tambov, 392000, Russian Federation, SPIN code: 8674-6046, +79606630093, monastyrev68@mail.ru

Tatyana Fedorovna Elchishcheva, Ph.D., Head of the Department of Architecture and Urban Planning, Tambov State Technical University, Associate Professor, room 2, 106/5, st. Sovetskaya, Tambov, 392000, Russian Federation, SPIN code: 9764-3898, +79158616308, elschevat@mail.ru

Maxim Valerievich Makarchuk, Ph.D., Associate Professor of the Department of Materials and Technology, Tambov State Technical University, room 2, 106/5, st. Sovetskaya, Tambov, 392000, Russian Federation, SPIN code: 2530-0886, +79107504045, energ-lab@yandex.ru

Vladimir Trofimovich Erofeev, Doctor of Technical Sciences, Professor of the Department of Construction Materials Science of the National Research University "Moscow State University of Civil Engineering", Professor, Academician of the Russian Academy of Architecture and Construction Sciences, 26, Yaroslavskoye sh., Moscow, 129337, Russian Federation, SPIN code: 4425-5045 , +79272760476, erofeevvt@bk.ru

Vladimir Ivanovich Rimshin, Doctor of Technical Sciences, Professor of the Department of Housing and Communal Complex of the National Research University of Moscow State University of Civil Engineering, 26, Yaroslavskoe sh., Moscow, 129337, Russian Federation, SPIN code: 9629-5322, +79265309315, RimshinVI@mgsu.ru

Irina Vladimirovna Erofeeva, Ph.D., senior lecturer of the department of fundamentals of architecture and artistic communications, National Research University "Moscow State University of Civil Engineering", 26, Yaroslavskoe sh., Moscow, 129337, Russian Federation, SPIN code: 5569-3057, +79375113575, ira.erofeeva.90@mail.ru

Павел Владиславович Монастырев, д.т.н., директор Института архитектуры, строительства и транспорта ФГБОУ ВО «Тамбовский государственный технический университет», доцент, член-корреспондент РААСН, помещение 2, д.106/5, ул. Советская, г. Тамбов, 392000, Российская Федерация, SPIN-код: 8674-6046, +79606630093, monastyrev68@mail.ru

Татьяна Федоровна Ельчищева, к.т.н., заведующий кафедрой «Архитектура и градостроительство» ФГБОУ ВО «Тамбовский государственный технический университет», доцент, помещение 2, д.106/5, ул. Советская, г. Тамбов, 392000, Российская Федерация, SPIN-код: 9764-3898, +79158616308, elschevat@mail.ru

Максим Валерьевич Макарчук, к.т.н., доцент кафедры «Материалы и технология» ФГБОУ ВО «Тамбовский государственный технический университет», помещение 2, д.106/5, ул. Советская, г. Тамбов, 392000, Российская Федерация, SPIN-код: 2530-0886, +79107504045, energ-lab@yandex.ru

Владимир Трофимович Ерофеев, д.т.н., профессор кафедры Строительного материаловедения НИУ «Московский государственный строительный университет», профессор, академик РААСН, 26, Ярославское ш., г. Москва, 129337, Российская Федерация, SPIN-код: 4425-5045, +79272760476, erofeevvt@bk.ru

Владимир Иванович Римшин, д.т.н., профессор кафедры Жилищно-коммунального комплекса НИУ Московского государственного строительного университета, 26, Ярославское ш., г. Москва, 129337, Российская Федерация, SPIN-код: 9629-5322, +79265309315, RimshinVI@mgsu.ru

Ирина Владимировна Ерофеева, к.т.н., старший преподаватель кафедры основ архитектуры и художественных коммуникаций НИУ «Московский государственный строительный университет», 26, Ярославское ш., г. Москва, 129337, Российская Федерация, SPIN-код: 5569-3057, +79375113575, ira.erofeeva.90@mail.ru

International Journal for Computational Civil and Structural Engineering, 20(2) 118–131 (2024)

DOI:10.22337/2587-9618-2024-20-2-118-131

CONCRETE DELAYED FAILURE TIME

Vu Ngoc Tuyen, Fedorova Nataliya Vitalyevna

Moscow State University of Civil Engineering National Research University, Moscow, RUSSIA

Abstract: At a single action on a concrete and reinforced concrete structure short-term dynamic load, the value of which may exceed the value of the static load-bearing capacity of the structure, it was observed that failure will occur not immediately, but after a certain time (delayed failure time t_d). If the dynamic load action is stopped before the moment t_d, the structure will not collapse. Therefore, the accurate determination of the delayed failure time of concrete is an important and relevant problem. To solve this problem, the paper presents a visco-elastic-plastic model to describe the stress-strain state of concrete under dynamic loading. This model consists of 2 elements: a nonlinear spring A and a piston B connected in parallel. Element A describes the nonlinear elastic-plastic properties of concrete, and element B takes into account the high-strain-rate effect of concrete. Under the action of sudden dynamic loads with an intensity greater than the static bearing capacity of the concrete, piston B helps to inhibit the development of deformations initiated in element A. Based on the proposed model, the delayed failure time is defined by the time interval required for the deformation of concrete to reach its ultimate value. The main factors affecting the deformation and failure of concrete such as concrete compressive strength, overload level, and viscosity are also investigated. Specifically, as follows: The higher the static compressive strength of concrete, the lower the delayed failure time. When a dynamic force of greater intensity is applied compared to the bearing capacity of the concrete, the faster the specimen will destroy. In addition, the viscosity coefficient significantly reduces the strain rate of concrete and the corresponding delayed failure time increases as the viscosity increases.

Keywords: Dynamic increase factor, delayed failure time, visco-elastic-plastic model, concrete, strain rate effect, viscosity, Kelvin–Voigt model

ВРЕМЯ ЗАДЕРЖКИ РАЗРУШЕНИЯ БЕТОНА

Ву Нгок Туен, Н.В. Федорова

Национальный исследовательский Московский государственный строительный университет, г. Москва, РОССИЯ

Аннотация: При однократном действии на бетонное и железобетонное сооружение кратковременной динамической нагрузки аварийного типа, величина которой может превышать величину статической несущей способности конструкции наблюдалось что разрушение произойдет не сразу, а по истечении определенного времени (время задержки разрушения t_d). Если действие динамической нагрузки прекратить до момента t_d, то конструкция не разрушится. Поэтому точного определение времени задержки разрушения бетона является важной и актуальной проблемой. Для решения данной проблемы, в статье представлена вязко-упруго-пластическая модель, позволяющая описывать напряженно-деформированное состояние бетона при динамическом нагружении. Эта модель состоит из 2-х элементов: нелинейная пружина А и поршень В, соединенных между собой параллельно. Элемент А описывает нелинейные упругопластические свойства бетона, а элемент В учитывает влияние скоростного деформирования бетона. Под действием внезапных динамических нагрузок с интенсивностью большей, чем статическая несущая способность бетона вязкий элемент В способствует торможению развития деформаций, инициируемых в элементе А. На основе предлагаемой модели время задержки разрушения определяется отрезком времени, необходимым для того, чтобы деформация бетона достигла своего предельного значения. Также доказаны основные факторы, влияющие на деформацию и разрушение бетона, такие как бетона по прочности на сжатие, уровень перенагружения и коэффициент вязкого сопротивления.

Ключевые слова: Коэффициент динамического упрочнения, время задержки разрушения, вязко-упруго-пластическая модель, бетон, скорость деформирования, модуль вязкого сопротивления, модель Кельвина-Фойгта

1. INTRODUCTION

In practical structural calculations, an important independent variable, time, is excluded from concrete deformation models. Such models adequately describe the inelastic behavior of a material only in the case of loading with low speeds, when the effect of strain lag can be neglected (quasi-static loading regime). Under high-speed loading, the deformation and fracture patterns of concrete specimens are very different from those under static loading . A large number of experimental studies have been devoted to the study of dynamic mechanical characteristics of concrete, conducted mainly under uniaxial loading [1–3]. Based on experimental results in uniaxial compression as well as in tension it was shown that with increasing strain rate there is an increase in concrete strength and modulus of elasticity [4] [5] [6]. In addition, the strain rate effect on the increase of concrete strength becomes significant when the strain rate is higher than a certain value, which is estimated differently in different scientific publications [7–9].

It has also been shown that the dynamic strength of concrete depends on the properties of the materials used, the characteristics of the concrete structure, and the moisture content [10–12]. The inhomogeneity of concrete microstructure and the presence of initial defects (especially large defects) affect the reduction of the dynamic strength of concrete to a greater extent than the static strength [13–15]. The dynamic strength of concrete increases when saturated with water [16,17].

One of the main criteria determining the behavior of concrete under dynamic loading is the dynamic increase factor (φ_d), i.e. the ratio of the strength of concrete under dynamic loading σ_d to its static strength R_b. To obtain the average dependence of the dynamic increase factor for concrete in compression and tension on the duration of increasing load intensity (τ) Y.M. Bazhenov tested 500 specimens of various concretes [1]. During this time, the load intensity is gradually increased from 0 to the maximum value σ_d.

The obtained empirical dependences of the dynamic increase factor by Y.M. Bazhenov for heavy concrete are presented in the form of:

In compression:

$$\varphi_d = 1.58 - 0.35\lg\tau + 0.07\left(\lg\tau\right)^2 \qquad (1)$$

In tension:

$$\varphi_{dt} = 1.42 - 0.15\lg\tau + 0.01\left(\lg\tau\right)^2 \qquad (1)$$

where the duration of increasing load intensity is expressed in milliseconds and is limited in the interval 1-2000 msec.

These results show that as the loading time decreases, i.e. as the strain rate increases, concrete hardening occurs. All these facts suggest that the basic physical law linking stresses to strains must contain time.

Further in [18] Y.M. Bazhenov, V.S. Udaltsov tested concrete specimens under sudden application of a constant load, the value of which is greater than the static compressive strength ($\sigma_d = const > R_b$). It has been found that failure will not occur immediately, but after a certain amount of time, and this will no longer require an increase in load. That is, a lag of deformations is observed. In scientific publications, the value of t_d is referred to as the delayed failure time (i.e., the time interval from the beginning of the loading moment until the element fails). The value of t_d depends mainly on the overload level, i.e., on $\varphi_d = \sigma_d / R_b$, and can be determined by the empirical formula applied by V.S. Udaltsov [18]:

$$\lg t_d = 7.55 - 4.88\varphi_d \qquad (3)$$

where t_d is expressed in milliseconds.

If the load action is stopped before the moment t_d that the strain in the concrete does not have time to reach its ultimate value, the concrete

will not fail. It should be noted that the values of t_d and τ are not identical due to different loading regimes in studies [1] and [18].

Similar conclusions are made in the work of V.A. Rakhmanov [19]. In addition, V.A. Rakhmanov also observed that the lag of transverse deformation is much larger than that of longitudinal deformation.

In recent years, numerous experiments have been conducted on reinforced concrete frames subjected to sudden column failure scenarios [20,21]. When observing the deformation and failure process of the frame under the slow-motion camera, it is seen that after the removal of the load-bearing column, progressive failure in characteristic cross-sections occurs only after a certain time interval t_d [22]. Therefore, the determination of the concrete delayed failure time is very important in calculations for the progressive collapse of buildings and structures.

It should be emphasized that the studies conducted by the above scientists are descriptive and will not explain the nature of concrete behavior under high-speed loading.

In parallel with the experimental studies, many theoretical studies on the establishment of analytical laws of deformation of concrete take into account the influence of strain rate. The complexity of this problem is because the concrete in its structure is an inhomogeneous material, which consists of cement stone forming a spatial lattice, aggregate of crushed stone and sand, and a large number of micropores and capillaries, containing water, water vapor, and air. The simultaneous presence of solid, liquid, and gaseous phases in concrete determines a complex picture of concrete behavior under loading.

Speed deformation of concrete structure causes the redistribution of liquid-gas phase in pores and capillaries and disturbs internal equilibrium between phases of the concrete. In this case, the greater the rate of deformation, the stronger the resistance of the liquid-gas medium. This explains the fact that the resistance of concrete increases under rapidly increasing loads. Taking into account all these factors inevitably leads to cumbersome dependencies that are of little use as a basis for practical methods of calculation of reinforced concrete and concrete structures.

To obtain sufficiently simple structure calculation formulas and dependencies between the level of overloading of concrete ($\varphi_d = T / T_s$) and the delayed failure time t_d, G.A. Geniev considered concrete as a two-phase medium consisting of solid and liquid-gas phases [23]. This allows us to explain many processes occurring in concrete, including the peculiarities of its behavior under short-term loading. Taking that the tangential stress intensity and shear strain intensity of the solid phase (element A of the model) are related by a nonlinear law $T_A = 2T_s\left(1-\Gamma / \Gamma_s\right)\Gamma / \Gamma_s$, and the stress state of the liquid phase (viscous element B of the model) depend on the strain rate and change according to the law of ideally viscous fluid $T_Б = Kd\Gamma / dt$, we obtained a model of elastic-plastic-viscous body (K- viscosity). When stress intensity $T = T_A + T_Б = const$ is applied to a structural element, shear strain intensity develops and reaches its maximum value $\Gamma_s = 2T_s / G_0$ within a very small time interval t_d (delayed failure time). During this time interval, the liquid phase contributes to the inhibition of the development of deformations initiated in the solid phase.

Based on the proposed model, A.G. Geniev established a relationship between the delayed failure time and the level of overloading of concrete φ_d:

$$t_d\omega = \frac{2arccot\sqrt{\varphi_d - 1}}{\sqrt{\varphi_d - 1}} \qquad (4)$$

It can be said that this model is the simplest and most successful for explaining the dynamic strength under the action of external dynamic (impact) loads in a short time. On the other hand, in the considered model, the ultimate deformation of concrete under uniaxial compression can be calculated by the formula $\varepsilon_{ult} = 2R_b / E_b$. This value is approximately 1.75

times less than the ultimate strain of concrete specified in the current normative documents ($\varepsilon_{b2} = 0.0035$). Therefore, the delayed failure time calculated from the ultimate strain $\varepsilon_{ult} = 2R_b / E_b$, will not be estimated accurately and is many times less than the actual value.

The purpose of the present work is to eliminate the above-mentioned shortcomings of A.G. Geniev's model to describe the nonlinear dynamic behavior of concrete under external (impact) loads. By correcting the solid phase deformation diagram, the delayed failure time of concrete is more accurately specified.

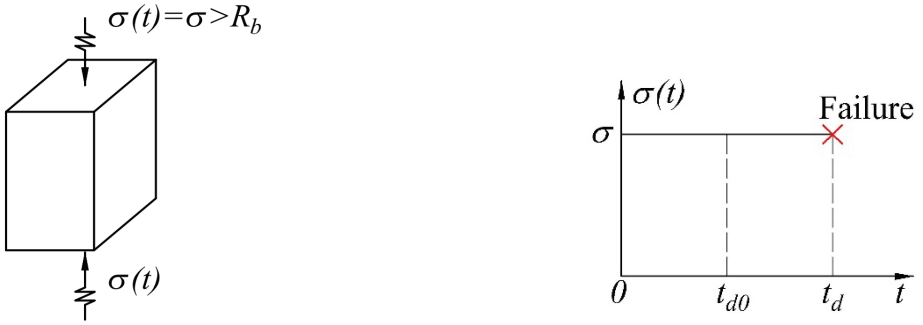
2. METHODS

Consider a specimen of heavy concrete with axial uniaxial compressive strength R_b and initial modulus of elasticity E_b. For simplicity, we will take only the case of the uniaxial stress state, in which it is easier to understand the essence of the phenomenon. At the initial moment of time $t = 0$, we suddenly apply a dynamic load with a constant value ($P(t) = P = const$) to this specimen (see Fig. 1a). Thus, the uniaxial stress arising in the concrete specimen under the action of an external dynamic force P can be determined by the formula

$$\sigma(t) = \frac{P(t)}{F} = \sigma = const \qquad (5)$$

where F is the cross-section area of the concrete specimen

When the stress in concrete exceeds the value of concrete compressive strength ($\sigma > R_b$) the above experimental studies show that concrete does not fail immediately at time $t = 0$, but deforms and then fails after a certain short period (delayed failure time t_d) (see Fig. 1a).



a) Concrete specimen loading scheme *b) graph of stress variation as a function of time*

Figure 1. Concrete specimen loading scheme and graph of stress variation as a function of time

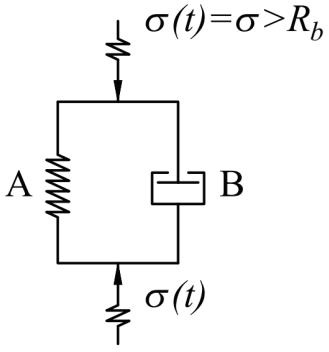


Figure 2. Model describing the behavior of concrete under dynamic loading

In this paper, we will determine the delayed failure time td of concrete by analytical methods based on the model of G.A. Geniev. This model includes two elements A and B connected in parallel and under stress $\sigma(t) = \sigma > R_b$ (see Fig. 2).

In this case, element A represents the nonlinear behavior of concrete under static loading and is depicted as a nonlinear spring (see Fig. 3). Under axial compression, we accept a nonlinear concrete deformation diagram according to the formula:

$$\sigma_A = \begin{cases} E_0\left(1-\dfrac{\varepsilon_A}{2\varepsilon_{b0}}\right)\varepsilon_A \ ; 0 \le \varepsilon_A \le \varepsilon_{b0} \\ R_b \ ; \ \varepsilon_{b0} \le \varepsilon_A \le \varepsilon_{b2} \end{cases} \quad (6)$$

Where σ_A and ε_A - stress and relative strain of element A, respectively; $\varepsilon_{b0} = 2R_b / E_b$ - relative strain of element A at the point corresponding to the maximum value of stress on the diagram σ_A - ε_A; ε_{b2} - limiting relative strain of element A.

The stress-strain diagram of spring A is shown graphically in Fig. 3.

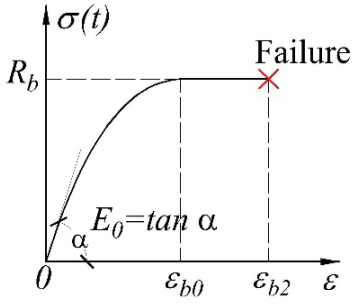


Figure 3. Concrete deformation diagram under uniaxial compression

Thus, according to Fig. 3, the concrete specimen is considered to be ruined under the action of sudden constant stress when the deformation in it reaches the value of ε_{b2}. According to the Russian standard for the design of concrete and reinforced concrete structures SP 63.13330.2012, this value is assumed to be 0.0035 for concrete of compressive strength class B60 and below.

Element B describes the viscosity of concrete and is represented as a piston as shown in Figure 2. The simplest law of deformation in time of piston B is established for an ideal fluid in which stresses are proportional to the strain rate

$$\sigma_B = K\frac{d\varepsilon_B}{dt} \quad (7)$$

where the value of K is the viscosity.

According to the adopted model, the relative deformation of element A and element B is equal

$$\varepsilon_A = \varepsilon_B = \varepsilon \quad (2)$$

The total stress in element A and element B is equal to the stress $\sigma(t) = \sigma > R_b$ caused by the external force:

$$\sigma_A + \sigma_B = \sigma \quad (9)$$

Let's consider two stages of concrete deformation: when the relative deformation of concrete is less than and $\varepsilon_{b0} = 2R_b / E_b$ when it is within the $[\varepsilon_{b0}, \varepsilon_{b2}]$.

Stage 1: $0 \le \varepsilon \le \varepsilon_{b0}$ - By substituting Eq. (6) and Eq. (7) into Eq. (9), we have

$$E_0\left(1-\frac{\varepsilon}{2\varepsilon_{b0}}\right)\varepsilon + K\frac{d\varepsilon}{dt} = \sigma \quad (10)$$

Eq. (10) is a first-order differential equation with separating variables. Using basic transformations, Eq. (10) takes the following form

$$\frac{d\varepsilon}{\frac{E_0}{2\varepsilon_{b0}}\varepsilon^2 - E_0\varepsilon + \sigma} = \frac{dt}{K} \quad (11)$$

To obtain the solution of the initial differential equation, it is necessary to integrate both parts of Eq. (11)

$$\int \frac{d\varepsilon}{\frac{E_0}{2\varepsilon_{b0}}\varepsilon^2 - E_0\varepsilon + \sigma} = \frac{t}{K} + C_1 \quad (12)$$

where C_1 - integration constant.

From Eq. (12) it is necessary to calculate the integral

$$f(\varepsilon)=\int\frac{d\varepsilon}{a\varepsilon^2+b\varepsilon+c} \tag{13}$$

The solution of the integral (13) depends on the sign of the discriminant

$$\begin{aligned}\Delta&=b^2-4ac=\left(-E_0\right)^2-4\frac{E_0}{2\varepsilon_{b0}}\sigma\\&=\left(-E_0\right)^2-4\frac{E_0}{2\dfrac{2R_b}{E_0}}\sigma=E_0^2-E_0^2\frac{\sigma}{R_b}\\&=E_0^2\left(1-\varphi_d\right)\end{aligned} \tag{14}$$

where $\varphi_d=\sigma/R_b$ - is called the level of concrete overload. According to the condition of the problem $\sigma>R_b$ it should be deduced that $\varphi_d>1$ and corresponds to the value $\Delta<0$. Thus, the solution of the integral is written in the form

$$\begin{aligned}f(\varepsilon)&=\int\frac{d\varepsilon}{a\varepsilon^2+b\varepsilon+c}\\&=\frac{2}{\sqrt{-\Delta}}\arctan\left(\frac{2a\varepsilon+b}{\sqrt{-\Delta}}\right)+C_1\end{aligned} \tag{15}$$

or

$$\begin{aligned}f(\varepsilon)&=\frac{2}{\sqrt{E_0^2\left(\varphi_d-1\right)}}\arctan\left(\frac{2\dfrac{E_0}{2\varepsilon_{b0}}\varepsilon-E_0}{\sqrt{E_0^2\left(\varphi_d-1\right)}}\right)\\&+C_1=\frac{2}{E_0\sqrt{\varphi_d-1}}\arctan\left(\frac{\dfrac{\varepsilon}{\varepsilon_{b0}}-1}{\sqrt{\varphi_d-1}}\right)+C_1\end{aligned} \tag{16}$$

Substituting Eq. (16) into Eq. (12) we obtain

$$\frac{2}{E_0\sqrt{\varphi_d-1}}\arctan\left(\frac{\dfrac{\varepsilon}{\varepsilon_{b0}}-1}{\sqrt{\varphi_d-1}}\right)=\frac{t}{K}+C_1 \tag{17}$$

To determine the value of the integration constant C_1, let us use the initial conditions of the problem: At time t=0, the relative deformation of the concrete specimen is 0 (ε=0). Substituting them into Eq. (17) we find the value of

$$C_1=\frac{2}{E_0\sqrt{\varphi_d-1}}\arctan\frac{-1}{\sqrt{\varphi_d-1}} \tag{18}$$

Thus, the partial solution of Eq. (9) satisfying the initial conditions has the form

$$\begin{aligned}&\frac{2}{E_0\sqrt{\varphi_d-1}}\arctan\left(\frac{\dfrac{\varepsilon}{\varepsilon_{b0}}-1}{\sqrt{\varphi_d-1}}\right)\\&=\frac{t}{K}+\frac{2}{E_0\sqrt{\varphi_d-1}}\arctan\frac{-1}{\sqrt{\varphi_d-1}}\end{aligned} \tag{19}$$

From Eq. (19), through some simple transformations, we obtain a formula representing the value of the relative strain of concrete over time

$$\varepsilon=\frac{\varepsilon_{b0}\cdot\varphi_d\cdot\tan\left(\dfrac{E_0\sqrt{\varphi_d-1}}{2K}t\right)}{tg\left(\dfrac{E_0\sqrt{\varphi_d-1}}{2K}t\right)+\sqrt{\varphi_d-1}}; \tag{20}$$

It is easy to see that Eq. (20) describes the change in the relative strain of concrete in the range $\varepsilon\in[0,\varepsilon_{b0}]$ with time t. At time t=0, the concrete is not deformed. At time $t=t_{d0}$, the concrete deformation reaches the value $\varepsilon_{b0}=2R_b/E_b$. We find the value of t_{d0} by substituting $\varepsilon=\varepsilon_{b0}$ into Eq. (20). We have

$$t_{d0}=\frac{2K}{E_0\sqrt{\varphi_d-1}}\arctan\frac{1}{\sqrt{\varphi_d-1}} \tag{21}$$

Taking the derivative of both parts of Eq. (20), we obtain the formula for the strain rate in time in the interval $t\in[0,t_{d0}]$

$$\dot{\varepsilon} = \frac{E_0 \varepsilon_{b0} \varphi_d (\varphi_d - 1)}{K\left[2\sqrt{\varphi_d - 1} \cdot \sin\left(\frac{E_0\sqrt{\varphi_d - 1}}{K} t\right) + (\varphi_d - 2)\cos\left(\frac{E_0\sqrt{\varphi_d - 1}}{K} t\right) + \varphi_d\right]} \quad (22)$$

Stage 2: $\varepsilon_{b0} \le \varepsilon \le \varepsilon_{b2}$ - then the stress of the non-linear spring A has a constant value and is equal to $\sigma_A = R_b$. Substituting Eq. (6) and Eq. (7) into Eq. (9), we have

$$R_b + K\frac{d\varepsilon}{dt} = \sigma \quad (23)$$

From Eq. (23) we obtain the formula for determining the strain rate

$$\dot{\varepsilon} = \frac{\sigma - R_b}{K} \quad (24)$$

Solving the differential Eq. (24), we find an expression for the relative strain of concrete as a function of time

$$\varepsilon = \frac{\sigma - R_b}{K} t + C_2 \quad (25)$$

The integration constant C_2 is determined from the initial condition as follows: at time $t = t_{b0}$ the relative strain of concrete reaches the value $\varepsilon = \varepsilon_{b0}$. We have

$$\varepsilon_{b0} = \frac{\sigma - R_b}{K} t_{b0} + C_2 \quad (26)$$

or

$$C_2 = \varepsilon_{b0} - \frac{\sigma - R_b}{K} t_{b0} \quad (27)$$

Substituting the found value C_2 into Eq. (25), we have

$$\varepsilon = \frac{\sigma - R_b}{K}(t - t_{b0}) + \varepsilon_{b0} \; ; \; \varepsilon \ge \varepsilon_{b0} \quad (28)$$

Note that Eq. (28) describes the change in the relative strain of concrete in the range $\varepsilon \in [\varepsilon_{b0}, \varepsilon_{b2}]$ with time t. When the relative strain reaches the limit value $\varepsilon = \varepsilon_{b2}$, the concrete specimen is considered to have failed. By substituting $\varepsilon = \varepsilon_{b2}$ into Eq. (28), we can find the time required for the concrete specimen to fail when subjected to a sudden dynamic load $\sigma(t) = \sigma > R_b$.

$$t_d = \frac{2K}{E_0\sqrt{\varphi_d - 1}} \arctan\frac{1}{\sqrt{\varphi_d - 1}} + \frac{(\varepsilon_{b2} - \varepsilon_{b0})K}{R_b(\varphi_d - 1)} \quad (29)$$

The values of t_{d0} and t_d in Eqs. (21)-(29) can be expressed as a function depending on the level of concrete overload, as shown in the following Fig. 4.

From Fig. 4, we see that the diagram t_d - φ_d can be obtained by moving the diagram t_{d0} - φ_d to the right - along the time axis t by a distance equal to $\frac{(\varepsilon_{b2} - \varepsilon_{b0})K}{R_b(\varphi_d - 1)}$.

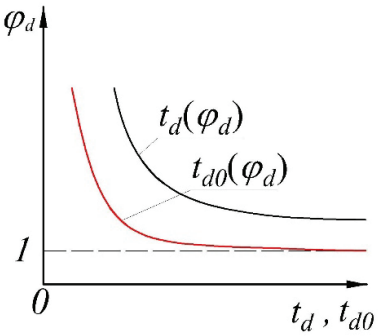


Figure 4. Dependence of t_{d0} and t_d on the level of overload φ_d

Generalizing the above two cases, we have a formula for determining the relative strain of concrete over time as follows:

$$\varepsilon = \begin{cases} \dfrac{\varepsilon_{b0} \cdot \varphi_d \cdot tg\left(\dfrac{E_0\sqrt{\varphi_d - 1}}{2K}t\right)}{tg\left(\dfrac{E_0\sqrt{\varphi_d - 1}}{2K}t\right) + \sqrt{\varphi_d - 1}}; \ 0 \le \varepsilon \le \varepsilon_{b0} \\ \dfrac{R_b(\varphi_d - 1)}{K}(t - t_{b0}) + \varepsilon_{b0} \ ; \ \varepsilon_{b0} \le \varepsilon \le \varepsilon_{b2} \end{cases} \quad (30)$$

and a formula for determining the strain rate of concrete over time:

$$\dot{\varepsilon} = \begin{cases} \dfrac{E_0 \varepsilon_{b0} \varphi_d (\varphi_d - 1)}{K\left[2\sqrt{\varphi_d - 1} \cdot \sin\left(\dfrac{E_0\sqrt{\varphi_d - 1}}{K}t\right) + (\varphi_d - 2)\cos\left(\dfrac{E_0\sqrt{\varphi_d - 1}}{K}t\right) + \varphi_d\right]} \ ; \ 0 \le \varepsilon \le \varepsilon_{b0} \\ \dfrac{R_b(\varphi_d - 1)}{K} \ ; \ \varepsilon_{b0} \le \varepsilon \le \varepsilon_{b2} \end{cases} \quad (31)$$

From Eqs. (30)-(31), we can plot the strain and strain rate versus time (see Fig. 5 and Fig. 6).

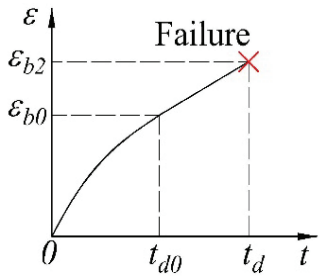


Figure 5. Dependence of $\varepsilon - t$

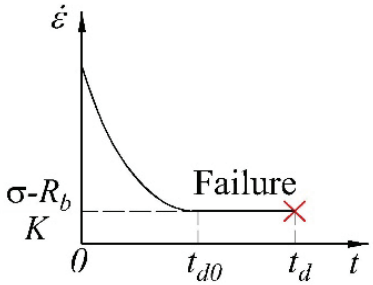


Figure 6. Dependence of $\dot{\varepsilon} - t$

3. RESULTS AND DISCUSSION

3.1 Effect of strength class on deformation and failure of concrete over time

Based on the proposed model, the influence of concrete compressive strength class R_b on the strain state, as well as the process of concrete failure over time under the action of an external load, the value of which exceeds the load-bearing capacity of concrete ($\sigma > R_b$), is considered. Mechanical parameters of concrete of different classes according to Russian standard SP 63.13330.2018 are presented in Table 1.

Table 1. Mechanical parameters of concrete of different compressive strength classes

	B20	B30	B40	B50
R_b(MPa)	15	22	29	36
$E_b \cdot 0,001$ (MPa)	27	32,5	36	39
$\varepsilon_{b0} = 2\dfrac{R_b}{E_b}$	0,0011	0,0014	0,0016	0,0018
ε_{b2}	0,0035			

Based on Eq. (6) and input data in Table 1, we can construct the stress-strain curves of concrete with different compressive strength classes when subjected to axial static force (see Fig. 7). It is noticed that as the compressive strength classes increase, the ultimate compressive strength of concrete and strain at that strength value become larger.

To facilitate the study of the influence of concrete compressive strength class on the delayed failure time, we assume the value of viscosity

K=400 MPa·sec, and the level of overload - $\varphi_d = \sigma / R_b = 1.4$. Then based on Eqs. (21)-(29) it is possible to plot the relationship between the delayed failure time and the compressive strength class of concrete (see Fig. 8).

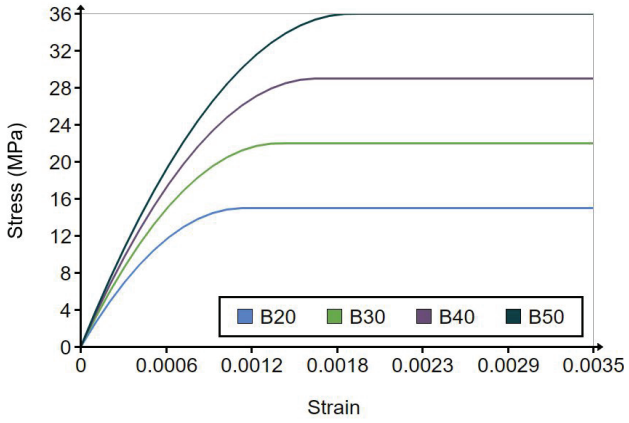


Figure 7. Stress-strain curves of concrete of different compressive strength classes under the static uniaxial compressive loading

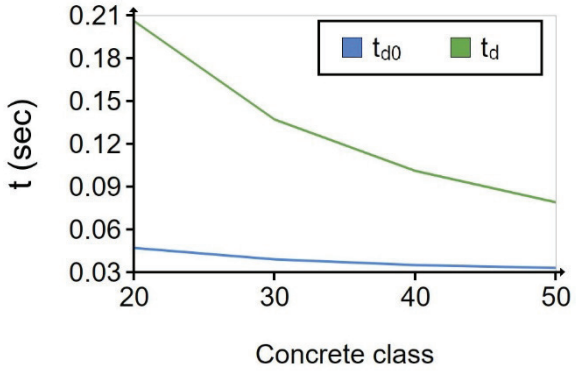


Figure 8. Relationship between concrete compressive strength class and delayed times

It is observed that for concrete B20 when the external dynamic load exceeds the bearing capacity 1.4 times, the relative strain reaches the value $\varepsilon_{b0} = 0.0011$ after a period of t_{d0}=0.047 sec. Concrete is considered to fail after a time interval t_d = 0.206 sec when the relative strain in it reaches the limit value $\varepsilon_{b2} = 0.0035$. When increasing the concrete class, the delayed failure time decreases significantly. In particular, when the concrete class is increased by 2.5 times (from concrete B20 to concrete B50), the time t_{d0} decreases by 1.4 times, and the delayed failure time t_d by 2.6 times. Thus, when increasing the concrete class, the delayed failure time will decrease faster than the time for the concrete to deform to the value ε_{b0}.This can be explained as follows. The compressive strength class of concrete is closely related to its brittleness. The higher the class of concrete, the more brittle it is. Consequently, when subjected to impact loads exceeding its bearing capacity, concrete with a high compressive strength class will undergo brittle failure, and the delayed failure time will be shorter than that of concrete with a low strength class.

3.2 Effect of level of overloading on deformation and failure of concrete over time

Based on Eqs. (21)-(29), it is possible to express the effect of the level of overloading on the time of delayed fracture in the case of B20 concrete with viscosity taken K=400 $MPa \cdot$sec (see Fig. 9).

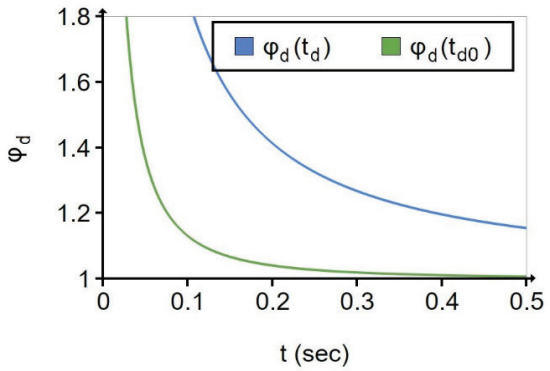


Figure 9. Dependence of delayed times on the level of overloading

From Fig. 9 we see that at sudden application of dynamic load with intensity exceeding the bearing capacity of the concrete specimen more than 1.1 times, the time required to reach the value of strain $\varepsilon_{b0} = 0.0011$, is t_{d0}= 0.118 c. And the concrete failure occurs at time t_d=0.756 c. Thus, the time t_d is 6.4 times longer than t_{d0}.

When the level of overload increases, the delay times will decrease dramatically. For example, when φ_d increases 1.6 times from 1.1 to 1.8, t_{d0} will decrease 4.2 times. The delayed failure time will accordingly be reduced by 7.1 times.

3.3 The influence of the viscosity on the deformation and failure of concrete over time

To study the effect of the viscosity on the deformation and failure of concrete over time, consider the example of concrete of class B20 with different viscosities (K = 200, 500, and 800 MPa/s). In practice, the viscosity can be adjusted by changing the porosity value or changing the water-cement ratio of the concrete mixture. Based on Eq. (29), we find out the effect of viscosity on the graph of "overload level - delayed failure time " (see Fig. 10). It is found that when the viscosity increases, the delayed failure time increases significantly. At an overload level of 1.4 and a viscosity of 200 MPa/s, the delayed failure time reaches a value of 0.103 s. When the viscosity increases by 2.5 times (K=500 MPa/s), the delayed failure time increases by 2.5 times (t_d=0.258 s).

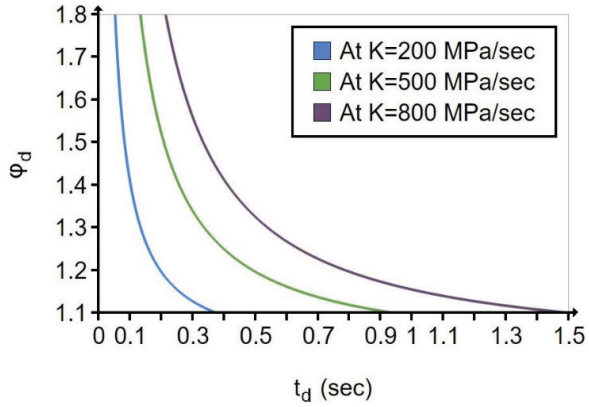


Figure 10. Effect of viscosity on delayed failure time

Eq. (30) gives us the characteristics of relative strain variation in time. Let's draw graphs "$\varepsilon - t$" for 3 cases (at K=200, 500, and 800 MPa/s) (see Fig. 11). It is easy to see that when t is in the range of $[0, t_{d0}]$, the graph has a curvilinear shape. When t is in the range of $[t_{d0}, t_d]$, the relative strain depends on time in a linear relationship. At any instant of time (e.g., t=0.05 s), the relative strain achieved is different in cases of different viscosity. At K=200 MPa/s, the relative strain at this moment is 0.002. At K=500 MPa/s the attainable strain is 2 times lower (ε=0.001). At K=800 MPa/s, the relative strain reaches 0.00075. Thus, it can be concluded that the relative strain of concrete at any moment in time depends on the value of viscosity.

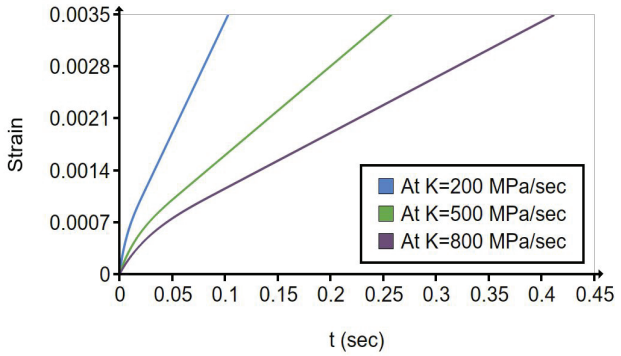


Figure 11. Effect of viscosity on $\varepsilon - t$ curves

Based on Eq. (31), we investigate the change of strain rate in time in cases of different K coefficients (see Fig. 12).

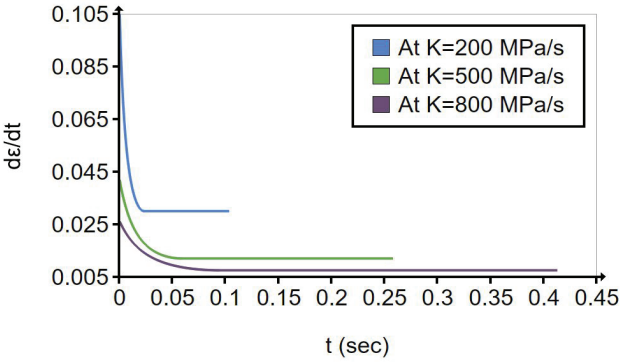


Figure 12. Effect of viscosity on the strain rate of concrete

It can be seen that when a sudden dynamic force with intensity $\sigma > R_b$ is applied to the concrete specimen, the strain rate in the concrete at the time of applying the force reaches its maximum

value. This maximum value can be determined by substituting t=0 into Eq. (22):

$$\dot{\varepsilon}_{\max} = \frac{E_0 \varepsilon_{b0} \varphi_d}{2K} \tag{32}$$

Eq. (32) shows that the maximum strain rate is proportional to the overload level and inversely proportional to the viscosity of the concrete. The strain rate decreases very rapidly over time in the range $[0, t_{d0}]$ and keeps a constant value in the range $[t_{d0}, t_d]$.

5. CONCLUSIONS

This paper presents a model that explains the phenomenon of delayed failure of concrete when a sudden dynamic load is applied to a structure, the intensity of which exceeds the bearing capacity of concrete. Using the analytical method, we can accurately determine the delayed failure time, relative strain, and strain rate at each time t. The main factors affecting the deformation and failure of concrete, such as concrete compressive strength, overload level, and viscosity, are thoroughly studied. The results of this study can be used in dynamic problems of reinforced concrete structures, for example, in the problem of calculating structural stability against progressive collapse of buildings and structures under the scenario of sudden removal of load-bearing elements.

ACKNOWLEDGMENTS

The research described in this paper was financially supported by the Russian Science Foundation grant No. 24-49-10010, https://rscf.ru//project/24-49-10010/.

REFERENCES

1. **Bazhenov Yu.M.** (1970) *Beton pri dinamicheskom nagruzhenii* [Concrete under dynamic loading]. Moscow: Stroyizdat. (in Russian)
2. **Rossi P.** (1991) Influence of cracking in the presence of free water on the mechanical behaviour of concrete. *Magazine of concrete research*, vol. 43, no 154, pp. 53-57. doi:10.1680/MACR.1991.43.154.53
3. **Cadoni E., Solomos G., Albertini C.** (2009) Mechanical characterisation of concrete in tension and compression at high strain rate using a modified Hopkinson bar. *Magazine of Concrete Research*, vol. 61, no 3, pp. 221-230. doi:10.1680/MACR.2006.00035
4. **Fedorova N.V., Medyankin M.D., Bushova O.B.** (2020) Eksperimentalnoe opredelenie parametrov statiko-dinamicheskogo deformirovaniya betona pri rezhimnom nagruzhenii [Experimental determination of the parameters of the static-dynamic deformation of concrete under loading modal]. *Stroitelstvo i rekonstruktsiya*, no 3, pp. 72–81.
5. **Korobkova M.V.** (2015) Ispytaniya betonnykh obraztsov s dempfiruyushchimi dobavkami na dinamicheskuyu prochnost [Tests of Concrete Samples with Damping Additives on Dynamic Strength]. *Stroitelnye materialy,* vol. 6, pp. 9–12.
6. **Fedorova N.V., Medyankin M.D., Bushova O.B.** (2020) Opredelenie parametrov statiko-dinamicheskogo deformirovaniya betona [Determination of static-dynamic deformation parameters of concrete]. *Promyshlennoe i grazhdanskoe stroitelstvo*, no 1, pp. 4–11.
7. **Al-Salloum Y., Almusallam T., Ibrahim S.M., Abbas H., Alsayed S.** (2015) Rate dependent behavior and modeling of concrete based on SHPB experiments. *Cement and Concrete Composites*, vol. 55, pp. 34–44. doi:10.1016/j.cemconcomp.2014.07.011
8. **Malvar L.J., Ross C.A.** (1998) Review of strain rate effects for concrete in tension. *ACI Materials Journal*, vol. 95, no 6, pp. 735-739. doi:10.14359/418

9. **Fu H.C., Erki M.A., Seckin M.** (1991) Review of Effects of Loading Rate on Concrete in Compression. *Journal of Structural Engineering*, vol. 117, no 12, pp. 3645–3659. doi:10.1061/(ASCE)0733-9445(1991)117:12(3645)
10. **Guo Y.B., Gao G.F., Jing L., Shim V.P.W.** (2022) Dynamic Properties of Mortar in High-strength Concrete. *International Journal of Impact Engineering*, vol. 165. doi:10.1016/J.IJIMPENG.2022.104216.
11. **Ali M.A., Tomann C., Aldakheel F., Mahlbacher M., Noii N., Oneschkow N., Drake K.H., Lohaus L., Wriggers P., Haist M.** (2022) Influence of Moisture Content and Wet Environment on the Fatigue Behaviour of High-Strength Concrete. *Materials*, vol. 15, no 3. doi:10.3390/MA15031025
12. **Salem S., Eissa E., Zarif E., Sherif S., Shazly M.** (2023) Influence of moisture content on the concrete response under dynamic loading. *Ain Shams Engineering Journal*, vol. 14, no 5. doi:10.1016/J.ASEJ.2022.101976.
13. **Qi C., Xia C., Dyskin A., Zhao F. (**2021) Effect of crack interaction and friction on the dynamic strength of rock-like materials with many cracks. *Engineering Fracture Mechanics*, vol. 257. doi:10.1016/J.ENGFRACMECH.2021.108006
14. **Yu W., Jin L., Du X.** (2021) Influence of pre-static loads on dynamic compression and corresponding size effect of concrete: Mesoscale analysis. *Construction and Building Materials*, vol. 300. doi:10.1016/J.CONBUILDMAT.2021.124302
15. **Alanazi N., Kolawole J.T., Buswell R., Susmel L.** (2022) The Theory of Critical Distances to assess the effect of cracks/manufacturing defects on the static strength of 3D-printed concrete. *Engineering Fracture Mechanics*, vol. 269. doi:10.1016/J.ENGFRACMECH.2022.108563
16. **Fu Q., Zhang Z., Zhao X., Hong M., Guo B., Yuan Q., Niu D.** (2021) Water saturation effect on the dynamic mechanical behaviour and scaling law effect on the dynamic strength of coral aggregate concrete. *Cement and Concrete Composites*, vol. 120. doi:10.1016/J.CEMCONCOMP.2021.104034
17. **Selyutina N.S., Petrov Y.V.** (2020) Fracture of saturated concrete and rocks under dynamic loading. *Engineering Fracture Mechanics*, vol. 225. doi:10.1016/J.ENGFRACMECH.2018.11.052
18. **Bazhenov Y.M., Udaltsov V.S.** (1964) Ob effekte zaderzhki razrusheniya betona na pri dinamicheskom nagruzhenii [On the effect of delaying the failure of concrete under dynamic loading]. *Materialy XV Itogovoy nauchno-issledovatelskoy konferentsii VNO VIKA,* no 11, pp. 8-11.
19. **Rakhmanov V.A., Rozovsky E.L., Tsupkov I.** (1987) Vliyanie dinamicheskogo vozdeystviya na prochnostnye i deformativnye svoystva tyazhelogo betona [The influence of dynamic influence on the strength and deformation properties of heavy concrete]. *Beton i zhelezobeton*, no 7, pp. 19-20.
20. **Fedorova N.V., Ngoc V.T.** (2020) Deformation and failure of monolithic reinforced concrete frames under special actions. *Journal of Physics: Conference Series*, vol. 1425, no 1. doi:10.1088/1742-6596/1425/1/012033
21. **Savin, S., Kolchunov, V., Fedorova, N., Tuyen Vu, N.** (2023) Experimental and Numerical Investigations of RC Frame Stability Failure under a Corner Column Removal Scenario. *Buildings*, Vol. 13, no 4. doi:10.3390/BUILDINGS13040908
22. **Tuyen V.N., Ivanovich K.V., Vitalyevna F.N.** (2024) Dynamic response model of reinforced concrete building frame under column removal scenario. *Structures*, vol. 63. doi:10.1016/J.ISTRUC.2024.106356
23. **Geniev G.A.** (1998) Metod opredeleniya dinamicheskikh predelov prochnosti betona [Method for determining the dynamic strength limits of concrete]. *Beton i zhelezobeton*, no 1, pp. 18-19.

СПИСОК ЛИТЕРАТУРЫ

1. **Баженов, Ю.М.** Бетон при динамическом нагружении. - М.: Стройиздат, 1970. - 272 с.
2. **Rossi P.** Influence of cracking in the presence of free water on the mechanical behaviour of concrete // Magazine of concrete research, 1991, No. 43(154), pp. 53-57.
3. **Cadoni E., Solomos G., Albertini C.** Mechanical characterisation of concrete in tension and compression at high strain rate using a modified Hopkinson bar // Magazine of Concrete Research, 2009, No. 61(3), pp. 221-230.
4. **Федорова Н. В., Медянкин М. Д., Бушова О. Б.** Экспериментальное определение параметров статико-динамического деформирования бетона при режимном нагружении // Строительство и реконструкция, 2020, №3. С. 72-81.
5. **Коробкова М. В.** Испытания бетонных образцов с демпфирующими добавками на динамическую прочность // Строительные материалы, 2015, №6. С. 9-12.
6. **Федорова Н.В., Медянкин М.Д., Бушова О.Б.** Определение параметров статико-динамического деформирования бетона // Промышленное и гражданское строительство, 2020, №1. С. 4-11.
7. **Al-Salloum Y., Almusallam T., Ibrahim S.M., Abbas H., Alsayed S.** Rate dependent behavior and modeling of concrete based on SHPB experiments // Cement and Concrete Composites, 2015, No. 55, pp. 34–44.
8. **Malvar L.J., Ross C.A.** Review of strain rate effects for concrete in tension // ACI Materials Journal, 1998, No. 95(6), pp. 735-739.
9. **Fu H.C., Erki M.A., Seckin M.** Review of Effects of Loading Rate on Concrete in Compression // Journal of Structural Engineering, 1991, No. 117(12), pp. 3645–3659.
10. **Guo Y.B., Gao G.F., Jing L., Shim V.P.W.** Dynamic Properties of Mortar in High-strength Concrete // International Journal of Impact Engineering, 2022, No. 165.
11. **Ali M.A., Tomann C., Aldakheel F., Mahlbacher M., Noii N., Oneschkow N., Drake K.H., Lohaus L., Wriggers P., Haist M.** Influence of Moisture Content and Wet Environment on the Fatigue Behaviour of High-Strength Concrete // Materials, 2022, No. 15(3).
12. **Salem S., Eissa E., Zarif E., Sherif S., Shazly M.** Influence of moisture content on the concrete response under dynamic loading // Ain Shams Engineering Journal, 2023, No. 14(5).
13. **Qi C., Xia C., Dyskin A., Zhao F.** Effect of crack interaction and friction on the dynamic strength of rock-like materials with many cracks // Engineering Fracture Mechanics, 2021, No. 257.
14. **Yu W., Jin L., Du X.** Influence of pre-static loads on dynamic compression and corresponding size effect of concrete: Mesoscale analysis // Construction and Building Materials, 2021, No. 300.
15. **Alanazi N., Kolawole J.T., Buswell R., Susmel L.** The Theory of Critical Distances to assess the effect of cracks/manufacturing defects on the static strength of 3D-printed concrete // *Engineering Fracture Mechanics*, 2022, No. 269.
16. **Fu Q., Zhang Z., Zhao X., Hong M., Guo B., Yuan Q., Niu D.** Water saturation effect on the dynamic mechanical behaviour and scaling law effect on the dynamic strength of coral aggregate concrete // Cement and Concrete Composites, 2021, No. 120.
17. **Selyutina N.S., Petrov Y.V.** Fracture of saturated concrete and rocks under dynamic loading // Engineering Fracture Mechanics, 2020, No. 225.
18. **Баженов Ю.М., Удальцов В.С.** Об эффекте задержки разрушения бетона на при динамическом нагружении // Материалы XV Итоговой научно-исследовательской конференции ВНО ВИКА. М., 1964. С. 8-11.
19. **Рахманов В.А., Розовский Е.Л., Цупков И.А.** Влияние динамического воздействия на прочностные и деформативные

свойства тяжелого бетона // Бетон и железобетон, 1987, №7. С. 19-20.
20. **Fedorova N.V., Ngoc V.T.** Deformation and failure of monolithic reinforced concrete frames under special actions // Journal of Physics: Conference Series, 2020, No. 1425(1).
21. **Savin, S., Kolchunov, V., Fedorova, N., Tuyen Vu, N.** Experimental and Numerical Investigations of RC Frame Stability Failure under a Corner Column Removal Scenario // Buildings, 2023, No. 13(4).
22. **Tuyen V.N., Ivanovich K.V., Vitalyevna F.N.** Dynamic response model of reinforced concrete building frame under column removal scenario // Structures, 2024, No. 63.
23. **Гениев Г.А.** Метод определения динамических пределов прочности бетона // Бетон и железобетон, 1998, №1. С. 18-19.

Vu Ngoc Tuyen — Candidate of Technical Sciences, Senior Lecturer, Department of Fundamental Education, National Research Moscow State University of Civil Engineering, 26, Yaroslavskoe Shosse, Moscow, 129337, Russia, WuNgokTuen@gic.mgsu.ru, +7 (495)-287-49-14*1751

Fedorova Natalia Vitalievna - Doctor of Technical Sciences, Professor, Head of the Department of Industrial and Civil Engineering, National Research Moscow State University of Civil Engineering, 26, Yaroslavskoye Shosse, Moscow, 129337, Russia, FedorovaNV@gic.mgsu.ru, +7(495) 583-79-04

Ву Нгок Туен — кандидат технических наук, старший преподаватель кафедры Фундаментального образования, Федеральное государственное бюджетное образовательное учреждение высшего образования «Национальный исследовательский Московский государственный строительный университет» (НИУ МГСУ), д. 26, Ярославское шоссе, г. Москва, 129337, Россия, WuNgokTuen@gic.mgsu.ru, +7 (495)-287-49-14*1751

Федорова Наталия Витальевна — доктор технических наук, профессор, заведующий кафедрой Промышленного и гражданского строительства, Федеральное государственное бюджетное образовательное учреждение высшего образования «Национальный исследовательский Московский государственный строительный университет» (НИУ МГСУ), д. 26, Ярославское шоссе, г. Москва, 129337, Россия, FedorovaNV@gic.mgsu.ru, +7(495) 583-79-04

International Journal for Computational Civil and Structural Engineering, 20(2) 132–140(2024)

DOI:10.22337/2587-9618-2024-20-2-132-140

CALIBRATION OF THE NONLOCAL DYNAMIC DEFORMATION MODEL OF A FLEXURAL BEAM BASED ON NUMERICAL EXPERIMENT RESULTS

Vladimir N. Sidorov [1,2], Elena S. Badina [1,2,3], Roman O. Tsarev [3]

[1] Moscow State University of Civil Engineering, Moscow, RUSSIA

[2] Russian University of Transport (MIIT), Moscow, RUSSIA

[3] Institute of Applied Mechanics of Russian Academy of Sciences, Moscow, RUSSIA

Abstract: In this paper, the problem of numerical modeling of the dynamic behavior of bending beams made of the materials with a developed internal structure is considered. The simulation is performed taking into account the non-local elastic properties of the material in time. According to the principals of nonlocal mechanics, it is assumed that elastic forces in a structure depend on the entire history of its deformation, and not only on the instantaneous deformed state. The proposed dynamic deformation model is proposed as an alternative to detailed three-dimensional models. The nonlocal dynamic deformation model is integrated into the algorithm of the FEA method to make it applicable to solving applied engineering problems. The numerical implementation of the model is performed in Python. A technique for selecting the scale parameter of a non-local model based on experimental data using the least squares method and the dichotomy method has also been developed and implemented. To identify the possibility of extrapolation of the scale parameter values determined according to the developed methodology, a series of numerical experiments were conducted, on the basis of which scale parameters for beams of different lengths were obtained and the stability of the nonlocal model was evaluated.

Keywords: Nonlocal mechanics, nonlocal damping, numerical simulation, finite element method

КАЛИБРОВКА НЕЛОКАЛЬНОЙ МОДЕЛИ ДИНАМИЧЕСКОГО ДЕФОРМИРОВАНИЯ ИЗГИБАЕМОЙ БАЛКИ ПО РЕЗУЛЬТАТАМ ЧИСЛЕННОГО ЭКСПЕРИМЕНТА

В.Н. Сидоров [1,2], Е.С. Бадьина [1,2,3], Р.О. Царёв [3]

[1] Российский университет транспорта (МИИТ), г. Москва, РОССИЯ

[2] Национальный исследовательский Московский государственный строительный университет, г. Москва, РОССИЯ

[3] Институт прикладной механики Российской академии наук, г. Москва, РОССИЯ

Аннотация: в настоящей работе рассматривается задача численного моделирования динамического поведения изгибаемых балок, выполненных из материалов с развитой внутренней структурой. Моделирование выполнено с учетом нелокальных во времени упругих свойств материала. Согласно положениям нелокальной механики предполагается, что упругие силы в конструкции зависят от всей истории её деформирования, а не только от мгновенного деформированного состояния. Представленная модель динамического деформирования предлагается в качестве альтернативы подробным трёхмерным моделям. Нелокальная модель динамического деформирования интегрирована в алгоритм метода конечных элементов, чтобы сделать её применимой для решения прикладных инженерных задач. Численная реализация модели выполнена на языке Python. Также разработана и реализована методика подбора масштабного параметра нелокальной модели на основании экспериментальных данных с применением метода наименьших квадратов и метода дихотомии. Для выявления возможности экстраполяции определённых по разработанной методике значений масштабного параметра, была проведена серия численных экспериментов, на основе которых были получены масштабные параметры для балок разной длины и проведена оценка устойчивости нелокальной модели.

Ключевые слова: Нелокальная механика, нелокальное демпфирование, численное моделирование, метод конечных элементов

INTRODUCTION

The active use of composite materials to address various production challenges requires new approaches to describe their behavior under dynamic loads. To achieve sufficient accuracy in numerical calculations, detailed three-dimensional finite element models are often employed, allowing for a reasonably accurate representation of materials with complex internal structures. However, such models are resource-intensive and laborious to analyze.

To optimize the calculation and design process, there arises a need to employ one-dimensional rod element models which are constructed on the base of specific mathematical hypotheses. Such hypotheses become necessary as classical viscoelastic models, proposed, for instance, in the works of W. Kelvin [1], J. Maxwell [2], J. Rayleigh [3], and Voigt [4], do not always accurately describe the behavior of materials with intricate internal structures.

As an alternative to classical models ones based on the principals of nonlocal mechanics can be used. Among such models the nonlocal elasticity model proposed in article [5], the model of nonlocal damping in space [6], and model [7] that combines the nonlocality of elastic and damping properties can be mentioned. The continuous spatial nonlocal damping model is described in article [8], while the nonlocal temporal internal friction model, based on the finite element method, is presented in article [9]. Article [10] discussed various damping mechanisms for a quasi-isotropic pultruded composite beam, including: viscous damping; internal damping dependent on strain rate; spatial hysteresis; and temporal hysteresis. Additionally, the article examines various combinations of these mechanisms [11].

In this work a proposed model is based on the assumption of the material's nonlocality in its elastic properties over time.

DYNAMIC MODEL OF BENDING BEAM DEFORMATION WITH CONSIDERING NON-LOCAL IN TIME ELASTIC PROPERTIES OF THE MATERIAL

The non-local model for dynamic deformation has been integrated into the finite element method algorithm. This approach allows using of the model in applied analyses of structures with the relatively complicated geometry. In the finite element method algorithm, the equation of motion is formulated in matrix form and is expressed in displacements [12]:

$$M \cdot \ddot{V}(t) + D \cdot \dot{V}(\tau) + K \cdot V(t) = F(t) \qquad (1)$$

Here: K is the stiffness matrix, M is the mass matrix, D is the damping matrix, $F(t)$ is the vector of external force influences, $V(t)$ is the displacement vector.

When accounting for non-local material properties, it is assumed that the elastic forces within the system at the considered time moment t depend not only upon the instantaneous value of displacement $V(t)$, but also upon the displacement values at prior time instances τ. Moreover, the impact of time points on each other weakens proportionally with increasing time gap [13]. To formulate a model for the deformation of a beam element considering material memory, let us express equation (1) in the subsequent manner:

$$M \cdot \ddot{V}(t) + D \cdot \dot{V}(\tau) + \\ +K \cdot \int_0^t R(t-\tau) \cdot V(t) d\tau = F(t) \qquad (2)$$

Here, the stiffness matrix K is superimposed with the kernel of the non-local elasticity operator $R(t-\tau)$ or influence function. This function characterizes the attenuation of the influence of displacements at previous time instances τ on the elastic forces at the current moment t, while ensuring adherence to the normalization condition.

$$\int_0^t R(t-\tau)\,d\tau = 1 \qquad (3)$$

For the memory function modeling, kernels of various types can be used [6]. In the present study, the non-local operator kernels employ the error function, which takes the form when condition (3) is satisfied:

$$R(t-\tau) = \frac{2\eta}{\sqrt{\pi}} \cdot e^{-\eta^2(t-\tau)^2} \qquad (4)$$

Like for all non-local models, in this case, a defining characteristic is the scale parameter η, which determines the nonlocality in the elastic properties of the material over time. Figure 1 illustrates how this parameter influences the shape of the kernel.

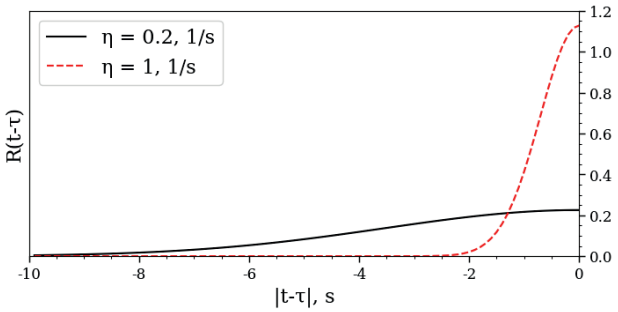


Figure 1. Graphs showing the effect of the parameter η on the nonlocality of the model

To solve the equation of motion, an implicit scheme (Newmark's method) [14] was employed. In this case, the velocities and accelerations of the finite element model nodes are represented as:

$$\dot{V}_{i+1} = \frac{V_{i+1} - V_i}{\Delta t};$$
$$\ddot{V}_{i+1} = \frac{2}{\Delta t^2}\left(V_{i+1} - V_i - \dot{V}_i \cdot \Delta t\right) - \ddot{V}_i \qquad (5)$$

Here: V_i is the vertical displacement of a node at a time t_i, $\dot{V}_i$ is the speed of the node at a given timet_i , $\ddot{V}_i$ is the node acceleration at a point in timet_i, Δt is the time step

Since, in the case of employing an implicit scheme, the memory function is imposed on the entire deformation process starting from the moment t_{i+1}, the discrete analog of the integral kernel has been divided into two parts [15]: α - the weighting coefficient associated with V_{i+1}, β - the sum of all other weights:

$$\alpha = \frac{2\eta}{\sqrt{\pi}} \cdot e^{-\eta^2(t_{i+1}-t_i)^2} \cdot \Delta t;$$
$$\beta = \Delta t \sum_{j=1}^{i} \frac{2\eta}{\sqrt{\pi}} \cdot e^{-\eta^2\left(t_i - t_{j-1}\right)^2} \qquad (6)$$

Then, the expression (1) can be presented as:

$$M \cdot \left[\frac{2}{\Delta t^2} \cdot \left(V_{i+1} - V_i - \dot{V}_i \cdot \Delta t\right) - \ddot{V}_i\right] + D \cdot \frac{1}{\Delta t} \cdot (V_{i+1} - V_i) + K \cdot \beta + K \cdot \alpha = \bar{F}_{i+1} \qquad (7)$$

After all transformations, the computational scheme takes the form:

$$Q \cdot V_{i+1} = F_{i+1} + \mathrm{M} \cdot \ddot{V}_i + Q_1 \cdot \dot{V}_i + Q_2 \cdot V_i - K \cdot \beta, \qquad (8)$$

here:

$$Q = \frac{2}{\Delta t^2} M + \frac{1}{\Delta t} D + K \cdot \alpha, \quad Q_1 = \frac{2}{\Delta t} M, \; Q_2 = \frac{2}{\Delta t^2} M + \frac{1}{\Delta t} D \qquad (9)$$

ASSESSMENT OF THE INFLUENCE OF THE SCALE PARAMETER ON THE NATURE OF THE OSCILLATORY PROCESS.

For further improvement of the model, it is necessary to determine how the variation of the scale parameter affects the nature of the vibrations. In the implementation of this model using the MATLAB software, a 12-meter beam clamped at both ends was considered. The material chosen for the beam is a thermoactive vinyl ester glass-reinforced plastic of Class I, with a Young's modulus in the longitudinal

direction equal to 17.2 GPa. The beam, in its cross-sectional profile, is a rectangle with a height of 0.3 meters and a width of 0.2 meters. The material's relative damping coefficient is set at 0.042. The beam is subjected to an instantly applied and uniformly distributed load with an intensity of -10 kN/m. At the first step, with i = 1, the initial conditions are set as $\bar{V}_0 = 0$.

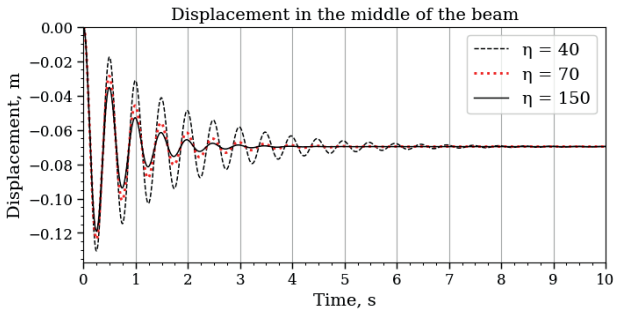


Figure 2. Graphs of the vertical displacement of the central node of the beam obtained for three calculation scenarios with different scale parameters

Analyzing the presented graphs, it can be observed that decreasing the parameter η (increasing the degree of non-locality) leads to an increase in the amplitude of oscillations.

DETERMINATION OF THE NON-LOCAL PARAMETER BASED ON THE RESULTS OF THE NUMERICAL EXPERIMENT.

In order to apply the non-local material model in practical calculations, it is necessary to determine the value of the non-local parameter. For this purpose, in the current study a calibration methodology of the non-local model using the least squares method was used based on the results of the numerical experiment [16]. The numerical experiment data consisted of the outcomes of three-dimensional finite element modeling of the beam. The geometrical and physical characteristics are the same the ones discussed in the previous section. The model was constructed using the MIDAS-Civil computational software, taking into account the orthotropic material properties. The material characteristics used in the modeling are presented in Table 1.

Table 1. Characteristics of thermoactive vinyl ester glass-reinforced plastic Class I:

Young's Modulus (Longitudinal), E_{lw}	17.2 GPa
Young's Modulus (Transverse), E_{cw}	12.2 GPa
Poisson's Ratio (Longitudinal), μ_{lw}	0.32
Poisson's Ratio (Transverse), μ_{cw}	0.15
Density, ρ	1900 kg/m^3
Damping Coefficient, γ	0.042

As a result of the calculation, a displacement diagram of the mid-section of the analyzed beam was obtained. Subsequently, the ordinate values of the oscillation graph obtained in MIDAS-Civil were exported and used to determine the scale parameter of the non-local model with an algorithm that was implemented with Python.

The numerical method employed to search for the minimum value of the sum of squared deviations between experimental data and numerical results was the bisection method.

The resulting diagrams are presented in Fig. 3 and Fig. 4. In comparison with the classical local deformation model (fig. 3), the calibrated non-local bending beam model (fig. 4) gives better alignment with the results of the numerical experiment.

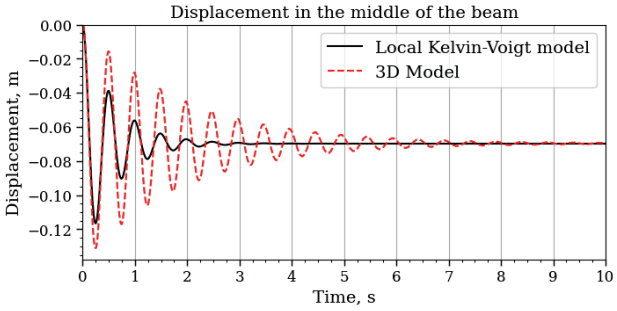


Figure 3. Comparison of numerical experiment results with one-dimensional modeling results using a model approximating the classical local Kelvin-Voigt model

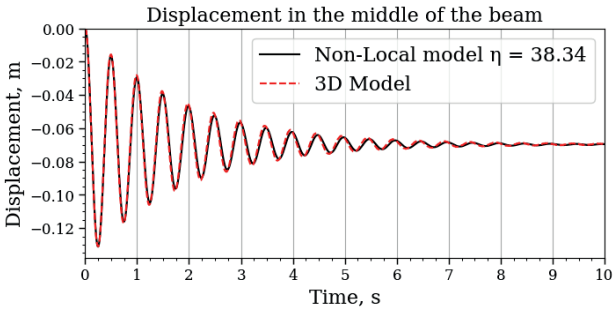


Figure 4. Comparison of numerical experiment results with one-dimensional modeling results using the calibrated time-nonlocal deformation model with the utilization of the error function kernel

As a result of calibration, the value of the scale parameter has been obtained η = 38.34 1/s. The root mean square error is 0.0034 m.

EVALUATION OF THE SCALE PARAMETER EXTRAPOLATION POSSIBILITY

The application of models requiring constant determination of the scale parameter by the experimental data may be impractical and can be extremely labor-intensive in application. Therefore, the question arises about the method for determining the scale parameter of a non-local model as a material constant or identifying dependencies that enable the determination of this parameter for elements of various geometry.

The damping model employed in conducting numerical experiments within the computational suite Midas is frequency dependent, hence the viscosity coefficient depends on the geometric attributes of the beam. Therefore, to demonstrate the correlation between the viscosity coefficient and the scale parameter, a series of numerical experiments were conducted involving beams of varied lengths. The outcomes tabulated in Table 2.

It can be seen from Table 2 that there is a correlation between the ratios of the viscosity coefficients and the ratios of the scale parameter. Consequently, given numerical or empirical data obtained for a beam of specific length and a non-local model calibrated by this data, it becomes possible to determine the scale parameter by values of frequency ratios or viscosity coefficients applicable to beams of different geometries but composed of the same material. Should damping in the material prove frequency-independence, the scale parameter for said material will inherently remain constant.

Table 2. The results of a series of experiments

L, m	χ, Pa·s	η, 1/s	The ratios of viscosity coefficients	The ratios of scale parameters
10	0,014	52.9	1,00	1.00
11	0,017	44.8	0,83	0.85
12	0,021	38.3	0,69	0.73
13	0,024	34	0,59	0.64
14	0,028	29.6	0,51	0.56
15	0,032	26.3	0,44	0.50
16	0,036	22.9	0,39	0.43
17	0,041	20.6	0,35	0.39
18	0,046	18.3	0,31	0.35

Here **L** is the Beam length, **χ** is the Viscosity coefficient, ***η*** is the Scale parameter

For clarity the proportion between viscosity coefficients and the proportion between scale parameters is visually presented in Figure 5.

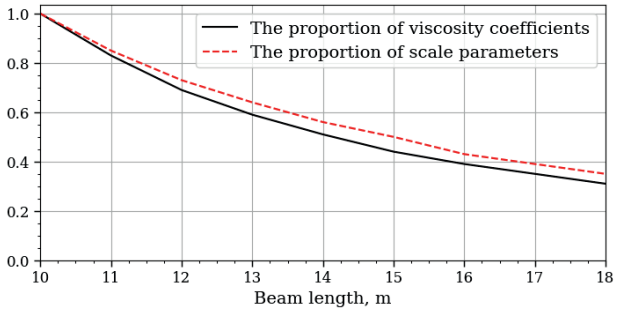


Figure 5. The correlation between the proportion of viscosity coefficients and the proportion of scale parameters

Thus, knowing the scale parameter for a 10-meter beam, it is possible to determine the scaling parameter for a 12-meter beam with

sufficient accuracy. According to Table 2, the scaling parameter for a 10-meter beam is η = 52.9 1/s, and the viscosity coefficient ratio for a 12-meter beam relative to a 10-meter beam is 0.69. Therefore, by multiplying these values, the approximate scaling parameter for a 12-meter beam can be determined, which in this example will be η = 36.50 1/s. The obtained root mean square error for the results obtained using the calculated scaling parameter will be 0.0051 м (Fig. 6).

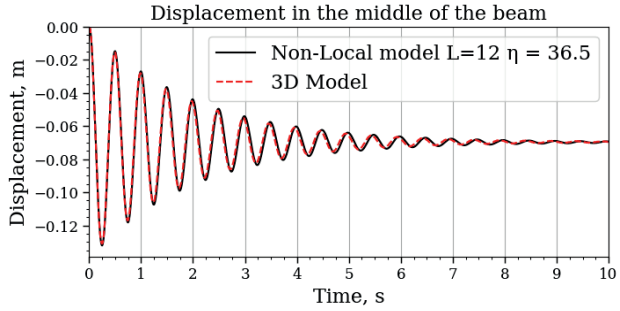


Figure 6. Comparison of numerical experiment results with one-dimensional modeling results using the time-nonlocal deformation model at the calculated scaling parameter η = 36.50 1/s

CONCLUSION

During the present study, a non-local deformation model of a bending beam was constructed using the finite element method. The Newmark method was applied for the numerical solution of the motion equation. The relationship between the scale parameter η and the amplitude of the bending beam oscillations has been demonstrated. It was shown that an increase in the material's nonlocality leads to an increase in the amplitude of oscillations. The model has been supplemented with a calibration algorithm for the scale parameter based on experimental results. The developed calibration algorithm has been tested using numerical experiment data, taking into account the orthotropic properties of the material. In comparison with the classical local model, the calibrated non-local deformation model of the bending beam allows for better convergence with the results of the numerical experiment. Additionally, a correlation between the viscosity coefficient of the model and the scale parameter has been identified, that allows to determine of the scale parameter through frequencies or viscosity coefficients ratio. Thus, the scale parameters can be determined for the beams of different geometry using this correlation, and there is no need to determine it from experimental data all over again. The correlation was obtained for the numerical experiment results obtained with the frequency dependent damping model. For the materials characterized by frequency independent damping properties, the scale parameter will be the constant of material.

ACKNOWLEDGEMENT

This research has been supported by the Program of Scientific Research of Moscow State University of Civil Engineering

REFERENCES

1. **Kelvin, (Thomson W.)** Proceedings of Royal Society / Kelvin // Proceedings of Royal Society of London. – 1865.
2. **Maxwell J. C.** Philosophical Transaction / J. C. Maxwell. - Philosophical Transaction, 1867
3. **Rayleigh, J.** Proceedings of the Mathematical Society / Rayleigh // Proceedings of the Mathematical Society. – 1873. - v.4.
4. **Alexandrov A.V., Potapov V. D., Zylyov V.B.**, 2008, Structural mechanics. In 2 books. Book 2. Dynamic and stability of the elastic systems. Highschool, Moscow (in Russian)
5. **Eringen, A.C.** Nonlocal elasticity / A.C. Eringen, D.G.B. Edelen // International Journal of Engineering Science. – 1972. - 10 (3), 233–248.

6. **Lei Y, Friswell M I and Adhikari S** 2006 A Galerkin Method for Distributed Systems with Non-local Damping Int.Journal of Solids and Structures 43 p 3381–3400
7. **Potapov V.D**. On the stability of the rod under the action of deterministic and stochastic loads, taking into account the nonlocal elasticity and nonlocal damping of the material. 2015. No. 1. S. 9–16.
8. **E.S. Shepitko, V.N. Sidorov**, 2019, Defining of nonlocal damping model parameters based on composite beam dynamic behaviour numerical simulation results // IOP Conf. Series: Materials Science and Engineering 675 012056
9. **Sidorov, V.N., Badina, E.S., Detina, E.P**, 2021. Nonlocal in Time Model of Material Damping in Composite Structural Elements Dynamic Analysis. International Journal for Computational Civil and Structural Engineering, 17(4), p. 14–21
10. **Banks H.T., Inman D.J.,** 1991, On damping Mechanisms in Beams Journal of Applied Mechanics 58(3) pp 716–723.
11. **V. N. Sidorov, E. S. Badina, R. O. Tsarev** / Dynamic Model of Beam Deformation with Consider Nonlocal in Time Elastic Properties of the Material // International Journal for Computational Civil and Structural Engineering. – 2022. – Vol. 18, No. 4. – P. 124-131.
12. **Bathe K. J., Wilson E.L.,** 1976, Numerical methods in finite element analysis. Prentice Hall, New York.
13. **Flugge W.** Viscoelasticity. Blaisdell Publishing Company, Waltham, Massachusetts, 1967. An introductory text dealing with both Kelvin-Voigt and Maxwell materials and their generalizations; 2d rev. ed. Springer-Verlag, Berlin, 1975.
14. **V.N. Sidorov, E.S. Badina.** The finite element method in problems of stability and vibrations of rod structures. Moscow. 2021. P. 172. (in Russian)
15. **Tsarev, R.O.** Calibration of a non-local model of dynamic deformation of a bent beam based on the results of a numerical experiment // Mechanics of composite materials and structures, complex and heterogeneous media: proceedings of the 13th All–Russian Scientific Conference with international participation named after I.F. Obraztsov and Yu.G. Yanovsky, Moscow, November 14-16, 2023. - pp. 143-148 (in Russian)
16. **V.N. Sidorov, M.V. Shitikova, E.S. Badjina, E.P. Detina** // Verification of the three-parameter nonlocal-in-time damping model by experimental data // 5th Novel Intelligent and Leading Emerging Sciences Conference NILES 2023 : Proceedings, Giza, Egypt, 21–23 октября 2023 года. – Giza, Egypt: Institute of Electrical and Electronics Engineers, 2023. – P. 373-376.

СПИСОК ЛИТЕРАТУРЫ

1. **Kelvin, (Thomson W.)** Proceedings of Royal Society / Kelvin // Proceedings of Royal Society of London. – 1865.
2. **Maxwell, J. C.** Philosophical Transaction / J. C. Maxwell. - Philosophical Transaction, 1867
3. **Rayleigh, J.** Proceedings of the Mathematical Society / Rayleigh // Proceedings of the Mathematical Society. – 1873. - v.4.
4. **Александров, А.В., Потапов В. Д., Зылёв В.Б.**, 2008, Строительная механика. В 2-х книгах. Книга 2. Динамика и устойчивость упругих систем. Издательство: Высшая школа.
5. **Eringen, A.C.,** 1972 Nonlocal elasticity / A.C. Eringen, D.G.B. Edelen // International Journal of Engineering Science. – 1972. - 10 (3), 233–248.
6. **Lei Y, Friswell M I and Adhikari S** 2006 A Galerkin Method for Distributed Systems

with Non-local Damping Int.Journal of Solids and Structures 43 p 3381–3400

7. **Потапов В.Д.** 2015. Об устойчивости стержня при действии детерминированной и стохастической нагрузки с учетом нелокальной упругости и нелокального демпфирования материала // Проблемы машиностроения и теории надежности. № 1. С. 9–16.
8. **E. S. Shepitko, V. N. Sidorov**, 2019, Defining of nonlocal damping model parameters based on composite beam dynamic behaviour numerical simulation results // IOP Conf. Series: Materials Science and Engineering 675 012056
9. **Sidorov, V.N., Badina, E.S., Detina, E.P** 2021. NONLOCAL IN TIME MODEL OF MATERIAL DAMPING IN COMPOSITE STRUCTURAL ELEMENTS DYNAMIC ANALYSIS. International Journal for Computational Civil and Structural Engineering, 17(4), p. 14–21
10. **Banks H. T., Inman D. J.,** 1991, On damping Mechanisms in Beams Journal of Applied Mechanics 58(3) pp 716–723.
11. **V. N. Sidorov, E. S. Badina, R. O. Tsarev** / Dynamic Model of Beam Deformation with Consider Nonlocal in Time Elastic Properties of the Material // International Journal for Computational Civil and Structural Engineering. – 2022. – Vol. 18, No. 4. – P. 124-131.
12. **Бате К.Ю., Вилсон Э.Л.** Численные методы анализа и метод конечных элементов. М., Стройиздат, 1982 – 448с
13. **Flugge W.** Viscoelasticity. Blaisdell Publishing Company, Waltham, Massachusetts, 1967. An introductory text dealing with both Kelvin-Voigt and Maxwell materials and their generalizations; 2d rev. ed. Springer-Verlag, Berlin, 1975.
14. **Сидоров В.Н., Бадьина Е.С.** Метод конечных элементов в задачах устойчивости и колебаний стержневых конструкций. Издательство АСВ, М. 2021. 172 с.
15. **Царев, Р.О.** Калибровка нелокальной модели динамического деформирования изгибаемой балки по результатам численного эксперимента // Механика композиционных материалов и конструкций, сложных и гетерогенных сред : сборник трудов 13ой Всероссийской научной конференции с международным участием им. И.Ф. Образцова и Ю.Г. Яновского, Москва, 14–16 ноября 2023 года. – С. 143-148.
16. **V.N. Sidorov, M.V. Shitikova, E.S. Badjina, E.P. Detina** // Verification of the three-parameter nonlocal-in-time damping model by experimental data // 5th Novel Intelligent and Leading Emerging Sciences Conference NILES 2023 : Proceedings, Giza, Egypt, 21–23 октября 2023 года. – Giza, Egypt: Institute of Electrical and Electronics Engineers, 2023. – P. 373-376.

Vladimir N. Sidorov, Academician of Russian Academy of Architecture and Construction Science, Professor, Dr.Sc, Rectorate Counselor, Head of the Department of Computer Science and Applied Mathematics, National Research University Moscow State University of Civil Engineering, Professor of «Building Structures, Buildings and Facilities» Department, Institute of Railway Track, Construction and Structures, Russian University of Transport (MIIT), 129337, Russia, Moscow, Yaroslavskoe Highway, 26, phone: +74956814381, e-mail: sidorov.vladimir@gmail.com.

Сидоров Владимир Николаевич, академик РААСН, профессор, доктор технических наук, советник при ректорате, заведующий кафедрой информатики и прикладной математики Национального исследовательского Московского государственного строительного университета, профессор кафедры «Строительные конструкции, здания и сооружения» Института пути, строительства и сооружений Российского университета транспорта (МИИТа); 129337, г. Москва, Ярославское шоссе, д. 26, телефон: +74956814381, e-mail: sidorov.vladimir@gmail.com.

Elena S. Badina, Associate Professor, Ph.D, Associate Professor of the Department of Computer Science and Applied Mathematics, National Research University Moscow State University of Civil Engineering, Associate Professor of «Computer Aided Design» Department, Institute of Railway Track, Construction and Structures, Russian University of Transport (MIIT), Senior Researcher at the Department of Mechanics of Structured and Heterogeneous Environment of the Institute of Applied Mechanics of the Russian Academy of Sciences; 129337, Russia, Moscow, Yaroslavskoe Highway, 26, phone: +74956092116, e-mail: shepitko-es@mail.ru.

Tsarev O. Roman, PhD student of the Department of Mechanics of Structured and Heterogeneous Environment of the Institute of Applied Mechanics of the Russian Academy of Sciences; 125040, Russia, Moscow Leningradsky Ave., 7, p. 1 telephone +7 (499) 257-03-58 e-mail: tsarev.r.o@yandex.ru

Бадьина Елена Сергеевна, доцент, кандидат технических наук, доцент кафедры информатики и прикладной математики Национального исследовательского Московского государственного строительного университета, доцент кафедры «Системы автоматизированного проектирования» Института пути, строительства и сооружений Российского университета транспорта (МИИТа), старший научный сотрудник Отдела механики структурированной и гетерогенной среды Института прикладной механики Российской академии наук, 129337, г. Москва, Ярославское шоссе, д. 26, телефон: +74956092116, e-mail: shepitko-es@mail.ru.

Царев Роман Олегович, аспирант Отдела механики структурированной и гетерогенной среды Института прикладной механики Российской академии наук; 125040, Россия, г. Москва Ленинградский просп., 7, стр. 1 телефон +7 (499) 257-03-58 e-mail: tsarev.r.o@yandex.ru

International Journal for Computational Civil and Structural Engineering, 20(2) 141–154(2024)

DOI:10.22337/2587-9618-2024-20-2-141-154

ANALYTICAL MODEL FOR BUCKLING LENGTH COEFFICIENT DETERMINATION IN STEEL TRUSSES: A LATERAL TORSIONAL BUCKLING APPROACH

D. Boukhalfa, T. Belaid, A. Slimani, F. Ammari

University of Science and Technology Houari Boumediene (USTHB), Algiers, ALGERIA

Abstract: This paper presents a contribution to the study of the stability of steel trusses. The paper proposes an analytical model for the determination of the buckling length coefficient of the truss N by the lateral torsional buckling approach. The model is derived by considering the equilibrium of the truss under the action of the applied loads and the buckling load. The buckling load is determined by considering the lateral buckling of the equivalent beam and the interaction between the members. The model is validated by comparing the predicted buckling loads with the experimental results of several steel trusses. The results show that the model can predict the buckling loads with good accuracy. The proposed model is a valuable tool for the design of steel trusses. The model can be used to determine the buckling length coefficient of the truss and to ensure that the truss is safe and reliable.

Keywords: Buckling, Truss, LTB, Equivalent Web, Ritz, Steel, Stability

АНАЛИТИЧЕСКАЯ МОДЕЛЬ ДЛЯ ОПРЕДЕЛЕНИЯ КОЭФФИЦИЕНТА ДЛИНЫ СМЯТИЯ В СТАЛЬНЫХ ФЕРМАХ: ПОДХОД К ОПРЕДЕЛЕНИЮ БОКОВОГО КРУТИЛЬНОГО СМЯТИЯ

Д. Бухалфа, Т. Белаид, А. Слимани, Ф. Аммари

Университет науки и технологии Уари Бумедьена (USTHB), г. Алжир, АЛЖИР

Аннотация: Данная работа представляет собой вклад в исследование устойчивости стальных ферм. Предложена аналитическая модель для определения коэффициента длины смятия N-фермы по методу бокового кручения. Модель построена с учетом равновесия фермы в условиях приложенных нагрузок и нагрузки смятия. Нагрузка смятия определяется с учетом бокового смятия эквивалентной балки и взаимодействия между элементами. Модель проверена путем сравнения прогнозируемых нагрузок на смятие с экспериментальными результатами для нескольких стальных ферм. Результаты показывают, что модель может предсказывать нагрузки на смятие с хорошей точностью. Предложенная модель является ценным инструментом для проектирования стальных ферм. Модель может быть использована для определения коэффициента длины смятия фермы и обеспечения ее безопасности и надежности**.**

Ключевые слова: Смятие, ферма, LTB, эквивалентное полотно, Ритц, сталь, устойчивость

INTRODUCTION

In steel frame buildings, trusses can provide better performance in terms of strength and stiffness than I-section beams. Trusses are made up of a series of interconnected members that form triangles. The triangles distribute the load evenly across the structure, making it more resistant to buckling and other forms of failure.

I-section beams, on the other hand, are made up of a solid web and two flanges. The web is responsible for carrying the shear force, while the flanges carry the bending moment. I-section beams are strong and stiff, but they are also more susceptible to buckling than trusses.

The equilibrium of a truss subjected to transverse loads can be obtained by developing exclusively axial forces in the bars that

constitute it. This means that the bars are only subjected to tension or compression, and not to bending. This makes trusses more efficient than I-section beams, as they can carry more load with less material.

However, trusses are susceptible to two kinds of instability: local buckling and overall transverse buckling. Local buckling occurs when the individual members of a truss buckle under compression. Overall transverse buckling occurs when the entire truss buckles under the combined action of compression and bending.

To prevent local buckling, the members of a truss must be designed to have a sufficient slenderness ratio. The slenderness ratio is a measure of the slenderness of a member, and it is calculated by dividing the member's length by its radius of gyration. To prevent overall transverse buckling, the truss must be designed to have a sufficient bracing system. The bracing system is a network of members that are used to prevent the truss from buckling under the combined action of compression and bending.

Despite the potential for instability, trusses are a very efficient and versatile structural system. They are often used in steel frame buildings because they can provide better performance in terms of strength, stiffness, and weight than I-section beams.

The local buckling of compressed bars occurs at a buckling length that is generally equal to the length of the bar. The buckling length can be less if the nodes are rigid. The buckling length depends on the type of connection and whether the bar belongs to a chord or a diagonal. The buckling length can be up to a factor of 1.0 times the length of the bar[1]or even less[2, 3];

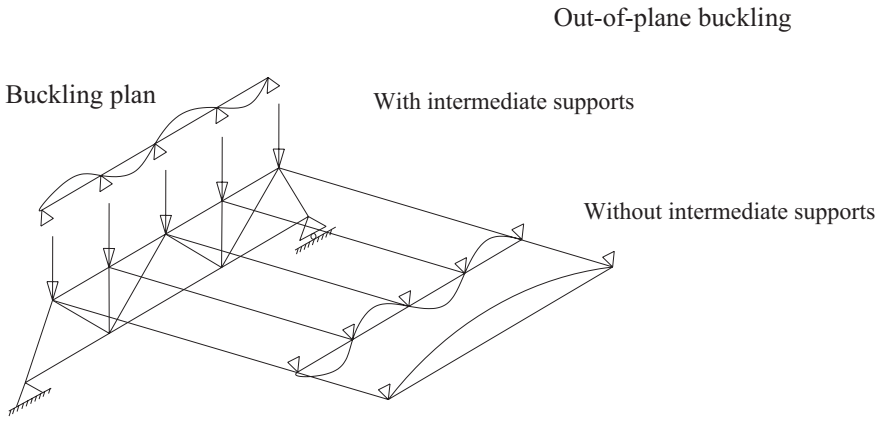


Figure 1. Buckling of a compressed chord

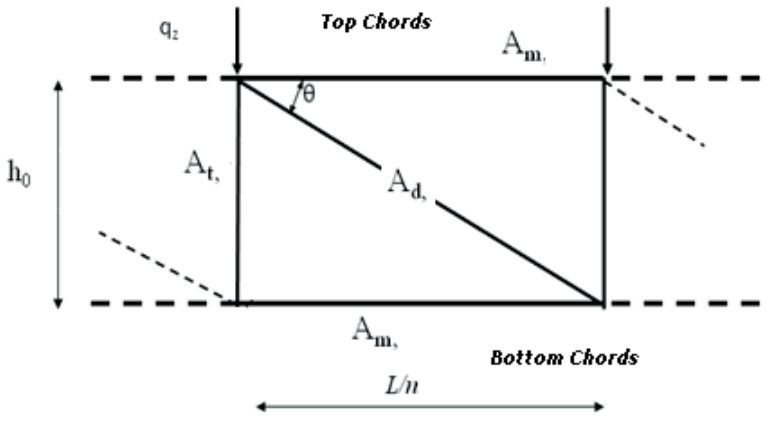


Figure 2. A panel of N-truss models for analyses

The overall transverse buckling, or Lateral torsional buckling (abbreviated as LTB), is induced by the transverse instability of a compressed chord involving several bars and carrying with it the rest of the truss. This can occur when the chord isn't braced laterally. Increasing chord component, therefore, has a transverse length of buckling greater than or less than its individual length.

This paper presents a contribution to the study of the stability of steel trusses. The paper proposes an analytical model for the determination of the buckling length coefficient of the truss N by the lateral torsional buckling approach.

The model is derived by considering the equilibrium of the truss under the action of the applied loads and the buckling load. The buckling load is determined by considering the lateral buckling of the equivalent beam and the interaction between the members.

The stability of steel structures has been the subject of many studies[4-11], starting with Horne [12], who equated truss stability to compressed member buckling, while modelling the truss as a bar with elastic supports to taking into account the contribution of braces and members. Morino & al [13] has produced a literature review of truss instabilities by assimilating the system to a lattice column. More recent analytical [14-16], numerical [3, 17] or experimental [2, 8, 9, 18, 19] works have been interested in the buckling stability of the trusses as well as in the buckling length coefficient of the compressed member, for different configurations. The design codes[1, 20], consider checking the lateral buckling stability of a truss beam by considering the buckling of the compressed chord; the results found [2, 3, 17], show that this solution is too safe. Moreover, consideration of the location of the load and consideration of the force of shear in the web of the beam remains limited [14].

Biegus and Wojczyszyn [3] evaluate the out-of-plane loss of stability of chords of one-way trusses. The values of the out-of-plane buckling length coefficients of the chords have been presented. The model of the compression chord as a straight member isolated from the one-way truss associated with the space model of lateral buckling of the truss has been analysed.

The problem has been studied parametrically by varying the number of web plates. For the models studied, comparative analyses of the out-of-plane buckling length coefficients have been carried out regarding the guidelines of selected design codes.

This article presents a general analytical approach to obtain the expression of the buckling length of a chord of N-truss by the LTB approach. The use of the notion of the equivalent web in the development of a critical moment formula of N trusses will allow us to analyze the effect of the position of the load in the calculation of the critical moment of LTB of an N truss considering the equivalent web. After that, an expression of the buckling length coefficient μ_z by the LTB approach with the equivalent web has been proposed. The results will be compared and discussed with those found in the literature.

1. METHODS

1.1. Basic assumptions

According to the Timoshenko theory [21], the model is based on the following assumptions:

The truss is composed of straight, slender members.

The members are connected by rigid joints.

The loads are applied at the joints.

The buckling is assumed to be elastic.

1.2. Critical moment expression

In the case of I-section beams, the usual differential equation of the elastic curve assumes that the curvature is proportional to the bending moment. In truss beams, the deformations due to shear stress cannot be neglected. The equivalent web of a truss beam is the cross-sectional area "A_a" of the web which would have the same deformation under the

influence of shear stress. It is only a convenient device for the calculation of deformations due to shear stress.

The value of "A_a" is determined so that the transverse deformation of a panel of length l_m of a reticulated member, whose distance between the neutral fibbers of the members is h_0, as shown in Figure 1 and which is subjected to a shear stress V_z, for N truss, is written under equation 1:

$$A_a = \frac{2{,}6\, A_d \dfrac{l_m}{h_0}}{\dfrac{A_d}{A_t} + \dfrac{l_d^3}{h_0^3}} = \frac{2{,}6\, A_d \cot g\, \theta}{\dfrac{A_d}{A_t} + \dfrac{1}{\sin^2 \theta}} \qquad (1)$$

Eurocode 3 [1] defines the critical moment of a double-symmetric beam subjected to a uniform load as given in equation (2).

$$M_{cr} = C_1 EI_z \frac{\pi^2}{L^2}\left[-C_2 e_z + \sqrt{\left[C_2 e_z\right]^2 + \left\{\frac{I_\omega}{I_z} + \frac{GJ}{EI_z}\frac{L^2}{\pi^2}\right\}}\right] \qquad (2)$$

Furthermore, the following parameters designate:

L length of steel beam;

E modulus of elasticity;

I_z second moment of the area to z axes;

I_ω warping constant;

J torsional constant;

G shear modulus;

e_z the eccentricity between the shear centre and load;

$C_1; C_2$ factors depending upon the loading and restraint conditions.

To take into account the effect of the equivalent web, we develop the expression of the critical moment from the total potential of a bi-symmetrical truss beam; This total potential is developed for an I-section beam from the kinematics by Belaid et al [7].

The potential of a Truss Beam, considered as an I beam with an equivalent web is given by: equation 3

$$\Pi_b = \frac{1}{2}\int_L \begin{bmatrix} EI_z (v'')^2 + GJ(\varphi_x')^2 + EI_\omega (\varphi''_x)^2 \\ +2(M_y - \rho q_z)(v''\varphi_x) \end{bmatrix} dx + \int_L \frac{1}{2}(z_Q - z_c) q_z \varphi^2{}_x\, dx \qquad (3)$$

With $\rho = \dfrac{EI_y}{GA_a}, q_z = -\dfrac{dV_z}{dx}, M_y(x) = \left[\left(\dfrac{q_z}{2} x\left[L - x\right]\right)\right]$ (4.a-4.b4.c)

Two main methods are used in the literature for the calculation of critical loads, namely the Ritz and Galerkin methods. With both methods, the displacement modes are first approached by functions that are compatible with the boundary conditions of the beam. While knowing that the resolution by the Galerkin method was solved by Ammari et al. [14]

It is important to note that solving an equation by approximate methods requires proposing a solution to that equation that satisfies the boundary conditions. The adopted solution represents the shape of the torsional deformation, which is taken as a trigonometric series. However, the solution of the buckling mode is known to be sinusoidal [7, 21].

Therefore, for the load cases studied in this paper, the solution will be of the first-order sinusoidal. This solution, which is an approximate solution, has been assumed by many authors[6, 7, 14, 21, 22].

Approximated functions are adopted for the solutions of the lateral displacement and the torsional rotation and are given as follows:

$$v = v_0 \sin\frac{\pi x}{L} \qquad \varphi_x = \varphi_0 \sin\frac{\pi x}{L} \qquad (5a\text{-}5b)$$

These functions fit ideally the boundary condition of the beam $v(0) = v''(0) = 0$ and: $\varphi_x(0) = \varphi_x''(0) = 0$

According to the theory of the minimum of total potential energy [6], one gets: $\dfrac{\partial \Pi}{\partial \varphi_0} = \dfrac{\partial \Pi}{\partial v_0} = 0$

The system of an equivalent simply supported steel beam loaded by uniform was developed,

Therefore, by setting the determinant equal to zero we obtain the expressions of the critical loads as given in(6)

$$q_{cr} = \frac{-EI_z(ez)\frac{L}{2} \pm \sqrt{\left[EI_z(ez)\frac{L}{2}\right]^2 + 4\left[\frac{(\pi^2+3)}{24}L - \rho\frac{\pi^2}{2L}\right]^2 \frac{2L^3}{\pi^4} EI_z \frac{\pi^2}{2L}\left\{EI_\omega \frac{\pi^2}{L^2} + GJ\right\}}}{2\left[\frac{(\pi^2+3)}{24}L - \rho\frac{\pi^2}{2L}\right]^2 \frac{2L^3}{\pi^4}} \quad (6)$$

Multiplication of the critical load by L²/8 and adaptation to the Eurocode, the critical moment become:

$$M = C_1^v EI_z \frac{\pi^2}{L^2}\left[-C_2^v e_z + \sqrt{\left[C_2^v e_z\right]^2 + \left\{\frac{I_\omega}{I_z} + \frac{GJ}{EI_z}\frac{L^2}{\pi^2}\right\}}\right] \quad (7)$$

Where C_1^v and C_2^v given by Eq. (8-a and 8-b) are factors depending upon the loading (uniform load for this case) taken into account the shear deformation of the equivalent web.

$$C_1^v = \frac{\pi^2}{16\left[\frac{(\pi^2+3)}{24} - \rho\frac{\pi^2}{2L^2}\right]}, C_2^v = \frac{1}{\left[\frac{(\pi^2+3)}{6} - 2\rho\frac{\pi^2}{L^2}\right]} \quad (8a; 8b)$$

2. RESULTS AND DISCUSSION

2.1. Parametric study

In the case of a symmetrical truss beam, the Top and Bottom Chords are the same, so the geometrical characteristics of the truss beam are calculated as follows:

$$I_y \approx 2 \times A_m \times \left(\frac{h_0}{2}\right)^2; \quad (9.a)$$

$$I_z = 2 \times I_{zm} \quad (9.b)$$

$$J = 2 \times J_m + J_{tr}$$

with $$J_{tr} = \frac{2{,}6\, K_{tr}\, I_d \cot g\,\theta}{\frac{I_d}{I_t} + \frac{1}{\sin^3\theta}} \quad (9.c)$$

$$I_\omega = \frac{I_z \times h^2}{4} \quad (9.d)$$

$$L = nh_0 tg\theta \quad (9.e)$$

Where:

A reference cross-sectional area (unit);

$A_m = m \times A$ cross-sectional area of a chord;

$A_t = t \times A$ cross-sectional area of a strut;

$A_d = d \times A$ cross-sectional area of a diagonal;

h_0 distance between the centres of gravity of the two chords;

I_{zm} second moment of area (for z axes of the truss beam) of a chord;

J_m torsional constant of a chord;

J_{tr} torsional constant moment of the truss beam;

K_{tr} coefficient of the connection conditions of the & trusses on the chords;

I_t et I_d second moment of area of struts and diagonals respectively;

n number of panels constituting the beam;

θ the degree of inclination of the diagonal about the chord.

Replacing equation (9) in equation (7) allows us to write the critical moment as a function of the characteristics of the components of the truss in equation (10)

2.2. Effect of the equivalent web section on coefficients C_1^v and C_2^v

While knowing that C_1 depends on the moment distribution and C_2 involves the position of the load and in the absence of the effect of the shearing force ($\rho = 0$), the coefficients defined in equation (8) whose values are 1.150 and 0.466 respectively are close and similar to those of Eurocode 3.

The use of Galerkin's method makes it possible to have in the case of ($\rho = 0$) the same values as those given by the codes[14].

When we compare C_1^v and C_1 of a truss beam excluding the effect of the shear force with that of a simply supported beam loaded by uniform load, the difference is not very significant, this value was obtained for I section beam solved by the Ritz method [6, 7] The development carried out in this work assumes that for a descending load on the Top chord we have ($e_z = +h_0 / 2$) and for an ascending load on the Bottom chord we have ($e_z = - h_0 / 2$). The relationship between the section height and the length of a beam is given by (9.e) and shown in Figure 1.

The coefficients C_1^v and C_2^v vary according to the ratio ρ / L^2. This ratio depends on the cross-sections of the chords, diagonals and trusts. So it depends on the ratios "m, t, d" respectively, as well as the number of truss panels "n".

Figures 3 a -b show the variation of the coefficients C_1^v and C_2^v respectively according to the number of panels "n" , for chord and diagonal section ratios (m/d =, 1, 1,5 and 2).

$$M_{cr} = 2C_1^v EI_{zm} \frac{\pi^2}{n^2 h_0^2 tg^2\theta} \left[-C_2^v \alpha \frac{h_0}{2} + \sqrt{\left[C_2^v \alpha \frac{h_0}{2} \right]^2 + \left\{ \frac{h_0^2}{4} + \frac{\left(J_m + \frac{J_{tr}}{2} \right)}{2.6 \times I_{zm}} \frac{n^2 h_0^2 tg^2\theta}{\pi^2} \right\}} \right] \quad (10)$$

α : Takes into account the position of the load.

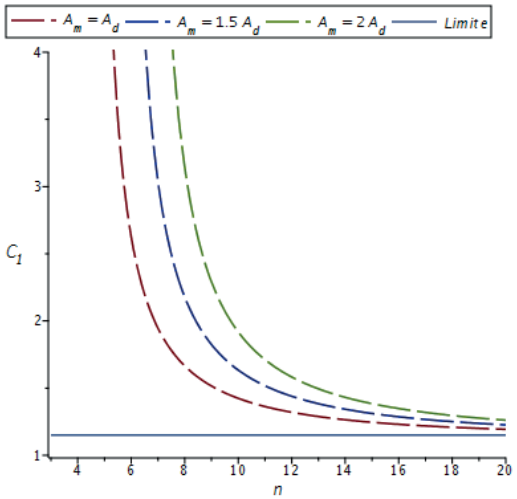


Figure 3-a : variation of C_1^v according to the number of panels "n"

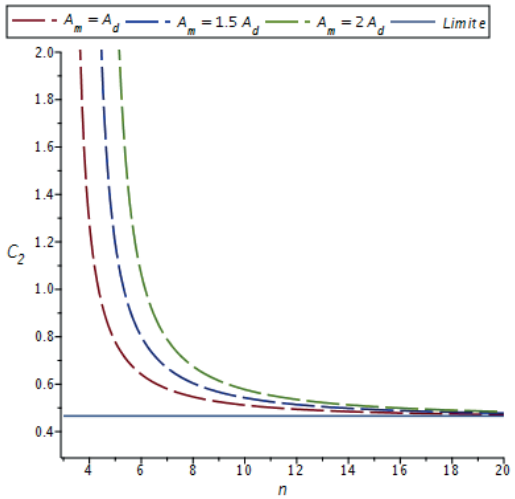


Figure 3-b: variation of C_2^v according to the number of panels "n

We observe that for the number of panels greater than 15, for any section ratio "m/d", the values of C_1^v and C_2^v tend towards the values of 1.150 and 0.466 respectively, which are obtained without taking into account the effect of the shear force or those of a free beam under uniform load. This can be explained by the fact that when the beam is slender, the shear effect

on the beam has a very small influence unlike the case of short beams, where we observe that the coefficients C_1^v et C_2^v take higher values and are inversely proportional to the number of panels. It is also important to note that the cross-section of the chords has a significant and proportional influence on the coefficients and thus on the critical moment, regardless of the ratio of the cross-sections.

2.3. Buckling length of the chord by the Lateral Torsional Buckling approach

The critical force N_{crz} of the chords for the out-of-plane buckling has been obtained by dividing the critical moment by h_0:

$$N_{crz} = M_{cr} / h_0 \tag{11}$$

The coefficients of buckling lengths have been determined using equation [1, 3, 17]:

$$\mu_z = \frac{\pi}{L}\sqrt{\frac{EI_{zm}}{N_{crz}}} \tag{12}$$

EI_{zm} : Represents bending stiffness of the chord in the plane of buckling.

By substituting (Eq. 10) and (Eq. 11) into (Eq. 12), then the coefficients of buckling lengths can be expressed as:

$$\frac{1}{\mu_z} = \sqrt{C_1^v\left[-C_2^v\alpha + \sqrt{\left[C_2^v\alpha\right]^2 + \left\{1 + 4\frac{G}{E}K\frac{n^2}{\pi^2}\right\}}\right]} \tag{13}$$

With: $K = \left(J_m + \frac{J_{tr}}{2}\right) / I_{zm}$ (14)

as mentioned above, the coefficient K takes into account the ratio of torsional and bending stiffness

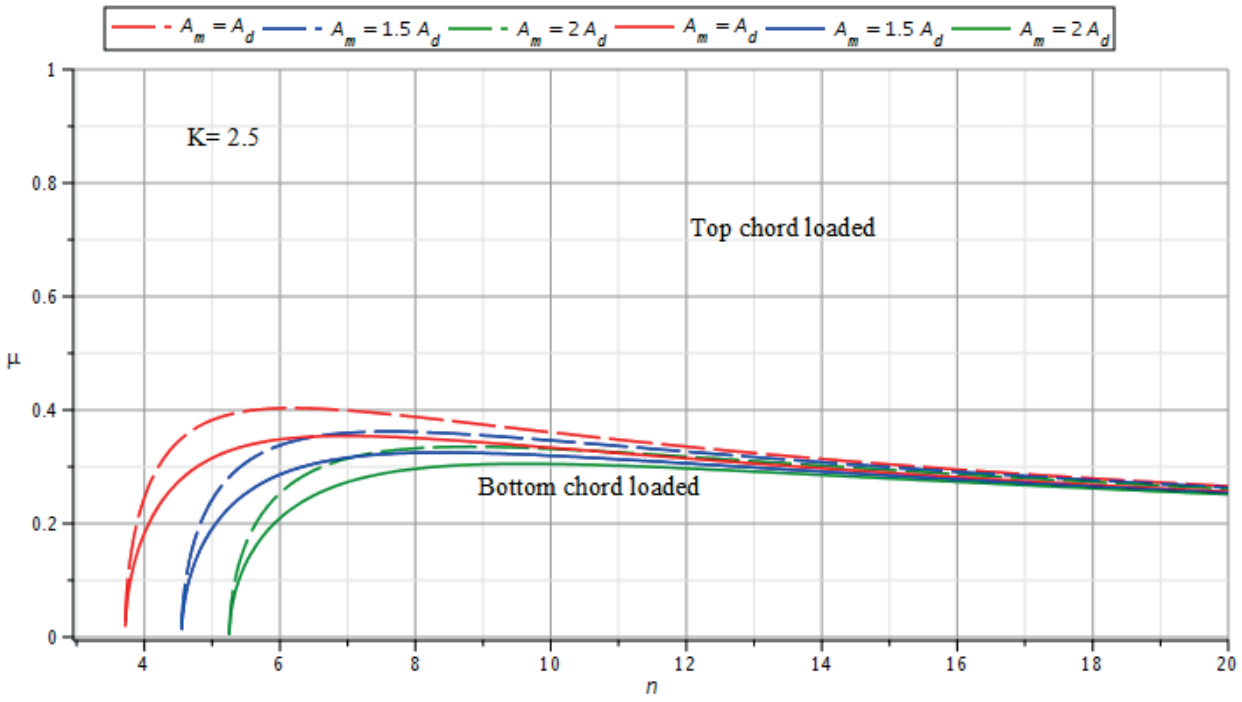


Figure 4. Coefficients of buckling lengths according to the number of panels K =2.5

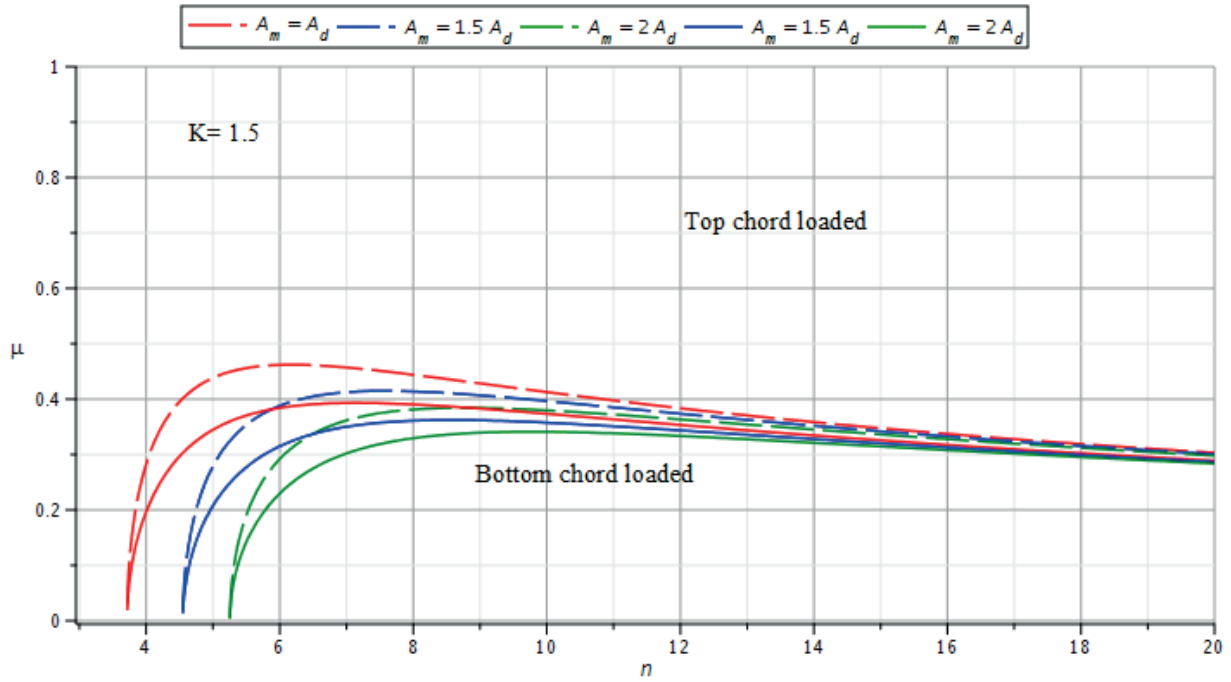


Figure 5. Coefficients of buckling lengths according to the number of panels K =1.5

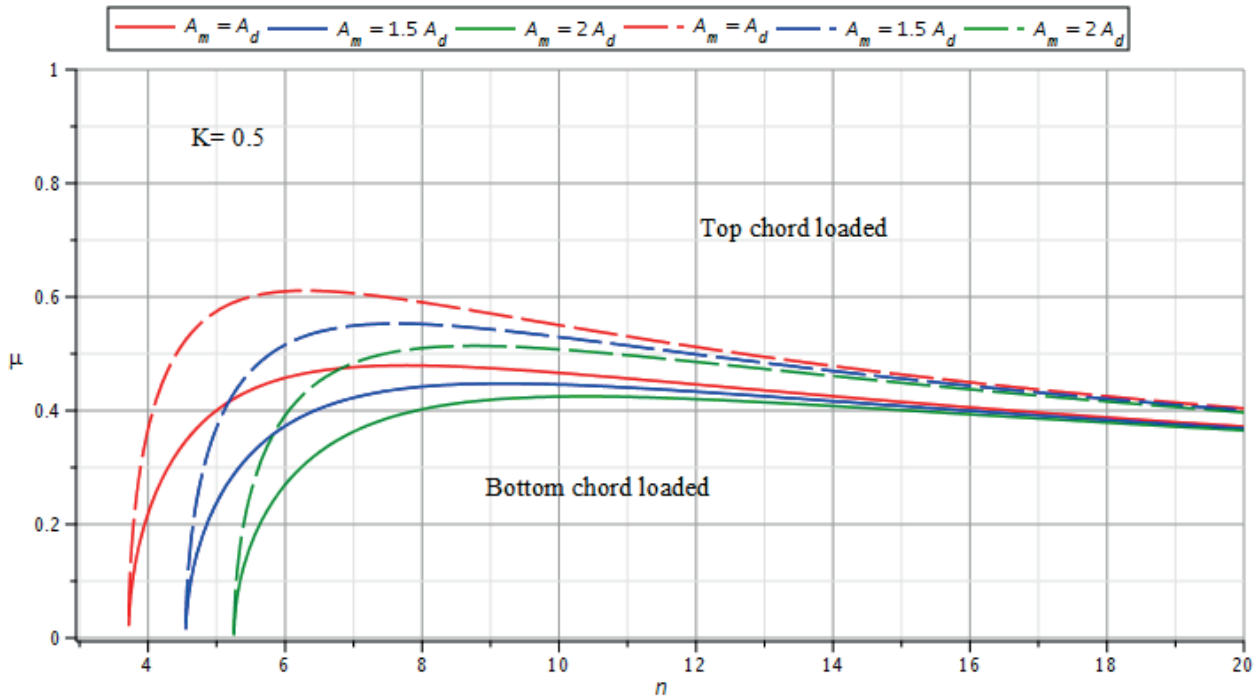


Figure 6. Coefficients of buckling lengths according to the number of panels K =0.5

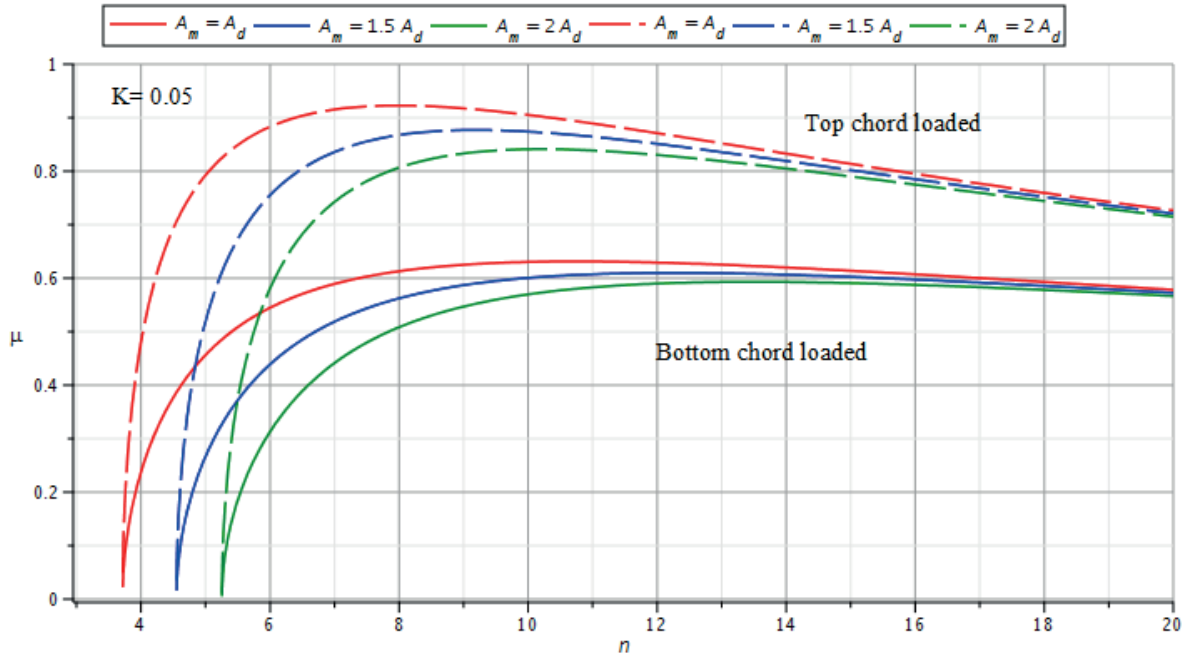


Figure 7. Coefficients of buckling lengths according to the number of panels K =0.05

This ratio depends on the support conditions which are represented by (Eq 9-c)

For $\theta = 45°$ and $A_d = A_t$, Figures 4, 5, 6 and 7 show the values of the coefficient μ_z as a function of the number of panels constituting the truss for chord and diagonal section ratios (m/d =, 1, 1,5 and 2), this for two cases of load, namely: load applied at the Top chord (TC); load applied at the Bottom chord (BC),

The values of K, are chosen to reflect the respective cases of a beam composed by :

- tubular section with a rigid connection K=2.5;
- hinged tubular section K= 1.5;
- open sections with rigid connection K=0.5;
- hinged open rolled sections K= 0.05;

We observe, for all the cases studied, that the coefficient μ_z varies significantly with the number of panels, and this occurs in two phases: For a number of panels less than 6, the coefficient shows an ascending variation. This can be explained by the fact that the beam is not highly slender, and thus, the effect of shear rigidity (equivalent web) favours the risk of local buckling of the components (diagonal and strut).

For a number of panels greater than 6, the effect of shear rigidity diminishes, favouring the risk of global buckling of the beam.

Nevertheless, for all the cases studied, the coefficient remains below the regulatory limits. The use of tubular sections, as observed in Figures 4 and 5, shows that the variation of the coefficient μ_z is not significantly affected by the variation in the sections composing the truss or the effect of load position, unlike the use of rolled sections (Figures 6-7). The maximum value that the coefficient μ_z can reach does not exceed 0.5 for the most unfavourable case, namely, a hinged connection of the components (K=1.5), the section of the web being the same as that of the uprights and diagonal, and the load being applied to the upper chord (destabilizing effect of the load). This leads us to confirm the remarks made by Biegus and Wojczyszyn **[3]**that, in this case, the calculation codes overestimate the values of μ_z.

The use of rolled sections (Figures 6-7) shows that the variation of the coefficient μ_z is

affected by the variation in the sections composing the truss or the effect of load position, unlike the use of tubular sections. The maximum value that the coefficient μ_z can reach is 0.9 for the most unfavourable case, namely, a hinged connection of the components (K=0.05), the section of the web being the same as that of the uprights and diagonal, and the load being applied to the upper chord (destabilizing effect of the load). The value obtained by our approach is the one used by Eurocode 3 [1].
In comparison with the limits given by Eurocode [1], we can see that the buckling length coefficient varies considerably depending on the number of panels, the cross-sections constituting the truss as well as the position of the load. The values are given by Eurocode [1], remain too safe when the Bottom Chord is loaded.

2.4. Comparison and example

The purpose of this section is to compare the coefficient μ_z developed for the uniform load defined by Equation (13) with those reported in the literature and which is presented in Section 1. likewise, Table 1 compares the coefficient μ_z
In this table, columns from 1 to 8 represent respectively number of panel(1), limit given by NF EN 1993-1-1/NA [23](2), coefficients of buckling lengths obtained by the present work (3) and (5) , as well as those of Biegus and Wojczyszyn **[3]** (4) and (6) , and, comparison between the code and the present work are given on the columns (7) and (8) for the case of loads applied at the Top chord and Bottom chord respectively.
Although the model of beams developed by Biegus and Wojczyszyn **[3]**, and the model developed in the present work are different, as well as the method, the results are very similar for the case of loads applied at the upper chord. Table 1 shows the values obtained for K=1.5 using equation (13) and those obtained by Biegus and Wojczyszyn **[3]** in the case of a truss composed by RHS.
The buckling lengths assumed according to Eurocode for the out-of-plane instability of the truss may be overestimated for the cases when the buckled segment covers several panels of the system. This effect leads to the underestimation of the critical load and in sequence to uneconomical consumption of material.

Table 1. Comparison of coefficients of buckling lengths μ_z
coefficients of buckling lengths μ_z

number of panels	*EC3*	Top chord		Bottom chord		Comparison Δ=EC-Eq/EC	
1	*2*	3	4	5	6	7	8
"n"	[1]	Eq,(13)	[3]	Eq,(13)	[3]	α = +1	α = -1
4	0,9	0,7	0,71	0,57	0,64	22%	37%
5	0,9	0,63	0,65	0,53	0,6	30%	41%
6	0,9	0,57	0,6	0,49	0,56	37%	46%
7	0,9	0,53	0,56	0,47	0,52	41%	48%
8	0,9	0,49	0,53	0,44	0,5	46%	51%
9	0,9	0,46	0,5	0,41	0,47	49%	54%

The examination of the results has shown the significant effect of the Equivalent web, this model constitutes a more accurate basis of computation and material savings in comparison code. The buckling length coefficients of the studied cases have given μ_z = 0.70–0.57, which

increases the critical load about 22% and 37% (for n = 4), and 49% - 54% (for n = 9) referred to μ_z = 0.9 , for the load applied at Top and Bottom chord respectively

However, it is important to note that in all the cases studied, the coefficient μ_z remains below the regulatory limits, indicating that the truss structures analyzed meet the required stability criteria.

We also compared the influence of different types of sections on the coefficient μ_z. The use of tubular sections showed less significant variation in the coefficient compared to rolled sections, regardless of changes in section composition or load position. This highlights the advantage of using tubular sections in terms of stability performance.

Furthermore, our results aligned with previous findings by Biegus and Wojczyszyn, supporting the observation that existing calculation codes tend to overestimate the values of μ_z for the specific case analyzed.

CONCLUSION

This work has allowed establishing an analytical expression of the critical buckling moment for an N-truss, taking into account the influence of the load through the use of coefficients C_1^v and C_2^v . By using the LTB approach with "the equivalent web", an expression of the buckling length coefficient μ_z has been proposed. In comparison with the limits given by Eurocode [1], we can see that the buckling length coefficient varies considerably depending on the number of panels, the cross-sections constituting the truss as well as the position of the load. The values given by Eurocode [1] (1 and 0.9 respectively), remain too safe when the Bottom chord is loaded.

In conclusion, our study focused on the variation of the coefficient μ_z in truss structures. We observed that the coefficient exhibits two distinct phases depending on the number of panels. For a lower number of panels, the coefficient increases due to the beam's lower slenderness, which enhances the risk of local buckling. Conversely, for a higher number of panels, the effect of shear rigidity diminishes, leading to an increased risk of global buckling.

However, it is important to note that in all the cases studied, the coefficient μ_z remains below the regulatory limits, indicating that the truss structures analyzed meet the required stability criteria.

We also compared the influence of different types of sections on the coefficient μ_z. The use of tubular sections showed less significant variation in the coefficient compared to rolled sections, regardless of changes in section composition or load position. This highlights the advantage of using tubular sections in terms of stability performance.

Furthermore, our results aligned with previous findings by Biegus and Wojczyszyn, supporting the observation that existing calculation codes tend to overestimate the values of μ_z for the specific case analyzed.

Overall, our study provides valuable insights into the behaviour of truss structures and emphasizes the importance of considering the number of panels and section types when assessing their stability. These findings contribute to the ongoing refinement of design codes, such as Eurocode 3, for accurate and efficient structural analysis

REFERENCES

1. *EN 1993-1-1: Eurocode 3: Design of Steel Structures. Part 1-1: General Rules and Rules for Buildings*, 2005.
2. **J. Jankowska-Sandberg and J. Kołodziej,** "Experimental study of steel truss lateral–torsional buckling," *Engineering Structures,* vol. 46, pp. 165-172, 2013.
3. **A. Biegus and D. Wojczyszyn,** "Studies on buckling lengths of chords for out-of-plane instability," *Archives of Civil and*

Mechanical Engineering, vol. 11, pp. 507-517, 2011.

4. **A. Slimani, T. Belaid, M. Saidani, F. Ammari, and R. Adman**, "A new method for determining the effective length factor of columns in partially braced frames on elastic supports," *Structural Engineering and Mechanics,* vol. 85, p. 825, 2023.
5. **A. Beldjazia, R. Adman, A. Slimani, M. Saidani, T. Belaid, and F. Ammari,** "Mechanical Modeling and General Analytical Solution for the Dynamic Buckling of Plane Structures Using a Beam-Column Element with Varying End Restraints," *International Journal of Structural Stability and Dynamics,* p. 2250019, 2021.
6. **T. Belaid, F. Ammari, and R. Adman,** "Influence of load position on critical lateral torsional buckling moment of laterally restrained beam at tense flange," *Asian Journal of Civil Engineering,* vol. 19, pp. 839-848, 2018.
7. **T. Belaid, A. Slimani, F. Ammari, D. Boukhalfa, and R. Adman,** "Formulation of the critical lateral buckling moment of steel beams under asymmetric loadings," *Thin-Walled Structures,* vol. 182, p. 110163, 2023/01/01/ 2023.
8. **P. Lorkowski and B. Gosowski,** "Experimental and numerical research of the lateral buckling problem for steel two-chord columns with a single lacing plane," *Thin-Walled Structures,* vol. 165, p. 107897, 2021/08/01/ 2021.
9. **M. Piątkowski,** "Experimental research on load of transversal roof bracing due to geometrical imperfections of truss," *Engineering Structures,* vol. 242, p. 112558, 2021.
10. **T. Yılmaz,** "Rapid evaluation of lateral-torsional buckling of European standard I-section cantilevers," *Mechanics Based Design of Structures and Machines,* pp. 1-19.
11. **A. Slimani, T. Belaid, M. Saidani, F. Ammari, and R. Adman,** "The effective length factor of columns in steel framed buildings with end restraint effects," in *Structures*, 2023, p. 105521.
12. **M. Horne,** "The elastic lateral stability of trusses," *The Structural Engineer,* vol. 38, pp. 147-155, 1960.
13. **S. Morino and C. Matsui,** "A Survey on the Lateral-Torsional Buckling of Truss Beam-Columns," 1981.
14. **F. Ammari, R. Adman, and D. Boukhalfa**, "Lateral buckling stability of trussed beam with under uniformly distributed loads," *International Journal of Engineering Science and Technology (IJEST),* vol. 5, pp. 277-285, 2013.
15. "EN 1993-1-1: Eurocode 3: Design of Steel Structures. Part 1-1: General Rules and Rules for Buildings," ed: Comité Européen de Normalisation, 1992.
16. **Q. Cai, R. Feng, and Z. Zhang,** "Topology optimization of trusses incorporating practical local buckling stability considerations," *Structures,* vol. 41, pp. 1710-1718, 2022/07/01/ 2022.
17. **M. Krajewski and P. Iwicki,** "Stability of an imperfect truss loaded by wind," *Engineering Transactions,* vol. 64, pp. 509–516, 2016.
18. **J.C. Gan, J.H. Lim, S.K. Lim, and H.S. Lin,** "Experimental and Numerical Study on the Effect of Heel Plate Length and Thickness on the Structural Integrity of Cold-formed Steel Roof Trusses," *International Journal of Steel Structures,* vol. 21, pp. 22-34, 2021/02/01 2021.
19. **P. Sejkot, S. Ormarsson, J. Vessby, and B. Källsner,** "Numerical out-of-plane stability analysis of long span timber trusses with focus on buckling length calculations," *Engineering Structures,* vol. 204, p. 109670, 2020/02/01/ 2020.
20. **C. Règles**, "66, Règles de Calcul des Constructions en Acier," *Éditions Eyrolles. Décembre,* 1966.
21. **S. Timoshenko and J. Gere**, "Theory of elastic stability. New York: McGraw-Hill, 1961," 1961.

22. **F. Mohri, A. Brouki, and J. Roth,** "Theoretical and numerical stability analyses of unrestrained, mono-symmetric thin-walled beams," *Journal of Constructional Steel Research,* vol. 59, pp. 63-90, 2003.
23. **A. Andrade and D. Camotim,** "Lateral–torsional buckling of singly symmetric tapered beams: theory and applications," *Journal of engineering mechanics,* vol. 131, pp. 586-597, 2005.

СПИСОК ЛИТЕРАТУРЫ

1. *EN 1993-1-1: Eurocode 3: Design of Steel Structures. Part 1-1: General Rules and Rules for Buildings*, 2005.
2. **J. Jankowska-Sandberg and J. Kołodziej,** "Experimental study of steel truss lateral–torsional buckling," *Engineering Structures,* vol. 46, pp. 165-172, 2013.
3. **A. Biegus and D. Wojczyszyn,** "Studies on buckling lengths of chords for out-of-plane instability," *Archives of Civil and Mechanical Engineering,* vol. 11, pp. 507-517, 2011.
4. **A. Slimani, T. Belaid, M. Saidani, F. Ammari, and R. Adman**, "A new method for determining the effective length factor of columns in partially braced frames on elastic supports," *Structural Engineering and Mechanics,* vol. 85, p. 825, 2023.
5. **A. Beldjazia, R. Adman, A. Slimani, M. Saidani, T. Belaid, and F. Ammari,** "Mechanical Modeling and General Analytical Solution for the Dynamic Buckling of Plane Structures Using a Beam-Column Element with Varying End Restraints," *International Journal of Structural Stability and Dynamics,* p. 2250019, 2021.
6. **T. Belaid, F. Ammari, and R. Adman,** "Influence of load position on critical lateral torsional buckling moment of laterally restrained beam at tense flange," *Asian Journal of Civil Engineering,* vol. 19, pp. 839-848, 2018.
7. **T. Belaid, A. Slimani, F. Ammari, D. Boukhalfa, and R. Adman,** "Formulation of the critical lateral buckling moment of steel beams under asymmetric loadings," *Thin-Walled Structures,* vol. 182, p. 110163, 2023/01/01/ 2023.
8. **P. Lorkowski and B. Gosowski,** "Experimental and numerical research of the lateral buckling problem for steel two-chord columns with a single lacing plane," *Thin-Walled Structures,* vol. 165, p. 107897, 2021/08/01/ 2021.
9. **M. Piątkowski,** "Experimental research on load of transversal roof bracing due to geometrical imperfections of truss," *Engineering Structures,* vol. 242, p. 112558, 2021.
10. **T. Yılmaz,** "Rapid evaluation of lateral-torsional buckling of European standard I-section cantilevers," *Mechanics Based Design of Structures and Machines,* pp. 1-19.
11. **A. Slimani, T. Belaid, M. Saidani, F. Ammari, and R. Adman,** "The effective length factor of columns in steel framed buildings with end restraint effects," in *Structures*, 2023, p. 105521.
12. **M. Horne,** "The elastic lateral stability of trusses," *The Structural Engineer,* vol. 38, pp. 147-155, 1960.
13. **S. Morino and C. Matsui,** "A Survey on the Lateral-Torsional Buckling of Truss Beam-Columns," 1981.
14. **F. Ammari, R. Adman, and D. Boukhalfa**, "Lateral buckling stability of trussed beam with under uniformly distributed loads," *International Journal of Engineering Science and Technology (IJEST),* vol. 5, pp. 277-285, 2013.
15. "EN 1993-1-1: Eurocode 3: Design of Steel Structures. Part 1-1: General Rules and Rules for Buildings," ed: Comité Européen de Normalisation, 1992.
16. **Q. Cai, R. Feng, and Z. Zhang,** "Topology optimization of trusses incorporating practical local buckling

stability considerations," *Structures,* vol. 41, pp. 1710-1718, 2022/07/01/ 2022.
17. **M. Krajewski and P. Iwicki,** "Stability of an imperfect truss loaded by wind," *Engineering Transactions,* vol. 64, pp. 509–516, 2016.
18. **J.C. Gan, J.H. Lim, S.K. Lim, and H.S. Lin,** "Experimental and Numerical Study on the Effect of Heel Plate Length and Thickness on the Structural Integrity of Cold-formed Steel Roof Trusses," *International Journal of Steel Structures,* vol. 21, pp. 22-34, 2021/02/01 2021.
19. **P. Sejkot, S. Ormarsson, J. Vessby, and B. Källsner,** "Numerical out-of-plane stability analysis of long span timber trusses with focus on buckling length calculations," *Engineering Structures,* vol. 204, p. 109670, 2020/02/01/ 2020.
20. **C. Règles**, "66, Règles de Calcul des Constructions en Acier," *Éditions Eyrolles. Décembre,* 1966.
21. **S. Timoshenko and J. Gere**, "Theory of elastic stability. New York: McGraw-Hill, 1961," 1961.
22. **F. Mohri, A. Brouki, and J. Roth,** "Theoretical and numerical stability analyses of unrestrained, mono-symmetric thin-walled beams," *Journal of Constructional Steel Research,* vol. 59, pp. 63-90, 2003.
23. **A. Andrade and D. Camotim,** "Lateral–torsional buckling of singly symmetric tapered beams: theory and applications," *Journal of engineering mechanics,* vol. 131, pp. 586-597, 2005.

Boukhalfa Dalila — Phd Student, Ing-, Built Environment Research Laboratory Faculty of Civil Engineering, University of Science and Technology Houari Boumediene (USTHB), BP 32 El Alia 16111, Bab Ezzouar, Algiers, Algeria- d.boukhalfa@yahoo.fr

Belaid Toufik Doctor of Science - Built Environment Research Laboratory Faculty of Civil Engineering, University of Science and Technology Houari Boumediene (USTHB), BP 32 El Alia 16111, Bab Ezzouar, Algiers, Algeria- t.belaid@usthb.dz - +213 554 288 336

Slimani Adel Doctor - Built Environment Research Laboratory Faculty of Civil Engineering, University of Science and Technology Houari Boumediene (USTHB), BP 32 El Alia 16111, Bab Ezzouar, Algiers, Algeria- slimani_a_del@hotmail.fr

Ammari Professor - Built Environment Research Laboratory Faculty of Civil Engineering, University of Science and Technology Houari Boumediene (USTHB), BP 32 El Alia 16111, Bab Ezzouar, Algiers, Algeria- ammari_fat@yahoo.fr

DOI:10.22337/2587-9618-2024-20-2-155-162

IMPLEMENTATION OF BIM TECHNOLOGIES IN THE MANAGEMENT OF MULTI-APARTMENT BUILDINGS DURING THE OPERATION PHASE

Dmitry A. Matveev

National Research Moscow State University of Civil Engineering, Moscow, RUSSIA

Abstract: The paper discusses the main aspects of implementing BIM technologies in the management of multi-apartment buildings. It highlights the features of implementing the system, including the stages of creating a digital model of the building, requirements for personnel, and specific skills. The advantages and opportunities that arise in the management process of multi-apartment buildings with information modeling technologies are noted. Specifically, it simplifies processes such as document storage and transmission, organization of building operations, current repairs of buildings and structures, and more. The prospects for the implementation of information technologies in the housing and utilities sector in the Russian Federation are already outlined: by 2023, developers are required to use these technologies when planning and constructing multi-apartment buildings. The government is implementing a series of systemic initiatives and measures aimed at the digitalization of multi-apartment building management, supporting the development of the sector towards a service model, and ensuring comfortable living conditions for citizens. To support these initiatives, it is necessary to unify requirements for services, standards for data collection, transmission, processing, and access, and to clarify the rules of interaction among participants, taking into account the active implementation of digital technologies in practice. The primary principle of digitalization should be economic feasibility. The implementation of digital technologies should provide real value for developers, management organizations, owners of residential and non-residential premises, and authorities. To achieve digitalization results, it is necessary to create conditions that stimulate the efficiency of interaction between subjects involved in the digitalization of multi-apartment building management. In particular, it is required to establish requirements for the implementation of information technologies at the legislative level.

Keywords: BIM technologies, information modeling technologies, digitalization of housing and utilities sector, digital model, management organization, multi-apartment building

ВНЕДРЕНИЕ BIM-ТЕХНОЛОГИЙ В УПРАВЛЕНИЕ МНОГОКВАРТИРНЫМИ ДОМАМИ НА ЭТАПЕ ЭКСПЛУАТАЦИИ

Д.А. Матвеев

Национальный исследовательский Московский государственный строительный университет»,
г. Москва, РОССИЯ

Аннотация: Рассмотрены основные аспекты внедрения BIM-технологий в управление многоквартирными домами. Показаны особенности внедрения системы, в том числе - этапы создания цифровой модели дома, требования к кадровому персоналу и специальным навыкам. Отмечены преимущества и возможности, которые появляются в процессе управлении многоквартирным домом при наличии технологий информационного моделирования. В частности, упрощаются процессы хранения и передачи документов, организация эксплуатации конструкций здания, текущего ремонта зданий и сооружений и др. Перспективы внедрения информационных технологий в сферу жилищно-коммунального хозяйства в Российской Федерации уже намечены: в 2023 году застройщики должны использовать эти технологии при планировании и постройке многоквартирных домов. Государство реализует ряд системных инициатив и мероприятий, направленных на цифровизацию управления многоквартирными домами, поддержку развития отрасли в направлении сервисной модели и обеспечения граждан комфортными условиями проживания. Для поддержки этих инициатив необходимо провести унификацию требований к услугам, стандартам сбора, передачи, обработки и доступа к данным и работы с ними, уточнить правила

взаимодействия участников с учетом активного внедрения цифровых технологий в практику. При этом основным принципом цифровизации должна стать экономическая целесообразность. Внедрение цифровых технологий должно иметь реальную ценность и для застройщиков, и для управляющих организаций, и для собственников жилых и нежилых помещений, и для органов власти. Для достижения результатов цифровизации необходимо создать условия, стимулирующие повышение эффективности взаимодействия между субъектами цифровизации управления многоквартирными домами. В частности, на законодательном уровне требуется установить требования по внедрению информационных технологий.

Ключевые слова: BIM-технологии, технологии информационного моделирования, цифровизация жилищно-коммунального хозяйства, цифровая модель, управляющая организация, многоквартирный дом

INTRODUCTION

Digitalization of the housing and utilities sector (HUS) is one of the priorities of the Russian Federation. An example is the approval by the Government of the Russian Federation to use information modeling technologies (BIM) in the construction and operation of buildings, including multi-apartment buildings (MAB). The Government Decree of December 20, 2021, No. 3719-r contains a plan aimed at creating conditions for the implementation of BIM in the construction industry and improving the quality of construction projects [1]. Digitalization of HUS allows integrating interaction and reporting processes at all management levels into a single information field. This allows for the optimal allocation of common resources, including natural resources, to improve the overall quality of life in the country. In this regard, studying new technologies that can improve the management system of HUS in general and MAB in particular becomes especially relevant.

In relation to buildings, this is an approach to their construction, maintenance, and repair, which involves the collection and processing of comprehensive data about the building in digital format. The authors of the work consider that building information modeling is a modern innovative approach to designing, constructing, and operating buildings [2]. Technically, building information modeling represents a complex process based on the use of accurate and coordinated data at all stages – from the development of the building concept to its construction and commissioning. The theoretical analysis revealed trends in the construction sector and the directions of BIM use. The authors note that such technologies are most often used in the construction of stadiums in Moscow, St. Petersburg, Saransk, Volgograd, Nizhny Novgorod, Samara, Sochi, and Kazan. This is primarily due to the complexity of the objects and social responsibility since stadiums accommodate from 20,000 people and more, hence the increased responsibility for inadequate structures and risks associated with the safety of life and health of people.

The new Volgograd Arena stadium was built using BIM technologies due to the technical complexity of the object. 3D models of structurally complex elements were created, and the data from these models were directly transferred to the manufacturer of the structural elements. The oval Mordovia Arena stadium was characterized by a technical feature of 88 interconnected consoles 40 meters high with a span of 49 meters. Thanks to BIM, a solution was quickly found, and the stadium was built without problems. The Skolkovo Research Center was also built using digitized architectural structures, allowing for all the structural features of the future building to be considered.

As can be seen, specialized literature mainly identifies sports facilities or buildings and does not contain examples of how BIM helps in the management of MAB. Consequently, this issue is insufficiently studied, although some authors show interest in it [3].

MATERIALS AND METHODS

Building information modeling (BIM) is essential for managing the maintenance, current, and capital repairs of MABs, as well as for analyzing the operational characteristics of buildings [4]. The operational model (AIM) of an object contains complete information about the object [Figure 1], and this information can be used in various activities at the operation stage [5]. Moreover, the BIM model provides accurate construction data and can be integrated with other tools that perform energy efficiency analysis, schedule replacements, and maintenance of engineering systems [6]. Such a model can be considered an integrated set of technologies that facilitate building management throughout its life cycle [7].

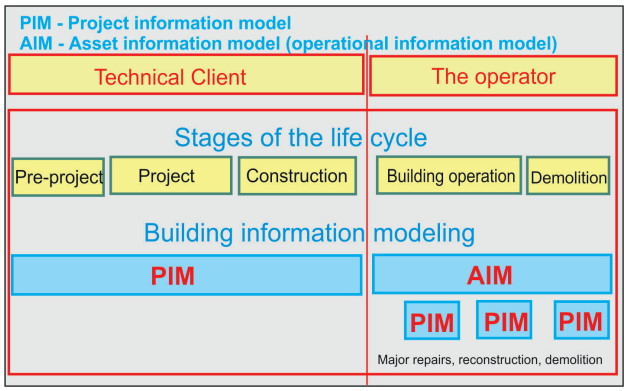


Figure 1. Stages of the Object's Life Cycle

Thus, the AIM information model has the potential to conduct maintenance and repair work on the building's engineering structures and systems more efficiently [18].

V.T. Talapov specifies [8] that BIM is aimed at calculating and modeling construction work and erecting new buildings, but it also finds application in housing and utilities management. In particular, the author shows how this technology can be applied to achieve the following goals:

1. The ability to model changes in the building's structure in case certain circumstances arise (works in non-residential premises by private property owners-entrepreneurs who may make adjustments to the structures);
2. Designing the re-equipment of the building with new engineering equipment, bringing its operational characteristics to the modern level of requirements (this situation is especially relevant for long-operated houses where heating equipment, particularly the piping system, has not been changed for many years, mainly due to lack of funding or the unwillingness of the managing organization (MO) to allocate funds for this, as the budget of such an event may increase during the equipment replacement process);
3. Monitoring the current state of the building (this process is currently outdated in the traditional view, as inspections and checks, as well as rounds by MO engineers, are conducted irregularly, and most often only in response to owners' complaints and inspections by municipal authorities);
4. Properly operating existing facilities (this is possible, for example, with the help of a digital model of the building, which clearly shows all the features of architecture, water supply, heating, and other engineering systems) (Figure. 2).

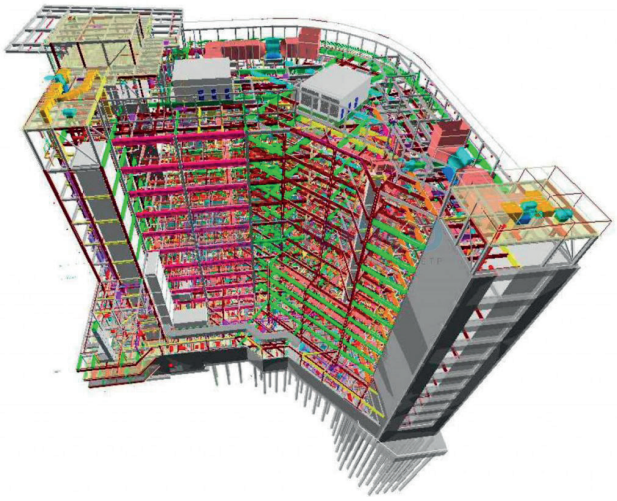


Figure 2. Information Model of Engineering Systems of Multi-Apartment Buildings

5. Managing the building's energy consumption, such measures can benefit both residents and society [9].
6. BIM provides accurate data about the object and can be integrated with other tools that perform energy efficiency analysis, resulting in reduced resource consumption costs [10].

Maintenance and current repairs of buildings and structures are very important and quite costly (considering the operating periods) types of day-to-day activities for managing organizations. This is the main type of work with the building during its service life, and here information modeling allows the listed tasks to be carried out timely and efficiently, minimizing overall costs.

BIM technologies can facilitate communication between various stakeholders involved in the management of multi-apartment residential buildings (MKB), such as building owners, managers, and tenants, by providing a common platform for sharing information and collaborating on building-related tasks. Thus, the information model can be applied for digital calculations and conducting financial activities between the managing organization and the owners of non-residential premises, who must pay monthly for maintenance and repairs. In practice, this process occurs "the old-fashioned way," by delivering paper payment receipts from the representative of the managing organization to the tenant's location. A digital version of this process would simplify the procedures for delivering receipts and generating reports.

One of the most important tasks in managing MAB is document management. The advantages provided by BIM technologies in managing MAB are that with their implementation, there is no need to maintain a paper archive with all the documentation about the object. The problem of paper archives is inherent in the entire bureaucratic system, and especially in the housing and utilities sector. Many managing organizations still store archives in folders without proper storage conditions, which affects their preservation.

Experts believe that the digital model of the house must also be included in the electronic technical passport of the house. This will allow the managing organization to control the state of all communications and load-bearing structures of the house, and the owners to see the real picture of what the managing organization has done in terms of building operation, preparation for the winter period, etc. [11].

Another aspect referred to by R.I. Surzhikov is the guarantee of the preservation of all executive and other documentation. Undoubtedly, when transferring management rights of the MAB, documentation is lost or deliberately damaged to hide disadvantages, risks, and deficiencies. With a digital model of the document archive, such situations will no longer concern companies entering the right to manage the MAB [12].

BIM allows for the creation of an accurate digital model of the MAB, which includes information about every part of it, from the foundation and walls to engineering systems and equipment. This facilitates the work of survey engineers, as they can easily access information about the building without the need to be physically present on site. Moreover, this approach reduces the time required for engineering surveys, as the information about the building is available in one digital place. It also helps reduce the costs of engineering surveys since there is no need for constant repeat trips to the site [9]. Overall, this optimizes the work of survey engineers, eliminating bureaucratic procedures.

Several authors address the topic of organizing new processes based on BIM: new technologies cannot simply be introduced into the housing and utilities sector [14], which is characterized by specific processes that have not changed for years. Thus, a number of authors [15] note the importance of personnel potential and the availability of special knowledge. To implement an operational information model of a multi-apartment residential building, it is necessary to

have appropriate personnel. The authors divide the process into two parts: in the first part, the building is designed and put into operation, in the second, the object continues to be operated by the specialists of the managing organization or the homeowners' association (HOA). The first part requires specialists such as BIM manager, BIM master, BIM coordinator, and BIM technician. In the subsequent operation of the object, the specialists should be provided by the staff of the managing organization or other controlling organizations for the operational information model of the multi-apartment residential building (FIM) [16]. These specialists include:

- FIM manager (specialist in modifying the 3D model and its implementation during operation);
- FIM dispatcher (specialist operating the building based on the 6D model: 3D model + time + information + operation);
- FIM engineer (specialist in developing engineering transformations of the building, such as major repairs, reconstruction, restoration, implementation of new technologies, and engineering networks) [15].

The application of BIM technologies in managing MAB in Russia is still at an early stage, and full-scale implementation will require investments in infrastructure and personnel training for interested parties.

K.V. Borodulin raises an important topic in his article [17] about the implementation of BIM in the management of MAB. The author envisages the implementation of information modeling in three stages:

1. Formation of the project team and development of the regulatory framework.
2. Collection and analysis of information about the object and organization.
3. Conducting laser scanning of the object and creating the information model.

Digitization of the housing and utilities sector faces specific problems, such as low demand for quality IT solutions: lack of initiative from housing and utilities organizations, resistance from managing organizations and HOAs, and lack of a competitive environment [18, 19]. However, the advantages of BIM make them a promising tool for increasing the efficiency of MAB management. There are already promising steps in this direction. For instance, the Ministry of Construction has mandated developers to implement BIM even at the foundation and planning stages. In 2023, this work was conducted in the construction of MAB, and in 2024, the technologies will be implemented in the construction of individual housing.

CONCLUSIONS

BIM technologies can help optimize the management of multi-apartment buildings by providing a comprehensive digital building model that can be used for monitoring and controlling various aspects of building operation, such as energy consumption, maintenance, and repairs. Moreover, BIM technologies will definitely help reduce costs associated with building maintenance and repairs by providing a more accurate and detailed understanding of the building's condition and needs.

REFERENCES

1. Plan of Activities ("Roadmap") for the Use of Information Modeling Technologies in the Design and Construction of Capital Construction Projects, as well as for Stimulating the Use of Energy-Efficient and Environmentally Friendly Materials, including Considering the Need for Their Production in the Russian Federation. Order No. 3719-r dated December 20, 2021. Available online: http://static.aovemment.ru/media/files/imFWAlUfdHZMmSMvdqfFRkvscqve7UYF.pdf (accessed on 24 October 2023) (in Russian)
2. **Demenev, A.V.; Artamonov, A.S.** Information Modeling in the Operation of

Buildings and Structures. Internet Journal "Naukovedenie" 2015, 7(3), 160-165 (in Russian).
3. **Surzhikov, R.I.** Implementation of BIM Technologies in the Management of a Residential Complex. Available online: https://cyberleninka.ru/article/n7vnedrenie-bim-tehnobaiv-v-upravlenie-zhitym-kompleksom?vsdid=b3aul7uel47382600 (accessed on 24 October 2023) (in Russian)
4. **Gonzalez-Caceres, A.; Bobadilla, A.; Karlshoj, J.** Implementing Post-Occupancy Evaluation in Social Housing Complemented with BIM: A Case Study in Chile. Building and Environment 2019, 158, 260-280. https://doi.org/10.1016/j.buildenv.2019.05.019
5. **Naghshbandi, S.N.** BIM for Facility Management: Challenges and Research Gaps. Civil Engineering Journal 2017, 2, 679-684. DOI: 10.28991/cej-2016-00000067
6. **Mohanta, A.; Das, S**. BIM as a Facilities Management Tool: A Brief Review. In Proceedings of the 7th International Conference on Sustainable Built Environment, Earl's Regency Hotel, Kandy, Sri Lanka, 16-18 December 2017.
7. **Li, X.; Wu, P.; Shen, G.Q.; Wang, X.; Teng, Y**. Mapping the Knowledge Domains of Building Information Modeling (BIM): A Bibliometric Approach. Automation in Construction 2017, 84, 195-206. https://doi.org/10.1016/j.autcon.2017.09.011
8. **Talapov, V.T.** BIM and Housing and Utilities: An Inevitable Union. Available online: https://ardexpert.ru/artide/13727?vsdid=b3aupwhjb276312012 (accessed on 15 April 2024) (in Russian)/
9. **Monteiro, C.S.; Causone, F.; Cunha, S.; Pina, A.; Erba, S.** Addressing the Challenges of Public Housing Retrofits. Energy Procedia 2017, 134, 442-451. https://doi.org/10.1016/j.egypro.2017.09.600
10. **Silva, M.C.d.C.; Silva, A.D.O.; Kohlman Rabbani, E.R.; Alencar, L.H.; Passos Neto, G.d.M.; Couto, J.P.; Valdes-Vasquez, R**. Guidelines for the Implementation of BIM for Post-Occupancy Management of Social Housing in Brazil. Energies 2022, 15, 6802. https://doi.org/10.3390/en15186802
11. Ministry of Construction Plans to Implement Information Modeling Technologies in Housing and Utilities. Available online: https://finance.rambler.ru/realty/48885921/?utm_content=finance_media&utm_medium=read_more&utm_source=copylink (accessed on 24 April 2024) (in Russian)
12. **Papadonikolaki, E., Vrijhoef, R., & Wamelink, H.** The Interdependences of BIM and Supply Chain Partnering: Empirical Explorations. Architectural Engineering and Design Management 2016, 12(6), 476-494. DOI: 10.1080/17452007.2016.1212693.
13. **Altohami, A.B.A.; Haron, N.A.; Ales@Alias, A.H.; Law, T.H.** Investigating Approaches of Integrating BIM, IoT, and Facility Management for Renovating Existing Buildings: A Review. Sustainability 2021, 13, 3930. https://doi.org/10.3390/su13073930
14. **Korneyeva, E.V.** Information Technologies in the Management of Housing and Utilities. International Journal of Applied and Fundamental Research 2017, 11-2, 357-359 (in Russian).
15. **Dolgov, O.V.; Shalobaev, E.V.; Perepelitsa, F.A.; Nigmatulin, T.A.** BIM Technologies for Housing and Utilities. Available online: https://isap.ru/bim (accessed on 24 October 2023) (in Russian).
16. What is FM — Definition of Facility Management. Available online: http://www.ifma.org/about/what-is-facility-management#sthash.GjARNDWg.dpuf (accessed on 19 October 2023).
17. **Borodulin, K.V.** Implementation of Information Modeling Technologies in the Process of Building and Structure Operation. Young Scientist 2019, 2 (240), 200-202. Available online:

https://moluch.ru/archive/240/55593/ (accessed on 24 April 2024) (in Russian)
18. **Naml, E., Isikdag, U., & Kocakaya, M.** Building Information Management (BIM), A New Approach to Project Management. Journal of Sustainable Construction Materials and Technologies 2019, 4, 323-332. DOI: 10.29187/jscmt.2019.36.
19. **Edirisinghe, R., & London, K.A.** Comparative Analysis of International and National Level BIM Standardization Efforts and BIM Adoption. 2015.

СПИСОК ЛИТЕРАТУРЫ

1. План мероприятий («Дорожная карта» по использованию технологий информационного моделирования при проектировании и строительстве объектов капитального строительства, а также по стимулированию применения энергоэффективных и экологичных материалов, в том числе с учетом необходимости их производства в Российской Федерации. Распоряжение от 20 декабря 2021 г. № 3719-р. URL: http://static.aovemment.ru/media/files/imFWAlUfdHZMmSMvdqfFRkvscqve7UYF.pdf (дата обращения: 24.10.2023).
2. **Деменев А.В., Артамонов А.С.** Информационное моделирование при эксплуатации зданий и сооружений // Интернет-журнал «Науковедение». – 2015. – Том 7. – №3. – С. 160-165.
3. **Суржиков Р.И.** Внедрение BIM технологий в управление жилым комплексом. URL: https://cyberleninka.ru/article/n7vnedrenie-bim-tehnobaiv-v-upravlenie-zhitym-kompleksom?vsdid=b3aul7u el47382600 (дата обращения: 24.04.2024).
4. **Gonzalez-Caceres, A.; Bobadilla, A.; Karlshoj, J.** Implementing post-occupancy evaluation in social housing complemented with BIM: A case study in Chile. Build. Environ. 2019,158, 260-280. https://doi.org/10.1016/j.buildenv.2019.05.019
5. **Naghshbandi, S.N.** BIM for facility management: Challenges and research gaps. Civ. Eng. J. 2017, 2, 679-684. DOI: 10.28991/cej-2016-00000067
6. **Mohanta, A.; Das, S.** BIM as facilities management tool a brief review. In Proceedings of the 7th International Conference on Sustainable Built Environment, Earl's Regency Hotel, Kandy, Sri Lanka, 16-18 December 2017.
7. **Li, X.; Wu, P.; Shen, G.Q.; Wang, X.; Teng, Y.** Mapping the knowledge domains of Building Information Modeling (BIM): A bibliometric approach. Autom. Constr. 2017, 84,195-206. https://doi.org/10.1016/j.autcon.2017.09.011
8. **Талапов В.Т.** BIM и ЖКХ: союз неизбежен. URL: https://ardexpert.ru/artide/13727?vsdid=b3aupwhjb276312012 (дата обращения: 15.04.2024).
9. **Monteiro, C.S.; Causone, F.; Cunha, S.; Pina, A.; Erba, S.** Addressing the Challenges of Public Housing Retrofits. Energy Procedia 2017, 134, 442-451. https://dbibra/10.1016/j.eav-pro.2017.09.600
10. **Silva, M.C.d.C.; Silva, A.D.O.; Kohlman Rabbani, E.R.; Alencar, L.H.; Passos Neto, G.d.M.; Couto, J.P.; Valdes-Vasquez, R.** Guidelines for the Implementation of BIM for Post-Occupancy Management of Social Housing in Brazil. Energies 2022,15, 6802. https://doi.org/10.3390/en15186802
11. Минстрой планирует внедрять технологии информационного моделирования в ЖКХ. URL: https://finance.rambler.ru/realtv/48885921/?utm_content=finance_media&utm_medium=read_more&utm_source=copvlink (дата обращения: 24.10.2023).
12. **Eleni Papadonikolaki, Ruben Vrijhoef & Hans Wamelink** (2016) The interdependences of BIM and supply chain

partnering: empirical explorations, Architectural Engineering and Design Management, 12:6, 476-494, DOI: 10.1080/17452007.2016.1212693.
13. **Altohami, A.B.A.; Haron, N.A.; Ales@Alias, A.H.; Law, T.H.** Investigating Approaches of Integrating BIM, IoT, and Facility Management for Renovating Existing Buildings: A Review. Sustainability 2021, 13,3930. https://doi.ora/ 10.3390/su13073930
14. **Корнеева Е.В.** Информационные технологии в управлении жилищно-коммунальным хозяйством // Международный журнал прикладных и фундаментальных исследований. – 2017. - № 11, – С. 357-359.
15. **Долгов О.В., Шалобаев Е.В., Перепелица Ф.А., Нигматулин Т.А.** BIM-технологии для ЖКХ. URL: https://lsap.ru/bim (дата обращения: 24.10.2023).
16. What is FM – Definition of Facility Management [Электронный ресурс]. URL: http://www.ifma.ora/about/what-is-facility-manage-ment#sthash.GjARNDWg.dpuf (дата обращения: 19.04.2024).
17. **Бородулин К.В.** Внедрение технологий информационного моделирования в процесс эксплуатации зданий и сооружений // Молодой ученый. - 2019. - № 2 (240). – С. 200-202. – URL: https://moluch.ru/archive/240/55593/ (дата обращения: 24.04.2024).
18. **Naml, Ersin & Isikdag, Umit & Kocakaya, Mustafa.** (2019). Building Information Management (BIM), A New Approach to Project Management. Journal of Sustainable Construction Materials and Technologies. 4. 323-332. 10.29187/jscmt.2019.36.
19. **Edirisinghe, R., & London, K.A.** (2015). Comparative analysis of international and national level BIM standardization efforts and BIM adoption.

Matveev Dmitry Aleksandrovich – Ingineer, Master student of the Department of construction organization and real estate management, National Research Moscow State University of Civil Engineering (NRU MGSU), 26 Yaroslavskoe Sh., Moscow, 129337, E-mail: d.a.matveev@gmail.com

Матвеев Дмитрий Александрович – инженер, магистрант кафедры оганизации строительства и управления недвижимость (ОСУН), ФГБОУ ВО «Национальный исследовательский Московский государственный строительный университет», ФГБОУ ВО «НИУ МГСУ», 26, Ярославское шоссе, г. Москва, Россия, d.a.matveev@gmail.com

International Journal for Computational Civil and Structural Engineering, 20(2) 163–176(2024)

DOI:10.22337/2587-9618-2024-20-2-163-176

OVERALL ASSESSMENT OF DEFORMATION AND FORCE OF DIAPHRAGM WALL JOINTS DURING THE STAGES OF DEEP EXCAVATION CONSTRUCTION

Phuong Tuan Nguyen [1], Truong Xuan Dang [2], Thuan Anh Nguyen [3], Hoa Van Vu Tran [3]

[1] Mien Tay Construction University, Vinh Long Province, VIETNAM
[2] Ho Chi Minh University of Natural Resources and Environment, Ho Chi Minh City, VIETNAM
[3] University of Transport Ho Chi Minh City, Ho Chi Minh City, VIETNAM

Abstract: In the realm of geotechnical engineering, deep excavation projects face intricate challenges, especially concerning the stability of barrette walls, which are highly susceptible to deformation and stress at their joints. This study focuses on evaluating the deformation and force behavior of barrette wall joints at the position of greatest deformation. The Finite Element Method (FEM) is utilized to simulate the behavior of these structures under various load conditions. The Analysis of Variance (ANOVA) method is employed to statistically analyze the FEM data, assessing the impact of different factors on deformation and force distributions within the barrette wall joints. The specific objective of this study is to determine the statistical significance of the observed deformations and understand the influence of construction stages on joint integrity. This methodological synergy enhances the predictability of engineering assessments and ensures that design and construction decisions are grounded in solid empirical evidence. The study's findings emphasize the importance of precise monitoring and advanced predictive techniques to mitigate potential risks associated with deep excavations, particularly at critical joint locations. The results indicate that the deformation patterns are primarily influenced by the geometrical setup of the walls and the mechanical properties of the soils. The greatest deformations were typically observed where the wall joints experienced the highest bending moments and shear forces, conditions exacerbated by unfavorable soil mechanics and hydrostatic pressures. The clear and consistent increase in total displacement highlights the progressive destabilization of the wall as the excavation depth increases. By integrating ANOVA with FEM, this study contributes to enhancing safety and efficiency in deep excavation projects by ensuring that decisions are grounded in empirical evidence.

Keywords: Barrette walls, Deep excavation, Finite element method, Wall thickness optimization, ANOVA tests, Deformation, Construction strategies

ОБОБЩЕННАЯ ОЦЕНКА ДЕФОРМАЦИЙ И УСИЛИЙ В СОЕДИНЕНИЯХ МЕМБРАННЫХ СТЕН НА ЭТАПАХ ВОЗВЕДЕНИЯ ОБЪЕКТОВ ГЛУБОКОГО ЗАЛОЖЕНИЯ

Фыонг Туан Нгуен [1], Чыонг Суан Данг [2], Туан Ань Нгуен [3], Хоа Ван Ву Чан [3]

[1] Миентай строительный университет, г. Виньлонг, ВЬЕТНАМ
[2] Хошиминский университет природных ресурсов и окружающей среды, г. Хошимин, ВЬЕТНАМ
[3] Хошиминский университет транспорта, г. Хошимин, ВЬЕТНАМ

Аннотация: В сфере геотехнической инженерии, при проектировании объектов глубоких заложения сталкиваются со сложными проблемами, особенно касающихся устойчивости барретных стенок, которые очень чувствительны к деформациям и напряжениям в местах их стыков. Данное исследование направлено на оценку деформации и силового поведения соединений стеновых заколок в состоянии наибольших деформаций. Метод конечных элементов (МКЭ) используется для моделирования поведения этих конструкций при различных условиях нагрузки. Метод дисперсионного анализа (ANOVA) используется для статистического анализа данных полученных МКЭ, оценки влияния различных факторов на деформацию и распределение усилий внутри заколочных соединений стенок.

Конкретная цель данного исследования – определить статистическую значимость наблюдаемых деформаций и понять влияние этапов строительства на целостность соединений. Такая методологическая синергия повышает предсказуемость инженерных оценок и гарантирует, что решения по проектированию и строительству основываются на надежных эмпирических данных. Результаты исследования подчеркивают важность точного мониторинга и передовых методов прогнозирования для снижения потенциальных рисков, связанных с эксплуатацией объектов глубокого заложения, особенно в критических местах соединений. Результаты показывают, что на характер деформаций в первую очередь влияют геометрическое расположение стен и механические свойства грунтов. Наибольшие деформации обычно наблюдались там, где стыки стен испытывали самые высокие изгибающие моменты и усилия сдвига, причем это состояние усугублялось неблагоприятной механикой грунта и гидростатическим давлением. Явное и последовательное увеличение общего смещения подчеркивает прогрессирующую дестабилизацию стены по мере увеличения глубины положения объекта. Интегрирация ANOVA с МКЭ в этом исследовании способствует повышению безопасности и эффективности проектов объектов глубоких заложения, гарантируя, что решения основаны на эмпирических данных.

Ключевые слова: Стены-барреты, глубокое заложение, метод конечных элементов, оптимизация толщины стен, тесты ANOVA, деформация, стратегии строительства

1. INTRODUCTION

In the realm of geotechnical engineering, the structural stability of deep excavation projects presents a complex interplay of challenges that demand rigorous analysis and precise monitoring [1]. As urban centers grow and the demand for underground space increases, so too does the complexity of ensuring the safety and integrity of deep foundations such as barrette walls [2, 3]. These structures, crucial for supporting large loads in poor soil conditions, are particularly susceptible to deformation and stress at their joints, which can compromise the overall stability of the construction project. The evaluation of deformation and forces at the most critical points of these structures is not just a technical necessity but a safety imperative. This study focuses on providing a comprehensive evaluation of the deformation and force behavior of barrette wall joints at the point of greatest deformation, utilizing the Finite Element Method (FEM) to simulate the intricate behaviors of these structures under various load conditions. The FEM is renowned for its ability to provide detailed insights into the stress-strain relationships and deformation characteristics of complex structures [4, 5], making it an indispensable tool in modern geotechnical engineering.

However, the vast amount of data generated by FEM simulations poses a significant challenge in terms of analysis and interpretation. This is where the Analysis of Variance (ANOVA) method comes into play [6, 7]. ANOVA is employed in this research to statistically analyze the FEM data, allowing us to systematically assess the impact of different factors on the deformation and force distributions within the barrette wall joints [8]. This statistical approach not only enhances the reliability of the simulation results but also helps in identifying key patterns and anomalies that could inform better construction practices and risk management strategies. The criticality of this approach stems from recent failures observed in similar engineering projects, where unforeseen deformations led to catastrophic failures, causing not only financial losses but also endangering human lives. Such incidents underscore the urgent need for advanced predictive and analytical techniques that can provide a more accurate and comprehensive understanding of potential risks associated with deep excavations.

By integrating ANOVA with FEM, this study aims to evaluate the overall deformation and force of the diaphragm wall joint at the weakest position [9, 10]. The specific objectives are to determine the statistical significance of the observed deformations and understand the

influence of different construction stages on joint integrity. This methodological synergy enhances the predictability of engineering assessments and ensures that design and construction decisions are grounded in solid empirical evidence.

2. METHODS

2.1. Materials

The geological setup of the excavation site comprises two primary layers: the upper layer consists of mixed clay extending 7.5 meters deep, followed by a sandy soil layer with a thickness of 32.5 meters. At this site, an excavation pit measuring 11 meters by 44 meters is situated adjacent to a single-story building, with a targeted depth of 15 meters. Excavation activities are initiated from both ends of the site to optimize access and efficiency [11, 12].

To ensure the stability of the excavation walls and prevent any structural failures, a comprehensive shoring system consisting of four layers is strategically employed. These layers are positioned at various depths: -1 meter, -4.6 meters, -7.1 meters, and -9.6 meters. The structure of the shoring system is reinforced with H-beam steel sections, each measuring 400x400 mm, which are critical in maintaining the structural integrity of the excavation walls (Table 1).

Table 1. Parameters describing shoring system materials

Parameter	Value
Material type	Elastic
Y (kN/m3)	78.5
A (m2)	0.02187
I2 (m4)	0.666E-3
I3 (m4)	0.224E-3
E (kN/m2)	210.0E6

Above these walls, a cap beam with dimensions of 800x800 mm is installed to connect the barrette walls, further enhancing the stability of the overall structure. The barrette walls themselves are 800 mm thick and extend down to a length of 25 meters (Table 2). The presence of groundwater at a depth of -4 meters adds an additional layer of complexity to the excavation process [13].

The methodology employed for excavating this site starts with the installation of the cap beam, which is crucial for providing lateral support and stability from the outset. This initial step forms the foundation for all subsequent excavation and shoring activities. After the cap beam is securely in place, excavation begins with the careful removal of the soil layer (Table 3). Following this, the first layer of the shoring system is constructed. This system is vital as it offers temporary support to the excavation walls, effectively preventing their collapse.

As the excavation progresses deeper, careful management of the groundwater table is necessary [14-16]. The water table is gradually lowered to counteract hydrostatic pressure, thus mitigating the risk of water inflow that could destabilize the excavation site. This iterative process of excavation, shoring installation, and water table management is repeated meticulously with each descending layer of soil, ensuring that the excavation progresses in a controlled and safe manner toward the desired depth (Figure 1).

Table 2. Cap beam material description parameters

Parameter	Value
Material type	Elastic
Y (kN/m3)	25
Height (m)	0.8
Width (m)	0.8
A (m2)	0.02187
I2 (m4)	0.666E-3
I3 (m4)	0.224E-3
E (kN/m2)	210.0E6

Table 3. Altitude of excavated soil layers

No	The soil layer	Altitude (m)
1	Layer 1	0 – (-2)
2	Layer 2	(-2) – (-5.1)
3	Layer 3	(-5.1) – (-7.6)
4	Layer 4	(-7.6) – (-10.1)
5	Layer 5	(-10.1)–(-13.1)
6	Layer 6	(-13.1) – (-15)

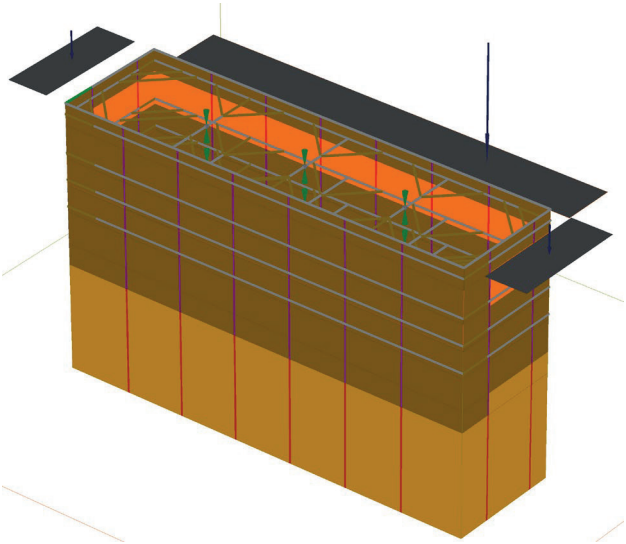


Figure 1. Overview of excavation pit models

2.2. Methods

This research meticulously investigates the deformation of barrette wall joints in deep excavation sites, employing the Finite Element Method (FEM) to conduct a detailed analysis of the soil-structure interactions under various loading and environmental conditions [17, 18]. The complex dynamics inherent in such constructions require a nuanced understanding of how different stressors—such as soil pressure, moisture variations, and adjacent structural activities—affect the structural integrity and behavior of excavation walls.

In the methodological framework of this study, a generic FEM model is constructed to represent both the geometry and material properties of the barrette walls and the surrounding soil (Table 4) [19].

This model effectively incorporates key parameters, including the elasticity, permeability, and plasticity of the soil, as well as the mechanical properties of the concrete used in the barrette walls and diaphragm wall joints has a length of 200 mm (Table 5).

By simulating the excavation process, a comprehensive analysis of how deformations collectively affect the barrette wall joint and the overall structural integrity of the walls is enabled.

In this study, we employed the Analysis of Variance (ANOVA) to examine whether there are statistically significant differences in technical parameters across various excavation stages (Figure 2) [20]. Data were collected for axial forces, bending moments, shear forces, and torsion moments from six distinct stages of excavation. Each parameter was measured at specific nodes and elements, providing a comprehensive dataset suitable for multivariate analysis. The primary goal was to evaluate the impact of changes in excavation techniques and geotechnical conditions on structural integrity and to identify any patterns or anomalies.

Table 4. Soil description parameters with Hardening soil model

Parameter	Soil type	
	Clay	Sand
Soil model	Hardening soil	Hardening soil
Drainage	Undrained	Undrained
γ_w (kN/m^2)	20.25	20.12
γ_{sat}	20.57	20.55
e_{init}	0.5879	0.5810
n_{init}	0.3702	0.3675
E_{50}^{ref}	6875	13.45E3
E_{ode}^{ref}	6875	13.45E3
E_{ur}^{ref}	20.63E3	40.35E3
V_{ur}	0.2	0.2
Power (m)	0.8	0.65
P^{ref}	38	400
C' ^{ref}	7.1	5.7
φ' (°)	30.40	30
Ψ (°)	0.4	0
K_z (m/day)	1.43E-05	6.91E-6
$K_x = K_y$	3.59E-05	0.138E-3

Table 5. Description parameters of barrette wall and diaphragm wall joints material

Parameter	Barrette Walls	Diaphragm Wall Joints
Material type	Elastic	Elastic
Y (kN/m3)	8	8
E1 (kN/m2)	32.50E6	32.50E6
E2 (kN/m2)	32.50E6	32.50E6
D (m)	0.8	0.8
G12 (kN/m2)	16.25E6	0.0001
G13 (kN/m2)	16.25E6	13.54E6
G23 (kN/m2)	16.25E6	0.0001

2.3. ANOVA Analysis

ANOVA was conducted by first ensuring that the data met the assumptions of normality and homogeneity of variances, which were assessed using Levene's test, respectively [21]. After confirming the assumptions, one-way ANOVA was applied to compare the mean values of each technical parameter between different stages [22, 23]. Post-hoc comparisons were performed using the Games-Howell test to determine which stages differed significantly from each other [24, 25]. This statistical approach provided a robust framework for interpreting the complexities of geotechnical behavior during progressive excavation stages [26].

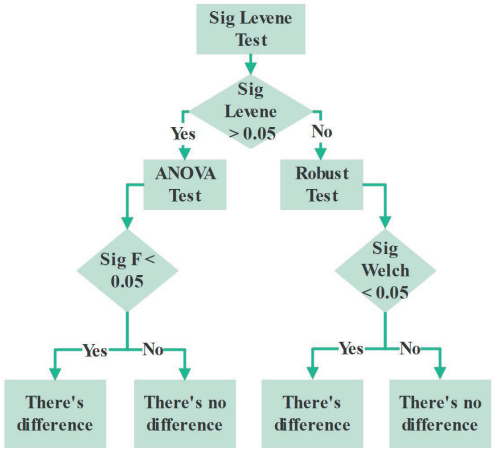


Figure 2. ANOVA General Inspection Process

3. RESULTS AND DISCUSSION

3.1. Analyze model deformation and forces

The research, through the application of the Finite Element Method (FEM), reveals that the deformation of barrette walls is significantly influenced by a combination of soil characteristics, wall geometry, and external loading conditions (Figure 3).

Total displacements |U| The largest is 0.0555 m at the red spot in Figure 3. This is the deformation analyzed at the time when it was dug to a height of -15 m.

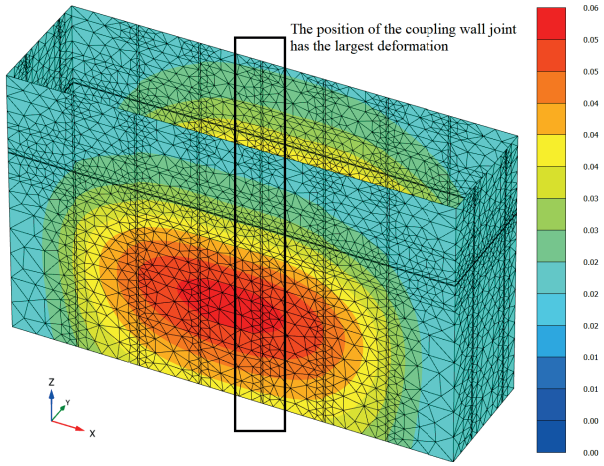


Figure 3. Deformation |U| of the barrette wall and the location of the largest deformed diaphragm wall joints

The research conducts an analysis of the deformation, shear force, and moment parameters at this diaphragm wall joint site.

From the initial to the final stage of excavation, there is a clear and consistent increase in the total displacement (|U|), which suggests a progressive destabilization of the wall as the excavation depth increases (Table 6). Starting from a minimal displacement of 0.0063 meters in the first stage, the displacement escalates to 0.0532 meters by the sixth stage. This pattern of increasing displacement is a typical response in excavation projects, reflecting the cumulative effect of stress and strain on the structure as more soil layers are removed. Deformation |U| through the stages of earthdigging are depicted in Figure 4.

Table 6. Deformation statistics of diaphragm wall joints during earthworks

Stages	Total displacements |U|	Total displacements Ux		Total displacements Uy		Total displacements Uz	
		min	max	min	max	min	max
1	6.30E-03	-1.22E-05	1.21E-05	1.66E-03	4.55E-03	4.30E-03	4.37E-03
2	0.01707	-3.7E-05	3.97E-05	0.003566	0.0128	0.0112	0.0113
3	2.64E-02	-6.16E-05	5.78E-05	2.44E-03	2.10E-02	1.59E-02	1.61E-02
4	3.46E-02	-9.41E-05	7.23E-05	1.47E-03	2.83E-02	1.98E-02	2.00E-02
5	4.41E-02	-1.41E-04	8.38E-05	6.80E-04	3.78E-02	2.25E-02	2.28E-02
6	5.32E-02	-1.73E-04	8.78E-05	1.53E-04	4.80E-02	2.27E-02	2.30E-02

Displacements in the Ux axis (lateral) show a fluctuation within a narrow range, but there's a noticeable trend where the maximum displacement slightly increases from 0.0000121 meters in the first stage to 0.0000878 meters in the last stage. This indicates lateral movements are relatively controlled but do increase as the excavation progresses. Uy and Uz displacements (vertical and longitudinal), however, exhibit more substantial changes. The vertical displacement (Uz) increases significantly from 0.0043 meters in the first stage to 0.023 meters in the sixth stage, highlighting a notable vertical settling or sinking of the wall under the excavation load.

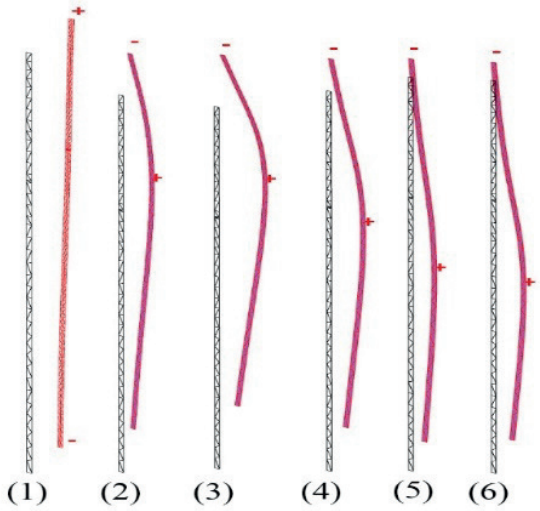


Figure 4. Deformation change |U| through the stages

The observed displacement patterns across Ux, Uy, and Uz axes suggest that while lateral stability is maintained to a certain extent, the primary challenge lies in managing vertical and longitudinal stresses. The consistent increase in these displacements indicates that the wall experiences significant downward and outward forces, which could be attributed to the unloading of soil and the consequent redistribution of stresses within the soil mass and the wall structure.

Throughout these stages of earthwork, there is a noticeable trend of increasing absolute values in both minimum and maximum axial forces for N1 and N2 (Table 7). This suggests a progressive escalation in structural loads as the excavation deepens, which is typical in such operations due to the increasing depth and the subsequent impact on lateral earth pressures.

Table 7. Axial forces value statistics

	Axial forces N1		Axial forces N2	
Stages	min	max	min	max
1	-81.04	55.05	-327	248.1
2	-257	264.5	-553.5	447.2
3	-418.6	416.4	-611.2	507.1
4	-662.8	536.6	-620.7	522.2
5	-1050	627.3	-612	519.1
6	-1329	653.7	-839.3	502.8

In the initial stage, axial forces are relatively low, indicating lesser stress and strain on the structure. As the excavation progresses to stages 2 through 6, there is a significant increase in both the compressive and tensile forces. This increment points towards growing challenges in maintaining structural stability, demanding enhanced reinforcement or support systems in deeper excavation stages.

For axial force N1, the shift from predominantly negative values in the early stages to a mixed range in the later stages highlights varying stress conditions, possibly due to changes in earth pressure or the activation of support systems like anchors or struts. Similarly, axial force N2 shows a broadening range between the minimum and maximum values, reflecting the uneven distribution of loads across the structure, which could be attributed to asymmetrical excavation or irregular soil conditions.

Notably, as the stages progress, both M11 and M22 show substantial increases in their maximum values, indicating heightened structural stresses due to deeper excavation (Table 8).

For M11, the minimum value starts at -14.07 kN/m in the first stage and drops slightly to -29.4 kN/m by the sixth stage, showing a moderate downward trend. On the other hand, the maximum value significantly increases from 20.5 kN/m in the first stage to 229.5 kN/m in

the sixth stage. This sharp rise suggests that elements experiencing M11 forces are increasingly subjected to tensile stress as the excavation deepens.

M22 illustrates a more pronounced trend with even larger fluctuations. Starting from a minimum of -28.51 kN/m in stage one and plummeting to -716.5 kN/m in stage six, coupled with a maximum of 10.53 kN/m in the first stage surging to 1306 kN/m in the last stage. These values are indicative of the critical bending loads that the structure must withstand as lateral earth pressures intensify with each subsequent stage of excavation.

Table 8. Moment value statistics through mining stages

	Bending M11		Bending M22	
Stages	**min**	**max**	**min**	**max**
1	-14.07	20.5	-28.51	10.53
2	-12.4	43.08	-53.6	289.2
3	-7.627	87.1	-124.4	527.9
4	-10.2	116.7	-251.4	688.5
5	-21.14	174.8	-479.9	930.5
6	-29.4	229.5	-716.5	1306

Table 9. Shear forces value statistics

	Shear Q12		Shear Q13		Shear Q23	
Stages	**min**	**max**	**min**	**max**	**min**	**max**
1		1.47E-07	-13.92	19.96		1.25E-07
2		5E-07	-62.69	53.48	5.13E-08	1.11E-06
3	-2.89E-07	7.82E-07	-112.6	89.9	6.50E-08	1.90E-06
4	-2.90E-07	8.73E-07	-173.6	108.6	7.09E-08	2.62E-06
5	-2.91E-07	8.46E-07	-265.8	112.8	7.10E-08	3.63E-06
6	-2.93E-07	7.88E-07	-414.3	167.6	7.08E-08	4.59E-06

The values presented indicate significant differences in the behavior of shear forces across three different shear directions, namely Q12, Q13, and Q23, across all stages (Table 9).

In the case of Shear Q12, the values remain relatively small and consistent, exhibiting minimal variations from 1.47E-07 to 8.73E-07 kN/m. This consistency suggests that the excavation process does not significantly affect shear forces in this direction, possibly due to the orientation of the excavation or the inherent structural properties resisting changes in this shear direction.

Conversely, Shear Q13 shows a substantial increase in both the maximum and minimum shear values as the excavation progresses, ranging from -13.92 kN/m to 19.96 kN/m in the first stage to -414.3 kN/m to 167.6 kN/m in the sixth stage. This trend indicates a growing imbalance or redistribution of forces within the structure as deeper layers are excavated, highlighting potential areas of structural stress or failure that could require reinforcement or careful monitoring.

Similarly, the maximum values for Shear Q23 escalate dramatically from 1.25E-07 kN/m in the initial stage to 4.59E-06 kN/m in the final stage. This progressive increase in shear forces could be indicative of increasing lateral pressures as the excavation depth increases, potentially compromising the stability of the excavation sides and necessitating the implementation of adequate shoring systems to prevent collapse.

Table 10. Torsion moments M12 value statistics

	Torsion moments M12	
Stages	min	max
1		1.98E-07
2	-1.8E-06	1.81E-06
3	-3.05E-06	3.04E-06
4	-4.18E-06	4.16E-06
5	-5.78E-06	5.76E-06
6	-7.30E-06	7.27E-06

The analysis of torsion moments M12 across the six stages of excavation reveals a consistent pattern of increase in both the maximum and minimum values (Table 10). Initially, the torsion moments are extremely low, with the

first stage having a maximum value of only 1.98E-07 kN/m. This indicates minimal torsional stress at the commencement of excavation.

As excavation progresses to deeper levels, there is a significant increase in torsional moments, indicating increased structural stress. By the second stage, torsion moments fluctuate around zero, showing a slight increase to -0.000001812 kN/m and 0.000001808 kN/m for the minimum and maximum values, respectively. This shift from nearly negligible initial values suggests that the torsional demands on the structure begin to become more significant as the depth of excavation increases.

The trend continues with more pronounced increases through stages three to six. The third stage shows torsion moments at -3.05E-06 kN/m and 3.04E-06 kN/m, nearly doubling by the fourth stage to -4.18E-06 kN/m and 4.16E-06 kN/m. The increasing trend underscores the cumulative effect of excavation depth on torsional stresses within the structure.

By the fifth and sixth stages, torsion moments reach -5.78E-06 kN/m and 5.76E-06 kN/m, and -7.30E-06 kN/m and 7.27E-06 kN/m, respectively. These values illustrate a steady increase in torsional demands, reflecting the ongoing impact of successive excavation layers on structural integrity.

3.2. Statistical analysis of inspection

The results of ANOVA analysis given with the independent variable are the parameters Torsion moments, shear force, Bending moment, Axial forces, U, Ux, Uy, and Uz deformation values. The dependent variable is the stages.

The variables Ux, Uy, Uz, U, N1, N2, Q12, Q23, Q13, M11, M22, and M12 all have a P-value of 0.000, which indicates that there is a significant difference in variance between groups for each variable (Table 11). This implies that the assumption of homogeneity of variance is rejected at the level of statistical significance. Therefore, reviewing the Robust Test analysis results is necessary (Figure 2) in Table 12.

Table 11. Test of Homogeneity of Variances

	Levene Statistic	df1	df2	Sig.
Ux	388,483	5	2730	,000
Uy	550,886	5	2730	,000
Uz	246,247	5	2730	,000
U	741,690	5	2730	,000
N1	401,832	5	2730	,000
N2	139,325	5	2730	,000
Q12	130,977	5	2730	,000
Q23	320,255	5	2730	,000
Q13	123,458	5	2730	,000
M11	423,197	5	2730	,000
M22	195,237	5	2730	,000
M12	83,469	5	2730	,000

Table 12. Robust Tests of Equality of Means

		Statistic[a]	df1	df2	Sig.
Ux	Welch	264,606	5	1109,881	,000
Uy	Welch	1600,059	5	1115,924	,000
Uz	Welch	12643168,594	5	1197,841	,000
U	Welch	8531,537	5	1111,466	,000
N1	Welch	340,604	5	1098,680	,000
N2	Welch	269,004	5	1200,865	,000
Q12	Welch	364,783	5	1197,433	,000
Q23	Welch	550,395	5	1067,969	,000
Q13	Welch	10,313	5	1100,477	,000
M11	Welch	1233,368	5	1193,499	,000
M22	Welch	14,136	5	1068,621	,000
M12	Welch	,096	5	1069,925	,993

a. Asymptotically F distributed.

In the Robust Test table, the Sig values of the variables Ux, Uy, Uz, U, N1, N2, Q12, Q23, Q13, M11, and M22 are all 0, proving that these variables have differences between stages. Only variable M12 has Sig = 0.993, this variable has no difference between digging stages.

Use Games-Howell analysis to post-test to find the variable with the largest difference among the variables with differences between construction stages. The results of the Ux variable compared between stages have a significant difference (Sig. = 0.000), the Uy variable decreases significantly as the stages progress (from Stage 1 to Stage 2 the difference is -0.006072711, Sig. = 0.000), Uz is similar to Uy, Uz also decreases significantly in later stages (from Stage 1 to Stage 6, the difference is -0.018497660, Sig. = 0.000), U changes greatly across stages. Period (significant decrease from

Period 1 to Period 6, difference is -0.032850999, Sig. = 0.000), Group of variables N1 and N2 show a significant increase in later periods compared to previous periods (N1 increases from 121,921 at Stage 1 to Stage 2 up to 460,343 from Stage 1 to Stage 6 with Sig = 0.000), Groups Q12 and Q23 show a significant change, although the actual values are very different. small, reflecting small but statistically significant differences (Q12 from Phase 1 to Phase 2 is -0.000000187, Sig. = 0.000), M11 and M22 show significant changes across phases (M11 decreased from -27,638 in Stage 1 to Stage 2 to -134,048 from Stage 1 to Stage 6 with Sig. = 0.000).

In the analysis from the Games-Howell post hoc tests, the variable Uz exhibits the most substantial differences between stages. This difference is quantitatively significant and is represented with very precise statistical values. For instance, the mean difference between Stage 1 and Stage 3 for Uz is -0.011647417, with an exceptionally low standard error of 0.000002713 and a significance level (Sig.) of 0.000, indicating not only a significant difference but also one with high precision. The magnitude of the changes in Uz is notably larger than those observed in other variables, with p-values consistently indicating these differences are statistically significant.

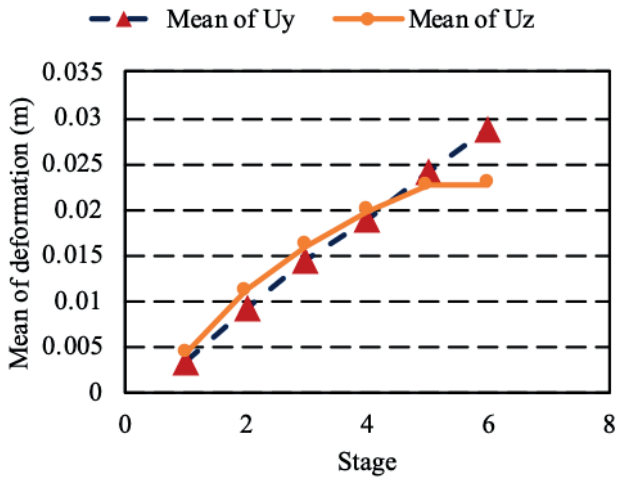


Figure 5. Mean plot of deformation Uy and Uz

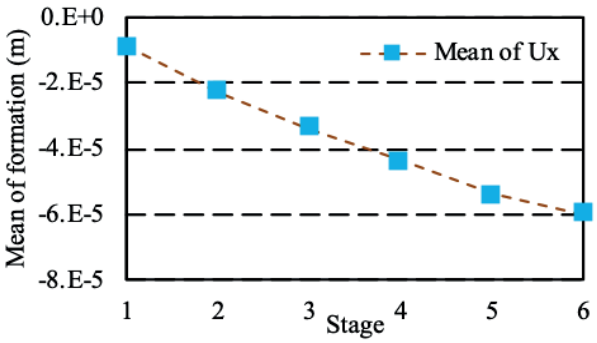


Figure 6. Mean plot of Ux

In addition to the variable Uz, which shows the most significant differences among the stages studied, attention should also be directed towards the variable Uy. This variable, similar to Uz, displays substantial stage-to-stage variations with consistently significant results, indicating its critical role in the study. Uy demonstrates a clear creasing trend as the stages progress, which could suggest a systematic change in the experimental conditions or the effect of accumulating variables across stages. The increment in Uy from Stage 1 to Stage 6 is notably significant, with the difference marked at 0.025413693, a p-value of 0.000 underscoring its importance in reflecting the underlying phenomena being studied (Figure 5).

Besides the variables that increase according to the stage, the variable Ux also decreases according to the construction stage (Figure 6).

3.3. Discussion

This research has underscored the critical importance of monitoring and evaluating deformations within geotechnical engineering projects, particularly those involving deep excavations like the one studied. The detailed analysis of deformation across different stages of the excavation process has highlighted significant transformations in the structure's behavior under varying geotechnical conditions. Integrating the Finite Element Method (FEM) with the Analysis of Variance (ANOVA), provides a nuanced understanding of the structural behaviors underpinning deep excavation projects, specifically focusing on barrette wall joints. The significance of the

deformations observed at these joints, the underlying causes, and their implications for structural safety are crucial for refining construction practices and enhancing project outcomes. Through the FEM, we have been able to simulate detailed scenarios that reflect real-world conditions under which these deep excavations are subjected. The FEM results reveal that the deformation patterns are primarily influenced by the geometrical setup of the walls and the mechanical properties of the soils. For instance, the greatest deformations were typically observed where the wall joints experienced the highest bending moments and shear forces, conditions that are exacerbated by unfavorable soil mechanics and hydrostatic pressures. The ANOVA analysis further assists in decoding the influence of various factors such as load conditions, soil consistency, and construction stages on these deformations. Significant findings from the ANOVA suggest that variations in soil properties across different layers significantly affect the deformation outcomes. For example, softer soil layers were associated with higher degrees of deformation at wall joints. This relationship underscores the necessity for precise soil assessment and characterization in the planning stages of construction to mitigate potential risks.

In this context, the variable Uz, which records vertical displacements, has demonstrated the largest and most significant changes across all stages. These findings are particularly important as they provide clear evidence of the progressive destabilization that can occur as excavation depths increase. The substantial increases in deformation measurements from the earliest to the final stages suggest that the structural integrity of the excavation walls could be compromised without adequate monitoring and intervention. Additionally, the variable Uy, indicative of lateral displacements, also shows significant transformations, reinforcing the necessity of a comprehensive monitoring strategy that encompasses multiple axes of deformation. The clear decreasing trend in Uy values as the excavation progresses could indicate lateral shifts or bending of the walls under load, which, if not adequately braced, could lead to catastrophic failures. The interaction of these variables with the mechanical properties of the soil and the construction materials used (as detailed in the earlier tables of material properties and design specifics) provides a complex picture of the dynamic interactions within the excavation site. For instance, changes in soil moisture, which affect soil stiffness and permeability, could further exacerbate the deformation rates observed.

By comparing these results with existing studies, such as those by Arabaninezhad, A., & Fakher, A. (2021) who investigated similar deep excavation projects in urban environments, it becomes evident that our findings align with broader observations in the field. These studies also highlighted the critical impact of soil heterogeneity on wall stability and emphasized the value of integrated approaches in predicting and managing structural responses.

One of the critical insights from our study is the demonstration of how specific deformation patterns, identified statistically through ANOVA, correlate strongly with increased risks of structural failure. For instance, where significant statistical differences in deformation across stages of excavation were noted, these often coincided with stages where historical data indicate a higher incidence of structural failures. This correlation not only validates the FEM and ANOVA as effective tools for this field of study but also enhances our ability to predict and prevent failures.

Moreover, the application of these analytical methods allows for a proactive approach to construction management. By understanding which stages of the excavation process are most susceptible to critical deformations, project managers can implement targeted reinforcement strategies and adjust construction plans in real time to ensure structural integrity.

4. CONCLUSIONS

This research has provided comprehensive insights into the deformation behaviors of barrette wall joints under various construction conditions

through the combined use of the Finite Element Method (FEM) and Analysis of Variance (ANOVA). By integrating these two powerful analytical tools, we have been able to pinpoint critical factors influencing structural deformations and thereby propose more effective risk management and mitigation strategies in geotechnical engineering projects. The application of FEM has allowed for a detailed simulation of the complex interplay between soil properties, wall geometry, and loading conditions. This method revealed that deformations at the barrette wall joints are significantly affected by variations in soil composition and moisture content, as well as by the physical constraints imposed by the surrounding structures. The results have highlighted the critical need for precise monitoring and evaluation mechanisms in geotechnical engineering projects, especially those involving significant changes in the structural environment. The variables Uz and Uy, which measure vertical and lateral displacements respectively, have shown significant increases in deformation with Uz experiencing a peak deformation of 0.0555 meters at the maximum excavation depth of -15 meters. This significant deformation underscores the progressive destabilization of the excavation walls as the depth increases. For instance, the increase in Uz from 0.0043 meters at the first stage to 0.023 meters in the final stage illustrates a more than fivefold increase in vertical displacement, which clearly indicates the gravity of structural shifts that could potentially lead to wall failures if not properly managed.

Similarly, Uy presented a significant reduction from an initial deformation at the first stage to a decrease by the sixth stage, which corresponds to the lateral adjustments of the wall under different loading conditions. These quantitative changes in Uy from 0.00455 meters in the initial stage to of 0.0480 meters by the final stage highlight the lateral movement tendencies that need continuous monitoring to prevent any unforeseen structural failures. Furthermore, the utilization of ANOVA has provided a robust statistical framework to assess the impact of these variables systematically, confirming the hypothesis that certain construction stages and soil conditions pose greater risks than others.

The major contributions of this study include the identification of specific stages in construction that are prone to critical deformations, and the clarification of how different soil layers' properties can drastically influence the stability of deep excavation sites. Such insights are invaluable for construction engineers and project managers, as they highlight the need for tailored construction strategies based on the specific conditions of each site. Additionally, the research findings advocate for the implementation of continuous monitoring systems at construction sites to dynamically assess and respond to potential structural failures. Real-time data obtained from such systems can be analyzed using the methodologies described in this study to make immediate adjustments to the construction process, thereby enhancing safety and efficiency. For future research, it is recommended to expand the application of these methodologies to a wider range of geotechnical structures and conditions. Investigating different types of soil and more varied construction scenarios will further validate the versatility and robustness of the FEM and ANOVA integration. Moreover, longitudinal studies that track structural integrity over time post-construction could provide deeper insights into the long-term impacts of the identified factors on structural health and safety.

In practical terms, this study serves as a foundation for developing advanced predictive models that can be incorporated into construction planning and management software. These models, equipped with the ability to simulate various scenarios and predict outcomes, could significantly improve decision-making processes in construction projects, especially those involving complex underground constructions. By identifying key factors affecting structural integrity and demonstrating the effective use of advanced analytical techniques, this study contributes to the enhancement of safety standards and the optimization of construction practices globally.

REFERENCES

1. **Nguyen, N.-N., L.H. To, and B.V. Le**. Behavior of Isotropic and Anisotropic Diaphragm Walls in Finite Element Analysis Model of Deep Excavation. in The International Conference on Sustainable Civil Engineering and Architecture. 2023. Springer.
2. **Qiao, Y.-K., et al.**, Socio-environmental costs of underground space use for urban sustainability. Sustainable Cities and Society, 2019. 51: p. 101757.
3. **Council, N.R., et al.,** Underground engineering for sustainable urban development. 2013: National Academies Press.
4. **Espinosa, H.D., et al.,** Merger of structure and material in nacre and bone–Perspectives on de novo biomimetic materials. Progress in Materials Science, 2009. 54(8): p. 1059-1100.
5. **Bardenhagen, S., A. Brydon, and J. Guilkey,** Insight into the physics of foam densification via numerical simulation. Journal of the Mechanics and Physics of Solids, 2005. 53(3): p. 597-617.
6. **Gelman, A.,** Analysis of variance—why it is more important than ever. 2005.
7. **Christensen, R.,** Analysis of variance, design, and regression: applied statistical methods. 1996: CRC press.
8. **Alzyod, H. and P. Ficzere,** Material-dependent effect of common printing parameters on residual stress and warpage deformation in 3D printing: A comprehensive finite element analysis study. Polymers, 2023. 15(13): p. 2893.
9. **Li, C., et al.,** Aero-mechanical multidisciplinary optimization of a high speed centrifugal impeller. Aerospace Science and Technology, 2019. 95: p. 105452.
10. **Sivareddy, D.V., et al.,** Parameter optimisation in vibration assisted turning of Ti6Al4V alloy using ANOVA and grey relational analysis. International Journal of Automotive and Mechanical Engineering, 2018. 15(3): p. 5400-5420.
11. **Read, R.,** 20 years of excavation response studies at AECL's Underground Research Laboratory. International Journal of Rock Mechanics and Mining Sciences, 2004. 41(8): p. 1251-1275.
12. **Martino, J. and N. Chandler,** Excavation-induced damage studies at the underground research laboratory. International Journal of Rock Mechanics and Mining Sciences, 2004. 41(8): p. 1413-1426.
13. **Do, T., et al.,** A combined finite difference and finite element model for temperature and stress predictions of cast-in-place cap beam on precast columns. Construction and Building Materials, 2019. 217: p. 172-184.
14. **Cashman, P.M. and M. Preene,** Groundwater lowering in construction: a practical guide to dewatering. 2020: CRC Press.
15. **Council, N.R., et al.,** Alternatives for managing the nation's complex contaminated groundwater sites. 2013: National Academies Press.
16. **Powers, J.P., et al.,** Construction dewatering and groundwater control: new methods and applications. 2007: John Wiley & Sons.
17. **David, T.K., R.R. Krishnamoorthy, and M.J. IB,** Finite element modelling of soil-structure interaction. Jurnal Teknologi, 2015. 76(8).
18. **Phuor, T., et al.,** Development of the skew boundary condition for soil-structure interaction in three-dimensional finite element analysis. Computers and Geotechnics, 2021. 137: p. 104264.
19. **IBST,** Geological survey report file. 2016.
20. **Hox, J. and H. Hoijtink,** Analysis of Variance: Why It Is More Important than Ever: Discussion. The Annals of Statistics, 2005. 33(1): p. 39-42.
21. **Levine, D.W., et al.,** A self-administered questionnaire for the assessment of severity of symptoms and functional status

in carpal tunnel syndrome. JBJS, 1993. 75(11): p. 1585-1592.
22. **Kim, Y.-K., S.-M. Kim, and H. Myoung,** Musical intervention reduces patients' anxiety in surgical extraction of an impacted mandibular third molar. Journal of oral and maxillofacial surgery, 2011. 69(4): p. 1036-1045.
23. **Leandri, M., et al.,** Balance features in Alzheimer's disease and amnestic mild cognitive impairment. Journal of Alzheimer's Disease, 2009. 16(1): p. 113-120.
24. **O'Toole, S., et al.,** Investigation into the accuracy and measurement methods of sequential 3D dental scan alignment. Dental Materials, 2019. 35(3): p. 495-500.
25. **Trattnig, S., et al.,** Lumbar intervertebral disc abnormalities: comparison of quantitative T2 mapping with conventional MR at 3.0 T. European radiology, 2010. 20: p. 2715-2722.
26. **Wang, J., et al.,** Multi-source data integration and multi-scale modeling framework for progressive prediction of complex geological interfaces in tunneling. Underground Space, 2024. 15: p. 1-25.

СПИСОК ЛИТЕРАТУРЫ

1. **Nguyen, N.-N., L.H. To, and B.V. Le**. Behavior of Isotropic and Anisotropic Diaphragm Walls in Finite Element Analysis Model of Deep Excavation. in The International Conference on Sustainable Civil Engineering and Architecture. 2023. Springer.
2. **Qiao, Y.-K., et al.**, Socio-environmental costs of underground space use for urban sustainability. Sustainable Cities and Society, 2019. 51: p. 101757.
3. **Council, N.R., et al.,** Underground engineering for sustainable urban development. 2013: National Academies Press.
4. **Espinosa, H.D., et al.,** Merger of structure and material in nacre and bone–Perspectives on de novo biomimetic materials. Progress in Materials Science, 2009. 54(8): p. 1059-1100.
5. **Bardenhagen, S., A. Brydon, and J. Guilkey,** Insight into the physics of foam densification via numerical simulation. Journal of the Mechanics and Physics of Solids, 2005. 53(3): p. 597-617.
6. **Gelman, A.,** Analysis of variance—why it is more important than ever. 2005.
7. **Christensen, R.,** Analysis of variance, design, and regression: applied statistical methods. 1996: CRC press.
8. **Alzyod, H. and P. Ficzere,** Material-dependent effect of common printing parameters on residual stress and warpage deformation in 3D printing: A comprehensive finite element analysis study. Polymers, 2023. 15(13): p. 2893.
9. **Li, C., et al.,** Aero-mechanical multidisciplinary optimization of a high speed centrifugal impeller. Aerospace Science and Technology, 2019. 95: p. 105452.
10. **Sivareddy, D.V., et al.,** Parameter optimisation in vibration assisted turning of Ti6Al4V alloy using ANOVA and grey relational analysis. International Journal of Automotive and Mechanical Engineering, 2018. 15(3): p. 5400-5420.
11. **Read, R.,** 20 years of excavation response studies at AECL's Underground Research Laboratory. International Journal of Rock Mechanics and Mining Sciences, 2004. 41(8): p. 1251-1275.
12. **Martino, J. and N. Chandler,** Excavation-induced damage studies at the underground research laboratory. International Journal of Rock Mechanics and Mining Sciences, 2004. 41(8): p. 1413-1426.
13. **Do, T., et al.,** A combined finite difference and finite element model for temperature and stress predictions of cast-in-place cap beam on precast columns. Construction and Building Materials, 2019. 217: p. 172-184.

14. **Cashman, P.M. and M. Preene,** Groundwater lowering in construction: a practical guide to dewatering. 2020: CRC Press.
15. **Council, N.R., et al.,** Alternatives for managing the nation's complex contaminated groundwater sites. 2013: National Academies Press.
16. **Powers, J.P., et al.,** Construction dewatering and groundwater control: new methods and applications. 2007: John Wiley & Sons.
17. **David, T.K., R.R. Krishnamoorthy, and M.J. IB,** Finite element modelling of soil-structure interaction. Jurnal Teknologi, 2015. 76(8).
18. **Phuor, T., et al.,** Development of the skew boundary condition for soil-structure interaction in three-dimensional finite element analysis. Computers and Geotechnics, 2021. 137: p. 104264.
19. **IBST,** Geological survey report file. 2016.
20. **Hox, J. and H. Hoijtink,** Analysis of Variance: Why It Is More Important than Ever: Discussion. The Annals of Statistics, 2005. 33(1): p. 39-42.
21. **Levine, D.W., et al.,** A self-administered questionnaire for the assessment of severity of symptoms and functional status in carpal tunnel syndrome. JBJS, 1993. 75(11): p. 1585-1592.
22. **Kim, Y.-K., S.-M. Kim, and H. Myoung,** Musical intervention reduces patients' anxiety in surgical extraction of an impacted mandibular third molar. Journal of oral and maxillofacial surgery, 2011. 69(4): p. 1036-1045.
23. **Leandri, M., et al.,** Balance features in Alzheimer's disease and amnestic mild cognitive impairment. Journal of Alzheimer's Disease, 2009. 16(1): p. 113-120.
24. **O'Toole, S., et al.,** Investigation into the accuracy and measurement methods of sequential 3D dental scan alignment. Dental Materials, 2019. 35(3): p. 495-500.
25. **Trattnig, S., et al.,** Lumbar intervertebral disc abnormalities: comparison of quantitative T2 mapping with conventional MR at 3.0 T. European radiology, 2010. 20: p. 2715-2722.
26. **Wang, J., et al.,** Multi-source data integration and multi-scale modeling framework for progressive prediction of complex geological interfaces in tunneling. Underground Space, 2024. 15: p. 1-25.

Phuong Tuan Nguyen, Doctor of Phylosophy, Lecturer, Mien Tay Construction University, Vinh Long Province, VIETNAM, 20B Pho Co Dieu, Ward 3, Vinh Long City. Mobile: +84919070096. Email: tuanphuongvk@gmail.com

Truong Xuan Dang, Doctor of Phylosophy, Lecturer, Ho Chi Minh University of Natural Resources and Environment, Ho Chi Minh City, VIETNAM, No 236B Le Van Sy, Tan Binh district. Mobile: +84913804068. Email: dxtruong@hcmunre.edu.vn

Thuan Anh Nguyen, Associate Professor, Lecturer, Department of Railways and Metro, University of Transport Ho Chi Minh City, Ho Chi Minh City, 717066, VIETNAM, No 2, Vo Oanh street, Binh Thanh district. Mobile: +849839097793. Email: tuanna@ut.edu.vn

Hoa Van Vu Tran, Expert of the SDCT Research Group, University of Transport Ho Chi Minh City, Ho Chi Minh City, 717066, VIETNAM, No 2, Vo Oanh street, Binh Thanh district. Mobile: +84902227137. Email: hoa.tranvu.htgroup@gmail.com

Фыонг Туан Нгуен, к.т.н., преподаватель, Миентай строительный университет, Виньлонг, ВЬЕТНАМ, 20В ул. Co Dieu, город Виньлонг. Мобильный: +84919070096. Электронная почта: tuanphuongvk@gmail.com

Чыонг Суан Данг, к.т.н., преподаватель, Хошиминский университет природных ресурсов и окружающей среды, Хошимин, ВЬЕТНАМ, № 236В Ле Ван Си, район Тан Бинь. Мобильный: +84913804068. Электронная почта: dxtruong@hcmunre.edu.vn

Туан Ань Нгуен, к.т.н., доцент, преподаватель кафедры железных дорог и метро, Хошиминский университет транспорта, г. Хошимин, 717066, ВЬЕТНАМ, № 2, улица Во Оан, район Бинь Тхань. Мобильный: +849839097793. Электронная почта: tuanna@ut.edu.vn

Хоа Ван Ву Чан, эксперт исследовательской группы SDCT, Хошиминский университет транспорта, Хошимин, 717066, ВЬЕТНАМ, № 2, улица Во Оан, район Бинь Тхань. Мобильный: +84902227137. Электронная почта: hoa.tranvu.htgroup@gmail.com

International Journal for Computational Civil and Structural Engineering, 20(2) 177–191(2024)

DOI:10.22337/2587-9618-2024-20-2-177-191

THE COEFFICIENT OF LONGITUDINAL BENDING FOR COMPOSITE STEEL-CONCRETE RODS UNDER SHORT-TERM LOADS

Denis V. Konin

Research Institute of Building Constructions (TSNIISK) Named After V. A. Koucherenko JSC "Research center of Construction", Moscow, RUSSIA

Abstract: The norms (codes) for calculations of compressed composite steel and concrete columns, as well as experimental and theoretical studies by other authors, are considered. An experimental study of compressed columns with small eccentricity at a range of flexibility l_0/h from 6 to 20 was performed. Finite-elements modeling of various variants of structures has been performed: with concrete class from B30 (C25/30) to B100 (C90/105), with I-beam core, with square form core. The experimental and FEM data obtained are compared with theoretical curves of the longitudinal bending coefficient. It was found that the coefficient curves in SP 266.1325800 and Eurocode 4 are not in the correct shape and do not reflect actual work of composite compressed columns. The use of SP 266.1325800 curve, based on the curve for reinforced concrete structures, as well as Eurocode 4 curves, which are accepted as for steel sections by Eurocode 3, does not provide load-bearing capacity reserve and does not ensure reliability. Both codes ignore different work of low- and high-strength concretes. As a result of the research, it was found that class of concrete affects the stability of columns with flexibility l_0/h from 6 to 10, while there is no influence on the shape of the cross-section of the core (type of rigid reinforcement). For flexibility l_0/h from 10 to 20, a uniform coefficient curve can be adopted for all concretes. Curves of the coefficient φ have been developed for calculating compressed elements at small eccentricities and short-term action of loads; a formula for calculating the bearing capacity of compressed racks has been proposed.

Keywords: concrete, high-strength concrete, steel, composite structure, rigid reinforcement, eccentrical compression, stability, buckling, coefficient of longitudinal bending

КОЭФФИЦИЕНТ ПРОДОЛЬНОГО ИЗГИБА СТАЛЕЖЕЛЕЗОБЕТОННЫХ СТОЕК ПРИ КРАТКОВРЕМЕННОМ ДЕЙСТВИИ НАГРУЗОК

Д.В. Конин

ЦНИИСК им. В. А. Кучеренко АО "НИЦ "Строительство", г. Москва, РОССИЯ

Аннотация: Рассмотрены нормы по расчету сжатых сталежелезобетонных стоек, а также экспериментально-теоретические исследования других авторов. Выполнено экспериментальное исследование работы сжатых стоек с малым эксцентриситетом на диапазоне гибкостей l_0/h от 6 до 20. Выполнено численное моделирование различных вариантов конструкций: с бетонами от В30 (С25/30) до В100 (С90/105), с сердечником в виде двутавра, с сердечником в виде квадрата. Полученные данные экспериментов и расчетов сопоставлены с теоретическими кривыми коэффициента продольного изгиба. Установлено, что кривые коэффициента в СП 266.1325800 и Eurocode 4 имеют не корректную форму и не отражают действительной работы сталежелезобетонных сжатых элементов. Использование кривой СП 266.1325800, основанной на кривой для железобетонных конструкций, а также кривых Eurocode 4, которые приняты как для стальных сечений (по Eurocode 3) – не дает нормального запаса конструкций и не обеспечивает надежность. Оба норматива игнорируют различный характер работы бетонов обычной и высокой прочности. В результате исследований установлено, что класс прочности бетона на сжатие влияет на устойчивость стержней с гибкостью от 6 до 10, при этом влияния формы поперечного сечения сердечника (вида жесткого армирования) практически нет. Для гибкостей от 10 до 20 может быть принята единая для всех бетонов кривая коэффициента. Разработаны кривые коэффициента φ для

расчета сжатых элементов при малых эксцентриситетах и кратковременном действии нагрузок; предложена формула расчета несущей способности сжатых стоек.

Ключевые слова: бетон, высокопрочный бетон, сталь, сталежелезобетонная конструкция, жесткая арматура, внецентренное сжатие, устойчивость, коэффициент продольного изгиба

INTRODUCTION

Consideration of buckling effects for steel reinforced concrete compressed struts is an extremely actual problem. Ignoring the effects of buckling in the design of columns of multi-storey buildings, supports of large-span roofs, bridge piers with large effective lengths can lead to design errors and accidents. Using only idealized design schemes, even taking into account geometric and physical nonlinearities, cannot fully account for the variety of random factors, which in combination can lead to premature failure of a critical building structure. Such random factors include: external eccentricities; internal eccentricities resulting from misalignment of steel and reinforced concrete sections; inaccuracy of manufacturing and assembly of structures; quality and variability of material properties, etc. Some effects can be accounted for by introducing appropriate coefficients in calculations, but the determination of these coefficients must be based on experimental studies of models or full-scale structures. The buckling coefficient simultaneously takes into account the nonlinear behavior of materials in the cross-section. In steel-reinforced concrete structures, this is primarily nonlinear deformation and cracking in concrete. As well as it is possible eccentricities of the load applied to the columns and "internal" eccentricities due to inaccurate assembly.

For long-term loading, the coefficient φ for reinforced concrete elements with rigid reinforcement should be taken from the table of SP 266.1325800.2016 depending on the slenderness ratio of the element and the compressive strength of the concrete. For short-term loading, it should be calculated using the following linear relationship: φ =0,9 at $\frac{l_0}{h} = 10$ ($\lambda = 34.5$) and φ = 0.85 at $\frac{l_0}{h} = 20$ ($\lambda = 69$), where l_0 is the effective length of the element, h is the depth of the section in the plane of determination of the coefficient φ. The values of the coefficient φ are shown in Figure 1 with a red line. The values of the coefficient φ for a rectangular cross-section at central compression taken from [1] are marked with a black dotted line.

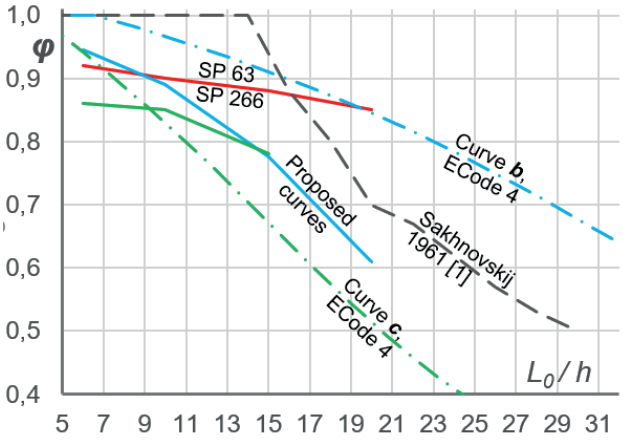


Figure 1. Comparison of coefficients φ

EN 1994-1-1 (2004) "Eurocode 4: Design of composite steel and concrete structures..." (hereinafter referred to as Eurocode 4) requires that the condition 6.44 must be met when designing compressed bars

$$\frac{N_{Ed}}{\chi N_{pl,Rd}} \leq 1 \qquad (1),$$

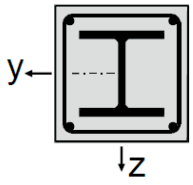
where N_{Ed} is the design load acting on element, and $N_{pl,Rd}$ is the 'plastic' cross-section bearing capacity, defined by formula 2. The nomenclature of parameters in the formula is taken in accordance with SP 266.1325800). Value $N_{pl,Rd}$ is calculated by simply summing up the constituent parts of the cross-section:

$$N_{pl,Rd} = R_y A_{st} + 0{,}85 R_{b,c} A + R_{sc} A_{s,tot} \qquad (2)$$

where R_y, R_{sc} are the design yield strength for rigid steel profile and for rebars, $R_{b,c}$ is the

design compressive strength of concrete cylinder specimens, A_{st}, A, $A_{s,tot}$ are the cross-section areas of rigid reinforcement, concrete and steel rebars respectively. Also formula 1 utilizes the buckling coefficient χ, which is defined according to the corresponding table 6.5 in Eurocode 4. This table specifies the type of curve of the χ coefficient depending on the type of section and refers to the provisions of clause 6.3.1.2 of EN 1993-1-1: 2005 "Eurocode 3: Design of Steel Structures..." (hereinafter referred to as Eurocode 3). An extract from Table 6.5 of Eurocode 4 and from the corresponding section of Eurocode 3 is given in Table 1. The curve types for the I-beam section, in the corresponding planes (column 5), are also shown there for comparison.

Table 1 – Comparison of Eurocode 3 and Eurocode 4 stability calculation requirements

Type of cross section	Design axes	**Curve type** according to Table 6.5 **Eurocode 4**	Imperfect element	**Curve type** for steel I-beam from steel S355 according to table 6.2 **Eurocode 3**	
				$h/b > 1{,}2$, $t_f \leq 40$ mm	$h/b \leq 1{,}2$, $t_f \leq 100$ mm
1	2	3	4	5	6
	*y-y*	*b*	$L/200$	*a*	*b*
	z-z	*c*	$L/150$	*b*	*c*

The data given in the table shows that curves for hot-rolled column I-beams (column 3) which have approximately the same flange height and width (column 6) are adopted when designing steel reinforced concrete structures of compressed struts in the form of fully concreted I-beams. Note that there is a differentiation in Table 6.2 of Eurocode 3 in the assignment of buckling curves for hot-rolled beam (column 5) and column I-beams, and for welded and hot-rolled sections. Table 6.5 in Eurocode 4 does not take into account the actual design of the I-beam (welded or rolled), its shape (column or beam) or the concrete class. Curve types are taken as the most unfavorable, i.e., in margin. In addition to the one considered in Table 1, there are partially concreted section made of I-beams, for which the curve types are the same as for the one considered. There is also partially concreted section made of two I-beams made in a cross (curve type b), pipe-concrete section with the percentage of reinforcement up to 3% and from 3 to 6% (curve types a and b, respectively), pipe-concrete section with rigid reinforcement in the form of I-beams (curve type b). In Figure 1, the dashed blue and green lines represent curves b and c, respectively. The slenderness ratios are given for the l_0/h ratio used in SP 63.13330 and SP 266.1325800, as for the S355 steel bar.

Steel reinforced concrete structures working in compression have been studied quite well in the USSR and Russia since the second half of the 20th century by A.N. Vasiliev [2], E.L. Zhitnitskaya [3], N.A. Slavinsky, S.K. Mikadze, N.A. Egorov [4], Khandzhi V.V. [8], Travush V.I. with the participation of the author [12] and others. The paper [24] provides justification of the possibility of calculating such structures using a nonlinear deformation model. Among foreign studies in recent years, the researchs of PRC scientists [15, 18, 19], as well as Western scientists [20, 21, 22, 23] have drawn attention. However, they investigate relatively short steel-reinforced concrete bars (l_0/h from 3 to 6), where the stability effects or the influence of deformation of the bar are minimal. Nevertheless, they will be used to analyze the results in the future.

The stability of reinforced concrete bars has been investigated in the studies of E.A. Chistyakov [11], V.M. Bondarenko, V.I. Murashev, as well as

A.D. Beglov and R.S. Sanzharovsky et al [9, 10], V.V. Gichko [7], A.L. Krishan. [17], Teryanik V.V. [16] and others. The studies of E.A. Chistyakov formed the basis of the current norms for the design of reinforced concrete structures SP 63.13330. The stability of reinforced concrete bars taking into account creep phenomena, including under the application of short-term acting loads, is studied in [13, 14]. The performance of modern concretes under load with different aggregates, their deformation diagrams and Poisson's ratio are studied in [25, 26].

2. RESEARCH METHODS

To verify the existing buckling coefficient curves (Figure 1), it is necessary to analyze the available experimental data on the performance of bars of different slenderness with different percentages of reinforcement. Due to the relatively small number of experiments on steel-reinforced concrete structures, test data on reinforced concrete bars of different slenderness are analyzed. This is justified, since the strains of concrete in steel-reinforced concrete bars at the central location of rigid reinforcement elements fully correspond to the strains of reinforced concrete structures. The comparison does not include the results of tests of pipe-concrete structures, since their operation is significantly influenced by the presence of a steel enclosed shell and concrete strains in such structures have certain peculiarities.

In order to supplement the existing test base, a full-scale test of steel-reinforced concrete strut models in the range of slenderness l_0/h from 6 to 20 was carried out. The general cross-sectional view and the view of one of the failed models are shown in Figure 2. The slenderness of the elements was varied by changing the length of the models. The steel of rigid reinforcement was C355 and that of steel rebars was A500C. The concrete had a compressive strength class of B100, which was confirmed by cube specimen tests. The percentage of cross-sectional reinforcement for all models is 10.3%. All models were tested under eccentric compression with an eccentricity of 5 mm along the flanges of the I-beam, which is close in value to random eccentricity (h/30=5.3 mm). During testing, the strains on the surface of steel and concrete, vertical absolute displacements, and the value of compressive load at the beginning and end of the holding time were recorded at each step.

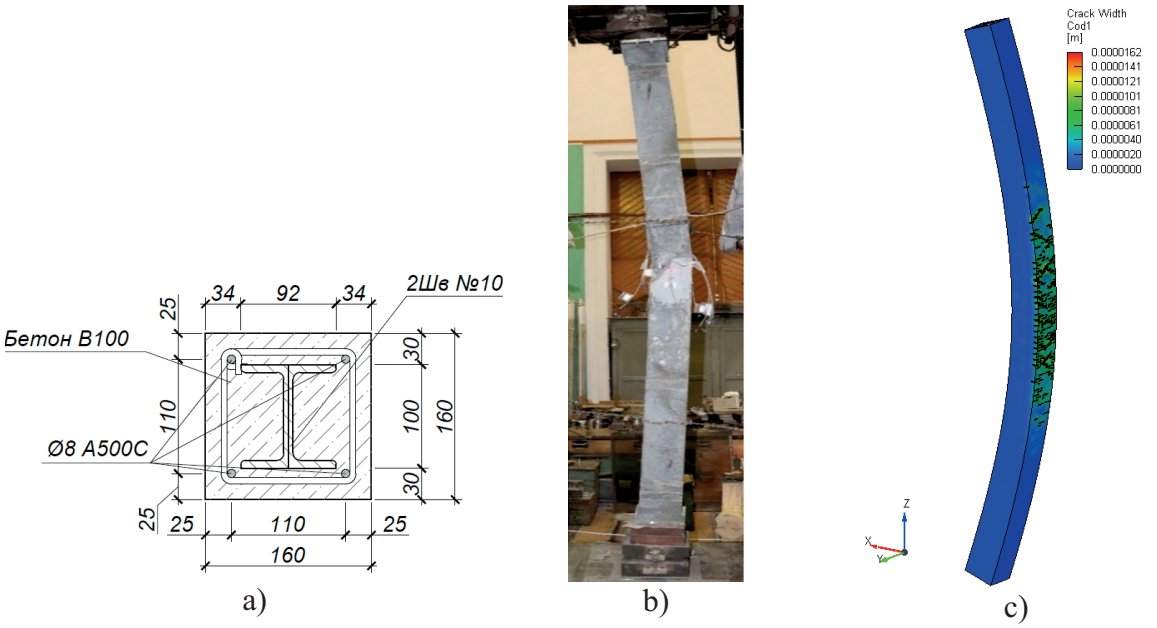


Figure 2. Experimental models: a - cross section, b - fractured model with slenderness ratio of 20, c - ultimate state of the model with slenderness ratio of 20 according to FEA

Similar struts were also studied using finite element modeling in ATENA software, considering the nonlinear performance of the materials: a three-line diagram for concrete and a two-line diagram for steel. Models were created that fully replicate the experimental models in terms of geometry, boundary conditions, eccentricities and materials. In addition, struts with concrete of compressive strength classes B30, B60, and B80 were modeled to extend the results to all material strength ranges. Poisson's ratio was assumed differentially according to the strength class of concrete [26]. The number of steps and mesh size for each model was also selected individually. The minimum number of loading steps was at least 20 and the mesh size was about 20 mm. The Fracture-Plastic Constitutive Material Model (CC3DCementitious2), which is based on a combination of a tensile fracture model (Rankine-Fracturing Model) with a compressive material fracture model (Menétrey-Willam), was used to describe the performance of the concrete. The calculations of all structures were performed considering the formation and opening of cracks in concrete. The limit state of the slender column is shown in Figure 2, c. Also, as part of preliminary finite element modeling, strut models with simulation of contact interaction between steel and concrete were tested. It was found that for struts with small eccentricities, regardless of the slenderness and shape of the core, the presence of a certain contact interaction at the steel-concrete joint practically does not affect the results of calculations. That is, there is no influence of the contact on the value of the ultimate load, the value of the ultimate longitudinal strain of the core. There is influence on the buckling deformation within 3-5%. The difference between forces and deformations for the same type of models with and without contact interaction modeling is less than 0.5%. Therefore, further analysis and modeling were performed for finite element models of struts in which the contact interaction at the steel-concrete joint was not modeled in a special way, and the steel and concrete FEs had common nodes in the design scheme.

3. RESULTS AND DISCUSSION

The main difficulty in analyzing previously conducted studies is that it is not always possible to reliably determine from descriptive materials the design length of elements that should be considered from hinge to hinge of the test bench. In some studies, only the length of the tested structures is given, which introduces a distortion in the results of the analysis. Often tests with small or zero eccentricities were performed in one or two instances, which did not allow to establish reliably the magnitude of the failure load. Therefore, it was possible to analyze 79 tests of reinforced concrete and steel-reinforced concrete struts out of the whole variety of studies based on the works [4, 6, 7, 11, 12, 22, 23], in which the eccentricity value did not exceed the value of $h/30$, as well as the tests described above, conducted by the author. The selected test results fall within the range of slenderness l_0/h from 5 to 32, for concrete on heavy aggregate with compressive strength classes from B20 to B100. The rigid reinforcement elements in almost all experiments are in the form of a single I-beam made of steel similar to C255...C390. In experiments [22, 23] 4 I-beams made of S460 steel were used as a rigid reinforcement. The investigated reinforcement percentage over the whole range of the study is from 0.08 to 46.6%. The cross sections were all rectangular or circular. Thus, a fairly representative array of experimental data was investigated over a wide range of slenderness, percent reinforcement, and compressive strength class of concrete. The longitudinal bending coefficient was calculated from the experimental results using the formula:

$$\varphi = N_{test}/N_{theor.} \quad (3)$$

where N_{test} is the fracture load based on test results, $N_{theor.}$ is the theoretical load-bearing

capacity of the strut, defined as the sum of the compressive load-bearing capacity of concrete, steel, reinforcement according to the actual values of material strengths and their actual dimensions. Figure 3 shows the test results as discrete values, as well as the theoretical values of the coefficient φ according to various sources. Reinforced concrete structures are marked in the figure with round markers, steel-reinforced concrete structures are marked with triangular markers.

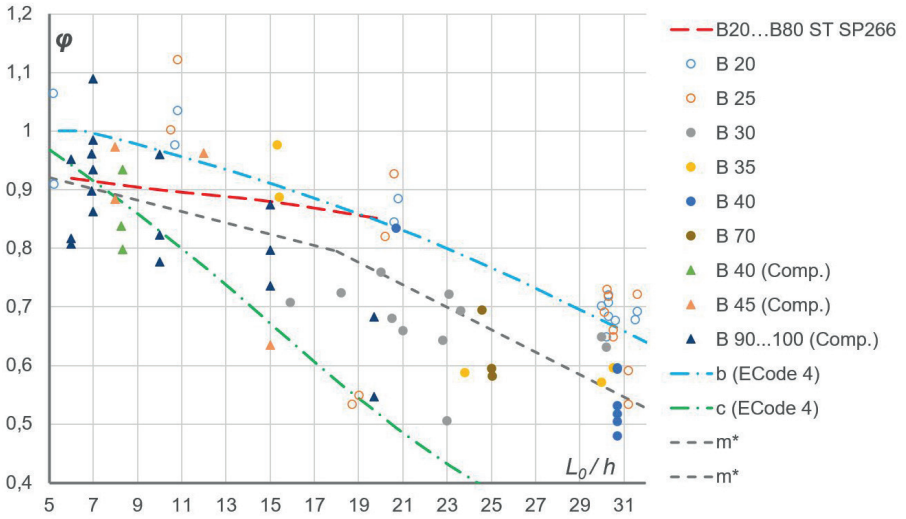


Figure 3. Comparison of theoretical curves of the coefficient φ with experimental data

While considering the data of the experiments, a rather large variation in the values of the coefficient φ attracts attention. At slenderness 6 the variation is from 0.81 to 1.0 (Δφ=0.19), at slenderness 10 - from 0.78 to 0.96 (Δφ=0.18), at slenderness 15 - from 0.64 to 0.98 (Δφ=0.34), at slenderness 20 - from 0.55 to 0.84 (Δφ=0.29), at slenderness 30 - from 0.48 to 0.65 (Δφ=0.17). The minimum squares approximation by a linear function leads to the following system of equations for the coefficient φ (shown in Figure 3 by the gray dashed line):

$$\begin{cases} \varphi = 0{,}97 - \frac{0{,}001 l_0}{h}, for \;\; 5 < l_0/h \leq 18 \\ \varphi = 1{,}14 - \frac{0{,}019 l_0}{h}, for \; 18 < l_0/h \leq 32 \end{cases} \quad (4)$$

Significant variation of test results is related to the complexity of the modeled structures. First of all, it is steel and reinforced concrete structures, in which the influence of internal eccentricities is high. In addition, it is difficult to take correct readings from load cells and displacement sensors in case of sudden brittle failure of the structure at the last stages of testing. These features are typical for all analyzed studies. A significant variation of data within one study is representative if model fabrication and measurements are performed by the same groups of specialists. The line of the characteristic coefficient according to SP 266.1325800 (red dotted line) lies above a significant number of tests and has a smaller slope with increasing slenderness than expessions (4).

Eurocode 4 lines b and c (blue and green dashed lines) also have an unsatisfactory correlation with lines plotted by expressions (4). Line b lies above a significant number of tests, i.e., calculations that use it will not give a margin. Line c lies substantially below almost all tests, which will lead to unjustified overconsumption of materials. At the same time, both of these lines at the value of slenderness of 5 are practically equal to 1, which does not ensure the reliability of structures and does not take into account the peculiarities of nonlinear operation of the combined steel-reinforced concrete section.

Expressions (4) are constructed for all concretes and slenderness ratios. If other smaller samples

by concrete strength classes, reinforcement percentages or other design parameters were to be separated in the investigated sample. The size would be unsatisfactory for approximation (n=3...5) and statistical analysis of the test results. Therefore, the mean function of the coefficient φ presented in expressions (4) over the entire range of concretes, reinforcement percentages and slenderness ratios can only be a guide. For example, the results of tests of steel-reinforced concrete structures with rigid reinforcement and concrete of strength class B90...B100 by different groups of specialists show that mainly at slenderness ratios from 10 to 20 the values of the coefficient φ lie below the approximation lines (4). This indicates the peculiarities of the performance of such structures and the need for a separate analysis. The peculiarities of the performance of structures with different types of cores can be investigated in detail using verified finite element models.

Finite element analysis of models with different slenderness ratios and concretes allowed us to construct curves of the coefficient φ, which was calculated using Formula 3. In this formula, the value of N_{FEM} is the ultimate compressive force based on the results of the finite element modeling that was utilized used instead of the failure load during the tests N_{test}. Extremes of the force-displacemt graphs for strut shortening and buckling were taken as the ultimate state (Figure 4, a). The plots of the coefficient φ for the whole considered range of slenderness ratios and B30, B60, B80 and B100 concretes are shown in Figure 4, b. The curves for all concretes at slenderness greater than 15 follow practically the same trajectory, and at slenderness from 6 to 15 they lie one under the another. The least strong concrete (B30) has the maximum coefficient φ=0.95 at slenderness of 6 (blue line). A core of the stronger concrete (B100) at the same slenderness has a value of φ=0.85 (green line).

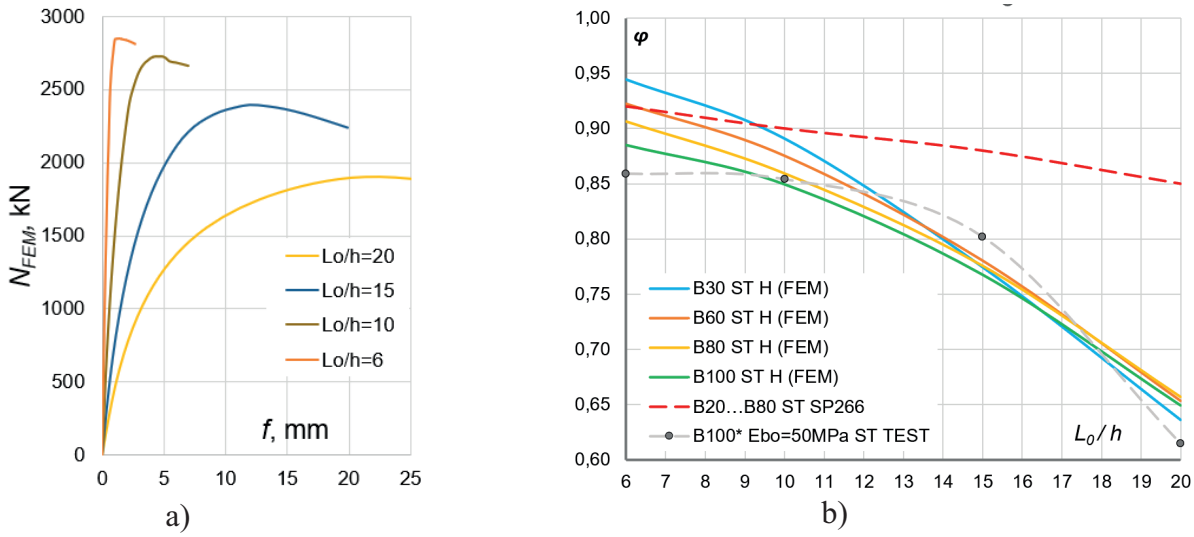


Figure 4. Comparison of finite element analysis results for different concretes: a - force-displacement graphs for identifying the buckling of struts made of B100 concrete for different slenderness ratios; b - diagrams of the coefficient φ for different slenderness ratios and concretes

Compared to the normative line of the coefficient φ (red dashed line, Figure 4), all obtained lines are lower, especially for slenderness ratio of 20 and more. At a slenderness of 20, the difference is more than 30%. Based on the obtained data from the analysis of validated finite element models, the refined graphs of the coefficient φ can be plotted.

In addition, we evaluate the influence of the cross-sectional shape of the rigid reinforcement on the performance of a bar compressed with a small eccentricity. For this purpose, finite element models of bars of different slenderness were created with a core in the form of a solid square section that is equivalent in area to the previously

studied bars with I-beams (Figure 5). The same options for creating and for analysis of models in ATENA were used for simulation as presented above. According to the results of the simulations, we can plot the buckling coefficients and compare them with those previously obtained for the bars with I-beam reinforcement (Figure 6). Solid lines in the graphs show the curves of the coefficient φ for bars with I-beam core, dotted lines indicate the curves of the coefficient φ for bars with square core. Despite the insignificant difference in the coefficient values (about 5-10%), the curves run parallel and there is almost no significant influence of the shape of the core cross-section. Unlike steel bars in compression, where the influence of cross-sectional shape on the type of φ coefficient curve has been established, here the effect is minimal and can be ignored for most common cross-sections with central and symmetrical arrangement of rigid reinforcement elements. This is primarily due to the fact that the value of the coefficient φ in steel-reinforced concrete structures is primarily influenced by the concrete and its deformation diagram. Therefore, the different character of deformation of concretes of different strengths should be accounted by the new curves of the φ coefficient, also taking into account the studies [25, 26].

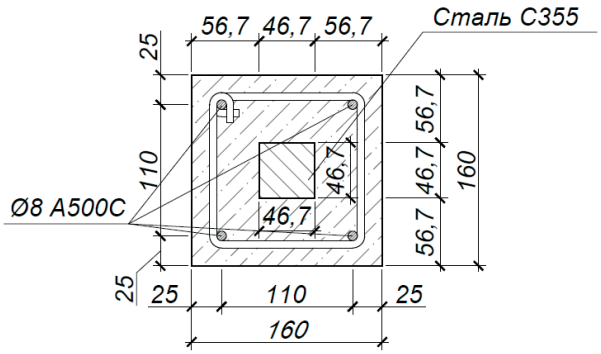


Figure 5. Cross-section of a strut with a square core

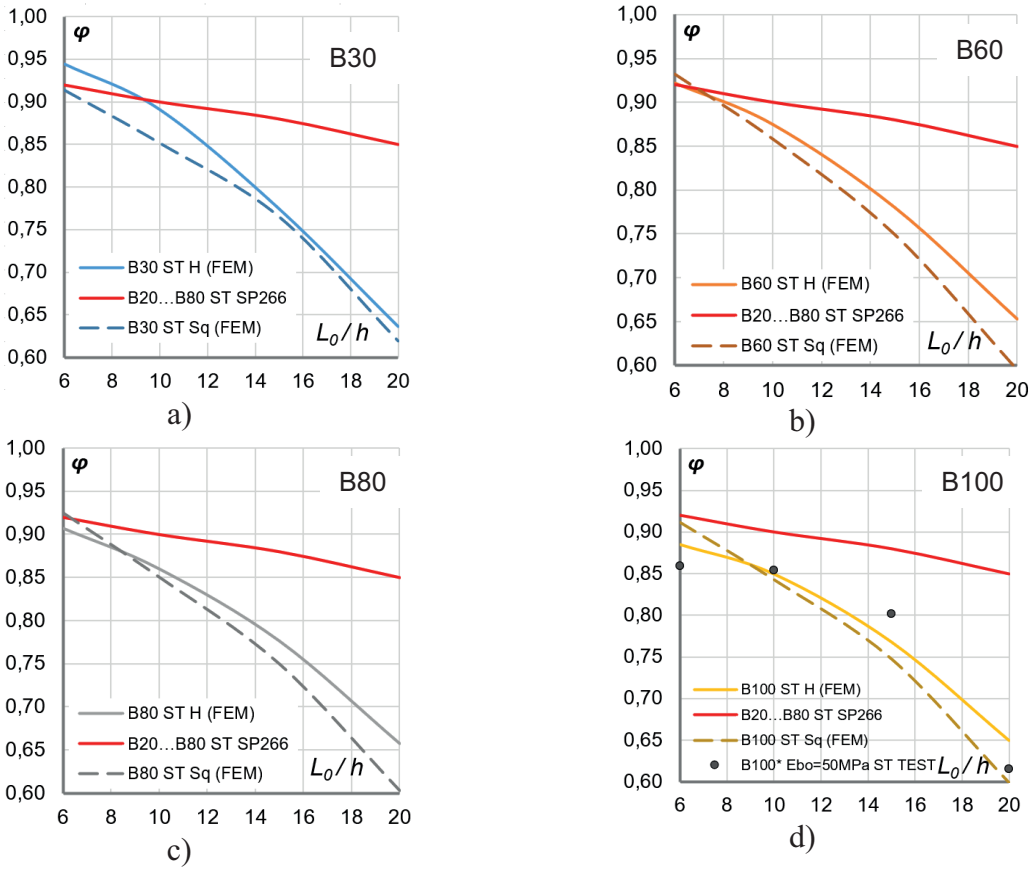
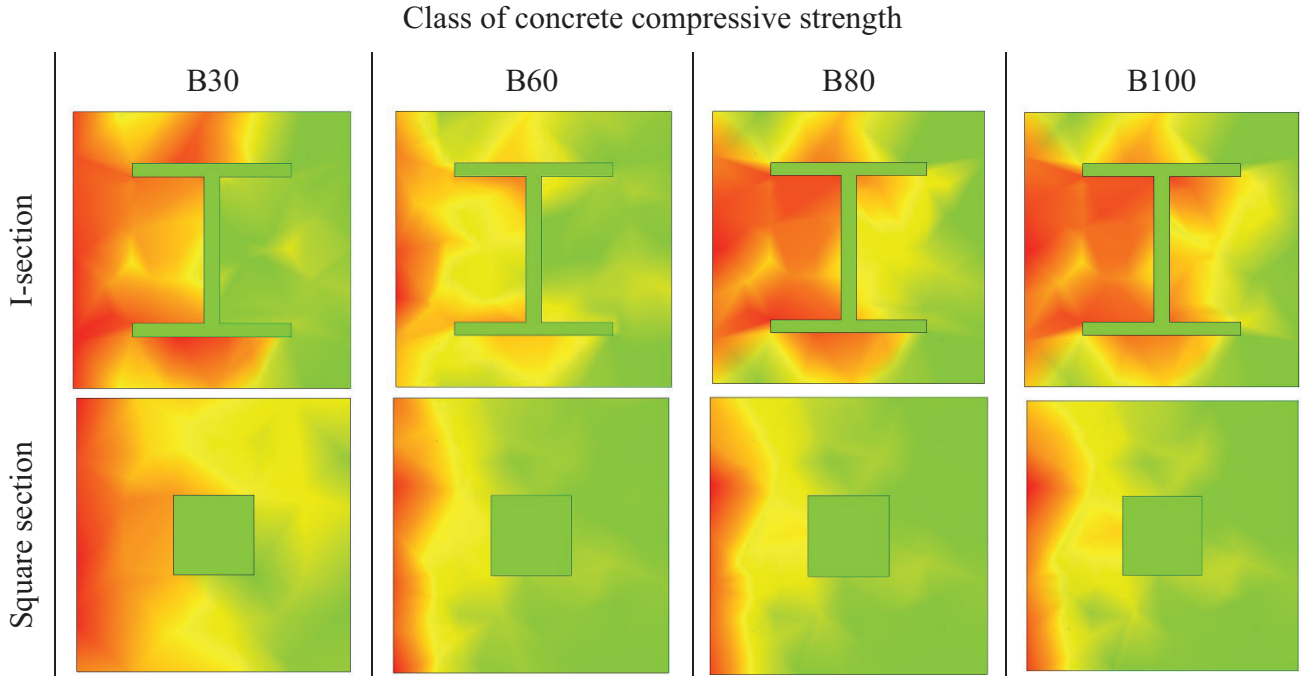


Figure 6. Comparison of calculation results for bars with I-beam and square core with different concretes: a - B30, b - B60, c - B80, d - B100

Additionally, let us analyze the pattern of cracking in the cross-section of struts with different types of rigid reinforcement. Table 2 shows comparative cracking patterns at the last calculation step before the ultimate state is reached. Crack patterns are given for a strut of slenderness 20 for an example with varying concrete performance diagrams from B30 to B100. It can be seen that the struts with B30 concrete exhibit more active material involvement throughout the cross-section. That is, cracks (and thus plastic strains in concrete under compression) propagate more actively from the periphery of the most compressed fiber to the axial areas of the cross-section. Thus, in structures made of concrete B30 the steel core is more actively involved in the work. In the case of high-strength concrete the steel core is used less effectively. In the actual performance of structures, this pattern will also be confirmed due to the fact that ordinary strength concrete (B20...B35) has a smoother deformation diagram and a descending branch after reaching the tensile strength [25]. Unlike high-strength concretes (B80...B100), which have brittle fracture behavior, the use of ordinary strength concretes increases the reliability of the structure, although it has the effect of increasing material consumption.

Table 2. Comparison of cracking patterns for different concretes and cross sections for slender struts l_0/h =20



There is also a pronounced cracking in the space between the flanges of the I-beam in the most compressed part of the cross-section. The analysis of the principal stresses, as well as stresses in separate directions shows that the concrete actively works not only in compression along the main axis of the core, but also in compression in the horizontal plane due to the constraint of lateral strains by the I-beam flanges. A "cage" effect is observed. This causes the I-beam core columns to work more efficiently (see Figure 6) and have a slightly higher value of the φ coefficient and ultimate bearing capacity than the square core columns. The comparison of ultimate bearing capacity of cores with different cores is summarized in Table 3. The maximum bearing capacity difference of 9.8% in favor of I-beam core is recorded in columns with maximum slenderness made of B60...B100 concrete. The fact that the

difference will be maximum for high-strength concrete is obvious since as the strength class of concrete increases, the actual value of Poisson's ratio also increases from 0.2 for B30 to 0.245 for B100 according to [26].

Table 3. Comparison of ultimate bearing capacity of struts with different reinforcement

Concrete class	l_0/h	I-section			Square section			$1-\frac{N_{FEM(3)}}{N_{FEM(6)}}$
		N_{FEM}, kN	N_{theor}, kN	φ	N_{FEM}, kN	N_{theor}, kN	φ	
1	2	3	4	5	6	7	8	9
B100	20	1628	2507	0,649	1502	2507	0,599	-8,4%
	15	1925		0,768	1874		0,748	-2,7%
	10	2130		0,849	2113		0,843	-0,8%
	6	2219		0,885	2285		0,911	2,9%
B80	20	1434	2182	0,657	1315	2182	0,603	-9,1%
	15	1693		0,776	1635		0,749	-3,6%
	10	1876		0,860	1855		0,850	-1,1%
	6	1979		0,907	2017		0,924	1,9%
B60	20	1213	1857	0,653	1105	1857	0,595	-9,8%
	15	1449		0,780	1392		0,749	-4,2%
	10	1626		0,875	1594		0,859	-1,9%
	6	1713		0,922	1732		0,932	1,1%
B30	20	872	1370	0,636	848	1370	0,619	-2,8%
	15	1061		0,775	1048		0,765	-1,2%
	10	1221		0,891	1166		0,851	-4,7%
	6	1294		0,945	1251		0,914	-3,4%

Summarizing the research data presented above, and also considering the peculiarities of steel-reinforced concrete structures in the form of reinforced concrete struts with rigid reinforcement, it is proposed to carry out the bearing capacity calculation for compressed elements with eccentricities not exceeding the random eccentricities by the following formula:

$$\frac{N}{\varphi(R_b A+R_{sc}A_{s,tot}+R_y A_{st})} \leq 1, \qquad (5)$$

where R_b, R_y, R_{sc} are the design strengths of concrete in compression, yield strength for rigid reinforcement and rebars respectively, A_{st}, A, $A_{s,tot}$ are the cross-section areas for rigid reinforcement, concrete and steel rebars respectively. The values of the coefficient φ for continuous action of loads are accepted according to Table 7.1 of SP 266.1325800, and for short-term action of loads are accepted according to Table 4 of this paper. Comparison of the proposed coefficients (blue and green lines) with the requirements of SP 266.1325800 (red dashed line) and Eurocode 4 (blue and green dashed lines) is shown in Figure 1.

The proposed values of the coefficient φ take into account the nature of the performance of concrete of different compressive strengths, as well as the peculiarities of the performance of steel-reinforced concrete compressed elements under load with different types of cores, the operation of the structure under deformed scheme.

Table 4. Coefficient φ for short-term loads

Concrete class	Slenderness ratio of the element			
	$l_0/h =$ 6	10	15	20
	$\lambda =$ 20.8	34.6	52.0	69.3
1	2	3	4	5
B30	0.945	0.891	0.78	0.61
B60	0.920	0.875		
B80	0.890	0.860		
B100	0.860	0.850		

4. CONCLUSIONS

1) Experimental and theoretical studies of the performance of compressed steel-reinforced concrete struts of different slenderness ratio have been performed. Russian and foreign studies of the stability of compressed reinforced concrete and steel reinforced concrete bars have been analyzed.

2) The curves of buckling coefficient contained in SP 266.1325800 and Eurocode 4 do not accurately reflect the peculiarities of steel-reinforced concrete compressed bars with small eccentricities. The coefficient of SP 266.1325800, which is based on the standards for the design of reinforced concrete structures, does not correspond to the theoretical assumptions in its current form, as it does not smoothly decrease with increasing slenderness ratio. It is also not confirmed by the analyzed experimental data. The coefficient in Eurocode 4, which gives a reference to the curves of a similar coefficient for steel structures from Eurocode 3, also cannot be considered sufficiently justified. It actually ignores the performance of reinforced concrete in the cross-section. The concrete at the periphery of the cross-section is included in the work at the very first stages of loading of the structure and significantly changes the performance and hence the coefficient curve of the compressed steel column surrounded by concrete. The concrete significantly improves the stability performance of the compressed strut, which should be taken into account in the calculations.

3) It is found that the compressive strength class of concrete affects the stability of bars with slenderness ratios from 6 to 10, with little or no influence of the shape of the cross-section of the core type of rigid reinforcement. The curves of the φ coefficient for the calculation of compressed elements at small eccentricities and short-term action of loads have been developed. A formula for calculating the load-bearing capacity of compressed struts has been proposed.

4) Based on the analysis performed, the buckling coefficients should be checked and updated when calculating the long-term action of loads, taking into account the shrinkage and creep of materials. Due to the presence of cracking concentrators in the form of steel-concrete joints, studs, etc., the creep measure used to calculate steel-reinforced concrete structures may differ from standard reinforced concrete structures.

REFERENCES

1. **Sahnovskij K.V.** (1961) *Zhelezobetonnye konstrukcii* [Reinforced concrete structures]. Moscow: Gosudarstvennoe Izdatel'stvo literatury po stroitel'stvu, arhitekture i stroitel'nym materialam, 840 p. (in Russian)
2. **Vasiliev, A.P.** (1941) *Zhelezobeton s zhestkoj armaturoj* [Reinforced concrete with rigid reinforcement]. Moscow: State Publishing House of Construction Literature, 123 p. (in Russian)
3. **Zhitnitskaya, E.L.** (1957) *Issledovanie vnecentrenno szhatyh zhelezobetonnyh kolonn s nesushchej armaturoj pri malyh*

ekscentrisitetah [Investigation of out-of-center compressed reinforced concrete columns with load-bearing reinforcement at small eccentricities] (PhD Thesis). Moscow. (In Russian)

4. **Egorov, N.A.** (1975) *Issledovanie vnecentrenno szhatyh zhelezobetonnyh kolonn s nesushchej armaturoj pri malyh ekscentrisitetah* [Investigation of the strength and deformability of reinforced concrete columns with rigid reinforcement made of low-alloy steel] (PhD Thesis). Moscow, 142 p. (In Russian)
5. **Kajumov R.H.** (1972) *Ustojchivost' gibkih zhelezobetonnyh sterzhnej iz vysokoprochnogo betona* [Stability of flexible reinforced concrete rods made of high-strength concrete] (PhD Thesis). Kiev, 201 p. (In Russian)
6. **Bambura A.N.** (1978) *Issledovanie kratkovremennoj ustojchivosti szhatyh zhelezobetonnyh jelementov pri nesharnirnom zakreplenii na koncah* [Research of short-term stability of compressed reinforced concrete elements with non-hinged fastening at the ends] (PhD Thesis). Kiev, 199 p. (In Russian)
7. **Gichko V.V.** (2015) *Rozrahunok stijkosti gnuchkih zalizobetonnih stijok za deformacijnim metodom* [Calculation of the stability of flexible reinforced concrete struts using the deformation method] (PhD Thesis). Kiev, 137 p. (in Ukrainian)
8. **Handzhi V.V.** (1977) *Raschet mnogojetazhnyh zdanij so svjazevym karkasom* [Calculation of multi-storey buildings with a connection frame]. Moscow: Strojizdat, 189 s.
9. **Beglov, A.D., Sanzharovsky, R.S.** (2006) *Teoriya rascheta zhelezobetonnyh konstrukcij na prochnost i ustojchivost. Sovremennye normy i Evrostandarty* [Theory of calculation of reinforced concrete structures for strength and stability. Modern norms and European standards]. St. Petersburg – Moscow. ACB, 221 p. (In Russian)
10. **Sanzharovsky, R.S.** (2015) Zhelezobeton: aktualizirovannyj normativ [Reinforced concrete: updated standard]. *Construction newspaper*. Moscow, no. 21.
11. **Chistjakov E.A.** (1988) Osnovy teorii, metody rascheta i jeksperimental'nye issledovanija nesushhej sposobnosti szhatyh zhelezobetonnyh jelementov pri staticheskom nagruzhenii [Fundamentals of theory, calculation methods and experimental studies of the bearing capacity of compressed reinforced concrete elements under static loading] (doctoral Thesis). Moscow, 498 p. (In Russian)
12. **Travush V.I., Konin, D.V., Rozhkova, L.S., Krylov, A.S.** (2016) Eksperimentalnyye issledovaniya stalezhelezobetonnykh konstruktsiy, rabotayushchikh na vnetsentrennoye szhatiye [Experimental study of composite structures, working for eccentric compression]. *Academia. Architecture and Construction*, no. 3, pp. 127-135.
13. **Arleninov P.D**. (2016) Deformirovanie i ustojchivost' szhatyh i vnecentrenno szhatyh sterzhnevyh zhelezobetonnyh jelementov s uchetom polzuchesti i treshhinoobrazovanija [Deformation and stability of compressed and non-centrally compressed core reinforced concrete elements, taking into account creep and cracking] (PhD Thesis) Moscow, AO «NIC «Stroitel'stvo» (NIIZhB im. A.A. Gvozdeva), Moscow, 143 p. (In Russian)
14. **Krylov S.B., Arleninov P.D.** (2012) Kriticheskaja sila dlja zhelezobetonnyh sterzhnevyh jelementov [Critical force for reinforced concrete core elements] Academia. Architecture and Construction. *Foresight-Russia*, no 2, pp. 136-138.
15. **S.P. Chiew, Y.Q. Cai.** (2018) *Design of high strength steel reinforced concrete columns: a Eurocode 4 approach*, Boca Raton: CRC Press, 105 p.
16. **Terjanik V.V**. (2003) O probleme ustojchivosti vnecentrenno szhatyh betonnyh i zhelezobetonnyh jelementov

srednej i bol'shoj gibkosti [On the problem of stability of non-centrally compressed concrete and reinforced concrete elements of medium and high flexibility] *Vestnik Samarskogo Gosudarstvennogo Tehnicheskogo Universiteta. Fiziko-Matematicheskie Nauki*, Samara, no 19, pp. 167-169.

17. **Krishan A.L., Krishan M.A.** (2014) Vlijanie gibkosti na nesushhuju sposobnost' szhatyh zhelezobetonnyh jelementov [The effect of flexibility on the bearing capacity of compressed reinforced concrete elements] // *Novye idei novogo veka,* Habarovsk, no 3, pp. 308-314.
18. **Lu T., Jin H., Guan K.** (2023) Experimental Research on Axial Compression Performance of High-Performance-Fiber-Reinforced-Cement-Composite-Prefabricated Monolithic Composite Columns. *Buildings*, no.13, pp. 1748-1763.
19. **Liu X., Pan M., Li W., Jing C., Chang W., Zhang H.** (2024) Experimental Study and Bearing Capacity Calculation of Compression-Reinforced Concrete Columns Strengthened with Ultra-High-Performance Concrete. *Applied Sciences*, no 14, pp. 1911-1928.
20. **Ince E.G., Özkal F.M.** (2024) Optimization of Structural Steel Used in Concrete-Encased Steel Composite Columns via Topology Optimization. *Applied Sciences*, no. 14, pp. 1170-1182.
21. **Polskoy P.P, Mailyan D.** etc. (2023) Strength of Compressed Reinforced Concrete Elements Reinforced with CFRP at Different Load Application Eccentricity. *Polymers*, no. 15, p. 26.
22. **Deng F., Chen T., Xiao C.** (2014) *Performance and capacity of isolated steel reinforced concrete columns and design approaches*. Beijing: China Academy of Building Research (CABR) Technology Co., Ltd.
23. **Bogdan T., Gerardy J.-C., Davies D.W., Popa N.** (2017) *Performance and capacity of composite "mega columns" with encased hot rolled steel sections.* Copenhagen: Eurosteel, p. 11.
24. **Muhamediev T.A., Starichkova O.I.** (2006) Raschet prochnosti stalezhelezobetonnyh kolonn s ispol'zovaniem deformacionnoj modeli [Calculation of the strength of steel-reinforced concrete columns using a deformation model] *Beton i zhelezobeton*, no 4 (541), pp. 18-22.
25. **Bezgodov I., Kaprielov S., Sheynfeld A**. (2022) Relationship between strength and deformation characteristics of high-strength self-compacting concrete. *International Journal for Computational Civil and Structural Engineering*, no 18(2), pp. 175–183.
26. **Kaprielov S., Sheinfeld, A., Selyutin N.** (2022) Control of heavy concrete characteristics affecting structural stiffness. *International Journal for Computational Civil and Structural Engineering*, no 18(1), pp. 24–39.

СПИСОК ЛИТЕРАТУРЫ

1. **Сахновский К.В.** Железобетонные конструкции – М.: Государственное Издательство литературы по строительству, архитектуре и строительным материалам, 1961. – 840 с.
2. **Васильев А.П.** Железобетон с жесткой арматурой – М.: Государственное издательство строительной литературы, 1941. – 123 с.
3. **Житницкая Э.Л.** Исследование внецентренно сжатых железобетонных колонн с несущей арматурой при малых эксцентриситетах: диссертация … кандидата технических наук – М., 1957.
4. **Егоров Н.А.** Исследование прочности и деформативности железобетонных колонн с жесткой арматурой из низколегированной стали: диссертация … кандидата технических наук: 05.23.01 – М., 1975. – 142 с.

5. **Каюмов Р.Х.** Устойчивость гибких железобетонных стержней из высокопрочного бетона: диссертация … кандидата технических наук: 05.23.01 – Киев, 1972. – 201 с.
6. **Бамбура А.Н.** Исследование кратковременной устойчивости сжатых железобетонных элементов при нешарнирном закреплении на концах: диссертация … кандидата технических наук: 05.23.01 – Киев, 1978. – 199 с.
7. **Гичко В.В.** Расчет устойчивости гибких железобетонных стоек по деформационному методу (Розрахунок стійкості гнучких залізобетонних стійок за деформаційним методом): диссертация … кандидата технических наук: 05.23.01 – Киев, 2015. – 137 с.
8. **Ханджи В.В.** Расчет многоэтажных зданий со связевым каркасом – М.: Стройиздат, 1977. – 189 с.
9. **Беглов А.Д., Р.С. Санжаровский.** Теория расчета железобетонных конструкций на прочность и устойчивость. Современные нормы и Евростандарты – Санкт-Петербург – Москва: АСВ, 2006. – 221 с.
10. **Санжаровский Р.С.** Железобетон: актуализированный норматив // Строительная газета. – М., 2015, №21.
11. **Чистяков Е.А.** Основы теории, методы расчета и экспериментальные исследования несущей способности сжатых железобетонных элементов при статическом нагружении: диссертация … доктора технических наук: 05.23.01. – М., 1988. – 498 с.
12. **Травуш В.И., Конин Д.В., Рожкова Л.С., Крылов А.С. и др.** Экспериментальные исследования сталежелезобетонных конструкций, работающих на внецентренное сжатие // ACADEMIA. Архитектура и строительство. – М.: 2016, №3. С. 127-135.
13. **Арленинов П.Д.** Деформирование и устойчивость сжатых и внецентренно сжатых стержневых железобетонных элементов с учетом ползучести и трещинообразования – Кандидатская диссертация, АО «НИЦ «Строительство» (НИИЖБ им. А.А. Гвоздева) – М., 2016. – 143 с.
14. **Крылов С.Б., Арленинов П.Д.** Критическая сила для железобетонных стержневых элементов // Academia. Архитектура и строительство, 2012. №2. С. 136-138.
15. **S.P. Chiew, Y.Q. Cai.** Design of high strength steel reinforced concrete columns: a Eurocode 4 approach // Boca Raton: CRC Press, 2018, 105 p.
16. **Теряник В.В.** О проблеме устойчивости внецентренно сжатых бетонных и железобетонных элементов средней и большой гибкости // Вестник Самарского Государственного Технического Университета. Серия: Физико-Математические Науки. – Самара.: 2003, №19. С. 167-169.
17. **Кришан А.Л.**, **Кришан М.А**. Влияние гибкости на несущую способность сжатых железобетонных элементов // Новые идеи нового века. – Хабаровск: 2014. Том 3. С. 308-314.
18. **Lu T., Jin H., Guan K.** Experimental Research on Axial Compression Performance of High-Performance-Fiber-Reinforced-Cement-Composite-Prefabricated Monolithic Composite Columns // Buildings, 2023, No.13, pp. 1748-1763.
19. **Liu X., Pan M., Li W., Jing C., Chang W., Zhang H.** Experimental Study and Bearing Capacity Calculation of Compression-Reinforced Concrete Columns Strengthened with Ultra-High-Performance Concrete // Applied Sciences, 2024, No. 14, pp. 1911-1928.
20. **Ince E.G., Özkal F.M.** Optimization of Structural Steel Used in Concrete-Encased Steel Composite Columns via Topology Optimization. // Applied Sciences, 2024. No. 14, pp. 1170-1182.

21. **Polskoy P.P, Mailyan D. etc** Strength of Compressed Reinforced Concrete Elements Reinforced with CFRP at Different Load Application Eccentricity. // Polymers, 2023. No. 15, pp. 26.
22. **Deng F., Chen T., Xiao C.** Performance and capacity of isolated steel reinforced concrete columns and design approaches // Beijing: China Academy of Building Research (CABR) Technology Co., Ltd., 2014.
23. **Bogdan T., Gerardy J.-C., Davies D.W., Popa N.** Performance and capacity of composite "mega columns" with encased hot rolled steel sections // Eurosteel 2017, Copenhagen, 11 p.
24. **Мухамедиев Т.А., Старичкова О.И.** Расчет прочности сталежелезобетонных колонн с использованием деформационной модели // Бетон и железобетон, 2006, №4 (541). С. 18-22.
25. **Bezgodov I., Kaprielov S., Sheynfeld A.** Relationship between strength and deformation characteristics of high-strength self-compacting concrete // International Journal for Computational Civil and Structural Engineering, 2022, №18(2), pp. 175–183.
26. **Kaprielov S., Sheinfeld, A., Selyutin N.** Control of heavy concrete characteristics affecting structural stiffness // International Journal for Computational Civil and Structural Engineering, 2022, №18(1), pp. 24–39.

Denis V. Konin – Ph.D (Engineering), deputy director for scientific work Research Institute of Building Constructions (TSNIISK) named after V. A. Koucherenko JSC Research Center of Construction: 6, 2nd Institutskaya street, Moscow, 109428, Russia; E-mail: konden@inbox.ru, +7-926-853-99-73.

Конин Денис Владимирович - кандидат технических наук, заместитель директора по научной работе Центрального научно-исследовательского института строительных конструкций (ЦНИИСК) им. В.А. Кучеренко АО «Научно-исследовательский центр (НИЦ) «Строительство»): д. 6, 2-я Институтская ул., Москва, 109428, Россия,; E-mail: konden@inbox.ru, +7-926-853-99-73.

International Journal for Computational Civil and Structural Engineering, 20(2) 192–198(2024)

DOI:10.22337/2587-9618-2024-20-2-192-198

SOLUTION OF THE PROBLEM OF TWO-DIMENSIONAL THEORY OF ELASTICITY WITH THE USE OF DISCRETE-CONTINUAL FINITE ELEMENT METHOD IN THE PRESENCE OF A CRACK

Marina L. Mozgaleva, Pavel A. Akimov

National Research Moscow State University of Civil Engineering, Moscow, RUSSIA

Abstract: Solution of the problem of two-dimensional theory of elasticity with the use of discrete-continual finite element method in the presence of crack is under consideration in the distinctive paper. The original operational continual and discrete-continual formulations of the problem are given, an example of analysis are presented.

Keywords: discrete-continual finite element method, numerical solution, two-dimensional theory of elasticity, structural analysis

РЕШЕНИЕ ДВУМЕРНОЙ ЗАДАЧИ ТЕОРИИ УПРУГОСТИ С ИСПОЛЬЗОВАНИЕМ ДИСКРЕТНО-КОНТИНУАЛЬНОГО МЕТОДА КОНЕЧНЫХ ЭЛЕМЕНТОВ ПРИ НАЛИЧИИ ЩЕЛИ

М.Л. Мозгалева, П.А. Акимов

Национальный исследовательский Московский государственный строительный университет, г. Москва, РОССИЯ

Аннотация: В настоящей статье рассматривается решение двумерной задачи теории упругости с использованием дискретно-континуального метода конечных элементов при наличии щели. Приведены исходные операторные континуальная и дискретно-континуальная постановки задачи, представлен пример расчета.

Ключевые слова: дискретно-континуальный метод конечных элементов, численное решение, двумерная задача теории упругости, расчеты конструкций

INTRODUCTION

Numerical solution of the problem of two-dimensional theory of elasticity with the use of discrete-continual finite element method (DCFEM) has been already considered in [1, 2, 4-8, 12]. Systematic literature review has been presented in [1, 2, 4-8, 12] as well. In this regard, let us immediately move on to the main material of the distinctive paper in case of presence of a crack.

1. FORMULATIONS OF THE PROBLEM

Let the constancy of the parameters of the problem be in the direction corresponding to x_2 (main direction). The operational formulation of the problem with the use of so-called method of extended domain [5], taking into account the selection of the main direction, is determined by the equation [6]:

$$L\,\bar{u} = \bar{\bar{F}}, \quad 0 \le x_1 \le \ell_1,\ 0 \le x_2 \le \ell_2, \qquad (1.1)$$

where we have

$$L = -L_{vv}\,\partial_2^2 + L_{uv}\,\partial_2 + L_{uu}; \qquad (1.2)$$

$$L_{uu} = \partial_1^* D_1^T C D_1 \partial_1; \qquad (1.3)$$

$$L_{uv} = \partial_1^* D_1^T C D_2 - D_2^T C D_1 \partial_1; \qquad (1.4)$$

$$L_{vv} = D_2^T C D_2; \qquad (1.5)$$

$$D_1 = \begin{bmatrix} 1 & 0 \\ 0 & 0 \\ 0 & 1 \end{bmatrix}; \quad D_2 = \begin{bmatrix} 0 & 0 \\ 0 & 1 \\ 1 & 0 \end{bmatrix}; \tag{1.6}$$

$$C = \begin{bmatrix} 2\mu+\lambda & \lambda & 0 \\ \lambda & 2\mu+\lambda & 0 \\ 0 & 0 & \mu \end{bmatrix}; \tag{1.7}$$

ℓ_1, ℓ_2 are corresponding dimensions of extended domain (linear dimensions of considering structure) [3]; $x = (x_1,\ x_2)$; $x_1,\ x_2$ are Cartesian coordinates; μ and λ are Lame parameters; Ω is the domain, occupied by structure;

$$\Omega = \{\ (x_1,\ x_2):\quad 0 < x_1 < \ell_1;\quad 0 < x_2 < \ell_2\ \}; \tag{1.8}$$

$\theta(x_1, x_2)$ is characteristic function of domain Ω; $\delta_\Gamma = \delta_\Gamma(x_1, x_2)$ is the delta function of boundary $\Gamma = \partial\Omega$; $\overline{n} = [\ n_1\ \ n_2\ ]^T$ is boundary normal vector; $\overline{F}$ is the load vector in domain Ω; $\overline{f}$ is the corresponding boundary load vector; $\overline{u}$ is the vector of displacements (unknown vector function),

$$\overline{u} = \begin{bmatrix} u_1 \\ u_2 \end{bmatrix}; \tag{1.9}$$

$\partial_s = \partial / \partial x_s,\ s = 1, 2;\ \partial_s^* = -\partial / \partial x_s,\ s = 1, 2.$

Let us introduce the following notations

$$\overline{v} = \partial_2 \overline{u} = \begin{bmatrix} v_1 \\ v_2 \end{bmatrix}; \tag{1.10}$$

$$\overline{u}' = \partial_2 \overline{u};\quad \overline{v}' = \partial_2 \overline{v}. \tag{1.11}$$

Thus, we can rewrite (1.1):

$$L_{uu}\,\overline{u} + L_{uv}\overline{v} - L_{vv}\partial_2 \overline{v} = \overline{\tilde{F}}. \tag{1.12}$$

Finally we obtain system of differential equations with operational coefficients:

$$\begin{cases} \overline{u}' = \overline{v} \\ \overline{v}' = L_{vv}^{-1} L_{uu}\overline{u} + L_{vv}^{-1} L_{uv}\overline{v} - L_{vv}^{-1}\overline{\tilde{F}} \end{cases} \tag{1.13}$$

or

$$\overline{z}' = \widetilde{L}\overline{z} + \overline{\tilde{F}}, \tag{1.14}$$

where

$$\widetilde{L} = \begin{bmatrix} 0 & E \\ L_{vv}^{-1} L_{uu} & L_{vv}^{-1} L_{uv} \end{bmatrix}; \quad \overline{\tilde{F}} = \begin{bmatrix} 0 \\ -L_{vv}^{-1}\overline{\tilde{F}} \end{bmatrix}; \tag{1.15}$$

$$\overline{z} = \begin{bmatrix} \overline{u} \\ \overline{v} \end{bmatrix}; \quad E = \begin{bmatrix} 1 & 0 \\ 0 & 1 \end{bmatrix}. \tag{1.16}$$

The system of equations (1.14) is supplemented by boundary conditions, which are set in sections with coordinates $x_2^1 = 0$ and $x_2^2 = \ell_2$.

The discrete component of the numerical solution is represented by direction along the axe x_1.

2. EXAMPLE OF ANALYSIS

2.1. Formulation of the problem.

As a model example, let us consider the determination of the displacements of a beam-wall, fixed along the side faces in three directions, under the influence of a load concentrated in the center (Figure 2.1).

Let us consider the following geometric parameters:

$$\ell_1 = 1\ \text{m};\quad \ell_2 = 1\ \text{m}.$$

Let us consider the following design parameters of material of the beam: coefficient of elasticity $E = 2650 \cdot 10^4\ \text{kN/m}^2$; Poisson's ratio $\nu = 0.15$.

Let external load parameter be equal to $P = 100\ \text{kN}$.

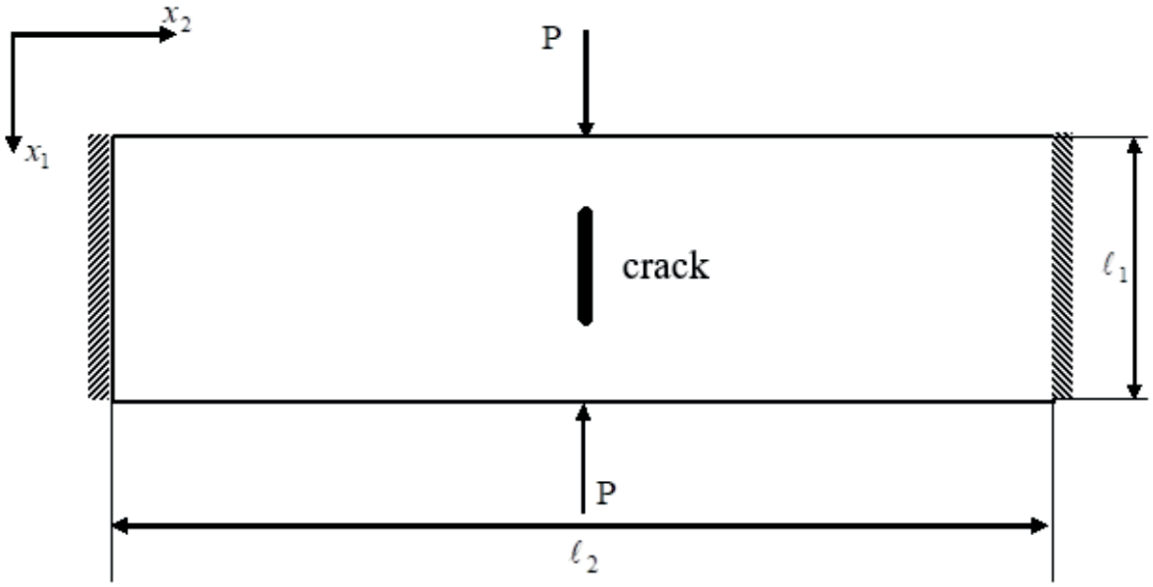


Figure 2.1. Example of analysis

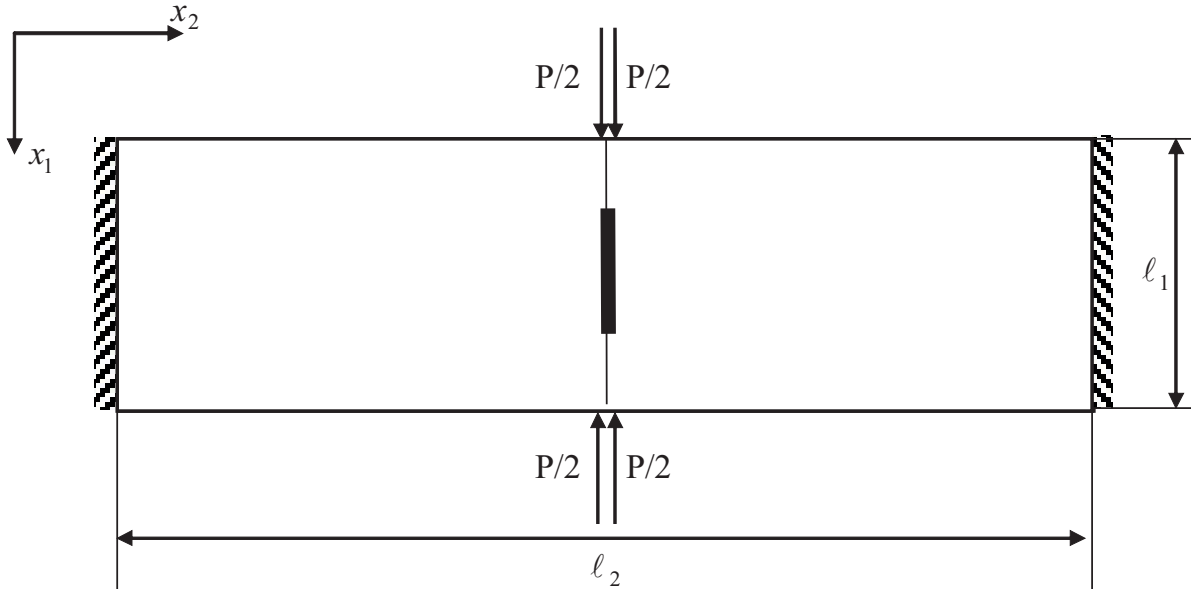


Figure 2.2. Design model

Let us consider the initial problem in the form of a combination of two boundary problems (Figure 2.2).

The contact boundary runs vertically, including the crack. In this case, the contact boundary equations at nodes outside the crack represent the conditions of ideal contact. The equations at the nodes that fall within the crack zone represent the free edge conditions. The load is specified on both sides of the contact boundary at a distance of $2 \cdot 10^{-7}$ m. The discrete component includes $n = 21$ nodes (finite elements): 20 upper and 7 lower nodes for ideal contact equations; internal 7 nodes for equations of free edges on the left side and right side.

Figures 2.3-2.6 are graphical visualizations of the numerical solution (displacements, stresses) at the contact nodes, while "*L*" means the solution for the boundary value problem on the left side, and "*P*" means the solution for the boundary value problem on the right side.

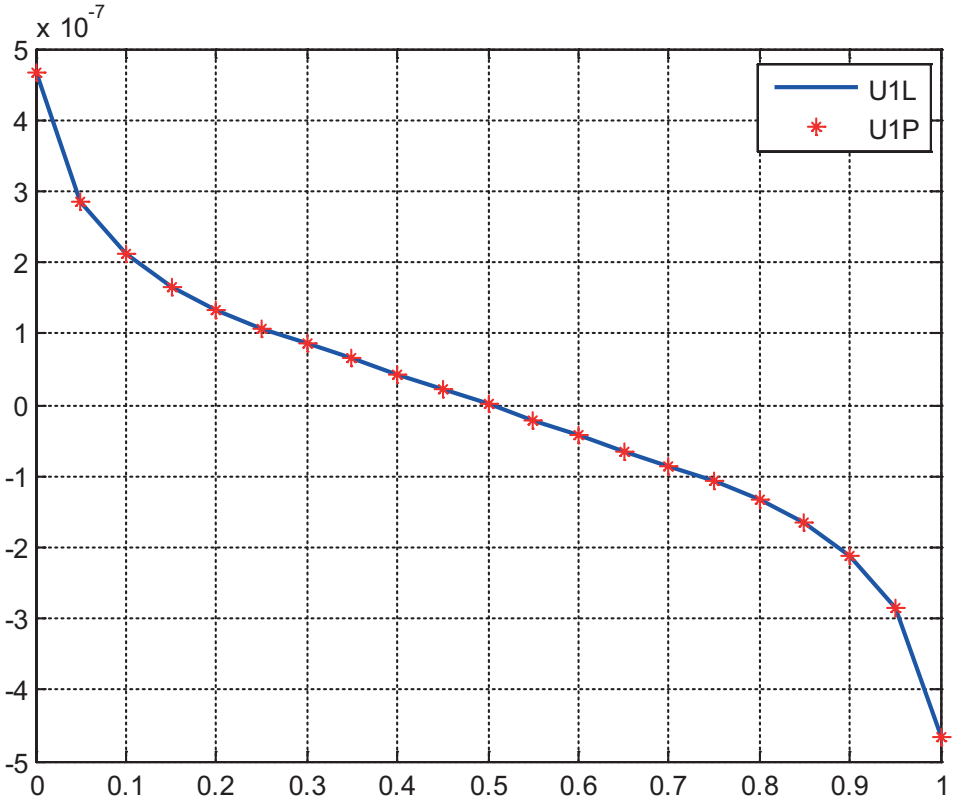


Figure 2.3. Displacements U1L and U1P

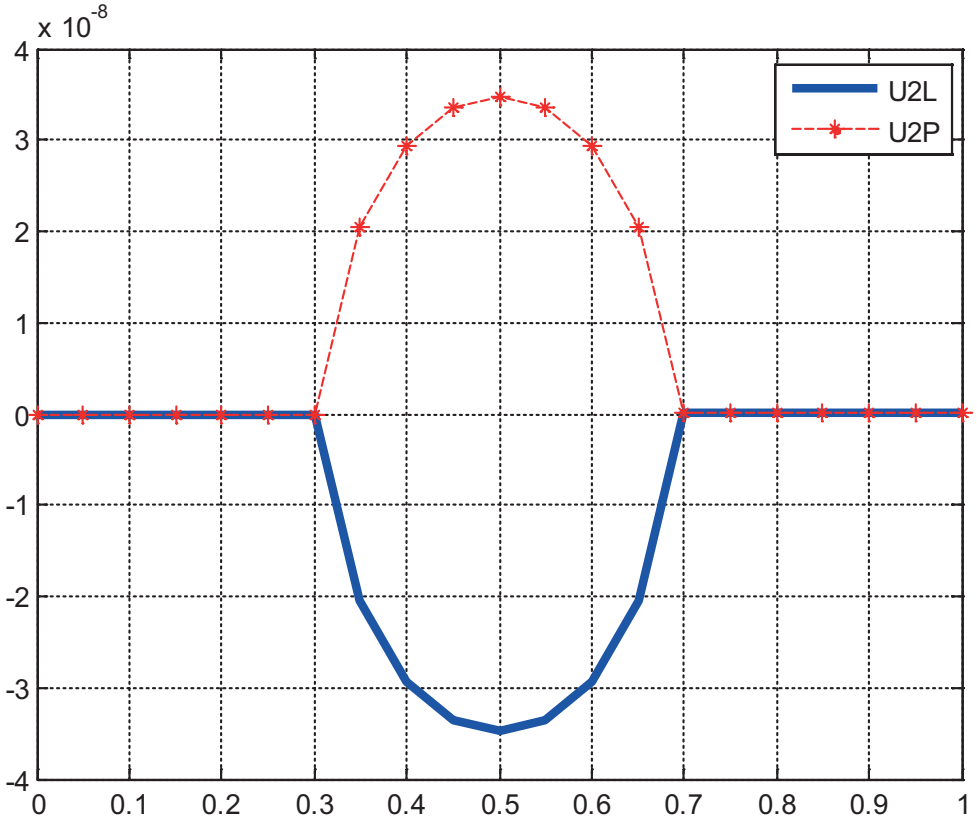


Figure 2.4. Displacements U2L and U2P

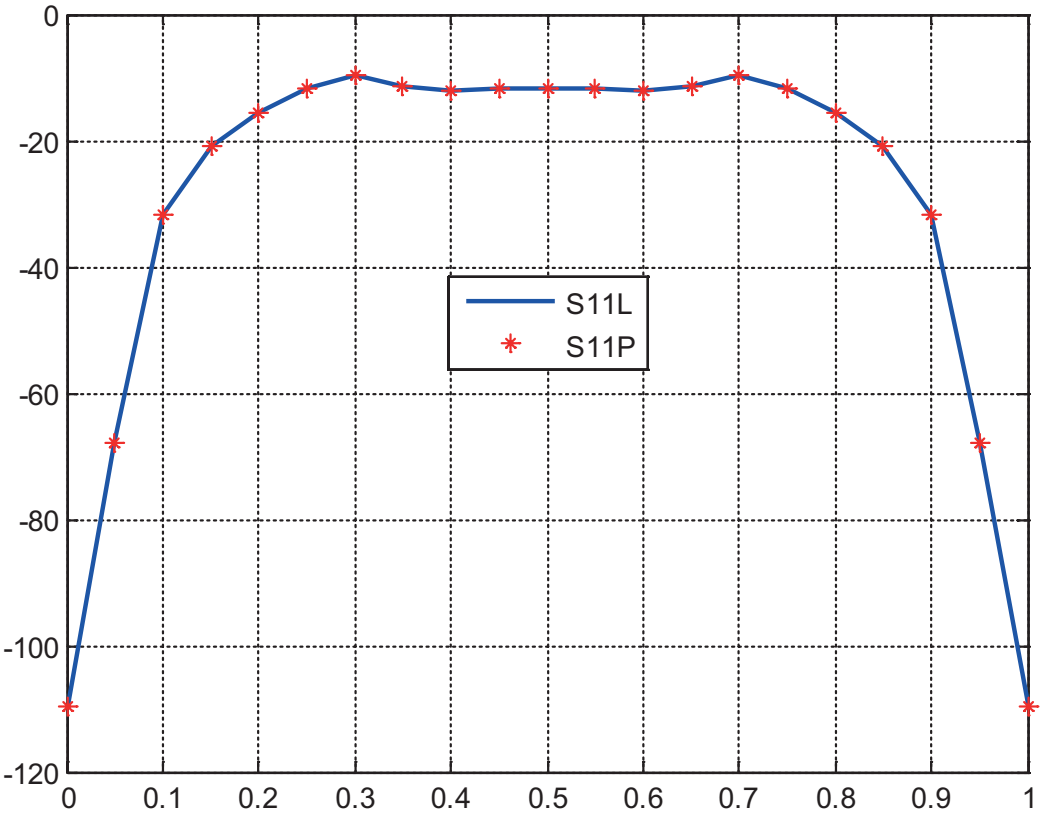


Figure 2.5. Stresses $\sigma 11L$ and $\sigma 11P$

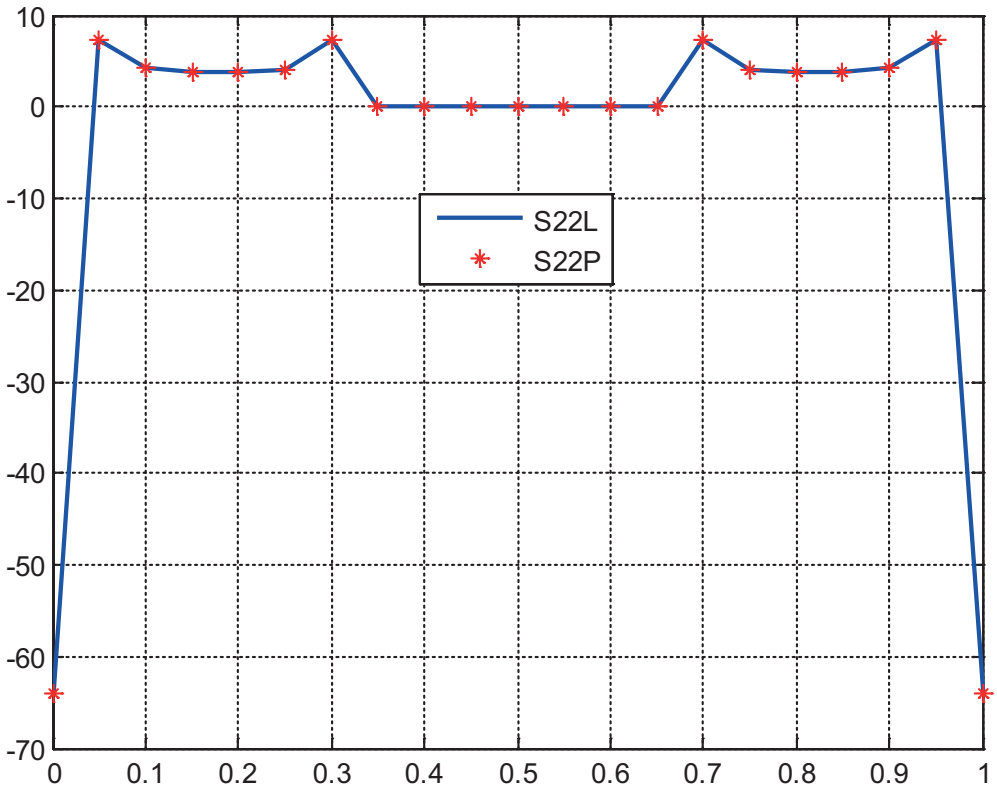


Figure 2.6. Stresses $\sigma 22L$ and $\sigma 22P$.

The presented sample of analysis illustrates the effectiveness of using the discrete-continuous finite element method, since the length significantly exceeds the width of the beam-wall, and the traditional finite element method [9-11] would lead to a significant increase in the nodes of the mesh region.

REFERENCES

1. **Akimov P.A.** Correct Direct Discrete-Continual Boundary Element Method of Structural Analysis. // Applied Mechanics and Materials Vols. 395-396 (2013), pp. 529-532.
2. **Akimov P.A., Sidorov V.N.** Correct Method of Analytical Solution of Multipoint Boundary Problems of Structural Analysis for Systems of Ordinary Differential Equations with Piecewise Constant Coefficients. // Advanced Materials Research Vols. 250-253, 2011, pp. 3652-3655.
3. **Akimov P.A., Mozgaleva M.L.** Method of Extended Domain and General Principles of Mesh Approximation for Boundary Problems of Structural Analysis. // Applied Mechanics and Materials, 2014, Vols. 580-583, pp. 2898-2902.
4. **Akimov P.A., Mozgaleva M.L.** Wavelet-based Multilevel Discrete-Continual Finite Element Method for Local Deep Beam Analysis. // Applied Mechanics and Materials Vols. 405-408 (2013), pp. 3165-3168.
5. **Akimov P.A., Mozgaleva M.L., Mojtaba Aslami, Negrozov O.A.** About Verification of Discrete-Continual Finite Element Method of Structural Analysis. Part 1: Two-Dimensional Problems // Procedia Engineering, Vol. 91 (2014), pp. 2-7.
6. **Akimov P.A., Mozgaleva M.L., Mojtaba Aslami, Negrozov O.A.** Wavelet-Based Discrete-Continual Finite Element Method of Local Structural Analysis for Two-Dimensional Problems // Procedia Engineering, Vol. 91 (2014), pp.8-13.
7. **Akimov P.A., Mozgaleva M.L., Negrozov O.A.** About Verification of Discrete-Continual Finite Element Method for Two-Dimensional Problems of Structural Analysis. Part 1: Deep Beam with Constant Physical and Geometrical Parameters Along Basic Direction. // Advanced Materials Research, Vols. 1025-1026 (2014), pp. 89-94.
8. **Akimov P.A., Mozgaleva M.L., Negrozov O.A.** About Verification of Discrete-Continual Finite Element Methodfor Two-Dimensional Problems of Structural Analysis. Part 2: Deep Beam with Piecewise Constant Physical and Geometrical Parameters Along Basic Direction. // Advanced Materials Research, Vols. 1025-1026 (2014), pp. 95-103.
9. **Zienkiewicz O.C., Morgan K.** Finite Elements and Approximation. Dover Publications, 2006, 352 pages.
10. **Zienkiewicz O.C., Taylor R.L., Zhu J.Z.** The Finite Element Method: Its Basis and Fundamentals. Butterworth-Heinemann, Sixth edition, 2005, 752 pages.
11. **Zienkiewicz O.C., Taylor R.L.** The Finite Element Method for Solid and Structural Mechanics. Volume 2. Butterworth-Heinemann, Sixth Edition, 2005, 736 pages.
12. **Zolotov A.B., Akimov P.A.** Semianalytical Finite Element Method for Two-dimensional and Three-dimensional Problems of Structural Analysis. // Proceedings of the International Symposium LSCE 2002 organized by Polish Chapter of IASS, Warsaw, Poland, 2002, pp. 431-440.
13. **Lur'e A.I.** Teorija uprugosti [Theory of Elasticity]. Moscow, Nauka, 1970, 939 pages (in Russian).

СПИСОК ЛИТЕРАТУРЫ

1. **Akimov P.A.** Correct Direct Discrete-Continual Boundary Element Method of Structural Analysis. // Applied Mechanics and Materials Vols. 395-396 (2013), pp. 529-532.
2. **Akimov P.A., Sidorov V.N.** Correct Method of Analytical Solution of Multipoint

Boundary Problems of Structural Analysis for Systems of Ordinary Differential Equations with Piecewise Constant Coefficients. // Advanced Materials Research Vols. 250-253, 2011, pp. 3652-3655.
3. **Akimov P.A., Mozgaleva M.L.** Method of Extended Domain and General Principles of Mesh Approximation for Boundary Problems of Structural Analysis. // Applied Mechanics and Materials, 2014, Vols. 580-583, pp. 2898-2902.
4. **Akimov P.A., Mozgaleva M.L.** Wavelet-based Multilevel Discrete-Continual Finite Element Method for Local Deep Beam Analysis. // Applied Mechanics and Materials Vols. 405-408 (2013), pp. 3165-3168.
5. **Akimov P.A., Mozgaleva M.L., Mojtaba Aslami, Negrozov O.A.** About Verification of Discrete-Continual Finite Element Method of Structural Analysis. Part 1: Two-Dimensional Problems // Procedia Engineering, Vol. 91 (2014), pp. 2-7.
6. **Akimov P.A., Mozgaleva M.L., Mojtaba Aslami, Negrozov O.A.** Wavelet-Based Discrete-Continual Finite Element Method of Local Structural Analysis for Two-Dimensional Problems // Procedia Engineering, Vol. 91 (2014), pp.8-13.
7. **Akimov P.A., Mozgaleva M.L., Negrozov O.A.** About Verification of Discrete-Continual Finite Element Method for Two-Dimensional Problems of Structural Analysis. Part 1: Deep Beam with Constant Physical and Geometrical Parameters Along Basic Direction. // Advanced Materials Research, Vols. 1025-1026 (2014), pp. 89-94.
8. **Akimov P.A., Mozgaleva M.L., Negrozov O.A.** About Verification of Discrete-Continual Finite Element Methodfor Two-Dimensional Problems of Structural Analysis. Part 2: Deep Beam with Piecewise Constant Physical and Geometrical Parameters Along Basic Direction. // Advanced Materials Research, Vols. 1025-1026 (2014), pp. 95-103.
9. **Zienkiewicz O.C., Morgan K.** Finite Elements and Approximation. Dover Publications, 2006, 352 pages.
10. **Zienkiewicz O.C., Taylor R.L., Zhu J.Z.** The Finite Element Method: Its Basis and Fundamentals. Butterworth-Heinemann, Sixth edition, 2005, 752 pages.
11. **Zienkiewicz O.C., Taylor R.L.** The Finite Element Method for Solid and Structural Mechanics. Volume 2. Butterworth-Heinemann, Sixth Edition, 2005, 736 pages.
12. **Zolotov A.B., Akimov P.A.** Semianalytical Finite Element Method for Two-dimensional and Three-dimensional Problems of Structural Analysis. // Proceedings of the International Symposium LSCE 2002 organized by Polish Chapter of IASS, Warsaw, Poland, 2002, pp. 431-440.
13. **Лурье А.И.** Теория упругости. – М.: Наука, 1970. – 939 с.

Pavel A. Akimov, Full Member of the Russian Academy of Architecture and Construction Sciences, Professor, Dr.Sc.; Rector of National Research Moscow State University of Civil Engineering; 26, Yaroslavskoe Shosse, Moscow, 129337, Russia; phone: +7(495) 651-81-85; Fax: +7(499) 183-44-38; E-mail: AkimovPA@mgsu.ru, rector@mgsu.ru, pavel.akimov@gmail.com.

Marina L. Mozgaleva, Senior Scientist Researcher, Dr.Sc.; Professor of Department of Applied Mathematics, National Research Moscow State University of Civil Engineering; 26, Yaroslavskoe Shosse, Moscow, 129337, Russia; phone/fax +7(499) 183-59-94; Fax: +7(499) 183-44-38; Email: marina.mozgaleva@gmail.com.

Мозгалева Марина Леонидовна, старший научный сотрудник, доктор технических наук; профессор кафедры прикладной математики Национального исследовательского Московского государственного строительного университета; 129337, Россия, г. Москва, Ярославское шоссе, дом 26; телефон/факс: +7(499) 183-59-94; Email: marina.mozgaleva@gmail.com.

Акимов Павел Алексеевич, академик РААСН, профессор, доктор технических наук; ректор Национального исследовательского Московского государственного строительного университета; 129337, Россия, г. Москва, Ярославское шоссе, дом 26; телефон: +7(495) 651-81-85; факс: +7(499) 183-44-38; Email: AkimovPA@mgsu.ru, rector@mgsu.ru, pavel.akimov@gmail.com.